1973-07

Design report of hybrid compressor and associated test rig

Vavra, Michael Hans

Monterey, California. Naval Postgraduate School

NAVAL POSTGRADUATE SCHOOL

Monterey, California

DESIGN REPORT OF HYBRID COMPRESSOR

AND

ASSOCIATED TEST RIG

by

M. H. Vavra

July 1973

NAVAL POSTGRADUATE SCHOOL
Monterey, California

Rear Admiral M. B. Freeman, USN
Superintendent

M. U. Clauser
Provost

ABSTRACT:

This report presents the aerodynamic calculations and describes the mechanical features of a test rig that has been designed at the Turbopropulsion Laboratory, Department of Aeronautics, for research work on a special type of centrifugal compressor. This so-called Hybrid compressor consists of a centrifugal rotor with 180° flow deflection in the meridional plane followed by an axial flow diffusor. The report establishes a method to predict the off-design performance of the subject compressor, which can be applied also to conventional centrifugal compressors. Extensive use is made of modern programmable calculators, and programs are presented to show the effectiveness of these tools in engineering endeavors.

This work was supported by:

Navy Department
Naval Air Systems Command, Code 330C
AIRTASK No. A3303300/186B/3F41432301

TABLE OF CONTENTS

		Page
	INTRODUCTION	1
I.	AERODYNAMIC DESIGN	2
	1. Impeller	2
	2. Inducer	6
	3. Diffusor	11
II.	DESIGN POINT PERFORMANCE	21
	1. Rotor	21
	2. Diffusor	24
	3. Flow Straightener and Discharge Duct	30
	4. Compressor Performance at Design Point	35
III.	OFF-DESIGN POINT PERFORMANCE	41
	1. General	41
	2. Rotor Performance	41
	3. Diffusor Performance	44
	4. Compressor Off-Design Performance	46
IV.	DRIVE TURBINE	49
	1. General	49
	2. Off-Design Turbine Performance	49
V.	MECHANICAL DESIGN	52
	1. Rotor	52
	2. Maximum Obtainable Pressure Ratios	54
	3. General Description of Test Rig	56
	REFERENCES	61
	TABLES (see list, page v.)	63
	FIGURES (see list, page vi.)	77
	APPENDIX A: Basic Elements for Advanced Design of Radial-Flow Compressors	110
	APPENDIX B: Manufacturing Drawings	153
	Dwg. 2103-A: Rotor Attachment	154
	" 2107 : Turbine Blade Profile	155
	" 2108-1: Turbine Rotors	156
	" 2109 : Turbine Stators	157
	" 2140 : Nozzle Casing	158
	" 2158 : Inlet Throttle Valve Assembly	159

Dwg. 2159 : Control Valve Actuator 160
" 2164-1: Inlet Plenum 161
" 2203 : Impeller of Hybrid Compressor 162
" 2204 : Inducer of Hybrid Compressor 163
" 2205 : Wheel Attachment 164
" 2207 : Stator Casing 165
" 2208 : Diffusor Sleeve 166
" 2209 : Diffusor Blade Holders and Spacers 167
" 2210-1: Diffusor Blades Type A1 168
" 2210-2: " " " A2 169
" 2210-3: " " " B1 170
" 2210-4: " " " B2 171
" 2212 : Shroud Support 172
" 2213 : Shroud 173
" 2214-2: Inlet Casing 174
" 2215 : Labyrinths 175
" 2216 : Nozzle Frame 176
" 2222 : Test Compressor Assembly 177
" 2223 : Installation of Hybrid Compressor Test Rig 178

APPENDIX C: Losses in Radial Compressor Wheels 179

APPENDIX D: Calculating Programs for Monroe Model 1655/6 and Model 1880-20 Programmable Calculators: 195

Program No. 102: Flow Rate through Radial Compressor for Given Conditions at Discharge 196

Program No. 103: Determination of Pressure Ratio for Given Isentropic Flow Function for Different γ. 204

Program No. 104: Inlet Conditions of Radial Compressor with Axial Inlet Flow 211

Program No. 105: Relation between Rotor Efficiencies and Velocity Ratio of Radial Compressor Impeller 218

Program No. 106: Conditions at Discharge of Impeller of Radial Compressor 224

Program No. 108: Mass Flow Rate at Inducer Inlet as Function of V_{1o}/a_o 231

Program No. 109: Flow Conditions after Cascade for Given Inlet Conditions, Flow Deflections and Total Pressure Loss Coefficient 238

Program No. 110: Calculation of Curve $r/a = \theta^{-b}$ with Zero Curvature at One Point and $\delta_{MAX} = 90^{\circ}$ 248

Program No. 517: Off-Design Performance of Hybrid Compressor 251

LIST OF TABLES

		page
I.	Flow, Blade, and Incidence Angles at Inducer Leading Edge	64
II.	Loss Coefficients of First Blade Row of Diffusor	65
III.	Design Values of First Blade Rows of Diffusors A and B	66
IV.	Loss Coefficients of Second Blade Row of Diffusor	67
V.	Design Values of Second Blade Rows of Diffusors A and B	68
VI.	Determination of Diffusor Profile Data	69
VII.	Flow Properties in Diffusor	70
VIII.	Flow Conditions in Flow Straightener and Discharge Duct	71
IX.	Estimated Compressor Performance at Design Point	72
X.	Performance of Centrifugal Compressor Rotor (2 sheets)	73
XI.	Calculated Performance of Hybrid Compressor at 16,666 rpm	75
XII.	Calculated Performance of Hybrid Compressor at 12,018 rpm	76

LIST OF FIGURES

		page
1.	Hybrid Compressor (Symbols and Stations)	78
2.	Determination of Rotor and Hub Contours for Specified Blade Tip Contour	79
3.	Conditions at Leading Edge of Inducer	80
4.	Blade Angles of Straight Inducer Blades	81
5.	Properties of Elliptical Inducer Blade Surface	82
6.	Secondary Loss Coefficient of Ref. 6	83
7.	Overall Loss Coefficients of First Diffusor Row	84
8.	Overall Loss Coefficients of Second Diffusor Row	85
9.	Diffusor Blade Data	86
10.	Determination of Flow Conditions after Diffusor Row	87
11.	Conditions in Flow Straightener and Discharge Duct	88
12.	Rotor Dimensions	89
13.	Polytropic Rotor Efficiency as Function of Flow Angle β_{1o} at Inducer Tip Radius and Speed Ratio U_2/a_0	90
14.	Arc Length of Parabolic Mean Camber Line of Inducer Blade ...	91
15.	Flow Angle β_{1o}* for U_2/a_0 and M_{W1} ...	92
16.	Velocity Distributions at Inducer Tip at Different Incidence Angles	93
17.	Compressor Performance at $U_2/a_0 = 0.83$	94
18.	Meridian Curve $r/a = \theta^{-b}$ with $\delta_m = \pi/2$	95
19.	Relationship between y_o/x_o , $x_o k_m$ and y_o/x_o for Meridian Curve of Fig. 18	96
20.	Scale Drawing of Meridian Contours with $r/a = \theta^{-b}$ of Impeller of Fig. 12 ...	97
21.	Dimensionless Mass Flow Rate $(\dot{m})$* as Function of Flow Function φ_1 of Fig. 17 ...	98
22.	Polytropic Rotor Efficiency η_{RP} and Mach Number M_{W1} ... from Figs. 21 and 15 ...	99

23. Polytropic Rotor Efficiency η_{RP} and Mach Number M_{W1} as Function of Flow Angle from Fig. 21 ... and Fig. 13... 100

24. Adiabatic Rotor Efficiency η_R as Function of Mach Number M_{W1} , Peripheral Speed Ratio U_2/a_0, and Incidence Angle i'... 101

25. Adiabatic Rotor Efficiency as Function of M_{W1} and i' of Fig. 24 ... 102

26. Velocity Coefficient Ψ and Incidence Angle i' of Hybrid Compressor Rotor as Function of Deceleration Ratio W_2/W_{1o} ... 103

27. Assumed Change of Diffusor Pressure Loss Coefficient Y_t with Incidence Angle i 104

28. Calculated Performance of Hybrid Compressor Operating in Test Rig 105

29. Predicted Performance of Drive Turbine 106

30. Predicted Turbine Performance 107

31. Stress Distribution in Hybrid Rotor 108

32. Blade Stresses of Hybrid Rotor 109

INTRODUCTION

The idea of arranging an axial diffusor after a special centrifugal compressor rotor that turns the flow by 180° instead of 90°, as in conventional machines, has been conceived by Mr. George Derderian, Naval Air Systems Command, Code AIR-53622B. For this so-called Hybrid compressor concept, he was awarded U. S. Patent 3, 365, 892 dated January 30, 1968.

To verify the conditions that exist after a Hybrid impeller, and to investigate whether it is possible to convert the kinetic energy of the flow after such a rotor into useful pressure rise with acceptable efficiency, a research project was started at the Turbopropulsion Laboratory, NPS, which was funded by the Naval Air Systems Command, under: AIRTASK A3303300/186B/3F41432301.

The present report gives the particulars of the design that led to the manufacture of the test rig which is now operative and being used to carry out the afore-mentioned research work.

The project was supervised by Mr. K. H. Guttmann, AIR-330C, who has been extremely helpful in all phases of the program. The author is deeply grateful to Mr. Guttmann for the patience, understanding and considerateness which he received during a lengthy period of personal misfortune which delayed the research program and the completion of this report.

I. AERODYNAMIC DESIGN

1. Impeller

Because of its peculiar design the rotor of the Hybrid compressor of Fig. 1 is highly stressed. (See Section V.1) Therefore, it must have meridional blades at the discharge to eliminate additional blade bending stresses. Ahead of the rotor the absolute inlet velocity will be axial everywhere. Hence it is possible to establish the rotor dimensions with the method of Ref. 1 which is enclosed as Appendix A. The corresponding dimensions of the Hybrid rotor are shown in Fig. 1.

The symbols used in the following are identical with those listed in Appendix A. For easier reference, the figures and equations of Appendix A are denoted by Fig. A .... and Eq. A ..... Thus, Fig. A(3) is figure 3, and Eq. A II(4) is equation II(14) of Table II of Appendix A.

A parametric study indicated that optimum conditions were obtained for the following design values (see Fig. 1):

$$\beta_{1o} = 55^{\circ}$$

$$\alpha_2 = 65^{\circ}$$

$$R_{1o}/R_2 = 0.55$$

$$R_{1i}/R_2 = 0.18$$

The relatively small angle β_{1o} of 55° is necessary to be able to limit the ratio R_{1o}/R_2 to 0.55 and to obtain a sufficiently high flow rate so that the diffusor blade height b_2 does not become too small. For values of R_{1o}/R_2 larger than 0.55 the meridional flow channel would also have very large curvatures at the blade tip contour of the Hybrid rotor. This would produce large radial velocity gradients at the rotor discharge. The choice of $\alpha_2 = 65^{\circ}$ was predicated by the permissible loading of the axial diffusor blade rows, and the large losses that occur if α_2 is

larger than 65°. A radius ratio $R_{1i}/R_2 = 0.18$ of the hub at the inducer inlet was chosen to be able to arrange 17 rotor blades with a thickness of about 0.125 inches. With smaller ratios R_{1i}/R_2 it is not possible to have 17 blades and it would then be necessary to design the impeller with splitter vanes, a feature which did not seem to be warranted for the present tests.

Preliminary investigation also showed that the peripheral rotor speed U_2 at the mean discharge radius R_2 of Fig. 1 should not exceed about 800 ft/s because of critical speed considerations if the rotor is made of aluminum.

For air with $\gamma = c_p/c_v = 1.4$ and a gas constant $R_G = 53.35$ (ft-lb)/(lbm, $^{\circ}$R), the velocity of sound a_0 at an assumed total inlet temperature $T_0 = 520^{\circ}$R is

$$a_0 = \sqrt{g\ \gamma\ R_G\ T_0} = 1117.85 \text{ ft/s}$$

giving a ratio

$$U_2/a_0 = 0.7156$$

From Eq. A II(4) the Mach number M_{W1} of the relative velocity at the outer radius R_{1o} of the rotor inlet eye is then

$$M_{W1} = \left[\frac{\sin^2 \beta_{1o}}{\left(\frac{R_{1o}}{R_2} \frac{U_2}{a_0} \right)^2} - \frac{\gamma - 1}{2} \cos^2 \beta_{1o} \right]^{-\frac{1}{2}} = 0.4842 \qquad (1)$$

For a weight flow rate $\dot{w} = \dot{m}\ g$ (lbm/s) there is from Eq. A II(9)

$$\pi R_2^{\ 2}\ k_{B1} = \frac{\dot{w}}{P_0} \sqrt{\frac{R_G\ T_0}{g}}\ (11.7944) \qquad (2)$$

Figure A(3a) shows that the so-called slip factor μ depends of the number of rotor blades Z_R, the ratio R_{1o}/R_2, the rotor efficiency η_R, and the flow coefficient φ_2. Minor corrections for μ must be applied if

the tip clearance ratio δ/b_2 differs from 0.05 (see Fig. A(3b)) and if the flow in the rotor is turned by less than 90° in the meridian plane (see Fig. A(3c)). However, no data for μ are available if this turning is 180° as in the present wheel, and for this reason the slip factor is taken as that of a standard centrifugal compressor wheel with $\varepsilon = 90^\circ$.

In accordance with Eq. A II(6) the flow coefficient φ_2 depends on μ. For a chosen value $\mu = 0.86$ there is

$$\varphi_2' = (0.86)(\cot 65^\circ) = 0.401$$

For an assumed rotor efficiency $\eta_R = 0.86$, $Z_R = 17$, and $R_{1o}/R_2 = 0.55$, by extrapolating Fig. A(3a) to higher values of φ_2, there is $\mu = 0.847$. Hence, $\varphi_2 = 0.395$, and the slip factor for this velocity ratio is about 0.85, giving a final value $\varphi_2 = 0.3964$. For $\mu = 0.85$, from Eq. A II(5),

$$\frac{W_2}{W_{1o}} = 0.6312 \tag{3}$$

Appendix A discusses the different possibilities to express the frictional losses in radial wheels. From Eq. A(25)

$$C = 0.7200$$

and from Eq. A(27) the so-called wheel efficiency η_W for $\eta_R = 0.86$ is

$$\eta_W = 0.4999$$

With this value and Eq. 3, the velocity ratio Ψ of Eq. A (21) is

$$\Psi = \frac{W_2}{W_{2is}} = 0.7548$$

With these data the rotor dimensions at the discharge are obtained from Eq. A II(11)

$$\pi R_2^2 \frac{b_2}{R_2} k_{B2} = \frac{\dot{w}}{P_0} \sqrt{\frac{R_G T_0}{g}} \, (1.2739) \tag{4}$$

Hence, with Eq. 2

$$\frac{b_2}{R_2}\,\frac{k_{B2}}{k_{B1}} = \frac{1.2739}{11.7944} = 0.1080$$

The restriction factor k_{B1} at the inlet eye due to boundary layer growth is assumed to be 0.98, and $k_{B2} \cong 0.954$,

Thus

$$\frac{b_2}{R_2} = 0.1109 \qquad (5)$$

In accordance with Fig. A(16) this ratio is acceptable.

The mean radius R_2 is chosen as 5.5 in., primarily to be able to drive the impeller by an available turbine and to mount the compressor to this item. Then the rotative speed N for U_2 = 800 ft/s is

$$N = \frac{800}{\frac{\pi}{30}\frac{R_2}{12}} = \frac{(800)(360)}{\pi(5.5)} = 16{,}666 \text{ rpm}$$

The basic compressor dimensions in inches are then:

$$D_2 = 2\,R_2 = 11.0$$

$$D_{1o} = 2\,R_{1o} = 6.05$$

$$D_{1i} = 2\,R_{1i} = 1.98$$

$$b_2 = 0.61$$

The radial overlaps δ of Fig. 1 at the impeller discharge are chosen to be 0.025 in., so that the blade height b_2' at the wheel discharge equals

$$b_2' = 0.56 \text{ in.}$$

Drawing 2222 of Appendix B shows the design of the Hybrid compressor. Details of the impeller and the inducer are given in Dwgs. 2203 and 2304. The meridional channel of the wheel was laid out by assuming a blade tip contour with the smallest possible curvature changes between R_{1o} and the discharge. Drawings 2203 and 2204 show that such a contour could be

obtained with a two adjoining circular arcs with radii of 1.666 and 1.02 inches. By assuming that the meridional flow areas, without the restriction due to the blades, change linearly with the distance ℓ along the tip contour from A_1 at the inlet to A_2' at the impeller discharge the meridional channel could be laid out with the method explained in Fig. 2. As shown in Dwgs. 2203 and 2204 the hub contour thus obtained could be approximated by four adjoining circular arcs whose radii decrease from the rotor inlet to the rotor discharge. The clearance between the blade tips and the adjoining casing of Dwg. 2213 is everywhere equal to 0.025 inch.

2. Inducer

Although some designers propose that the leading edges of the inducer blading have to be so arranged that particular incidence angles occur, it is shown in Ref. 2 that the correct incidence angles are obtained if the blockage because of the blade thickness is taken into account in the design. Figure 3 shows the conditions at the inducer entrance where V_1, W_1, β_1 are the flow properties just ahead of the inducer leading edges. In particular, the relative flow angle β_{1o} at the radius R_{1o} is equal to 55°. At an arbitrary radius R_1 the blade spacing is

$$S = \frac{2 \pi R_1}{Z_R} \tag{6}$$

Because of the blade thickness t or its projected thickness t_u in peripheral direction, the axial component V_1' of the flow after entering the inducer is

$$V_1' = V_1 \frac{s}{s - t_u} \tag{7}$$

giving a flow angle β_1' of

$$\beta_1' = \tan^{-1}\left(\frac{\omega R_1}{V_1'}\right) = \beta_B \qquad (8)$$

If the blade has this angle β_1' at the leading edge there occurs an effective positive incidence angle

$$i = \beta_1 - \beta_1' = \beta_1 - \beta_B \qquad (9)$$

Although in actuality the projected blade width is then $t_u' = t/\cos \beta_1'$ it is sufficiently accurate to take $t_u = t/\cos \beta_1$ because of the small values of i, and because the blade leading edge will actually be profiled as shown by the dotted contours of Fig. 3. For the same reason the thickness t is taken as 0.10 in., although the blade thickness t farther downstream is actually 0.125 in.. With these assumptions the blade angle $\beta_B = \beta_1'$ at the leading edge can be determined from Eqs. 6 to 8, or

$$\tan \beta_B = \frac{\omega R_1}{V_1}\left(1 - \frac{t_u}{s}\right) = \frac{\omega R_1}{V_1}\left(1 - \frac{t Z_R}{\cos \beta_1 \, 2 \pi R_1}\right)$$

Assuming V_1 to be constant along R_1, and from the condition that at R_{1o}

$$\tan \beta_{1o} = \frac{\omega R_{1o}}{V_1} = \tan 55^\circ$$

there is with $R_{1o} = 3.025$ in.

$$\tan \beta_1 = \frac{R_1}{R_{1o}} \tan 55^\circ = \frac{R_1}{3.025} \tan 55^\circ$$

and

$$\tan \beta_B = \tan \beta_1 \left[1 - \frac{(0.1)(17)}{\cos \beta_1 \, 2 \pi R_1}\right]$$

Table I gives the angles β_1, β_B and the incidence angles i along the radius R_1 at the inducer inlet.

To be able to machine the impeller with simple means, it is assumed that its blade sufaces consist of generatrices that are everywhere parallel

to the radius at the inducer discharge where the blades must adjoin the radial impeller blades. As shown in Fig. 4, the camber line of the inducer blades can then be specified by a single function $y = f(x)$. At a point P the blade surface has the angle γ, where $\tan \gamma = dy/dx$. This angle, however, is the angle in planes A-A which are perpendicular to the radius at station Q, where the inducer blades line up with the impeller blades. To obtain the actual blade angle β_B at a radius R_1 the blade surface must be intersected with a cylinder of radius R_1. For a point $P(x,y)$ of the blade surface the blade angle β_B at the radius R_1 is from Fig. 4

$$\tan \beta_B = \frac{dy}{\cos \theta \, dx} = \frac{\tan \gamma}{\cos \theta}$$

However

$$\cos \theta = \frac{\sqrt{R_1^2 - y^2}}{R_1}$$

Thus

$$\tan \beta_B = \frac{\tan \gamma}{\sqrt{1 - (y/R_1)^2}} = \frac{dy/dx}{\sqrt{1 - (y/R_1)^2}} \qquad (10)$$

A function $y = f(x)$ for the blade surface will now be established such that the blade angles β_B of Table I can be obtained along the radius R_1 by varying the axial length x of the inducer blades, as indicated in Fig. 3. In particular, the camber line of the inducer blades is chosen to be an ellipse. In accordance with Fig. 5

$$y = b - \frac{b}{a}\sqrt{a^2 - x^2} \qquad (11)$$

where 2a and 2b are the lengths of the major and minor axes of the ellipse, respectively. From Eq. 11

$$\frac{dy}{dx} = \tan \gamma = \frac{b}{a} \frac{x}{\sqrt{a^2 - x^2}} \tag{12}$$

Referring to Fig. 3, the values of "a" and "b" will be determined by specifying the conditions at stations C and D at the radii $R_{lo} = 3.025$ in. and $R_{li} = 0.99$ in. where, in accordance with Table I, the flow angles β_B must be 50.32°, and 18.08°, respectively. As shown in Fig. 3, it is assumed also that the axial lengths x of the inducer blades are 1.8 in. at C and 1.255 in. at D. These data are sufficient to determine the values of "a" and "b". However if Eqs. 11 and 12 are introduced into Eq. 10, one obtains fourth-order equations which cannot be solved with simple means. For this reason a method of successive approximations is used by assuming values for the angles γ_T and γ_H of Fig. 5 at R_{lo} and R_{li} and calculating the corresponding angles β_B by means of Eq. 10. Let, in accordance with Fig. 5,

$$x_T = 1.8 = \ell$$

$$x_H = 1.255 = \zeta \ell = (0.697)\ell$$

Then, from Eq. 12, with $c = b/a$,

$$\tan^2 \gamma_T = \frac{c^2}{(a/\ell)^2 - 1}$$

$$\tan^2 \gamma_H = \frac{\zeta^2 c^2}{(a/\ell)^2 - \zeta^2}$$

giving

$$\left(\frac{a}{\ell}\right)^2 = \frac{\zeta^2(\tan^2 \gamma_T - \tan^2 \gamma_H)}{\zeta^2 \tan^2 \gamma_T - \tan^2 \gamma_H} \tag{13}$$

$$c^2 = \left(\frac{b/\ell}{a/\ell}\right)^2 = \frac{(1 - \zeta^2) \tan^2 \gamma_T \tan^2 \gamma_H}{\zeta^2 \tan^2 \gamma_T - \tan^2 \gamma_H} \tag{14}$$

Successive approximations of γ_T and γ_H established the following final values:

$$\gamma_T = 49.964^\circ; \tan \gamma_T = 1.1902$$

$$\gamma_H = 17.817^\circ; \tan \gamma_H = 0.3214$$

For these angles, from Eqs. 13 and 14,

$$\frac{a}{\ell} = 1.04442; \quad a = 1.8799$$

$$\frac{b}{\ell} = 0.37460; \quad b = 0.6743$$

and, by Eq. 11

$$\frac{y}{\ell} = 0.37460 - 0.35867 \sqrt{1.09081 - (x/\ell)^2} \tag{15}$$

For $x = \ell$ at $R_{1o} = 3.025$,

$$y = 0.47973$$

and for $x = (0.697)\ell$ at $R = 0.99$,

$$y = 0.1721$$

With these values, from Eq. 10, at $R_{1o} = 3.025$,

$$\tan \beta_{Bo} = \frac{1.1902}{\sqrt{1 - (0.47973/3.025)^2}} = 1.20545$$

and, at $R_{1i} = 0.99$,

$$\tan \beta_{Bi} = \frac{0.3214}{\sqrt{1 - (0.1721/0.99)^2}} = 0.32637$$

Table I shows that these angles coincide very closely with the required blade angles at these radii.

All blade angles β_B of Table I at the different radii R_1 can be obtained with the blade surface that is given by Eq. 15, for a particular change of the distance x of Figs. 3 and 5 with the radius R_1. This

relationship between x and R_1 must be determined with an iterative method. For chosen values of x there can be determined y and dy/dx from Eqs. 15 and 12. These values introduced into Eq. 10, for the radius R_1 under consideration, give the value of β_B. If the blade angle thus determined differs from the required blade angle of Table I, the distance x must be varied until the correct angle is obtained. Drawing 2204 gives the values of $z = 1.8 - x$ vs. R_1 that were obtained in this manner for the blade surface of Eq. 15 whose coordinates are listed also in Dwg. 2204.

With this design the inducer can be fabricated from a forging by first machining the tip controur of the blades and the surface of revolution of the leading edges that is given by z vs. R. Then the blade passages can be produced by an end-mill that is moved in x and y directions, and along the radius, to produce the hub contour, However, with the described design the axis of the end-mill need not be tilted to produce the correct inlet blade angles.

3. Diffusor

The diffusor is arranged in a cylindrical annulus downstream of the impeller discharge, having the mean radius $R_2 = 5.5$ in., and a radial height $b_2 = 0.61$ inches. Ahead of the diffusor at station (2) the flow properties are obtained with the relations of Table A I. From Eq. A I(7), and the data established earlier,

$$\frac{T_2}{T_0} = 1.08402$$

From Eq. A I (8)

$$\frac{T_2'}{T_0} = 1.07013$$

From Eq. A I (6)

$$\frac{T_{t2}}{T_0} = 1.17411$$

From Eq. A I (20)

$$\frac{p_2}{p_0} = 1.2677$$

and from Eq. A I (19)

$$\frac{p_{t2}}{p_0} = 1.6764$$

The Mach number M_{V2} of the velocity V_2 ahead of the diffusor is from Eq. A II(6)

$$M_{V2} = 0.6446$$

for the chosen flow angle

$$\alpha_2 = 65^\circ$$

A preliminary analysis showed that a minimum of two diffusor blade rows is necessary to produce an acceptable diffusor efficiency. These rows are designed in the same manner as bladings of axial-flow compressors by using the method of Ref. 3. In the following, station (3) is after the first diffusor blade row and station (4) is located after the second diffusor row, as shown in Fig. 1.

Neglecting the change of the through-flow velocity because of the density increase from station (2) to station (3) the diffusion factor D of the first diffusor blade row is

$$D = 1 - \frac{\cos \alpha_2}{\cos \alpha_3} + \frac{(\tan \alpha_2 - \tan \alpha_3)}{2\sigma} \cos \alpha_2 \qquad (16)$$

where α_3 is the average flow angle at station (3) and σ the cascade solidity defined by

$$\sigma = \frac{\text{blade chord}}{\text{blade spacing}} = \frac{c}{s}$$

For different deflections $\Delta\alpha = \alpha_2 - \alpha_3$ and σ it is possible therefore to evaluate D from Eq. 16. The losses increase with increasing values of D. For the first diffusor blade row these losses can be expressed by the total pressure loss coefficient Y_t defined by

$$Y_t = \frac{\Delta P}{P_{t2} - p_2} = \frac{P_{t2} - P_{t3}}{P_{t2} - p_2} \tag{17}$$

where ΔP is the loss in total pressure in the blade row, and P_{t2}, p_2, the total and static pressure, respectively, ahead of the cascade. Reference 4 shows that Y of a stator blade row with a discharge angle α_3, diffusion factor D, and solidity σ can be calculated from

$$Y = \frac{2\sigma}{\cos \alpha_3}\left[0.0004 + 0.0639(D + 0.1)^{2.91} + 0.057D^{2.02}\ (1 - \lambda)^{3.77}\right] \tag{18}$$

The factor λ is defined by

$$\lambda = \frac{R - R_H}{R_T - R_H} \tag{19}$$

where R is the radius at which Y is to be determined, and R_T, R_H are the tip and hub radii, respectively, of the blading. Since $1 - \lambda = 1$ at R_H, and $1 - \lambda = 0$ at R_T, the loss coefficient Y of Eq. 18 is higher at the hub than at the tip, if the other quantities in Eq. 18 do not vary radically along R. Equation 18 may give a realistic description of the loss variation in radial direction if the blade heights are large with respect to their chords, as for instance in axial compressors for jet engines. In such compressors the stator blades are attached at the tip and they usually have a clearance at the hub to prevent rubbing with the rotor assembly. The NASA calculating procedure of Refs. 3 or 4 does not separate the overall blade loss into profile losses, secondary or end losses, and tip clearance

losses. End and tip clearance losses depend on the ratio of blade height and chord and on the ratio of blade gap to blade height, respectively, and it is evident from Eq. 18 that these quantities do not influence the overall loss coefficient of the NASA design procedure. In the cascades to be determined the blade gap is zero but the ratio of blade height and chord, or b_2/c, is quite small compared with the values in jet engine compressors, and the end losses will be very much larger than those in stator cascades of such machines. It is assumed therefore that Eq. 18 for the mid-span, or for $\lambda = 0.5$, establishes the profile loss coefficients Y_p only, or

$$Y_p = \frac{2\sigma}{\cos \alpha_3}\left[0.004 + 0.0639(D + 0.1)^{2.91} + 0.0042\, D^{2.02}\right] \tag{20}$$

To this profile loss coefficient will be added the so-called secondary loss coefficient Y_S to give the total loss coefficient Y_t, such that

$$Y_t = Y_p + Y_S = \frac{P_{t2} - P_{t3}}{P_{t2} - p_2} \tag{21}$$

Eq. 13(76) of Ref. 5, p. 380, gives the so-called induced drag coefficient C_{Di} of axial-flow cascades where the first part is the drag coefficient C_{DS} due to secondary flow effects, whereas the second part is due to tip clearance losses. This part is taken to be zero because no radial blade gaps δ exist in the present diffusor configuration. Hence

$$C_{DS} = 0.04\, C_L^2\, \sigma \frac{s}{h} \tag{22}$$

where the blade height h equals b_2. The lift coefficient C_L is equal to (see Eq. 13(14), Ref. 5, p. 337)

$$C_L = \frac{2}{\sigma}(\tan \alpha_2 - \tan \alpha_3) \cos \alpha_\infty \tag{23}$$

The angle α_∞ is obtained from

$$\tan \alpha_\infty = \frac{\tan \alpha_2 + \tan \alpha_3}{2} \tag{24}$$

Equation 13(11) of Ref. 5 relates the drag coefficient to the total pressure loss coefficient ζ which, in the present application, would be defined by

$$\zeta = \frac{\Delta P}{P_{t3} - p_3}$$

It must be noted that ζ relates the drop in total pressure to the discharge conditions of a cascade. Then, since

$$Y_s \equiv \frac{\Delta P}{P_{t2} - p_2}$$

there is with Eqs. 22, 23, and 24

$$Y_S' = 0.16 \frac{s}{h} \cos^2 \alpha_2 \left[\tan \alpha_2 - \tan \alpha_3 \right]^2 \sqrt{1 + \tfrac{1}{4}[\tan \alpha_2 + \tan \alpha_3]^2} \tag{25}$$

since $1/\cos \alpha_\infty = \sqrt{1 + \tan^2 \alpha_\infty}$ The secondary loss coefficient of Eq. 25 is denoted by Y_S' to distinguish it from a secondary loss coefficient Y_s'' that has been proposed in Ref. 6. In Ref. 6 it is stated that the ratio $Y_s''/(Y_p + Y_s'') = Y_s''/Y_t''$ is a unique function of $\Delta\alpha(c/h)$, where $\Delta\alpha$ is the flow deflection in radians, and c/h the ratio of blade chord and blade height. This relationship is shown in Fig. 6. For known values of Y_p and Y_s''/Y_t'' there are

$$Y_s'' = Y_p \frac{(Y_s''/Y_t'')}{1 - (Y_s''/Y_t'')} \tag{26}$$

and

$$Y_t'' = \frac{Y_p}{1 - (Y_s''/Y_t'')} \tag{27}$$

The losses in the diffusor blade rows will be determined with Eq. 25 as well as with Eq. 26 for purposes of comparison. These two methods are

based on different models and concepts. It can be noted that for given flow angles the secondary losses of Eq. 25 are primarily a function of the ratio of blade spacing and blade height, whereas with the method of Ref. 6, or Eq. 26, they are depending mainly on the ratio of blade chord and blade height. Evidently, if Eq. 25 is used, one obtains different cascade arrangements for a specified total loss than if Eq. 26 is applied, and this situation is indicative of the present state of ignorance about secondary flows in general. A survey of the available analytical methods for the determination of secondary flow effects is given in Ref. 7.

As shown in Dwgs. 2202 and 2210-1, the diffusor blades will have a circular platform with a threaded cylindrical extension to attach them to the blade holders, which are shown as item 1 in Dwg. 2209. This design has been adopted to be able to change the blade stagger angle in the diffusor cascades if, because of the irregular flow conditions at the impeller discharge, the average flow angle α_2 differs from the design value of 65°. This diffusor blade attachment requires however, that each blade row does not have more than 38 blades. For Z = 38, the blade spacing s at the mean radius R_2 = 5.5 in. becomes

$$s = \frac{2\,\pi R_2}{Z} = 0.9094 \text{ in.}$$

and

$$\frac{s}{h} = \frac{s}{b_2} = \frac{0.9094}{0.61} = 1.4908 \tag{28}$$

For particular values of $\sigma = c/s$,

$$\frac{c}{h} = \sigma \frac{s}{h} = \sigma(1.4908) \tag{29}$$

For $\Delta\alpha$ in degrees, the variable $\Delta\alpha(c/h)$ of Fig. 6 is,

$$\Delta\alpha(c/h) = \Delta\alpha^{\circ}\frac{\pi}{180}\sigma(1.4908) = \frac{2.602}{100}\sigma\,\Delta\alpha^{\circ} \qquad (30)$$

Table II shows the diffusion factor D, the profile losses Y_p, and the overall loss coefficients Y_t' and Y_t'' as functions of solidity for flow deflections $\Delta\alpha$ = 10, 12 and 14° in the first blade row of the diffusor. The quantities Y_t' and Y_t'' are also plotted in Fig. 7.

Although it is desirable to have the highest possible flow deflection $\Delta\alpha$ in the first diffusor blade row, the general level of the losses as evidenced by Fig. 7, and the non-uniform and non-steady flow conditions at the impeller exit, make it advisable to limit $\Delta\alpha$ to 12°. For this deflection the data of Fig. 7 show that the solidity should be about unity to obtain loss coefficients Y_t that are smaller than about 0.12. Experience with diffusors of centrifugal compressors seems to indicate however that, in spite of the results of Fig. 7, more favorable conditions may be obtained for higher solidities, primarily because of the afore-mentioned irregular flow properties at the rotor discharge. At higher solidities the diffusor blades form channels with better guidance of the flow than if the solidity were low. These channels will act as flow straighteners which can equalize the flow irregularities with smaller flow separations than those which might occur in low-solidity cascades where the diffusion factors and the blade loadings are higher. It is likely then that the performance of the second diffusor blade row, and possibly that of the whole diffusor, is better than if the solidity of the first row is small. In general, the writer is of the opinion that the secondary losses do not increase as radically with the flow deflection $\Delta\alpha$ and the solidity σ as obtained by Ref. 6.

For these reasons it was decided to build two sets of diffusors. In one, denoted by A, the solidity of the first row was chosen as 1.6. In

another, which is denoted by B, the first row has a solidity of 0.95. The deflections $\Delta\alpha$ have been chosen as 12° for both first rows of A and B. However, since the effects due to the non-steady impeller exit flows cannot be evaluated, the performance of these cascades will be determined with the loss coefficients of Fig. 7. The design criteria of the two first diffusor blade rows are listed in Table III, which also gives the values of the chosen maximum blade thickness.

The flow angle α_3 ahead of the second diffusor blade row is then $65 - 12 = 53^\circ$. Theoretically, the highest pressure recovery would be obtained in the diffusor if this angle could be reduced to zero in the second row. It can be seen, however, that the blade loadings and the losses would become excessive for such deflections. Preliminary investigations showed that the deflections $\Delta\alpha = \alpha_3 - \alpha_4$ cannot exceed about 26° to 38° at reasonable loss coefficients, so that after the diffusor the flow angles α_4 will be between 27° and 15°. Even though the kinetic energy of these whirl components of the discharge flow at station (4) cannot be converted into pressure rise, the overall efficiency of the compressor will be better than the one obtainable if it were tried to reduce the flow angle α_4 to zero.

Because it is intended to orient the blades of the second row in such a manner that they form a so-called tandem foil arrangement with the blades of the first row, the second diffusor row must also have 38 blades. Thus, its geometrical properties are likewise given by Eqs. 28, 29, and 30. The profile losses Y_p of the second row of diffusor blades can be determined by Eq. 20 if α_3 is replaced by α_4. The diffusion factors of these rows are obtained by Eq. 16, replacing α_2 by α_3 and α_3 by α_4. The overall loss coefficient Y_t is, similarly to Eq. 17,

$$Y_t = \frac{P_{t3} - P_{t4}}{P_{t3} - p_3} \tag{31}$$

The secondary flow loss coefficients Y_s will be determined by Eq. 26, replacing α_2 by α_3, and α_3 by $\alpha_4 = \alpha_3 - \Delta\alpha$, and also with the method proposed in Ref. 6 by using the curve of Fig. 6. The results for different solidities and deflections $\Delta\alpha$ are listed in Table IV and plotted in Fig. 8.

Figure 8 shows that the overall losses increase very radically with solidity if the secondary flow losses are calculated in accordance with Ref. 6. If Eq. 25 is used however to determine Y_s, the overall losses Y_t' are almost constant for different values of σ, in fact they have a minimum for solidities of about unity. The data of Fig. 8 for Y_t''; that is, using Y_s'' of Ref. 6, suggest that with solidities much smaller than unity a diffusor with very low losses could be designed. However, not only would the blade chords be excessively small in such cascades, but the writer also believes that because of the high blade loading the flow would be too severely separated to make possible the small losses that Ref. 6 predicts. If in contrast to this opinion, the method of Ref. 6 should prove to give the correct values of Y_s'', a cascade with solidity of 1.6, which was chosen for blade row A1, would have excessive losses. It was decided, therefore, to design two second row diffusor cascades also. Both rows will have a deflection $\Delta\alpha = \alpha_3 - \alpha_4 = 32^\circ$ to keep the losses within acceptable limits, independent of whether the one or the other prediction method gives the correct loss coefficients. The so-called row A2 will be designed for $\sigma = 1.4$, and for row B2 the solidity is chosen as unity. If Eq. 25 predicts the secondary losses properly, both cascades should have about equal losses. On the other hand, if Ref. 6 gives realistic secondary losses, row A2 would be greatly inferior to row B2. Although it will be

possible to arrange row A2 or B2 after either of the two first rows A1 or B1, for calculating purposes the so-called diffusor A is supposed to consist of rows A1 and A2 and diffusor B of rows B1 and B2. The design parameters of the second diffusor blade rows are listed in Table V.

The blade profiles and their orientation in the cascade are determined with the method of Ref. 3. The necessary calculating steps are described in paragraph 8 of Ref. 8. The basic thickness distribution of the profiles is shown in Fig. 13 of Ref. 8. Except for slight modifications near the leading edge this distribution corresponds to that of a British C-4 profile. The camber line of the profiles is a circular arc with camber angle φ. For known values of φ and thickness ratios t/c the profile coordinates are obtained with the relations of Fig. 14 of Ref. 8.

Figure 9 shows the attitude of a blade in a diffusor cascade and explains the symbols that are used for the profile calculations in Table VI. By using the method of Ref. 3 one often obtains excessively large incidence angles. As seen from Table VI this situation occurs for row A1 where $i = +4.312^{\circ}$, for row B1 where $i = -2.95$, and for row B2 where $i = -7.002^{\circ}$. For these rows, incidence angles i^* of $+2^{\circ}$, -1°, and -2°, respectively, are chosen, and the corresponding camber angles φ^* and the stagger angles γ^* are calculated with the values of $d\delta/di$ of Fig. 177 of Ref. 3. Table VI also lists the drawings of Appendix B where the different blade profiles and their coordinates are shown. From these drawings the angles $\Delta\gamma$ of Fig. 9 were determined graphically and were used to establish the stagger angles γ' that are necessary for the installation of the blades in the blade holders of Dwg. 2209.

II. DESIGN POINT PERFORMANCE

1. Rotor

For a chosen total temperature $T_0 = 520^\circ R$ at the compressor inlet, and for $U_2/a_o = 0.7156$, $M_{W1} = 0.4842$ (see Eq. 1), the static temperature T_1, and the static pressure p_1 at the inlet eye of the impeller are obtained from Eqs. A I (5) and A I (18), or

$$\frac{T_1}{T_0} = 0.9848$$

$$\frac{p_1}{P_0} = 0.9478$$

The absolute value of the total pressure P_0 at the impeller inlet is as yet unknown because in the test rig the compressor operates as an exhauster. Drawing 2223 shows that the air entering the compressor is expanded in a throttle valve to a pressure below atmospheric pressure. From a plenum chamber (Dwg. 2164-1), where the kinetic energy of the flow through the throttle valve openings is destroyed by a system of adjustable screens, the air enters the suction pipe through a profiled orifice. This suction pipe with an inner diameter of 18 inches has a length of about 18 feet, so that non-uniformities of the flow which have not been removed in the plenum chamber will be equalized ahead of the flow measuring nozzle of Dwg. 2216. This nozzle has a diameter of 5.38 inches, hence its flow area is only about 9 percent of the cross sectional area of the suction pipe. The large acceleration of the flow in the nozzle will produce a uniform flow at its discharge. Drawing 2222 shows the location of the flow nozzle with respect to the compressor inlet. Drawing 2202 shows that provisions have been made in the nozzle casing (Dwg. 2140) to carry out flow surveys ahead of the 7 in. diameter duct ahead of the impeller by

means of Pitot probes.

Drawing 2222 shows that a honeycomb flow straightener is arranged after the diffusor blade rows to remove the whirl components of the flow at this station, and that the air is then discharged into the atmosphere. This arrangement has been adopted for simplicity of the design, since it does not require a scroll or a complicated collector after the compressor from where the flow is discharged into the atmosphere through a throttling valve. Moreover, with this arrangement the driving power of the compressor is lower than with a test set-up where the inlet flow of the compressor is at atmospheric pressure. However, the total inlet pressure P_0, which is equal to the total pressure in the 7 in. diameter inlet duct, depends on the pressure ratio that is produced by the compressor. If, as shown in Fig. 1, the conditions at the exit of the discharge duct, arranged after the annular flow straightener, are denoted by the subscript (6), the static pressure p_6 must be equal to the ambient atmospheric pressure P_{atm}, or

$$P_0 = P_{atm} \frac{1}{(p_6/P_0)} \tag{32}$$

Hence it is necessary to determine the pressure ratio p_6/P_0 to obtain P_0. Evidently, p_6/P_0 depends on the pressure drops in rotor, diffusor and flow straightener which will be evaluated in Section II.3.

The weight flow rate $\dot{w}$ through the compressor can be determined from Eq. 2. For the assumed blockage factor $k_{Bl} = 0.98$, and since $R_2 = 5.5$ inches,

$$\frac{\dot{w}}{P_0}\sqrt{\frac{R_G\, T_0}{g}} = \frac{\pi R_2^2\, k_{Bl}}{11.7944} = 7.8963\ (\text{in.}^2) \tag{33}$$

With $R_G = 53.35$ (ft-lb)/(lbm, $^\circ$R), $g = 32.174$ ft/s^2, $T_0 = 520^\circ$ R,

$$\dot{w} = 0.2689 \quad P_0 \quad \text{(lbm/s)} \tag{34}$$

In Eqs. 33 and 34, P_0 is the absolute total inlet pressure in psia.

In the rotor the total temperature of the fluid is increased from T_0 to T_{t2}. For an adiabatic process the energy increase due to this temperature rise is equal to the energy per unit flow rate that the rotor must transmit to the fluid. Hence, the power HP required to drive the rotor is, exclusive of bearing and other mechanical losses,

$$HP = \dot{w}\, c_p\, (T_{t2} - T_0)\, \frac{1}{550} \quad \text{(HP)} \tag{34a}$$

With

$$c_p = R_G \frac{\gamma}{\gamma - 1} \qquad \text{(ft-lb)/(lbm, }^{\circ}\text{R)}$$

and Eq. 33

$$HP = \frac{7.8963}{550} \frac{\gamma}{\gamma - 1} P_0 \sqrt{g R_G T_0} \left(\frac{T_{t2}}{T_0} - 1\right)$$

For $\gamma = 1.4$, and since $T_{t2}/T_0 = 1.17411$,

$$\frac{HP}{P_0 \sqrt{g R_G T_0}} = \frac{8.7489}{(10^3)} \tag{35}$$

For $T_0 = 520^{\circ}$ R, $\gamma = 1.4$, $R_G = 53.35$, there is also,

$$HP = 8.2656\, P_0 \qquad \text{(HP)} \tag{36}$$

In Eqs. 35 and 36 the pressure P_0 must be in psia.

The following data at the rotor discharge were obtained earlier:

$$\frac{T_2}{T_0} = 1.08402$$

$$\frac{p_2}{P_0} = 1.2677$$

$$\frac{P_{t2}}{P_0} = 1.6764$$

$$M_{V2} = \frac{V_2}{a_2} = 0.6446$$

With $T_o = 520^\circ R$, or $a_o = 1117.85$ ft/s, the velocity of sound a_2 at the rotor discharge is

$$a_2 = a_o \sqrt{T_2/T_o} = 1163.86 \quad \text{ft/s}$$

and

$$V_2 = 750.23 \quad \text{ft/s}$$

This average velocity at the rotor exit has an average flow angle $\alpha_2 = 65^\circ$.

2. Diffusor

The total pressure P_{t3} after the first diffusor blade row is obtained from Eq. 21, or

$$\frac{P_{t3}}{P_o} = (1 - Y_t) \frac{P_{t2}}{P_o} + Y_t \frac{P_2}{P_o} \tag{37}$$

where the pressure loss coefficients Y_t of the rows A1 and B1 are listed in Table III. At station (3), after the first diffusor row, the velocity V_3 has an average flow angle $\alpha_3 = 53^\circ$. Although the annulur flow areas are equal at the station (2) and (3), the boundary layer growth in the blade row will make the effective flow area smaller at (3) than at (2). At station (2) a restriction factor $k_{B2} = 0.954$ has been assumed earlier to establish the diffusor annulus, or

$$A_2 = k_{B2} A_{geom}$$

where A_{geom} is the cross-sectional area of the annulus. At station (3) it is assumed that the effective flow area A_3 is

$$A_3 = k_{B3} A_{geom}$$

and $k_{B3} = 0.92$ by assumption.

The flow conditions at station (3) must be determined analytically for the flow area A_3, the flow angle α_3, and the total pressure P_{t3}, by using the energy equation, the equation of motion, and the equation of continuity. The energy equation for an assumed adiabatic process of a steady flow gives

$$T_{t3} = T_{t2}$$

In fact, the same total temperature will occur at stations (4), (5) and (6), if the flow processes are adiabatic.

Since the conditions after the second diffusor row at station (4) must be established with the same approach as those at station (3), a calculating procedure will be developed with the symbols of Fig. 10. Figure 10a shows a diffusor cascade in an annulus. The effective flow areas are $A_e = k_{Be} A_{geom}$ and $A_d = k_{Bd} A_{geom}$ at entrance and discharge, respectively. The average axial components V_{ea} and V_{da} that are uniform over A_e and A_d, respectively are

$$V_{ea} = V_e \cos \alpha_e$$

$$V_{da} = V_d \cos \alpha_d$$

A section through the blading of the diffusor row is shown in Fig. 10b, and Fig. 10c depicts the thermodynamic process between entrance and discharge in an entropy diagram. From the equation of motion

$$T_{te} = T_{td} = T_e + \frac{V_e^2}{2 g c_p} = T_d + \frac{V_d^2}{2 g c_p} \tag{38}$$

From the equation of continuity, with $\rho = p/(g R_G T)$

$$A_d V_d \cos \alpha_d \frac{p_d}{R_G T_d} = A_e V_e \cos \alpha_e \frac{p_e}{R_G T_e} \tag{39}$$

With $A_e/A_d = k_{Be}/k_{Bd}$, Eq. 39 can be rewritten as

$$\frac{V_d}{\sqrt{g\,\gamma\,R_G\,T_d}} = \frac{k_{Be}}{k_{Bd}}\,\frac{\cos\alpha_e}{\cos\alpha_d}\,\frac{(p_e/P_0)}{\sqrt{(T_e/T_0)}}\,\frac{V_e}{\sqrt{g\,\gamma\,R_G\,T_e}}\,\frac{\sqrt{(T_d/T_0)}}{(p_d/P_0)} \tag{40}$$

With the Mach numbers

$$M_d = \frac{V_d}{\sqrt{g\,\gamma\,R_G\,T_d}} \tag{41}$$

$$M_e = \frac{V_e}{\sqrt{g\,\gamma\,R_G\,T_e}} \tag{42}$$

and

$$K = \frac{k_{Be}}{k_{Bd}}\,\frac{\cos\alpha_e}{\cos\alpha_d}\,\frac{p_e/P_0}{\sqrt{(T_e/T_0)}}\,M_e \tag{43}$$

which is a constant for known entrance conditions and area ratios, there is from Eq. 40,

$$M_d = K\,\frac{\sqrt{(T_d/T_0)}}{(p_d/P_0)} \tag{44}$$

From Fig. 10c at the entropy s_d, from Eq. 38,

$$\frac{T_{td}}{T_d} = \frac{T_{te}}{T_d} = 1 + \frac{\gamma - 1}{2}\,M_d^2$$

and

$$\frac{P_{td}}{p_d} = \left(1 + \frac{\gamma - 1}{2}\,M_d^2\right)^{\gamma/(\gamma - 1)}$$

From these relations

$$\frac{T_d}{T_0} = \frac{T_{te}/T_0}{1 + \frac{\gamma - 1}{2}\,M_d^2} \tag{45}$$

and

$$\frac{p_d}{P_0} = \frac{P_{td}/P_0}{(1 + \frac{\gamma - 1}{2} M_d^2)^{\gamma/(\gamma - 1)}} \tag{46}$$

where, similar to Eq. 37, with the pressure loss coefficient Y_t of the blade row,

$$\frac{P_{td}}{P_0} = (1 - Y_t) \frac{P_{te}}{P_0} + Y_t \frac{p_e}{P_0} \tag{47}$$

Because of their exponential expressions it is not possible to substitute Eqs. 45 and 46 into Eq. 44 to obtain a closed solution for M_d. It is necessary to choose values of M_d, say M_d^*, to calculate T_d/T_0 and p_d/P_0 from Eqs. 45 and 46. These quantities are then used in Eq. 44 to determine the Mach number M_d. If M_d differs from M_d^*, other values of M_d^* must be chosen until agreement is reached. With the final value of $M_d = M_d^*$ it is possible to calculate the ratios T_d/T_0 and p_d/P_0 with Eqs. 45 and 46, and the velocity V_d is obtained from Eq. 41, or

$$V_d = M_d \, a_0 \sqrt{(T_d/T_0)} \tag{48}$$

This iterative calculating process has been carried out for the rows A1 and B1, for both overall loss coefficients Y_t' and Y_t'' that are listed in Table III. In Table VII where the final data are presented, the columns designated by A1' and A1" give the performances of blade row A1 for the overall loss coefficients Y_t' and Y_t'', respectively, of Table III. A similar designation is used for the performance of blade row B1, for the losses Y_t' and Y_t''. With the flow conditions thus determined at (3), the flow properties at station (4), after the second diffusor blade row, can be calculated with the same method. These calculations are also carried out with both loss coefficients Y_t' and Y_t'' of Table V. The

quantity K of Eq. 43 is determined for $k_{Be} = k_{B3} = 0.92$ and $k_{Bd} = k_{B4} = 0.88$. The flow angles α_3 and α_4 are 53° and 21°, respectively, in accordance with Table VI.

The calculations of the flow conditions after the diffusor blade rows are quite lengthy and have to be carried out with great precision. On the other hand they do not warrant the use of a high-speed digital computer for which a rather elaborate program would have to be set up to perform the necessary iterations automatically. For the debugging of such a program several tries would probably be necessary until results could be obtained. However, for evaluations of the type discussed above, in fact for most calculations of this report, modern electronic and programmable display calculators are admirably suited. The Monroe Model 1655 with Card Reader CR-1 used at the Turbo-Propulsion Laboratory has proved to be an extremely valuable tool, and the writer believes that such calculators will completely revolutionize analytical engineering approaches. Libraries of programs for a variety of engineering calculations are already available, and programs for particular tasks can be established with great ease. Since most calculators, specifically the Monroe Model 1655, have provisions to verify and debug programs with a step by step procedure, program errors can be detected and corrected without delay by the programmer himself, without having to go to the trouble of submitting several modified programs as is necessary in most central computer facilities. At present, many high-speed computers are used for programs that do not really need the small access time and the large storage capacity of modern systems, and the use of programmable calculators will make available more time for those calculations that can be solved only by high-speed machines. Conversely the engineer or student is relieved of many routine calculations, without having to worry about inaccuracies and errors, and he obtains

results when needed during the progress of his work. Thus more time is available for creative efforts where the formulation of a problem is more important than the manipulation of numbers that is necessary for its solution.

To show the possibilities that exist in solving engineering problems with the Monroe 1655 calculator, some of the programs used for the calculations for this report are enclosed in Appendix D. Each program consists of a description, an operating instruction, and a listing of the program steps with their codes. The serial numbers of these programs refer to the private program library of the writer. The data of Table VII for the conditions after the two diffusor blade rows have been obtained with Program No. 109.

Appendix D also contains a more elaborate calculating program that requires the use of the Monroe calculator Model 1880 which is an advanced and more expensive machine with larger memory capacity.

The pressure ratios P_{t4}/P_0 of Table VII will be used to determine the so-called total-to-total compressor efficiency η_{t4}. For an isentropic compression from the total inlet pressure P_0 and the total inlet temperature T_0 to the total discharge pressure P_{t4}, the rise in total temperature ΔT_{tis} equals

$$\Delta T_{tis} = T_0 \left[(P_{t4}/P_0)^{(\gamma - 1)/\gamma} - 1 \right]$$

Since this temperature rise is proportional to the theoretical energy input per unit mass flow rate, and because for the actual process the energy per unit mass flow rate necessary to drive the rotor is proportional to $T_{t4} - T_0$, which equals $T_{t2} - T_0$, the compressor efficiency η_{t4} is

$$\eta_{t4} = \frac{(P_{t4}/P_0)^{(\gamma - 1)/\gamma} - 1}{(T_{t2}/T_0) - 1} \qquad (49)$$

The compressor efficiencies η_{t4} are given also in Table VII. If the secondary flow losses are calculated in accordance with Eq. 25, an efficiency of 81.5% is obtained for the compressor with diffusor A, whereas if the losses for this configuration are determined with the method of Ref. 6 the efficiency is 78.9% only. The calculated compressor efficiencies with diffusor B are 82.3% and 82.8%, respectively, with the two methods.

It would appear, therefore, that higher efficiencies can be reached with diffusor B than with diffusor A. However, for the reason mentioned earlier, it may be that more favorable conditions can be obtained with the high-solidity diffusor A. Moreover, the performance calculations cannot take account of the radial velocity gradients or the non-steady flow at the rotor discharge, and it is because of these uncertainties that tests must be carried out to verify which diffusor configuration gives the best performance.

3. Flow Straightener and Discharge Duct

The flow conditions in the flow straightener and the discharge duct of Fig. 11a can be determined with approximate methods since the Mach numbers of the flow are small. At station (4), at the diffusor discharge, the velocity V_4 has the angle $\alpha_4 = 21^\circ$ with the axial direction. The peripheral component $V_4 \sin \alpha_4$ will be destroyed as the flow enters the axial flow straightener. This element consists of a honeycomb with hexagonal channels that have a spacing of 0.125 inch, a wall thickness of about 0.002 to 0.003 inch, and an axial length of 1.38 inch. As shown in Dwg. 2212, twelve honeycomb segments are arranged in an annulus between spacers that are 0.25 inches thick. On assuming that the flow leaving the diffusor does not diverge in radial direction, the velocity V_S in the channels of the flow straightener is with the symbols of Fig. 11a, neglecting density

changes,

$$V_4\, 2\, \pi R_2\, b_2 = V_S \left[2\, \pi R_2\, b_2 - (12)(0.25)\, b_2 \right] \left(\frac{0.123}{0.125}\right)$$

where the fraction 0.123/0.125 is the blockage due to the wall thickness of the honeycomb straightener. With $V_{4a} = V_4 \cos 21^\circ = 0.933\, V_4$, $R_2 = 5.5$,

$$V_S = V_4 \cos 21^\circ \frac{(0.125/0.123)}{1 - \frac{(12)(0.25)}{2\,\pi\,(5.5)}} = 1.039\, V_4 \qquad (50)$$

As shown in Fig. 11a, it is supposed that after the honeycomb the flow will diverge radially to a height $b_5 = 0.65$ in. at station (5). Hence the velocity V_5 is assumed to be

$$V_5 = \frac{b_2}{b_5}\, V_{4a} = \frac{0.61}{0.65}\,(0.933)\, V_4 = 0.8764\, V_4 \qquad (51)$$

Because the discharge duct between stations (5) and (6) is not a properly designed diffusor it will be assumed that the flow will follow the dash-dotted boundaries of Fig. 11a. Neglecting the change in density from (5) to (6), the velocity V_6 is then

$$V_6 = V_5 \frac{2\,\pi\,(5.5)(0.65)}{2\,\pi\,(6.2)(0.70)} = 0.824\, V_5 = 0.722\, V_4$$

Figure 11b shows the flow process between stations (4) and (6) in an entropy diagram. If the flow is adiabatic the total temperature T_t is everywhere constant, equal to $T_{t4} = T_{t2}$. From the diffusor discharge at (4) to the entrance of the honeycomb the velocity V_4 is reduced to V_{4a} at the constant static pressure p_4. This process is associated with an increase in entropy from s_4 to s_4', reducing the total pressure from P_{t4} to P_{t4}'. The velocity is then increased from V_{4a} to V_S at station (4') just inside the entrance to the flow straightener. If this acceleration is isentropic the pressure p_4 is reduced to p_4'. With the symbols of Fig. 11b,

$$T_4^* = T_4 + \frac{V_4^2 - V_{4a}^2}{2\, g\, c_p}$$

Since $C_p = R_G\, \gamma/(\gamma - 1)$, and $V_{4a} = V_4 \cos \alpha_4$,

$$\frac{T_4^*}{T_0} = \frac{T_4}{T_0} + \frac{\gamma - 1}{2}\left(\frac{V_4 \sin \alpha_4}{a_0}\right)^2 \tag{53}$$

where $a_0 = 1117.85$ ft/s and $\alpha_4 = 21^\circ$. Further,

$$\frac{P_{t4}'}{P_0} = \frac{p_4}{P_0}\left(\frac{T_{t2}/T_0}{T_4^*/T_0}\right)^{\gamma/(\gamma - 1)} \tag{54}$$

The velocity increase from V_{4a} to V_S at the entropy s_4' reduces the static temperature from T_4^* to T_4', where

$$T_4' = T_{t2} - \frac{V_S^2}{2\, g\, c_p}$$

or, with Eq. 50,

$$\frac{T_4'}{T_0} = \frac{T_{t2}}{T_0} - \frac{\gamma - 1}{2}\left(\frac{1.039\, V_4}{a_0}\right)^2 \tag{55}$$

Also

$$\frac{p_4'}{P_{t4}'} = \left(\frac{T_4'}{T_{t2}}\right)^{\gamma/(\gamma - 1)}$$

and

$$\frac{p_4'}{P_0} = \frac{P_{t4}'}{P_0}\left(\frac{T_4'/T_0}{T_{t2}/T_0}\right)^{\gamma/(\gamma - 1)} \tag{56}$$

The loss in total pressure $\Delta P_S = P_{t4}' - P_{t4}''$ in the honeycomb will be determined with the frictional coefficient f of flows in pipes, or

$$\Delta P_S = \left(\frac{L}{d_h}\right) f \frac{\rho}{2} V_S^2 \qquad (57)$$

The hydraulic diameter d_h of the flow channels in the honeycomb straightener is 0.123 in., and L = 1.38 in. The factor f depends on the Reynolds number

$$R_e = \frac{V_S d_h}{\nu}$$

Table VII shows that the velocities V_4 do not differ greatly, hence R_e can be determined for an average value V_4 = 330 ft/s. Moreover the average ratio T_4/T_0 is about 1.157, and the pressure p_4 is nearly equal to the atmospheric pressure. For $T_4 = (1.157)(520) = 602^\circ$ R, and p_4 = 14.7 psia, there is $\nu = 1.97(10^{-4})$ ft/s^2. Hence, with Eq. 50,

$$R_e = \frac{(1.039)(330)(0.123/12)}{1.97(10^{-4})} = 1.78(10^4)$$

From Ref. 9 for smooth surfaces, f = 0.0265, and by Eq. 57

$$\Delta P_S = \frac{(1.38)}{(0.123)} (0.0265) \frac{\rho}{2} V_S^2 = 0.3 \frac{\rho}{2} V_S^2$$

At the low Mach numbers of the flow, there is approximately

$$\frac{\rho}{2} V_S^2 = P_{t4}' - p_4'$$

or

$$\frac{P_{t4}'}{P_0} = 0.7 \frac{P_{t4}'}{P_0} + 0.3 \frac{p_4'}{P_0} \qquad (58)$$

From Fig. 11b, and Eq. 56 the static pressure p_4'' is then obtained from

$$\frac{p_4''}{P_0} = \left(\frac{P_{t4}''/P_0}{P_{t4}'/P_0}\right)\left(\frac{p_4'}{P_0}\right) \qquad (59)$$

The reduction of the velocity from V_S to V_5 is supposed to occur at the static pressure p_4'', hence $p_5 = p_4''$, as indicated in Fig. 11b. The static temperature T_5 is with Eq. 51,

$$\frac{T_5}{T_0} = \frac{T_{t2}}{T_0} - \frac{\gamma - 1}{2}\left(\frac{0.8764\ V_4}{a_0}\right)^2 \tag{60}$$

and the pressure ratio P_{t5}/P_0 is

$$\frac{P_{t5}}{P_0} = \frac{p_4''}{P_0}\left(\frac{T_{t2}/T_0}{T_5/T_0}\right)^{\gamma/(\gamma - 1)} \tag{61}$$

The loss in the discharge duct between stations (5) and (6) is assumed to be

$$P_{t6} - P_{t5} = (0.4)(P_{t5} - p_5)$$

Thus, with $p_5 = p_4''$

$$\frac{P_{t6}}{P_0} = 0.6\ \frac{P_{t5}}{P_0} + 0.4\ \frac{p_4''}{P_0} \tag{62}$$

With Eq. 52

$$\frac{T_6}{T_0} = \frac{T_{t2}}{T_0} - \frac{\gamma - 1}{2}\left(\frac{0.722\ V_4}{a_0}\right)^2 \tag{63}$$

and

$$\frac{p_6}{P_0} = \frac{P_{t6}}{P_0}\left(\frac{T_6/T_0}{T_{t2}/T_0}\right)^{\gamma/(\gamma - 1)} \tag{64}$$

For the data at the diffusor discharge (station (4)) of Table VII the conditions of state in the flow straightener and the discharge duct have been calculated with the above relations. The results are summarized in Table VIII. As discussed earlier, the static pressure p_6 at the exit of the duct will equal the atmospheric pressure. If this ambient pressure

P_{atm} is taken as 14.7 psia, the total pressure P_0 at the compressor inlet is obtained from Eq. 32. The last line of Table VIII gives these pressures for diffusors A and B and the two different losses which were taken into account for their performance prediction.

4. Compressor Performance at Design Point

The weight flow rate $\dot{w}$ and the driving power of the compressor can be determined from Eqs. 34 and 36 for the values of P_0 from Table VIII. The pressures thus obtained are for a total inlet temperature $T_0 = 520^\circ$ R and a speed of rotation N = 16,666 rpm. Of interest is also the torque M that is necessary to turn the compressor, which equals

$$M = \frac{HP(550)}{\omega} = \frac{HP(550)}{\pi N/30} \qquad \text{(ft-lb)} \qquad (65)$$

With Eq. 34, and N = 16,666 rpm

$$M = 2.6045\ P_0 \qquad \text{(ft-lb)}$$

or

$$M = 31.2554\ P_0 \qquad \text{(in-lb)} \qquad (65)$$

where P_0 must be in psia. In Table IX the compressor performance data for the design point at N = 16,666 rpm and $T_0 = 520^\circ$ R are summarized. Also given are the pressure ratios P_{t4}/P_0 and p_6/P_0, and the efficiencies η_{t4} with the two diffusors A and B, for the two methods used for the determination of their secondary flow losses.

It is evident from Appendix A (Ref. 1), and the calculations of this report, that U_2/a_0, $\gamma = c_p/c_v$, and the flow angles are the prime variables that establish the performance of a particular compressor, in fact of all designs which are geometrically similar. Except for possible changes in the loss coefficients which will be discussed later, the pressure ratio P_{t4}/P_0 of these machines will be equal if U_2/a_0, γ, and the flow angles

are equal. This situation occurs because the density ratios of the fluid and the Mach numbers of the flow remain constant at particular stations in the compressors, which makes it possible to maintain the same flow angles with respect to the bladings. From Eq. A II(9) it is seen that the dimensionless mass flow rate $(\dot{m})^*$ defined by

$$(\dot{m})^* = \frac{(\dot{w}/g)\sqrt{g\, R_g\, T_0}}{\pi\, R_2^2\, P_0} \tag{66}$$

must be constant at these conditions. From Eq. 35 and Eq. A I(6) it is apparent that the dimensionless power $(HP)^*$, defined by

$$(HP)^* = \frac{(HP)(550)}{\pi\, R_2^2\, P_0 \sqrt{g\, R_G\, T_0}} \tag{67}$$

is invariant also for similar machines that operate at the same values U_2/a_0 and γ, and produce the same pressure ratio P_{t4}/P_0.

Since $\omega = U_2/R_2$, the moment of Eq. 65 becomes with Eq. 67, and

$a_0 = \sqrt{\gamma\, g\, T_G\, T_0}$,

$$M = \pi R_2^3\, P_0\, \frac{(HP)^*}{(U_2/a_0)\sqrt{\gamma}} \tag{68}$$

Hence, similar to Eqs. 66 and 67 the so-called dimensionless moment $(M)^*$ will be defined as

$$(M)^* = \frac{M}{\pi R_2^3\, P_0} \tag{69}$$

which is constant also for the conditions at which $(\dot{m})^*$ and $(HP)^*$ do not change.

Obviously the dimensionless quantities of Eqs. 66, 67, and 69 have equal magnitudes in any consistent system of units for geometrically

similar compressors that operate at the same values of U_2/a_0, γ, and P_{t4}/P_0, independent of their size and the magnitudes of P_0 and T_0. However, the losses in these machines do not depend only on the angles and the Mach numbers but also on the Reynolds numbers of the flow. That the Mach numbers remain constant at fixed values U_2/a_0, γ, and flow angles, independent of the magnitudes of T_0 and P_0, is shown by Eqs. A II(4) and A II(6). The flow angles, and therefore the blade incidence angles, remain equal at particular stations because the ratios T/T_0 and P/P_0, which establish the density ratios ρ/ρ_0, are also not affected by T_0 and P_0. The Reynolds number R_e at a particular station, where the velocity V exists at p and T, can be expressed by

$$R_e = \frac{V\, R_2}{\mu_v}\, \rho$$

since, for geometrically similar compressors, the dimensions of all flow channels are constant fractions of the mean compressor radius R_2. If M_V is the Mach number of V, or $V = M_V \sqrt{\gamma\, g\, R_G\, T}$, and, since $\rho = p/(g\, R_G\, T)$, there is also

$$R_e = \left[\frac{P_0\, R_2}{\mu_v \sqrt{g\, R_G\, T_0}} \right] \left(\frac{(p/P_0)\, M_V \sqrt{\gamma}}{\sqrt{(T/T_0)}} \right) \qquad (70)$$

Since the dynamic viscosity μ_v has the dimension $(lb\text{-}s)/ft^2$ in the system of units used in this report, the term in the square bracket is dimensionless. This is necessary because the term in the round bracket and R_e are dimensionless also.

Whereas, for reasons discussed earlier, the expression in the round bracket is constant for all geometrically similar compressors operating at particular values of U_2/a_0, P_{t4}/P_0 and γ, independent of P_0 and T_0, the term in the square bracket depends on the compressor size, the gas properties,

and the magnitudes of P_0 and T_0. Experience has shown, however, that the influence of Reynolds number on losses in turbomachines is quite small, and that large increases of the losses occur only below some critical value of R_e which is usually reached only at very low pressures or with small dimensions. For most gases the dynamic viscosities increase slightly with temperature but the absolute magnitudes of μ_v do not vary greatly for different gases. Most diatomic gases such as N_2, O_2, H_2, CO, and also air, have values of γ of about 1.4 at ambient temperature, and the ratio of the viscosities of the heaviest of these gases (O_2) and the lightest one (H_2) is only about 2. A change in Reynolds number by a factor of two has a very small influence on the losses, except near the above-mentioned critical value of R_e.

This discussion shows that geometrically similar compressors that operate with gases that have the same specific heat ratio will have almost equal values of $(\dot{m})^*$, $(HP)^*$, and $(M)^*$ at particular values of U_2/a_0 and P_{t4}/P_0, if the Reynolds numbers are sufficiently high. Evidently the efficiencies of the compressors at these operating conditions will then also be nearly equal, irrespective of the molecular weight of the gas and the magnitudes of inlet pressure and inlet temperature. The quantities $(\dot{m})^*$, $(HP)^*$ and $(M)^*$ are shown in Table IX for the ratio $U_2/a_0 = 0.7156$.

For a particular compressor operating with a particular gas, the dimensionless quantities of Eqs. 66, 67, and 69 can be simplified by introducing the ratios

$$\theta_C = \frac{T_0}{T_{REF}} \tag{71}$$

and

$$\delta_C = \frac{P_0}{P_{REF}} \tag{72}$$

where T_{REF} and P_{REF} are usually taken as 518.4° R and 14.7 psia. The subscript C was introduced to differientiate these ratios from similar ones that later on are used for the performance calculations of the drive turbine.

With Eq. 71, the ratio U_2/a_0 is also

$$\frac{U_2}{a_0} = \frac{(\pi/30)\ N\ R_2}{\sqrt{g\ \gamma\ R_G\ \theta_C\ T_{REF}}}$$

Hence in a compressor that handles a specific gas, equal values of U_2/a_0 are obtained for equal ratios $N/\sqrt{\theta_C}$. Thus,

$$N_{REF} = N/\sqrt{\theta_C} \qquad \text{(rpm)} \tag{73}$$

will be called the referred speed of the compressor. Similarly, from Eq. 66, the so-called referred weight flow rate is defined by

$$\dot{w}_{REF} = \frac{\dot{w}\sqrt{\theta_C}}{\delta_C} \qquad \text{(lbm/s)} \tag{74}$$

From Eq. 67 the referred power is

$$(HP)_{REF} = \frac{HP}{\delta_C\sqrt{\theta_C}} \qquad \text{(HP)} \tag{75}$$

and from Eq. 69 the so-called referred torque becomes

$$M_{REF} = \frac{M}{\delta_C} \qquad \text{(ft-lb) or (in-lb)} \tag{76}$$

On the basis of the previous discussion it can be stated that a compressor designed for and operated with a particular fluid will have the same pressure ratio at the same values of N_{REF} and $\dot{w}_{REF}$ independent of the absolute magnitudes of P_0 and T_0, provided that the possible variations of Reynolds number have a minor effect on the losses in the bladings of

the machine. Then the referred power required by the compressor will also be a unique function of $N/\sqrt{\theta_c}$ and $\dot{w}\sqrt{\theta_c}/\delta_c$, indicating that its efficiency is only depending on these two variables also. The main disadvantage of the so-called referred parameters is that they are not dimensionless, and that they cannot be used to compare the operating performance of different machines with each other, as it is possible with the earlier defined non-dimensional quantities.

The referred operating parameters of Eqs. 73 to 76 for the design point are given in Table IX.

III. OFF-DESIGN POINT PERFORMANCE

1. General

Because the Hybrid compressor operates as an exhauster in the test rig it is of interest to know its performance at pressure ratios and speed other than those for the design point. If the pressure ratio is smaller than the design value, the pressure P_0 will be higher and since the weight flow rate, and the driving power are proportional to P_0, it is likely that the maximum power occurs at pressure ratios lower than the values at the design point.

2. Rotor Performance

Prime variables for the rotor performance are the peripheral speed ratio U_2/a_0 and the absolute discharge angle α_2. If particular values of these quantities are chosen and if the slip factor μ and the velocity ratio ψ were known it would be possible to determine the dimensionless mass flow rate through the wheel by means of Eq. A II(11). These calculations can be carried out by means of program 102 of Appendix D, which also establishes the ratios T_2/T_0 and p_2/P_0 for the assumed values of μ and ψ. Actually, program 102 determines the quantities:

$$\frac{\dot{w}\sqrt{(R_G/g)\,T_0}}{P_0} = (\dot{m})^*\,\pi\,R_2^{\,2} \tag{77}$$

$$\Phi_2 = \frac{\dot{w}\sqrt{(R_G/g)\,T_0}}{A_2\,k_{B2}\,P_0} = \frac{\dot{w}\sqrt{(R_G/g)\,T_0}}{2\pi R_2\,b_2\,k_{B2}\,P_0} \tag{78}$$

and

$$\Phi_1 = \frac{\dot{w}\sqrt{(R_G/g)\,T_0}}{A_1\,k_{B1}\,P_0} = \frac{\dot{w}\sqrt{(R_G/g\,T_0}}{\pi\,(R_{1o}^{\,2} - R_{1i}^{\,2})\,k_{B1}\,P_0} \tag{79}$$

for chosen blockage factors k_{B1} and k_{B2}.

The dimensionless flow function Φ_1 of Eq. 79 can be used to establish the ratio of the static pressure p_1 and P_0, since P_0 is identical with the total pressure P_{t1} at station (1), with the relation

$$\Phi_1 = \sqrt{\frac{2\gamma}{\gamma - 1}\left[(p_1/P_0)^{2/\gamma} - (p_1/P_0)^{(\gamma + 1)/\gamma}\right]} \qquad (80)$$

Since for known values of Φ_1 and γ, it is not possible to calculate p_1/P_0 in closed form, the calculating program 103 of Ref. D has been set up to determine p_1/P_0 with an iterative process.

Program 104 of Appendix D can then be used to determine the flow properties at the inducer inlet with the relations of Appendix A which are listed in the program description. This program gives T_1/T_0, V_1/a_0, W_{1o}/a_0, and the quantities M_{W1} and i'. The latter is the incidence angle at the outer inlet radius R_{1o} if blockage due to inducer blade thickness is taken into account.

Appendix C analyzes available test data of losses in centrifugal compressor rotors, and shows that Fig. 24 can be used for the present off-design calculations. From Fig. 24 the rotor efficiencies η_R are obtained as functions of i' and M_{W1}. The efficiency η_R is defined by Eq. A (12). With Eqs. A II(5), A (27), and A (21) it is possible to calculate the velocity ratio $\psi = W_2/W_{2is}$ which is used for the performance calculations with the method of Appendix A. This conversion can be carried out with program 105 of Appendix D. The wheel efficiency η_W of Eq. A (15) and the deceleration ratio W_2/W_{1O} are outputs of this program also. The value of ψ thus obtained should coincide with that initially assumed for use in program 102, and ψ must be iterated by successive approximations till agreement is reached.

For the design point the slip factor $\mu = \mu_d = 0.85$ has been determined from Fig. A (3a) for the given rotor dimensions, the assumed rotor

efficiency $\eta_R = 0.86$, and the design flow coefficient $\varphi_2 = \varphi_{2d} = 0.3964$. Experience shows that Fig. A (3a) cannot be used to establish μ at off-design conditions. Most theoretical analyses predict that the slip factor for rotors with radial blades at the discharge remains constant if the flow coefficient and η_R change. As shown in Ref. 13, and by other authors, this condition does not occur in actuality. For the present calculations the conclusion reached in Ref. 13 is applied, namely, that the relative flow angle β_2 of Fig. 1 at the rotor exit remains constant at all operating conditions. Then, by Fig. 1

$$\tan \beta_2 = \frac{U_2 \, (1 - \mu)}{V_{m2}} = \frac{1 - \mu}{\varphi_2}$$

For the design point with μ_d and φ_{2d}, and for $\beta_2 = \beta_{2d}$

$$\frac{1 - \mu}{\varphi_2} = \frac{1 - \mu_d}{\varphi_{2d}}$$

and, since

$$\varphi_2 = \mu \cot \alpha_2$$

there is

$$\mu = \frac{1}{1 + \dfrac{1 - \mu_d}{\varphi_{2d}} \cot \alpha_2} \tag{81}$$

Then, for $\mu_d = 0.85$ and $\varphi_{2d} = 0.3964$

$$\mu = \frac{1}{1 + (0.3784) \cot \alpha_2} \tag{82}$$

Sheets 1 and 2 of Table X give the final results of the rotor performance for speed ratios $U_2/a_0 = 0.7156$ and $U_2/a_0 = 0.516$, respectively, obtained with the procedure outlined above. As pointed out earlier, a value of $\psi = \psi_j$ has to be assumed (line 7 of Table X) and must be changed until it and the value ψ calculated by program 105 (line 22 of Table X) coincide.

Table X only gives the final value of ψ_j for each chosen angle α_2, the intermediate results of the iterations in ψ have not been listed. The curves of Fig. 25 are identical with those of Fig. 24 which were used to obtain the rotor efficiencies η_R as functions of M_{W1} and i' for the calculations in Table X. In Fig. 25 the rotor efficiencies η_R of Table X are plotted vs. M_{W1} and i' to show the location of the curves U_1/a_0 = 0.7156 and U_1/a_0 = 0.516 in relation to the other curves U_1/a_0 = constant which were actually disregarded in establishing η_R for the calculations of Table X. It can be noticed that the two curves U_1/a_0 = constant, that could be drawn through the data points of Table X, are similar to the dashed curves of Figs. 24 and 25 but have somewhat different slopes.

A far more interesting representation of the data of Table X is given in Fig. 26 where the velocity coefficients ψ and the incidence angles i' are shown as function of the deceleration ratio W_2/W_{1o} of the relative velocities in the rotor. As expected, the velocity coefficients ψ decrease with decreasing ratios W_2/W_{1o}, and if W_2/W_{1o} approaches unity the values of ψ seem to reach an asymptotic value which is higher at the lower velocity ratio U_1/a_0 because of the lower Mach number of the flow. Figure 26 also shows that the incidence angles decrease almost linearly with W_2/W_{1o}. In the writer's opinion losses of centrifugal compressors rotors should be presented in the manner of Fig. 26. Data of this nature for different impellers would enable the engineer to arrive at optimum designs and make it possible to establish off-design performance maps with greater accuracy than with the rotor efficiencies η_R.

3. Diffusor Performance

To determine the compressor performance for the rotor data of Table X the conditions in the diffusor must be evaluated also. Experience shows that the pressure loss coefficient Y_t of a decelerating axial

cascade varies with incidence angle and inlet Mach number. Limited information is however available in the literature about these influences. Figure 27 has been established on the basis of Fig. 130 of Ref. 3, but these data are educated guesses at best, although they are representative of observed behavior. In particular, the solid curve will be used for $U_2/a_0 = 0.7156$ and the dashed curve for $U_2/a_0 = 0.516$, for the range of the Mach numbers indicated. Because of the approximate nature of these curves it is sufficient to treat the two diffusor rows together. At the design point the total pressure loss coefficient of rows A_1' and A_2' of diffusor A' is from Table VII

$$Y_t = (Y_t)_{i0} \frac{P_{t2}/P_0 - P_{t4}/P_0}{P_{t2}/P_0 - p_2/P_0} = \frac{1.6764 - 1.5910}{1.6764 - 1.2677} = 0.2089$$

This loss coefficient is supposed to occur at the design incidence angle $i = i_0 = +2^\circ$ of the first diffusor blade row A1 in accordance with Table VI. At other incidence angles

$$i = \alpha_2 - 63^\circ$$

the pressure loss coefficients Y_t are taken as

$$Y_t = 0.2089 \left[Y_t/(Y_t)_{i0} \right]$$

where the ratio in the square bracket is read from Fig. 27.

Reference 3 shows that the deviation angle δ is almost constant if the incidence angle of the flow of a particular cascade changes. Thus, the discharge flow angle of a cascade is nearly constant. This general phenomenon is evident also from Fig. 14 (7) of Ref. 5. Because of the approximate nature of the present investigation it is permissible, therefore, to assume that the flow angle after the second diffusor row A_2 is

constant, equal to $\alpha_4 = 21^\circ$, irrespective of incidence angle and Mach number of diffusor row A_1 (see Table VI).

The calculating method of program 109 of Appendix D will be used to establish the conditions of state of the fluid after the diffusor for the data of Table X. It is assumed that the blockage factors at inlet and exit of the diffusor are those at the design point, or

$$k_{Be} = k_{B2} = 0.954$$

$$k_{Bd} = k_{B4} = 0.88$$

The quantity K of Eq. D 109(2) is then, with $A_4 = A_2$, $\alpha_4 = 21^\circ$, and $M_2 = M_{V2}$

$$K = 1.161218 \cos \alpha_2 \frac{p_2/P_0}{\sqrt{T_2/T_0}} M_2$$

The Mach number M_4 and the velocity V_4 must be obtained with the iterative procedure outlined in program 109.

The processes in the flow straightener and discharge duct, illustrated in Figs. 11a and 11b, are determined with Eqs. 50 to 64. The objective of this procedure is to obtain the pressure ratio p_6/P_0. Since p_6 is equal to the ambient pressure, or 14.7 psia, these calculations establish the value of the total pressure P_0 ahead of the compressor rotor. It is assumed that the total temperature T_0 equals $520^\circ R$.

4. Compressor Off-Design Performance

From line 8 of Table X there are known the ratios $\dot{w}\sqrt{(R_G/g)T_0}/P_0$. Hence the flow rate $\dot{w}$ in lbm/s is obtained from

$$\dot{w} = 0.034055 \frac{\dot{w}\sqrt{(R_G/g)\ T_0}}{P_0} P_0 \ (\text{lbm/s}) \qquad (83)$$

for $R_G = 53.35$ (lb-ft)/(lbm, $^\circ R$), $g = 32.174$ ft/s^2, and $T_0 = 520^\circ R$, if P_0 is introduced in psia. The drive power of the compressor is, from Eq. 34a,

$$HP = 176.54\ \dot{w}\ \left[(T_{t2}/T_0) - 1\right]\ (HP) \tag{84}$$

where T_{t2}/T_0 is known from line 23 of Table X.

The total-to-total efficiency η_{t4} of Eq. 49 can be determined for the pressure ratio P_{t4}/P_0 that is obtained by the calculations. For $T_0 = 520\ ^{\circ}R$, and $R_2 = 5.5$ in., the speed N of the compressor is

$$N = 23290.21\ (U_2/a_0)\ (rpm) \tag{85}$$

These calculations have been performed with program 517 on a Monroe Model 1880-22 scientific programmable printing calculator. Program 517 contains the earlier mentioned program 109. With this advanced calculator the whole calculating procedure can be carried out without the need of introducing several programs as would have been necessary with Monroe Model 1556, which is limited to 256 program steps and seven active memory registers. Program 517 which is described in Appendix D requires 557 program steps and 40 data storage registers.

The results of the calculations for the data of Table X are listed in Table XI for the design velocity ratio $U_2/a_0 = 0.7156$ and in Table XII for $U_2/a_0 = 0.516$. The data of these tables are direct print-outs of the Model 1880 calculator.

The data at the design speed of 16,666 rpm and for $\alpha_2 = 65^{\circ}$ (Table XI) should coincide with the values of Table IX. It can be noted that the agreement is good, hence, it can be concluded that no arithmetic errors were made in the calculations.

Figure 28 is a graph of the data of Tables XI and XII. As expected, the driving power is higher at flow rates larger than that of the design point. It is necessary therefore to run the compressor with a turbine that is capable of producing at least 130 HP at 16,666 rpm, although only about 83 HP are required at the design point conditions. It can also be seen

from Fig. 28 that the calculated optimum compressor efficiencies at 12,018 and 16,666 rpm are nearly equal, namely, 81.35% at the lower and 81.49% at the higher speed. It seems possible, therefore, to obtain a good measure of the maximum compressor efficiency with tests at speeds lower than design, say, at about 13,000 to 14,000 rpm.

The data points in Fig. 28 at the lowest flow rates are for $\alpha_2 = 73^\circ$ at both speeds. As indicated in Fig. 25 these points lie on the curve labeled "surge limit." At $\alpha_2 = 73^\circ$ the diffusor incidence angle i is 10°. By Fig. 27 the ratio $Y_t/(Y_t)_0$ for $i = 10^\circ$ is 1.90 for $U_2/a_0 = 0.7156$ and 1.22 for $U_2/a_0 = 0.516$. A frequently applied rule assumes that an axial blade row stalls if the loss is twice that at the design incidence angle. If this condition were to hold for the tandem row of the present diffuser, it could be stated that compressor surge is due to rotor stall at both speed ratios. The surge limit indicated in Fig. 28 holds for this premise.

IV. DRIVE TURBINE

1. General

An available test stand for investigations of transonic axial compressor wheels is driven by a dual-flow air turbine with 50 percent reaction which is illustrated in Dwg. 2222 of Appendix B. The rotors of this turbine are shown in Dwg. 2108-1 and the guide vanes in Dwg. 2109. The blades of rotor and stator are identical with the profiles of Dwg. 2107, but to avoid wake interferences the stator row has 31 and the rotor 32 blades. The two parallel stages are designed for the following conditions

$$P_{t0}/p_2 = 2.8 \text{ for } p_2 = p_{AMB} = 14.7 \text{ psia}$$

$$T_{t0} = 640\ ^{\circ}R$$

$$\dot{w} = 10.85 \text{ lbm/s}$$

$$HP = 485 \text{ HP}$$

$$N = 30{,}500 \text{ rpm}$$

where P_{t0} and T_{t0} are total inlet pressure and total inlet temperature, respectively, and p_2 the static discharge pressure.

To be determined are the pressure ratio, inlet temperatures, and weight flow rates for turbine powers of 130 HP at 16,666 rpm, and 60 HP at 12,018 rpm.

2. Off-Design Turbine Performance

These calculations were performed by Prof. E. Macchi during his stay as Visiting Professor at NPS. Use was made of the computer program of Ref. 14 which treats the three-dimensional flow in a turbine stage by taking account of streamline curvatures and slopes, as well as energy and entropy gradients. In Ref. 14 it is possible to select one of five loss correlation methods that are included in the program. For the present

investigation the method of Traupel (Ref. 15) has been applied, since it was found to give good performance predictions for 50 percent reaction turbines. The results of these calculations are presented in Fig. 29, showing referred flow rate $\dot{w}\sqrt{\theta_T}/\delta_T$, and referred power $HP/(\delta_T \sqrt{\theta_T})$ as function of the referred speed $N/\sqrt{\theta_T}$ for different turbine pressure ratios. There are:

$$\delta_T = P_{t0}/14.7$$

$$\theta_T = T_{t0}/518.4$$

If the ambient pressure is assumed to be 14.7 psia the turbine pressure ratio P_{t0}/p_2 equals δ_T.

For ease of operation it will be endeavored to run the turbine at the lowest possible inlet temperature T_{t0}. A lower limit is given by the condensation or icing of the water vapor in the operating air which has nearly 100 percent relative humidity. It will therefore be assumed that the static turbine discharge temperature T_2 shall not be less than 45° F or 505° R. The off-design calculations showed that the total-to-static turbine efficiency η_s does not exceed about 81% in the range of operating conditions for the Hybrid compressor. The temperature T_2 is obtained from

$$T_2 = T_{t0} \left\{ 1 - \eta_s \left[1 - (1/\delta_T)^{(\gamma - 1)/\gamma} \right] \right\} \qquad (86)$$

For $T_2 = 505^\circ$ R and $\eta_s = 0.81$ the temperature T_{t0} can therefore be determined for different values of δ_T and $\gamma = 1.4$. Thus, the ratios $\theta_T = T_{t0}/518.4$ are known as functions of δ_T. For a particular speed N, or ratio $N/\sqrt{\theta_T}$, the referred turbine parameters are then obtained from Fig. 29 for the three values of δ_T. The results are listed in the following table:

N (rpm)	16,666			12,018		
δ_T	1.4	1.8	2.2	1.4	1.8	2.2
T_{t0} ($^{\circ}$R) (Eq. 86)	545.5	577.3	603.6	545.5	557.3	603.6
$\theta_T = T_{t0}/518.4$	1.05227	1.11360	1.16439	1.05227	1.11360	1.16439
$N/\sqrt{\theta_T}$	16,247	15,793	15,445	11,716	11,388	11,137
$\frac{\dot{w}\sqrt{\theta_T}}{\delta_T}$ (Fig. 29)	3.65	4.18	4.30	3.72	4.27	4.36
$\frac{HP}{\delta_T\sqrt{\theta_T}}$ (Fig. 29)	48.5	89.1	111.8	46.8	81.0	97.2
$\dot{w}$ (lbm/s)	4.98	7.13	8.77	5.08	7.28	8.89
HP	69.6	169.2	265.4	67.2	153.8	230.7

From the plot of these data in Fig. 30 it can be seen that the turbine is capable of producing 130 HP at 16,666 rpm with a pressure ratio of 1.64 at a flow rate of 6.4 lbm/s. The inlet temperature must be about 105° F. At the lower speed of 12,018 rpm a power of 60 HP is produced at a pressure ratio of 1.37 for a flow rate of 4.85 lbm/s with a turbine inlet temperature of 82° F.

The air supply system of the Turbopropulsion Laboratory is capable of producing these inlet conditions and no difficulty is expected to drive the compressor at all possible operating conditions.

V. MECHANICAL DESIGN

1. Rotor

An investigation of the stresses in the Hybrid rotor has been carried out to determine its maximum operating speed. As evident from Dwg. 2203 of Appendix B the outer rim of the rotor will produce bending stresses which will be reduced, in part, by the restraint of the radial blades. In Ref. 16 the stresses were calculated by ignoring these bending stresses and the support by the blades. Referred to the outer rotor radius $R_o = 5.94$ inch the maximum stress σ_{max} was determined to be

$$\sigma_{max} = 0.53\ \rho\omega^2\ R_o^2$$

where ρ is the density of the rotor material.

For aluminum alloy AL-7079 with $\rho = 2.616\ (10^{-4})$ lb $s^2/in.^4$, there is at N = 17,000 rpm

$$\rho\omega^2\ R_o^2 = 29{,}252 \text{ psi}$$

and

$$\sigma_{max} = 15{,}504 \text{ psi}$$

With a correction factor of about 1.25, to allow for the inaccuracies of the model used for the calculation, the design stress σ_d was taken as

$$\sigma_d = 1.25\ \sigma_{max} = 19{,}380 \text{ psi}$$

Aluminum alloy Al-7079-T6 was chosen as material. In forged condition this alloy has a 0.2% yield stress of 73 kpsi, and an ultimate stress of 83 kpsi.

During his stay at NPS as Visiting Assistant Professor, Dr. W. Schlachter undertook a more accurate stress analysis with the method of Ref. 17 which is discussed also in Ref. 18. This method takes account of the bending moments that occur in non-symmetrical disks with radial blades. Although the forces and moments produced by the blade elements are evaluated properly, these

effects are later distributed evenly along the periphery to obtain axi-symmetric conditions. Thus the rotor is supposed to have an infinite number of blades which have the same effect as the actual number of blades. Inspite of its complexity the method of Ref. 17 gives doubtful results in the vicinity of the outer radius of the Hybrid rotor, and finite-element methods should actually be employed to give more accurate conditions.

Figure 31 shows the dimensionless stresses $\sigma/(\rho\omega^2 R_o^2)$ in the disk in radial and peripheral directions. In Fig. 31 the shape of the Hybrid rotor is shown also to indicate that the plotted stress ratios exist on either the outer or the inner disk contour, which are designated by A and B, respectively. Evidently, high stresses occur at a radius ratio $R/R_o = 0.7$ where the disk has its smallest thickness. On contour A the disk is in compression and on contour B it is in tension. This is indicative of the bending moment that must occur at this station.

The highest stress occurs at the radius R_o on the inner contour B of the rotor but it has the nature of a stress concentration which, in ductile materials, will be reduced considerably by local plastic deformations if the yield stress is exceeded. For this reason ductile materials have to be used for rotors to equalize stress peaks. From Fig. 31 it can be concluded that a maximum stress of about $0.60\ (\rho\omega^2 R_o^2)$ can be used as a design criterion for the Hybrid rotor if it is made of a material with good ductility.

This criterion seems to be invalidated by Fig. 32 which shows the blade stresses at the tip, and at the base where they adjoin the disk. These stations are designated as contours D and C, respectively, of the rotor which is shown in Fig. 32, also. However, the high stress ratio at the blade tips at a radius ratio $R_D/R_o = 0.7$ is clearly a local condition which will be reduced by plastic yielding if the material has good

ductility. Drawing 2203 of Appendix B shows that the blades of the rotor have a thickness of 0.125 inch. If this thickness were increased to 0.16 inches the blade tip stress ratio could be reduced from 2 to about 1.22 without loss in efficiency. However, the writer believes that even with the thin blades the rotor is capable of operating at 17,000 rpm without danger. For a stress ratio of 0.6, the maximum stress σ_{max} is

$$\sigma_{max} = 17{,}500 \text{ psi}$$

If a maximum design stress of 55 kpsi is taken for AL-7075-T6, or about 75 percent of its 0.2% yield stress (73 kpsi), the maximum rotor speed could be

$$N_{max} = 17{,}000 \sqrt{\frac{55{,}000}{17{,}500}} = 30{,}100 \text{ rpm}$$

A design speed of 17,000 rpm was used because of the critical speed of the rotor assembly. For the overhung arrangement of Dwg. 2222, where the shaft is supported by ball bearings with 30 mm bore, and for an aluminum rotor that weighs about 19.5 lb, the critical speeds are:

$$N_{CI} = 21{,}620 \text{ rpm}$$

and

$$N_{CII} = 66{,}230 \text{ rpm}$$

These speeds were obtained without taking account of the flexibility of the bearing supports. Thus, the decision was made to limit the operating speed to 17,000 rpm or about 78 percent of the first critical shaft speed.

2. Maximum Obtainable Pressure Ratios

It is of interest to evaluate what pressure ratio could be produced by the Hybrid compressor if it were rotating at 30,100 instead of at 16,666 rpm. The peripheral speed ratio U_2/a_0 for a total inlet temperature $T_0 = 520^\circ$ R could then be increased from 0.7156 to

$$(U_2/a_0)_{max} = 1.2924$$

From Eq. A II(3)

$$\frac{P_{t4}}{P_0} = \left[1 + (\gamma - 1)\ \mu\ \eta_c\ (U_2/a_0)^2\right]^{\gamma/(\gamma - 1)} \tag{87}$$

For an assumed efficiency $\eta_c = 0.8$, and $\gamma = 1.4$, $\mu = 0.85$,

$$\left(\frac{P_{t4}}{P_0}\right)_{max} = 3.71$$

At this pressure ratio the static temperature T_2 at the rotor exit is from Eq. A I(7), for $T_0 = 520^\circ$ R,

$$(T_2)_{max} = 662.5^\circ \text{ R} = 202.5^\circ \text{ F}$$

This temperature is somewhat high for aluminum alloys since their physical properties are reduced considerably at higher temperatures. At 300° F, for instance, the 0.2% yield strength of AL-7075-T6 is reduced from 73 kpsi (at room temperature) to 22 kpsi.

Titanium alloy 6AL-4V would be a better rotor material for the higher speeds. At a temperature of about 300° F the 0.2% yield strength of a forging with an elongation of 13 percent is about 130 kpsi. For a design stress of 75 percent of this yield strength, or

$$\sigma_{max} = 97{,}500 \text{ psi}$$

and

$$\sigma_{max} = 0.6\ (\rho\omega^2\ R_o^{\ 2})$$

there is with

$$\rho = 4.144\ (10^{-4})\ \text{lb s}^2/\text{in.}^4$$

$$N_{max} = \frac{30}{\pi}\,\omega = \frac{30}{\pi}\sqrt{\frac{\sigma_{max}}{(0.6)\ \rho\ R_o^{\ 2}}} = 31{,}835 \text{ rpm}$$

Then

$$U_2/a_0 = 1.3669$$

From Eq. 87 the pressure ratio at this speed ratio is, for $\eta_c = .80$, $\gamma = 1.4$, $\mu = 0.85$,

$$\frac{P_{t4}}{P_0} = 4.213$$

at a temperature T_2 of

$$T_2 = 679.4^\circ \text{ R} = 219.4^\circ \text{ F}$$

These calculations indicate that pressure ratios larger than about 4.2 can be reached only in a Hybrid compressor of the design proposed here, if spin tests show that stress ratios $\sigma_{max}/(\rho\ \omega^2\ R_o^2)$ higher than 0.6 are permissible, or that the ratio of 75 percent of design and yield stress is too conservative.

3. General Description of Test Rig

Drawing No. 2222 of Appendix B shows that the compressor shaft is supported by two matched pairs of high-precision ball bearings. The rotor assembly is held together by a central tie-bolt which is prevented from turning by prongs in the quill shaft that connects the compressor to the drive turbine. At the compressor end of the assembly, a steel attachment, shown in Dwg. 2103-A, pre-loads the inner races of the ball bearings and serves as support for the aluminum rotor. To ensure that the rotor remains concentric with the shaft, even if it increases its diameter by centrifugal stresses, four matched bushings (part 2103-2) are inserted in holes in the rotor collar and part 2103-1, that are drilled and reamed together. These bushings center the rotor and transmit the torque. The maximum torque is about 605 in.-lb at 160 HP and 16,666 rpm. The cross-sectional area of one bushing (0.25 OD, 0.196 ID) is 0.0189 $in.^2$. The shear force acting at the

diameter of 3.2 in., where the rotor rests on the steel disk (part 2103-1) is 605/(2 x 3.2) = 94.5 lb if all bushings carry equal loads. Thus the shear stress per bushing is 94.5/0.0189 = 5000 psi. The bushings are of Steel AISI 4340, hardened to 360 Brinell, to obtain a yield strength of about 160 kpsi. Hence the allowable shear stress is 80,000 psi and it is possible for one bushing to transmit the whole torque without danger.

The axial thrust exerted by the impeller is eliminated by the rotating balance piston near the quill shaft. The ball bearings at this shaft end are floating but they are supported by flexures which are equipped with strain gages. Calibrations of the assembly with known applied axial forces will indicate how much thrust is acting on the bearings. The readout of the strain gages is displayed in the control room so that the balance air pressure can be adjusted for minimum thrust acting on the bearings. Because of its symmetrical design the drive turbine will not produce any axial thrust. The bearings are oil-mist lubricated, and the temperature of each outer race of the eight bearings is measured by a thermocouple which can be read in the control room also.

The diffusor blades are attached to blade holders (Part 1 of Dwg. 2209) by nuts and lock washers. Hence their stagger angles can be varied. These blade holders are inserted in a casing (Part 4 of Dwg. 2208). A number of spacer rings (see Dwg. 2209) were manufactured to be able to locate the diffusor blade rows at different distances from the rotor discharge. It is possible also to rotate the blade holders with respect to each other. With this arrangement it is possible to produce different arrangements of tandem blade rows. Part 4 of Dwg. 2208 is bolted to a casing (Part 1 of Dwg. 2207) on one side and to the shroud support of Dwg. 2212 on the other. To this support is attached the rotor shroud (Part 1 of Dwg. 2213) to form the floating stator assembly whose functions

are described in the next paragraph. Honeycomb flow straighteners are arranged between the fins of the shroud support.

At the design point the total temperature of the air passing through the compressor will increase by about 90° R. Hence a temperature error of one degree will result in a change of the calculated efficiency of about 1.2 points. Errors of temperature measurements of one degree easily occur in high speed flows, especially if they are non-steady. It was therefore decided to make arrangements for direct torque measurements. As shown in Dwg. 2222 the so-called floating stator assembly, consisting of the diffusor vanes, the flow straightener, the rotor shroud, and an outer casing, is supported by two special Kaydon ball bearings. The flow ahead of the inducer is in axial direction and the flow straightener after the diffusor will produce an axial discharge velocity. Then, the moment excerted on the rotor must be equal and opposite to the moment acting on the above-mentioned assembly. This moment is measured by flexures with strain gages (Part 4 of Dwg. 2215) which are calibrated against known torques, that are applied with a lever and known weights.

This arrangement requires labyrinth seals at the inner and outer diameters of the shroud of Dwg. 2213. These labyrinths are shown in Dwg. 2215. For radial clearances of 0.015 inch a leakage flow of about 0.012 lbm/s will pass through the inner labyrinth with 6.4 inch ID, from the region inside the shroud to the inducer inlet. This quantity is about 0.4 percent of the design flow rate. Through the outer labyrinth with an OD of 9.48 inch, however, a leakage flow of 0.064 lbm/s will occur from the opening after the flow straightener to the region inside the shroud. To maintain the required pressure between the labyrinths, an air flow of 0.064 - 0.012 = 0.054 lbs/s has to be vented from this region. For this reason the inlet casing, shown in Dwg. 2214-2, is hollow and is connected

by four 1 inch tubes to openings in the 18 inch suction pipe ahead of the flow measuring nozzle.

The measuring nozzle has a diameter of 5.375 inches and is formed of epoxy as shown in Dwg. 2222, with parts of the contour machined in the nozzle frame of Dwg. 2216. The shape of the nozzle conforms to the norms of VDI measuring orifices. A nozzle with a diameter of 5.375 inches will produce a pressure difference of about 20 inches of water for the measuring of the design flow rate of 2.7 lbm/s.

Drawing 2223 shows the general installation of the compressor test rig in Test Cell 2 of the Turbopropulsion Laboratory. Air supplied from a multi-stage axial compressor with a drive power of 1250 HP passes through a remote-controlled butterfly valve to the drive turbine. In case of runaway conditions, which could be caused by a compressor blade failure, the turbine air can be blown directly to the atmosphere through an emergency bypass valve.

The compressor air flow is controlled by the inlet throttle valve of Dwg. 2158. It consists of a fixed and a rotating plate that have the same arrangement of holes. The maximum flow area is 158 $in.^2$, corresponding to the area of a pipe of about 14 inch ID. The rotating plate is supported by ball bearings and can be moved with the oil pressure actuator of Dwg. 2159. This actuator can produce a force of about $1700^{lb}_{\Delta} \pm 1700$ lb for an oil pressure of 400 psi. It is controlled from the control room by a reversible electric motor of less than 1/10 HP. The actuator is inherently stable and maintains the same position irrespective of the force applied to it, provided it is less than about 2000 lb.

After the throttling valve the velocity of the air is destroyed in the plenum chamber of Dwg. 2164-1. It is equipped with six perforated plates, with 43 percent free opening, which can be located at arbitrary positions

along the axis of the plenum. A contoured plastic nozzle guides the flow into the 18 inch diameter suction pipes, which contain the measuring nozzle.

REFERENCES

1. Vavra, M. H., "Basic Elements for Advanced Design of Radial Flow Compressors", Article 6 of AGARD Lecture Series No. 39 on Advanced Compressors, Technical Editing and Reproduction Ltd., London, June 1970. (Enclosed as Appendix A)
2. Stiefel, W., "Theoretical and Experimental Research on Limit Loading of Radial Compressors" Part II, Course Note 53b, Von Karman Institute for Fluid Dynamics, Rhode-Saint-Genese, Belgium, March 1965.
3. Lieblein, S., "Experimental Flow in Two-Dimensional Cascades", Chapter VI of "Aerodynamic Design of Axial-Flow Compressors", Edited by I. A. Johnson and R. O. Bullock, NASA SP-36, Washington, D.C., 1965.
4. Steinke, R. J., and Crouse, J. E., "Analytical Studies of Aspect Ratio and Curvature Variations for Axial-Flow Compressor Inlet Stages under High Loading", NASA TN D-3959, May 1967.
5. Vavra, M. H., "Aerothermodynamics and Flow in Turbomachines," John Wiley & Sons, New York 1960.
6. Griepentrog, H., "Secondary Flow Losses in Axial Compressors", Article 5 of AGARD Lecture Series No. 39 on Advanced Compressors, Technical Editing and Reproduction Ltd., London, June 1970.
7. Woods, J. R. Jr., "The Analytical Treatment of Secondary Flows and Associated Losses in Axial-Flow Turbomachines", Report NPS-57W071121A, Naval Postgraduate School, Monterey, California, December 1971.
8. Vavra, M. H., "Aerodynamic Design of Symmetrical Blading for Three-Stage Axial Flow Compressor Test Rig" Report NPS-57VA70091A, Naval Postgraduate School, Monterey, California, September 1970.

9. Giles, R. V., "Fluid Mechanics and Hydraulics" 2nd. Ed., p. 257, Schaum Publishing Co., New York, 1962.

10. Linsi, U., "Experiments on the Radial Compressors of Turbochargers" Brown Boveri Review, Vol. 52, No. 3, pp. 161/170, March 1965.

11. Meldahl, A., "The Separation of Impeller and Diffusor Losses in Radial Blowers" Brown Boveri Review, Vol. 28, No. 8/9, pp. 203/206, Aug./Sept. 1941.

12. Traupel, W. "Die Theorie der Stroemung durch Radialmaschinen", p. 100, G. Braun, Karlsruhe, 1962.

13. Stahler, A. F., "The Slip Factor of a Radial Bladed Centrifugal Compressor", ASME Paper 64-GTP-1, March 1965.

14. Macchi, E., "Computer Program for Prediction of Axial Flow Turbine Performance", Report NPS-57MA70081A, Naval Postgraduate School, Monterey, California, August 1970.

15. Traupel, W., "Thermische Turbomaschinen", Vol. 1, pp. 269/298, Springer Verlag, Berlin, 1958.

16. Griepentrog, H., "Calculation of Hybrid Compressor", Encl. 3 of Progress Report, February 1970, on "Research in Hybrid Compressor Concept", Naval Postgraduate School, Monterey, California. AIR TASK A330536 0/551B/0F32432302

17. Schilhansl, M. J., "Stress Analysis of Radial-Flow Rotor", Trans. ASME J. of Engg. for Power, January 1962 pp. 124-130.

18. Vavra, M. H.,"Mechanical Problems in Radial Turbines", Short Course March 1968, Part C, p. C14/C26, Von Karman Institute for Fluid Dynamics, Rhode-Saint-Genese, Belgium.

TABLES

TABLE I: Flow, Blade, and Incidence Angles

at Inducer Leading Edge

R_1 (in.)	β_1 ($^\circ$)	β_B ($^\circ$)	tan β_B	$i=\beta_1-\beta_B$ ($^\circ$)
3.025	55	50.32	1.20545	4.68
2.8	52.89	47.99	1.11016	4.90
2.6	50.83	45.71	1.02525	5.12
2.4	48.57	43.23	0.94024	5.34
2.2	46.09	40.51	0.85449	5.58
2.0	43.36	37.54	0.76852	5.82
1.8	40.36	34.30	0.68216	6.06
1.6	37.07	30.76	0.59530	6.31
1.5	35.30	28.88	0.55166	6.42
1.4	33.46	26.92	0.50784	6.54
1.3	31.54	24.88	0.46388	6.66
1.2	29.53	22.77	0.41973	6.76
1.1	27.44	20.57	0.37538	6.87
1.023	25.78	18.83	0.34111	6.95
1.00	25.27	18.30	0.33085	6.97
0.99	25.05	18.08	0.32639	6.97

TABLE II: Loss Coefficients of First Blade Row of Diffusor

$\Delta\alpha$	σ =	0.8	1.0	1.2	1.4	1.6	1.8
10°	D	0.4524	0.4146	0.3893	0.3713	0.3578	0.3473
	Y_P	0.0452	0.0486	0.0527	0.0572	0.0619	0.0668
	Y_t'	0.0900	0.0934	0.0975	0.1020	0.1067	0.1116
	Y_t''	0.0680	0.0788	0.0902	0.1031	0.1169	0.1323
12°	D	0.5137	0.4705	0.4417	0.4211	0.4057	0.3937
	Y_P	0.0545	0.0578	0.0620	0.0666	0.0716	0.0768
	Y_t'	0.1116	0.1148	0.1190	0.1236	0.1286	0.1338
	Y_t''	0.0873	0.0988	0.1127	0.1289	0.1470	0.1669
14°	D	0.5687	0.5207	0.4886	0.4657	0.4485	0.4352
	Y_P	0.0639	0.0670	0.0711	0.0760	0.0812	0.0857
	Y_t'	0.1332	0.1362	0.1403	0.1452	0.1504	0.1549
	Y_t''	0.1069	0.1207	0.1376	0.1569	0.1788	0.2017

$\Delta\alpha = \alpha_2 - \alpha_3 = 65^\circ - \alpha_3$ = Flow Deflection

σ = Solidity = (Blade Chord/Blade Spacing)

D = Diffusion Factor (Eq. 16)

Y_P = Profile Loss Coefficient (Eq. 20)

$Y_t' = Y_P + Y_s'$ = Overall Loss Coefficient

$Y_t'' = Y_P + Y_s''$ = Overall Loss Coefficient (Eq. 27)

Y_s' = Secondary Flow Loss Coefficient (Eq. 25)

Y_s'' = Secondary Flow Loss Coefficient (Eq. 26 with Y_s''/Y_t'' from Fig. 6)

TABLE III: Design Values of First Blade Rows

of Diffusors A and B

Diffusor	A	B
Diffusor Blade Row Designation	A_1	B_1
Flow Deflection $\Delta\alpha^\circ = \alpha_2 - \alpha_3$	12	12
Number of Blades	38	38
Solidity σ	1.6	0.95
Diffusion Factor D	0.4057	0.4796
Profile Loss Coefficient Y_P	0.0716	0.0569
Total Loss Coefficient Y_t'	0.1286	0.1139
Total Loss Coefficient Y_t''	0.1470	0.0958
Blade Chord c (in.)	1.455	0.864
Maximum Blade Thickness t (in.)	0.090	0.085
Thickness Ratio t/c	0.062	0.098

TABLE IV: Loss Coefficients of Second Blade Row of Diffusor

$\Delta\alpha$	σ =	0.8	1.0	1.2	1.4	1.6	1.8
26°	D	0.6321	0.5706	0.5296	0.5003	0.4783	0.4612
	Y_P	0.0565	0.0568	0.0587	0.0613	0.0644	0.0678
	Y_t'	0.1349	0.1352	0.1371	0.1397	0.1428	0.1462
	Y_t''	0.1201	0.1354	0.1553	0.1793	0.2077	0.2387
32°	D	0.7101	0.6392	0.5919	0.5581	0.5327	0.5130
	Y_P	0.0698	0.0690	0.0703	0.0726	0.0755	0.0789
	Y_t'	0.1709	0.1702	0.1714	0.1737	0.1767	0.1801
	Y_t''	0.1654	0.1856	0.2129	0.2461	0.2906	0.3432
38°	D	0.7753	0.6956	0.6425	0.6046	0.5761	0.5540
	Y_P	0.0826	0.0805	0.0810	0.0829	0.0856	0.0889
	Y_t'	0.2066	0.2044	0.2049	0.2068	0.2095	0.2128
	Y_t''	0.2135	0.2439	0.2811	0.3288	0.3926	0.4677

$\Delta\alpha = \alpha_3 - \alpha_4 = 53^\circ - \alpha_4$ = Flow Deflection

σ = Solidity = (Blade Chord/Blade Spacing)

D = Diffusion Factor (Eq. 16 with $\alpha_2 = \alpha_3$, $\alpha_3 = \alpha_4$)

Y_P = Profile Loss Coefficient (Eq. 26 with $\alpha_3 = \alpha_4$)

$Y_t' = Y_P + Y_s'$ = Overall Loss Coefficient

$Y_t'' = Y_P + Y_s''$ = Overall Loss Coefficient

Y_s' = Secondary Flow Loss Coefficient (Eq. 25 with $\alpha_2 = \alpha_3$, $\alpha_3 = \alpha_4$)

Y_s'' = Secondary Flow Loss Coefficient (Eq. 26 with Y_s''/Y_t'' from Fig. 6)

TABLE V: Design Values of Second Blade Rows of Diffusors A and B

Diffusor	A	B
Diffusor Blade Row Designation	A2	B2
Flow Deflection $\Delta\alpha^{\circ} = \alpha_3 - \alpha_4$	32	32
Number of Blades	38	38
Solidity σ	1.4	1.0
Diffusion Factor D	0.5581	0.6392
Profile Loss Coefficient Y_P	0.0726	0.0690
Total Loss Coefficient Y_t'	0.1737	0.1702
Total Loss Coefficient Y_t''	0.2461	0.1856
Blade Chord c (in.)	1.275	0.910
Maximum Blade Thickness t (in.)	0.090	0.085
Thickness Ratio t/c	0.070	0.093

TABLE VI: Determination of Diffusor Profile Data

(For Symbols see Fig. 9)

Diffusor Blade Row	A1	B1	A2	B2
α_e (°)	65	65	53	53
$\Delta\alpha$ (°)	12	12	32	32
α_d (°)	53	53	21	21
σ	1.6	0.95	1.4	1.0
t/c	0.062	0.098	0.07	0.093
From Ref. 3: $(k_i)_{sh}$	1.1	1.1	1.1	1.1
From Ref. 3: $(k_\delta)_{sh}$	1.1	1.1	1.1	1.1
From Ref. 3: $(i_0)_{10}$	7.85°	4.55°	5.80°	4.10°
From Ref. 3: $(\delta_0)_{10}$	3.22°	2.05°	1.40°	1.80°
From Ref. 3: m	0.245	0.338	0.231	0.300
From Ref. 3: n	-0.197	-0.293	-0.140	-0.195
From Ref. 3: $(k_i)_t$	0.79	0.99	0.845	0.970
From Ref. 3: $(k_\delta)_t$	0.545	0.925	0.630	0.955
$i_0 = (i_0)_{10}(k_i)_t(k_i)_{sh}$	6.822°	4.955°	5.391°	4.375°
$\delta_0 = (\delta_0)_{10}(k_\delta)_t(k_\delta)_{sh}$	1.930°	2.086°	0.97°	1.891°
$\varphi = (\Delta\alpha - i_0 + \delta_0)/(1 - m + n)$	12.738°	24.74°	43.846°	58.447°
$i = i_0 + n\varphi$	4.312°	-2.95°	-0.747°	-7.022°
$\delta = \delta_0 + m\varphi$	5.051°	10.50°	11.098°	19.425°
$\gamma = \alpha_e - \varphi/2 - i$	54.319	54.922	31.824	30.798
Chosen incidence i*	+2°	-1°	0°45'	-2°
From Ref. 3: $(d\delta/di)$	0.04	0.13	--	0.085
$\varphi^* = \varphi - (i^* - i)(1 - d\delta/di)$	14.957	23.613	43.846	53.852
$\gamma^* = \alpha_e - \varphi^*/2 - i^*$	55°31'	54°11'	31°50'	28°04'
Profile coordinates:	Dwg 2210-1	Dwg 2210-3	Dwg 2210-2	Dwg 2210-4
$\Delta\gamma$	0°39'	1°09'	0°	0°06'
$\gamma' = \gamma + \Delta\gamma$ or $\gamma^* + \Delta\gamma$	56°10'	55°20'	31°50'	28°10'

TABLE VII: Flow Properties in Diffusor

Blade Row	A1'	A1"	B1'	B1"
P_{t2}/P_0	———	1.6764	———	
$T_{t2}/T_0 = T_{t3}/T_0 = T_{t4}/T_0$	———	1.17411	———	
p_2/P_0	———	1.2677	———	
T_2/T_0	———	1.08402	———	
K (Eq. 43)	———	0.571523	———	
Y_t (Table III)	0.1286	0.1470	0.1139	0.0958
P_{t3}/P_0 (Eq. 47)	1.6238	1.6163	1.6298	1.6372
M_3* (chosen)	0.4240	0.4265	0.4220	0.4196
T_3/T_0 (Eq. 45)	1.13336	1.13290	1.13373	1.13417
p_3/P_0 (Eq. 46)	1.4350	1.4263	1.4419	1.4505
M_3 (Eq. 44)	0.4240	0.4265	0.4220	0.4196
V_3 (ft/s) (Eq. 48)	504.6	507.7	502.3	499.5
Blade Row	A2'	A2"	B2'	B2"
K (Eq. 43)	0.385168	0.385168	0.385132	0.385150
Y_t (Table V)	0.1737	0.2461	0.1702	0.1856
P_{t4}/P_0 (Eq. 47)	1.5910	1.5695	1.5978	1.6025
M_4* (chosen)	0.2743	0.2784	0.2730	0.2722
T_4/T_0 (Eq. 45)	1.15670	1.15618	1.15686	1.15670
P_4/P_0 (Eq. 46)	1.5100	1.4872	1.5172	1.5221
M_4 (Eq. 44)	0.2743	0.2785	0.2730	0.2722
V_4 (ft/s) (Eq. 48)	329.8	334.7	328.2	327.2
η_{t4} (Eq. 49)	81.5%	78.9%	82.3%	82.8%

TABLE VIII: Flow Conditions in Flow Straightener and Discharge Duct

(See Fig. 11 for Symbols and Location of Stations)

Diffusor	A'	A"	B'	B"
V_4 (ft/s) (From Table VII)	329.8	334.6	328.2	327.2
P_{t4}/P_0 (From Table VII)	1.5910	1.5696	1.5979	1.6026
p_4/P_0 (From Table VII)	1.5100	1.4873	1.5172	1.5222
T_4/T_0 (From Table VII)	1.15670	1.15619	1.15686	1.15698
$V_4/a_0 = V_4/(1117.85)$	0.2950	0.2993	0.2936	0.2927
T_4^*/T_0 (Eq. 53)	1.15893	1.15849	1.15907	1.15918
P_{t4}'/P_0 (Eq. 54)	1.5803	1.5587	1.5872	1.5919
T_4'/T_0 (Eq. 55)	1.15532	1.15477	1.15550	1.15561
p_4'/P_0 (Eq. 56)	1.4935	1.4706	1.5009	1.5059
$P_{t4}"/P_0$ (Eq. 58)	1.5543	1.5323	1.5613	1.5661
$p_4"/P_0$ (Eq. 59)	1.4689	1.4457	1.4764	1.4814
T_5/T_0 (Eq. 60)	1.16074	1.16035	1.16087	1.16095
P_{t5}/P_0 (Eq. 61)	1.5290	1.5066	1.5362	1.5410
P_{t6}/P_0 (Eq. 62)	1.5050	1.4822	1.5123	1.5172
T_6/T_0 (Eq. 63)	1.16503	1.16477	1.16512	1.16518
p_6/P_0 (Eq. 64)	1.4647	1.4414	1.4721	1.4772
$P_0 = \frac{14.7}{(p_6/P_0)}$ (psia)	10.036	10.198	9.985	9.951

TABLE IX: Estimated Compressor Performance

at Design Point (N = 16,666 rpm, $T_0 = 520^{\circ}R$)

Diffusor	A'	A"	B'	B"
P_{t4}/P_0 (Table VII)	1.5910	1.5696	1.5979	1.6026
η_{t4} (Table VII)	81.5%	78.9%	82.3%	82.8%
p_6/P_0 (Table VIII)	1.4647	1.4414	1.4721	1.4772
P_0 (Table VIII), (psia)	10.036	10.198	9.985	9.951
$\dot{w}$ (Eq. 34), (lbm/s)	2.698	2.742	2.685	2.676
HP (Eq. 36), (HP)	83.0	84.3	82.5	82.2
M (Eq. 65), (in.-lb)	313.7	318.7	312.1	311.0
U_2/a_0	0.7156			
$(\dot{m})^*$ (Eq. 66)	0.08309			
$(HP)^*$ (Eq. 67)	0.05063			
$(M)^*$ (Eq. 69)	0.05980			
$\theta_c = 520/518.4$	1.0031			
$\delta_c = P_0/14.7$	0.6827	0.6937	0.6792	0.6769
N_{REF} (Eq. 73), (rpm)	16,642			
$\dot{w}_{REF}$ (Eq. 74), (lbm/s)	3.9591			
$(HP)_{REF}$ (Eq. 75), (HP)	121.317			
M_{REF} (Eq. 76), (in.-lb)	459.45			

TABLE X (SHEET 1 OF 2) PERFORMANCE OF CENTRIFUGAL COMPRESSOR ROTOR

(MONROE CALCULATOR 1655/6)

ROTOR DIMENSIONS:

γ of Fluid = 1.4	A_2 = 21.0801 (in^2)	A_1 = 25.6685 (in^2)	R_{1o}/R_2 = 0.55	β_B = 50.32 (^{o})	k = 0.8599

SELECTED PARAMETERS	U_2/a_0	1	←	—	—	0.7156	—	—	—	→
	α_2	2	65	62	58	54	67	69	71	73
	k_{B2}	3	←	—	—	0.954	—	—	—	→
	k_{B1}	4	←	—	—	0.980	—	—	—	→
Eq. 82	ω	5	.85	.8325	.8088	.7844	.8616	.8732	.8847	.8963
ITERATION OF Ψ	No.=j	6	DESIGN POINT	FINAL	FINAL	FINAL	FINAL	FINAL	FINAL	FINAL
	Ψ_j	7	.7548	.788	.780	.781	.717	.6686	.6116	.548
PROGR.102	$\dot{w}\sqrt{(R_G/g)T_0}/P_0$	8	7.892 906	8.717 619	9.622 001	10.461 233	7.307 976	6.705 048	6.088 361	5.462 317
	Φ_2	9	.392 478	.433 488	.478 458	.520 190	.363 393	.333 412	.302 747	.271 616
	Φ_1	10	.313 769	.346 554	.382 506	.415 869	.290 516	.266 548	.242 032	.217 145
PROGR.103	P_1/P_0	11	.947 862	.935 492	.919 985	.903 564	.955 697	.963 010	.969 728	.975 796
PROGR.104	T_1/T_0	12	.984 817	.981 128	.976 454	.971 442	.987 136	.989 289	.991 256	.993 024
	V_1/a_0	13	.275 522	.307 180	.343 120	.377 877	.253 608	.231 421	.209 096	.186 761
	W_{1o}/a_0	14	.480 435	.499 264	.522 146	.545 615	.468 212	.456 577	.445 675	.435 643
	β_{1o} (^{o})	15	55.006	52.029	48.918	46.166	57.204	59.545	62.020	64.615
	β_{1o}' (^{o})	16	50.851	47.772	44.606	41.849	53.154	55.636	58.291	61.109
	M_{W1}	17	.4841	.5040	.5284	.5536	.4712	.4590	.4476	.4372
	i' (^{o})	18	+0.531	−2.548	−5.713	−8.471	+2.834	+ 5.316	+ 7.971	+10. 789
FIG. 24	η_R	19	.86	.8574	.80	.7396	.8514	.8373	.8187	.7964
PROGR.105	W_2/W_{1o}	20	.6312	.6783	.7405	.7991	.5976	.5617	.5229	.4813
	η_y	21	.4999	.4789	.2198	−.1250	.4747	.4300	.3699	.2977
	Ψ	22	.7548	.7878	.7802	.7817	.7170	.6686	.6116	.5480
PROGR.106	T_{t2}/T_0	23	1.174 108	1.170 524	1.165 669	1.160 671	1.176 484	1.178 860	1.181 216	1.183 592
	P_{t2}/P_0	24	1.676 382	1.657 610	1.605 044	1.554 246	1.683 471	1.687 492	1.688 961	1.688 362
	T_2/T_0	25	1.084 022	1.079 476	1.072 513	1.064 392	1.086 756	1.089 263	1.091 551	1.093 625
	P_2/P_0	26	1.267 734	1.248 524	1.199 174	1.147 873	1.275 311	1.279 641	1.281 213	1.280 258
	M_{V2}	27	.6446	.6494	.6590	.6725	.6425	.6413	.6409	.6413

TABLE X (SHEET 1 OF 2) PERFORMANCE OF CENTRIFUGAL COMPRESSOR ROTOR (MONROE 1655/6)

TABLE X (SHEET 2 OF 2) PERFORMANCE OF CENTRIFUGAL COMPRESSOR ROTOR

(MONROE CALCULATOR 1655/6)

ROTOR DIMENSIONS:

γ of Fluid = 1.4	A_2 = 21.0801 (in^2)	A_1 = 25.6685 (in^2)	R_{1o}/R_2 = 0.55	β_B = 50.32 (^{o})	k = 0.8599

SELECTED PARAMETERS	U_2/a_0	1	←				0.516			→
	α_2	2	65	62	58	54	50	67	69	71	73
	k_{B2}	3	←				0.954				→
	k_{B1}	4	←				0.98				→
Eq. 82	ω	5	.85	.8325	.8088	.7844	.7590	.8616	.8732	.8847	.8963
ITERATION OF Ψ	No.=j	6	FINAL	FINAL	FINAL	FINAL	FINAL	FINAL	FINAL	FINAL	FINAL
	Ψ_j	7	.7546	.7955	.8351	.8381	.840	.7111	.665	.612	.554
PROGR.102	$\dot{w}\sqrt{(R_G/g)T_0}/P_0$	8	5.265 458	5.875 178	6.653 236	7.384 474	8.099 555	4.881 731	4.478 169	4.070 451	3.660 138
	Φ_2	9	.262 822	.292 146	.330 835	.367 196	.402 754	.242 746	.222 679	.202 405	.182 002
	Φ_1	10	.210 114	.233 558	.264 488	.293 557	.321 984	.194 065	.178 022	.161 814	.145 503
PROGR.103	P_1/P_0	11	.977 378	.971 878	.963 604	.954 715	.944 912	.980 773	.983 875	.986 719	.989 292
PROGR.104	T_1/T_0	12	.993 483	.991 883	.989 463	.986 846	.983 941	.994 468	.995 366	.996 187	.996 929
	V_1/a_0	13	.180 505	.201 455	.229 532	.256 451	.283 366	.166 305	.152 213	.138 070	.123 921
	W_{1o}/a_0	14	.336 340	.348 033	.365 003	.382 504	.401 047	.328 937	.322 042	.315 604	.309 676
	β_{1o} (^{o})	15	57.542	54.631	51.035	47.898	45.044	59.630	61.793	64.057	66.411
	β_{1o}' (^{o})	16	53.511	50.460	46.755	43.579	40.735	55.727	58.047	60.500	63.079
	M_{W1}	17	.3374	.3494	.3669	.3850	.4043	.3298	.3228	.3162	.3101
	i' (^{o})	18	+ 3.191	+ 0.14	-3.565	-6.740	-9.584	+ 5.407	+ 7.727	+ 10.180	+ 12.759
FIG. 24	η_R	19	.856	.86	.86	.8204	.7680	.8428	.8315	.8164	.8006
PROGR.105	W_2/W_{1o}	20	.6502	.7017	.7639	.8220	.8761	.6134	.5742	.5325	.4882
	η_W	21	.4465	.4371	.3914	.1176	-.3847	.4102	.3813	.3386	.2936
	Ψ	22	.7547	.7955	.8350	.8381	.8394	.7111	.6655	.6119	.5541
PROGR.10[illegible]	T_{t2}/T_0	23	1.090 552	1.088 663	1.086 139	1.083 540	1.080 835	1.091 762	1.092 998	1.094 223	1.095 458
	P_{t2}/P_0	24	1.321 777	1.315 198	1.305 222	1.287 029	1.267 233	1.323 813	1.326 128	1.327 759	1.329 071
	T_2/T_0	25	1.043 687	1.041 323	1.037 703	1.033 481	1.028 559	1.045 108	1.046 412	1.047 602	1.048 680
	P_2/P_0	26	1.133 514	1.125 676	1.112 604	1.090 658	1.065 369	1.136 169	1.138 616	1.140 082	1.140 810
	M_{V2}	27	.473 705	.476 767	.483 096	.492 128	.504 107	.472 442	.471 802	.471 713	.472 264

TABLE X (SHEET 2 OF 2) PERFORMANCE OF CENTRIFUGAL COMPRESSOR ROTOR (MONROE 1655/6)

TABLE XI CALCULATED PERFORMANCE OF HYBRID COMPRESSOR AT 16,666 RPM

$T_0 = 520^\circ R$; $P_0 = 14.7/(p_6/P_0)$ (psia)

U_2/a_0	0.7156	0.7156	0.7156	0.7156
α_2	65.0000	62.0000	58.0000	54.0000
P_{t4}/P_0	1.5910	1.5722	1.5135	1.4235
P_4/P_0	1.5100	1.4708	1.3825	1.2527
T_4/T_0	1.1567	1.1485	1.1359	1.1190
M_{V4}	0.2743	0.3100	0.3620	0.4313
V_4/a_0	0.2951	0.3322	0.3858	0.4562
P_{t4}'/P_0	1.5803	1.5586	1.4958	1.4000
P_4'/P_0	1.4935	1.4504	1.3563	1.2193
P_{t4}''/P_0	1.5543	1.5262	1.4539	1.3458
P_4''/P_0	1.4689	1.4202	1.3184	1.1720
P_{t5}/P_0	1.5290	1.4946	1.4131	1.2924
P_{t6}/P_0	1.5050	1.4648	1.3752	1.2443
P_6/P_0	1.4646	1.4151	1.3122	1.1647
P_0 (psia)	10.0367	10.3883	11.2026	12.6209
$\dot{w}$ (lbm/s)	2.6978	3.0841	3.6709	4.4963
HP	82.9226	92.8442	107.3626	127.5371
N (rpm)	16,666.	16,666.	16,666.	16,666.
η_T	0.8149	0.8093	0.7587	0.6607

U_2/a_0	0.7156	0.7156	0.7156	0.7156
α_2	67.0000	69.0000	71.0000	73.0000
P_{t4}/P_0	1.5982	1.5997	1.5816	1.5264
P_4/P_0	1.5295	1.5423	1.5339	1.4867
T_4/T_0	1.1618	1.1666	1.1709	1.1747
M_{V4}	0.2513	0.2292	0.2096	0.1943
V_4/a_0	0.2709	0.2475	0.2268	0.2106
P_{t4}'/P_0	1.5892	1.5922	1.5754	1.5212
P_4'/P_0	1.5155	1.5306	1.5242	1.4786
P_{t4}''/P_0	1.5671	1.5737	1.5600	1.5084
P_4''/P_0	1.4944	1.5128	1.5093	1.4661
P_{t5}/P_0	1.5457	1.5558	1.5452	1.4961
P_{t6}/P_0	1.5252	1.5386	1.5308	1.4841
P_6/P_0	1.4907	1.5096	1.5066	1.4639
P_0 (psia)	9.8609	9.7375	9.7569	10.0417
$\dot{w}$ (lbm/s)	2.4541	2.2235	2.0230	1.8680
HP	76.4618	70.2088	64.7194	60.5433
N (rpm)	16,666.	16,666.	16,666.	16,666.
η_T	0.8123	0.8032	0.7723	0.6995

TABLE XII CALCULATED PERFORMANCE OF HYBRID COMPRESSOR AT 12,018 RPM

T_0= 520°R ; P_0= 14.7/(p_6/P_0) (psia)

U_2/a_0	0.5160	0.5160	0.5160	0.5160	0.516
α_2	65.0000	62.0000	58.0000	54.0000	50.000
P_{t4}/P_0	1.2824	1.2756	1.2642	1.2362	1.193
p_4/P_0	1.2414	1.2243	1.1969	1.1501	1.083
T_4/T_0	1.0805	1.0760	1.0693	1.0614	1.051
M_{V4}	0.2160	0.2429	0.2805	0.3228	0.374
V_4/a_0	0.2245	0.2520	0.2901	0.3326	0.383
P_{t4}'/P_0	1.2771	1.2689	1.2553	1.2246	1.178
p_4'/P_0	1.2330	1.2138	1.1833	1.1327	1.061
P_{t4}''/P_0	1.2639	1.2523	1.2337	1.1971	1.143
p_4''/P_0	1.2203	1.1980	1.1630	1.1072	1.029
P_{t5}/P_0	1.2511	1.2364	1.2127	1.1702	1.108
P_{t6}/P_0	1.2388	1.2210	1.1928	1.1450	1.077
p_6/P_0	1.2180	1.1952	1.1595	1.1029	1.024
P_0(psia)	12.0689	12.2989	12.6784	13.3279	14.346
$\dot{w}$ (lbm/s)	2.1724	2.4608	2.8726	3.3517	3.957
H P	34.7276	38.5173	43.6842	49.4315	56.478
N(rpm)	12,018.	12,018.	12,018.	12,018.	12,018
η_T	0.8135	0.8123	0.8042	0.7475	0.639

U_2/a_0	0.5160	0.5160	0.5160	0.5160	
α_2	67.0000	69.0000	71.0000	73.0000	
P_{t4}/P_0	1.2846	1.2870	1.2870	1.2811	
p_4/P_0	1.2498	1.2579	1.2630	1.2617	
T_4/T_0	1.0832	1.0859	1.0884	1.0907	
M_{V4}	0.1984	0.1810	0.1641	0.1479	
V_4/a_0	0.2065	0.1887	0.1712	0.1544	
P_{t4}'/P_0	1.2801	1.2832	1.2839	1.2786	
p_4'/P_0	1.2427	1.2519	1.2581	1.2577	
P_{t4}''/P_0	1.2689	1.2738	1.2761	1.2723	
p_4''/P_0	1.2318	1.2427	1.2505	1.2515	
P_{t5}/P_0	1.2580	1.2647	1.2687	1.2663	
P_{t6}/P_0	1.2475	1.2559	1.2614	1.2604	
p_6/P_0	1.2299	1.2411	1.2491	1.2504	
P_0(psia)	11.9526	11.8448	11.7683	11.7565	
$\dot{w}$ (lbm/s)	1.9871	1.8064	1.6313	1.4654	
HP	32.1903	29.6570	27.1356	24.6953	
N (rpm)	12,018.	12,018.	12,018.	12,018.	
η_T	0.8084	0.8037	0.7933	0.7683	

FIGURES

FIG. 1 HYBRID COMPRESSOR (SYMBOLS AND STATIONS)
(NOT TO SCALE)

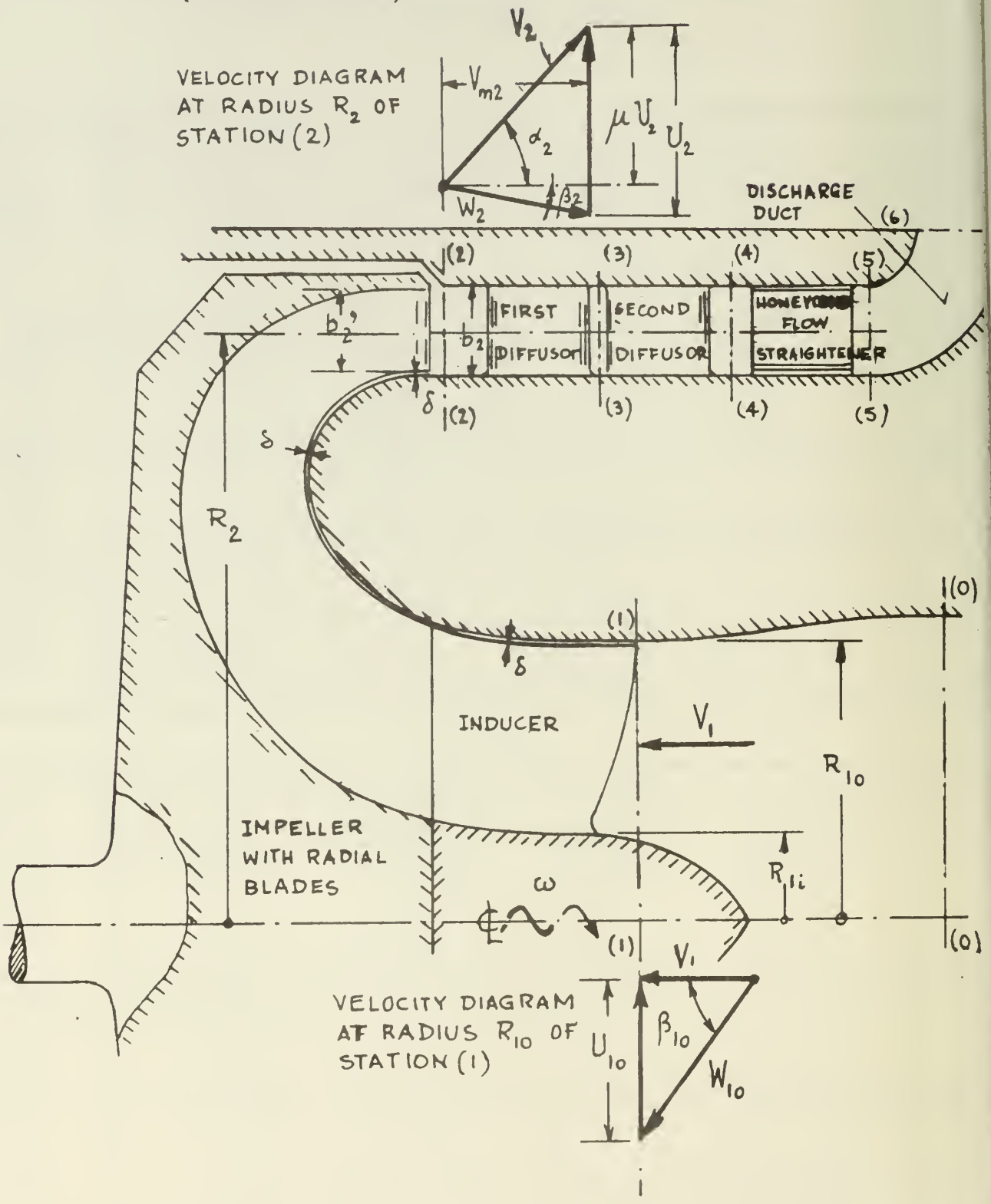

MHV 1/21/7

FIG. 2 DETERMINATION OF ROTOR HUB CONTOUR FOR SPECIFIED BLADE TIP CONTOUR

(TO SCALE)

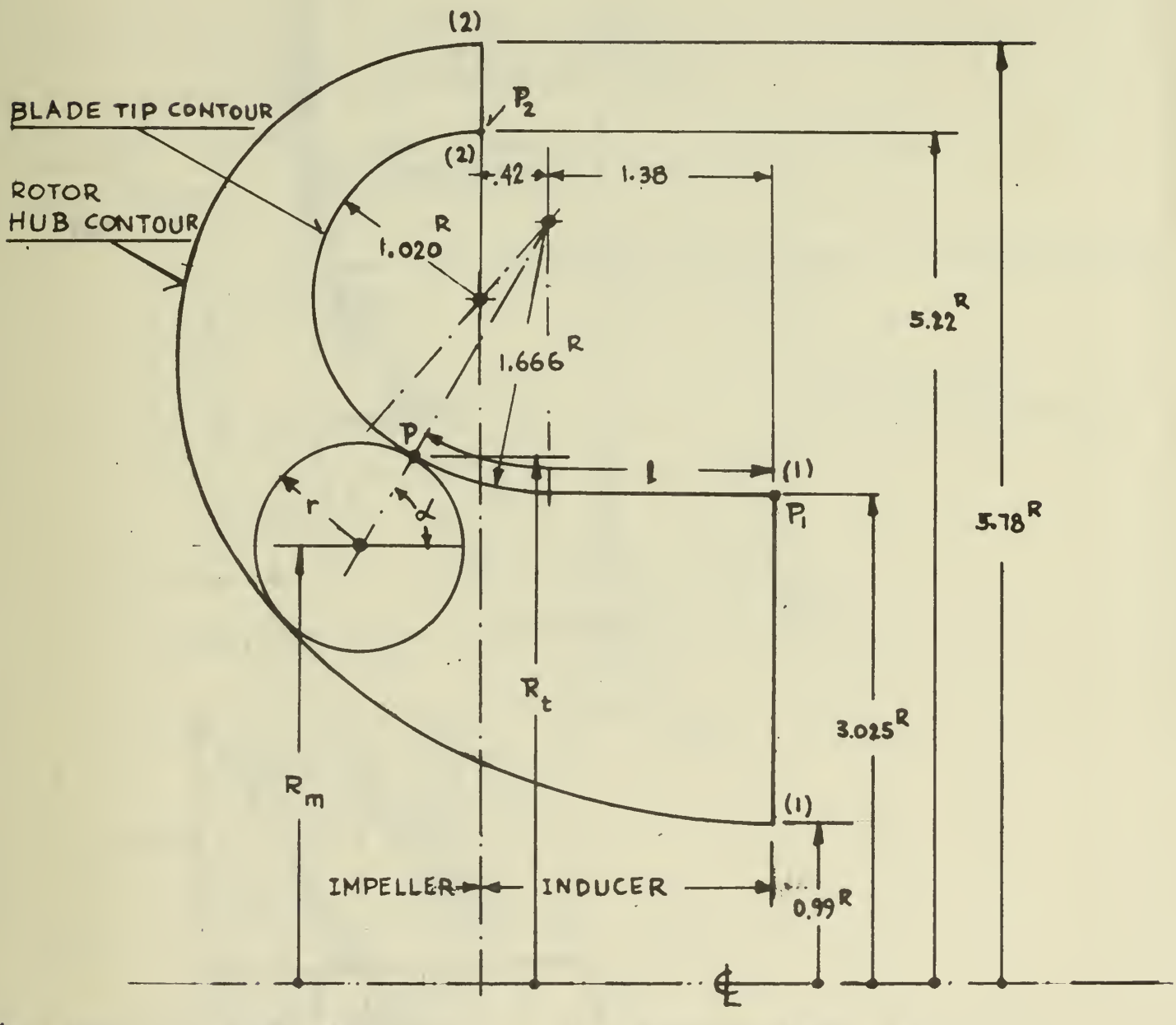

A_1 = ANNULUS AREA AT (1)-(1) ; A_2 = ANNULUS AREA AT (2)-(2)

AT POINT P: l = LENGTH OF TIP CONTOUR FROM P_1 TO P

l_o = LENGTH OF TIP CONTOUR FROM P_1 TO P2

$$A = 2\pi R_m r = A_1 - (A_1 - A_2)\frac{l}{l_o}$$

$$R_m = R_t - r \sin\alpha$$

$$r = \frac{R_t}{2\sin\alpha} - \sqrt{\left(\frac{R_t}{2\sin\alpha}\right)^2 - \frac{A_1 - (A_1 - A_2)(l/l_o)}{4\pi \sin\alpha}}$$

MHV 1/21/72

FIG. 3 CONDITIONS AT LEADING EDGE OF INDUCER

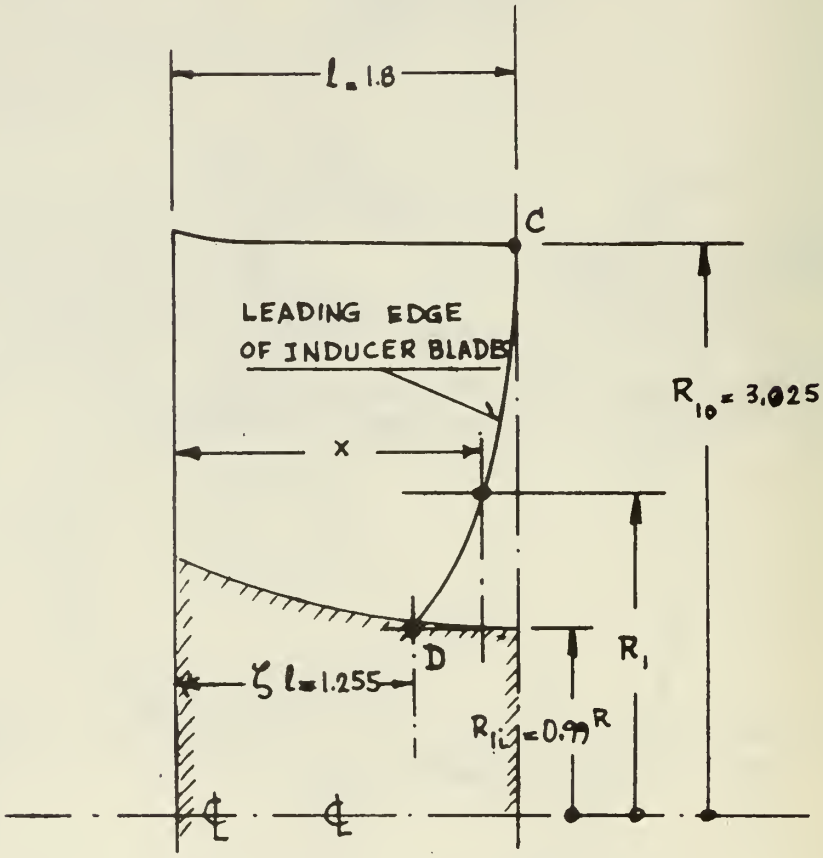

FIG. 3a MERIDIONAL CROSS-SECTION

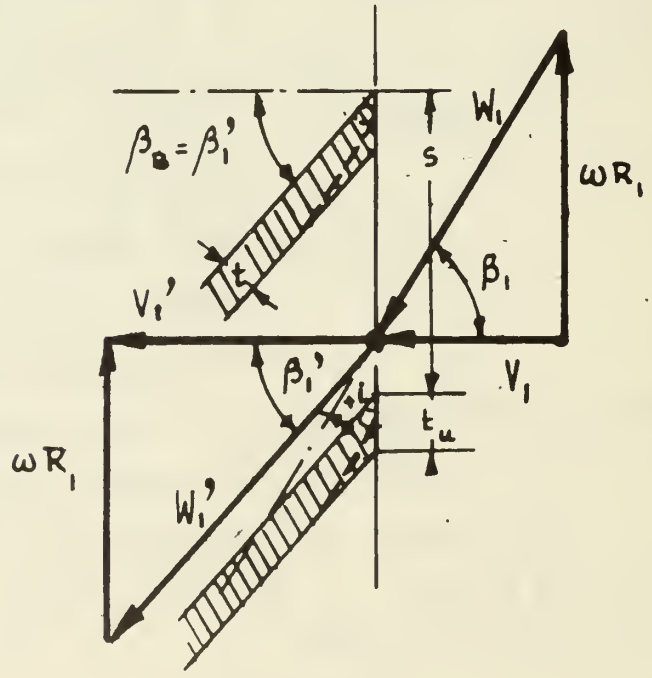

FIG. 3b CONDITIONS AT RADIUS R_1

FIG. 4 BLADE ANGLES OF STRAIGHT INDUCER BLADES

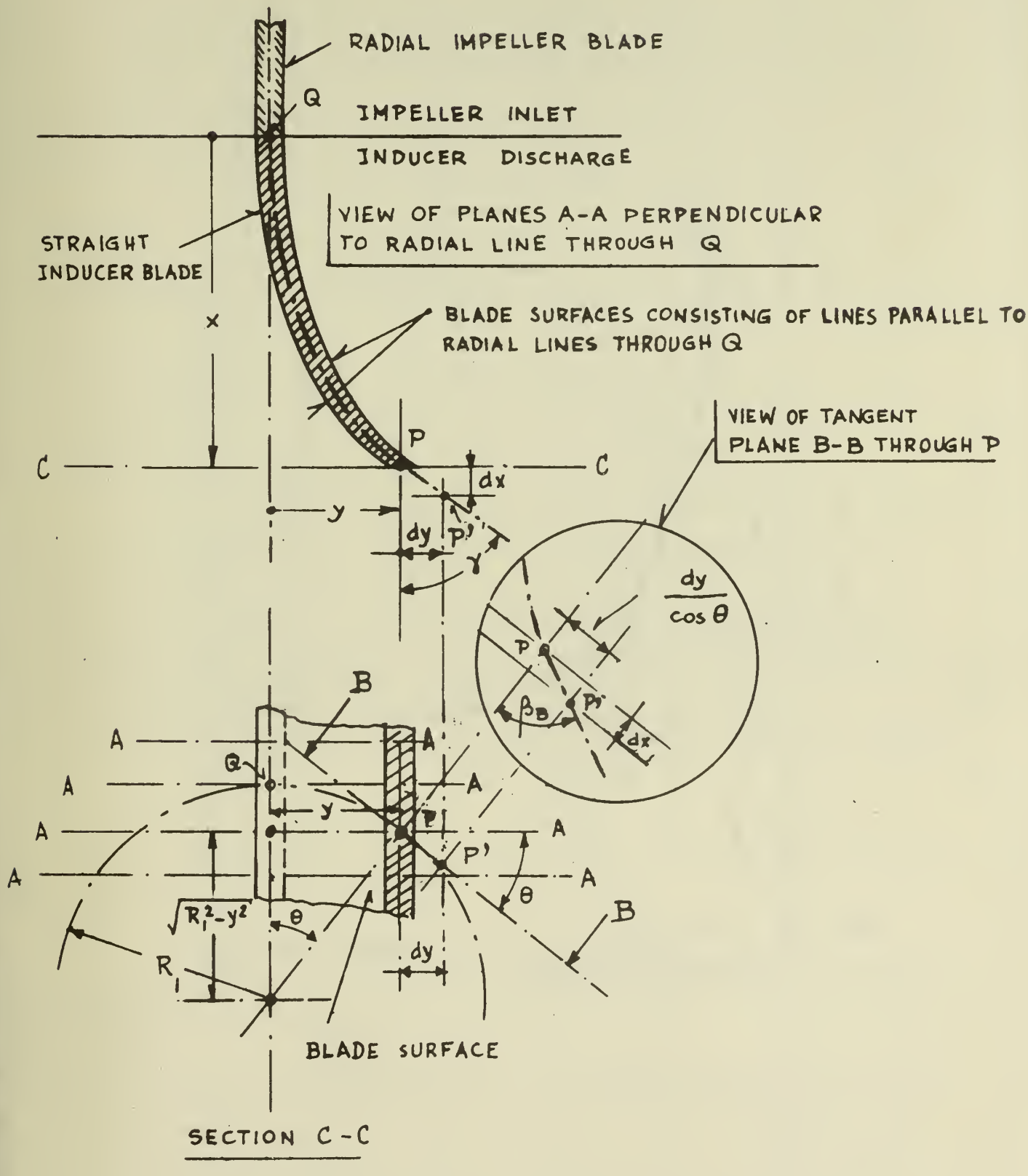

MHV 1/21/72

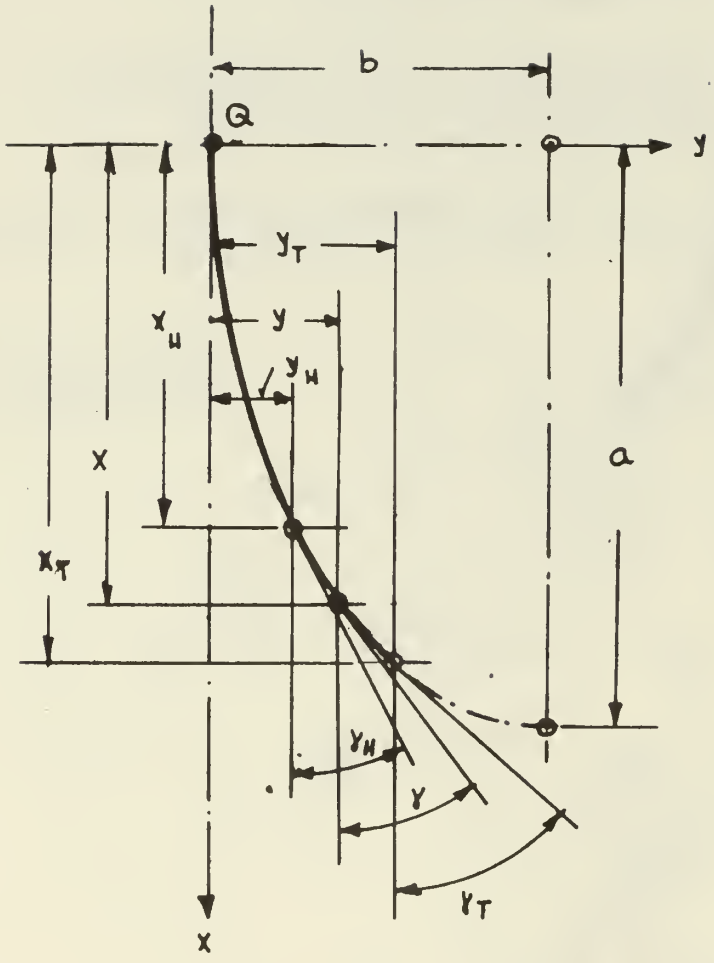

FIG. 5 PROPERTIES OF ELLIPTICAL INDUCER BLADE SURFACE

MHV 1/21/7

FIG. 6 SECONDARY LOSS COEFFICIENT OF REF. 6

Y_s'' = SECONDARY LOSS COEFFICIENT , Y_t'' = TOTAL LOSS COEFFICIENT

$\Delta\alpha$ = FLOW DEFLECTION (RADIANS)

c = BLADE CHORD , h = BLADE HEIGHT

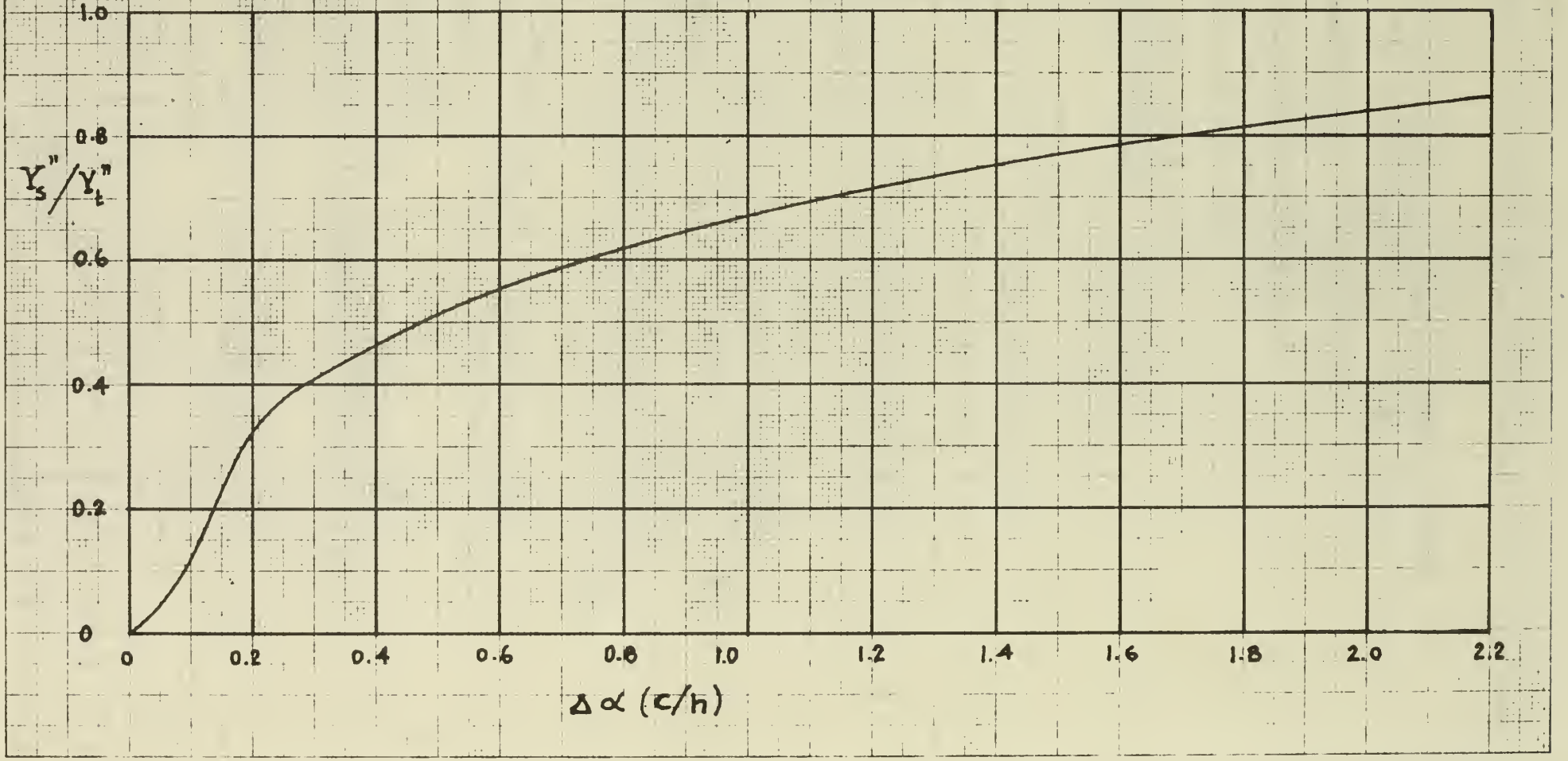

FIG. 7 OVERALL LOSS COEFFICIENTS Y_t', Y_t'' OF FIRST DIFFUSOR ROW

——— Y_t' WITH SECONDARY FLOW LOSSES OF EQ. 26

— — — Y_t'' WITH SECONDARY FLOW LOSSES FROM FIG. 6

$\Delta\alpha = \alpha_2 - \alpha_3 = 65° - \alpha_3$

$\sigma = \frac{\text{BLADE CHORD}}{\text{BLADE SPACING}}$

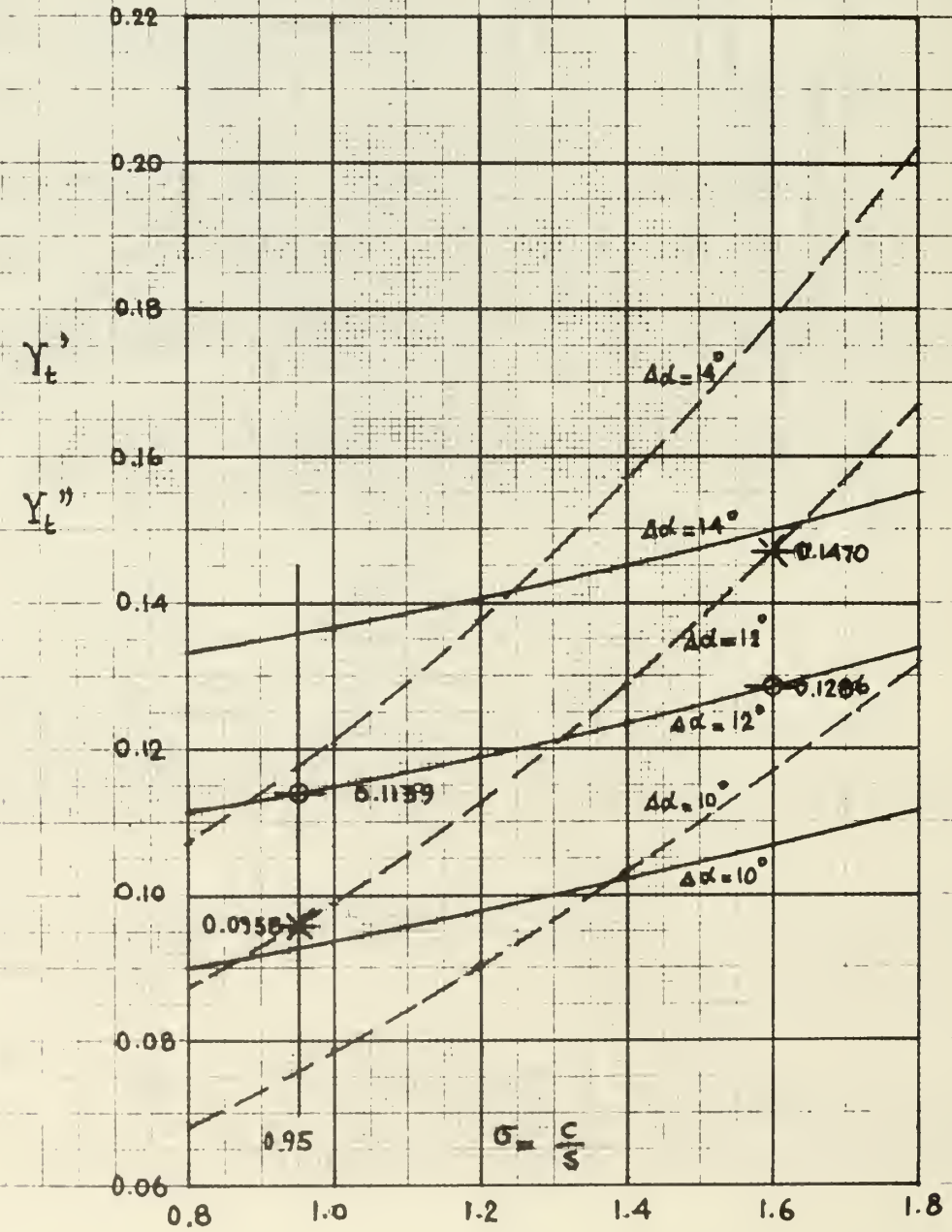

M.H.V

FIG. 8 OVERALL LOSS COEFFICIENTS Y_t', Y_t'' OF SECOND DIFFUSOR ROW

——— Y_t' WITH SECONDARY FLOW LOSSES OF EQ. 26

— — — Y_t'' WITH SECONDARY FLOW LOSSES FROM FIG. 6

$\Delta\alpha = \alpha_3 - \alpha_4 = 53° - \alpha_4$

$\sigma = \frac{\text{BLADE CHORD}}{\text{BLADE SPACING}}$

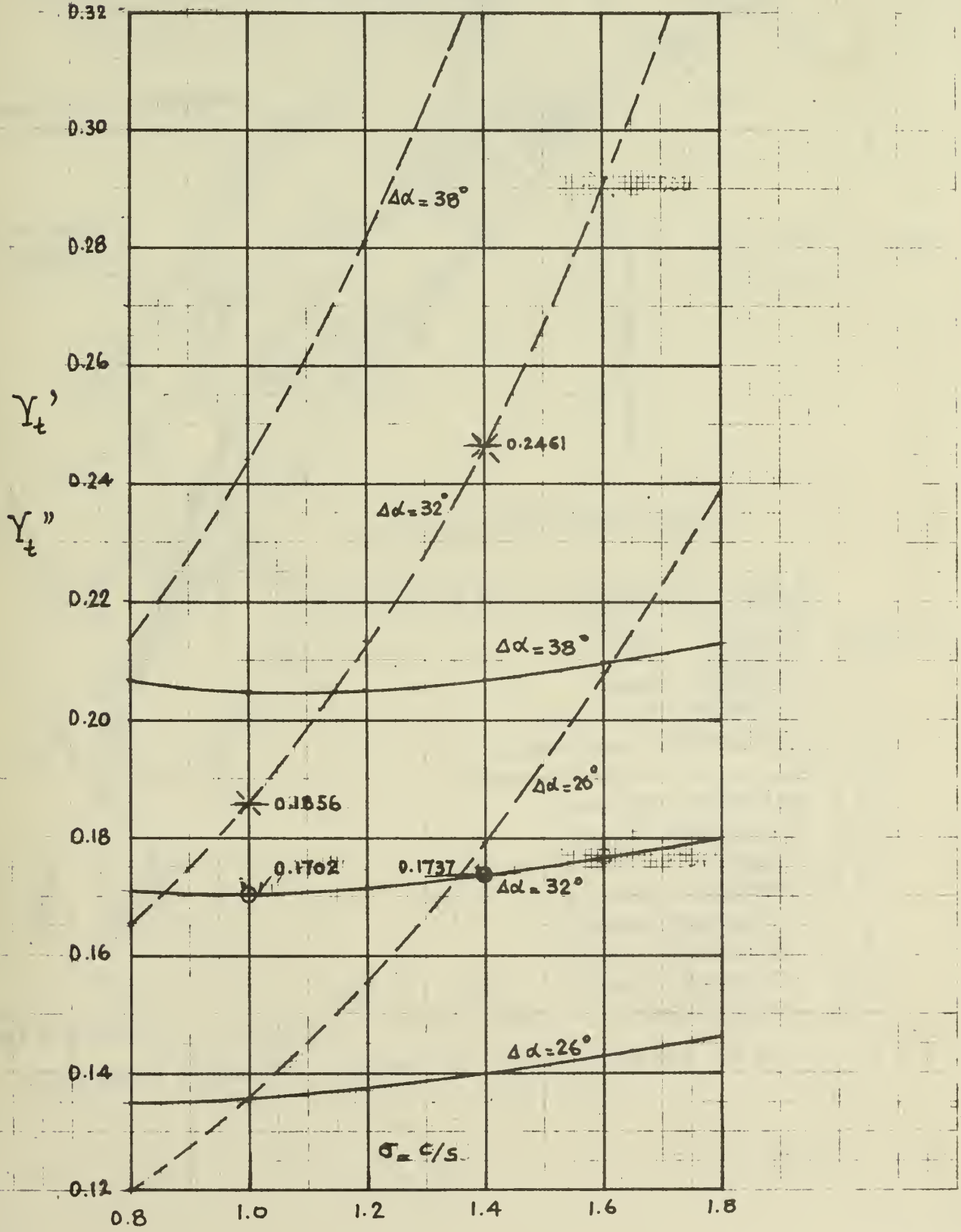

FIG. 9 DIFFUSOR BLADE DATA

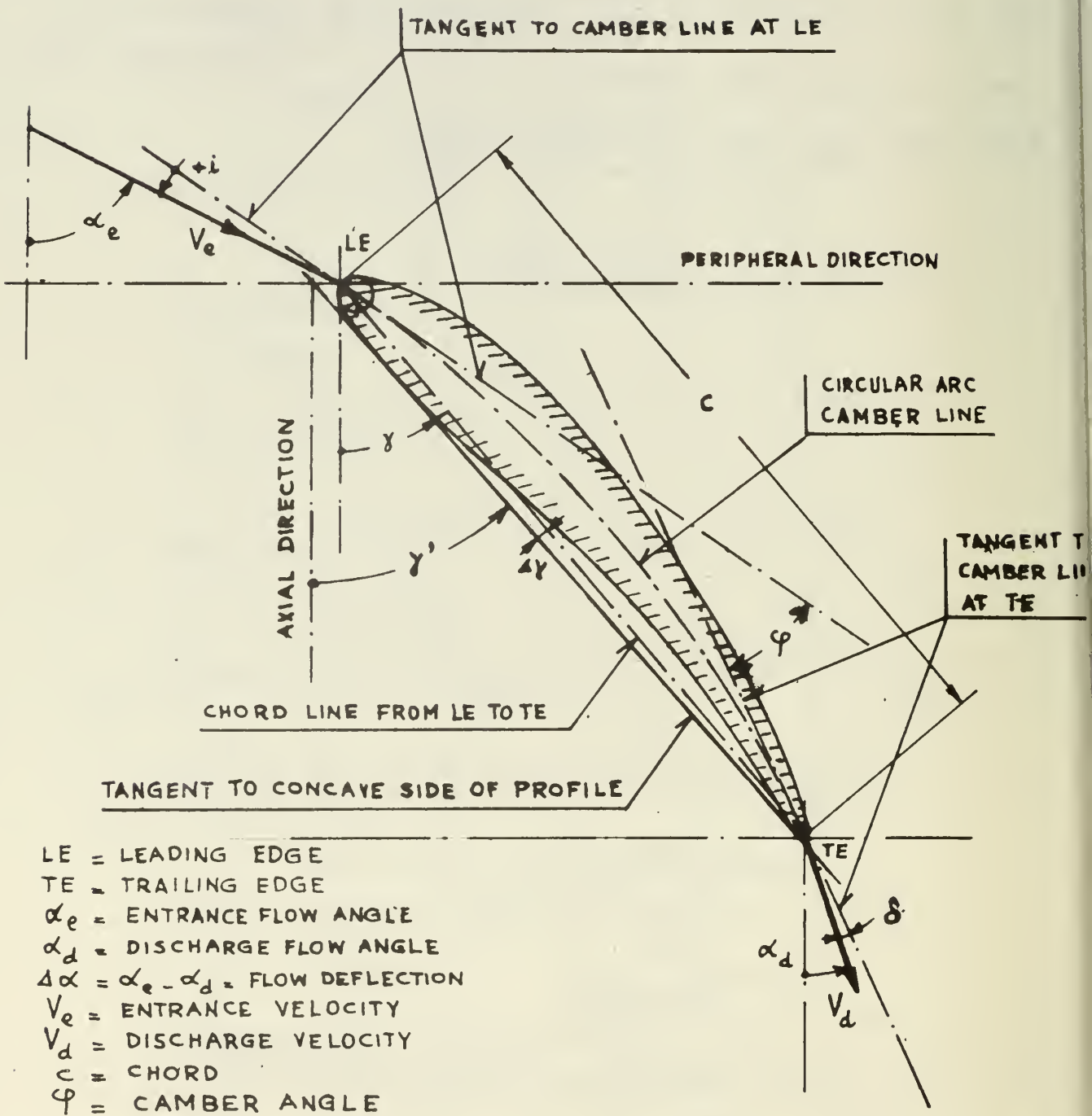

LE = LEADING EDGE
TE = TRAILING EDGE
α_e = ENTRANCE FLOW ANGLE
α_d = DISCHARGE FLOW ANGLE
$\Delta\alpha = \alpha_e - \alpha_d$ = FLOW DEFLECTION
V_e = ENTRANCE VELOCITY
V_d = DISCHARGE VELOCITY
c = CHORD
φ = CAMBER ANGLE
i = INCIDENCE ANGLE
δ = DEVIATION ANGLE
γ = STAGGER ANGLE $= \alpha_e - i - \varphi/2$
$\Delta\gamma$ = ANGLE BETWEEN CHORD LINE AND TANGENT TO CONCAVE PROFILE SIDE
$\gamma' = \gamma + \Delta\gamma$ = STAGGER ANGLE OF TANGENT TO CONCAVE PROFILE SIDE

M.H.V. 1/20

FIG. 10 DETERMINATION OF FLOW CONDITIONS AFTER DIFFUSOR ROW

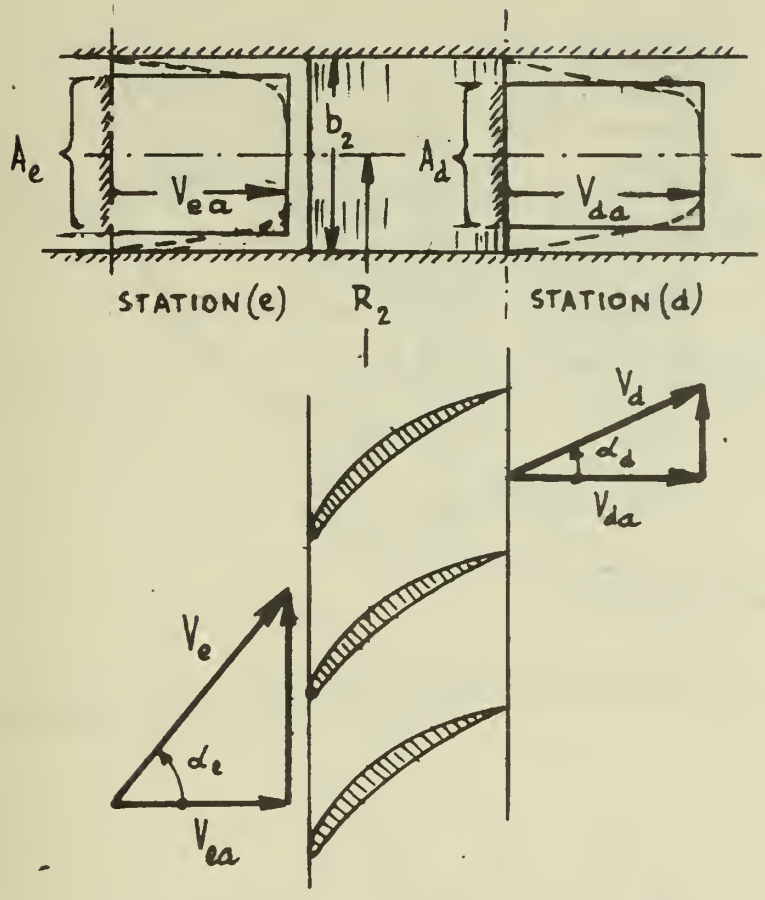

FIG. 10a. MERIDIONAL SECTION

FIG. 10b. DEVELOPED CASCADE AT RADIUS R_2

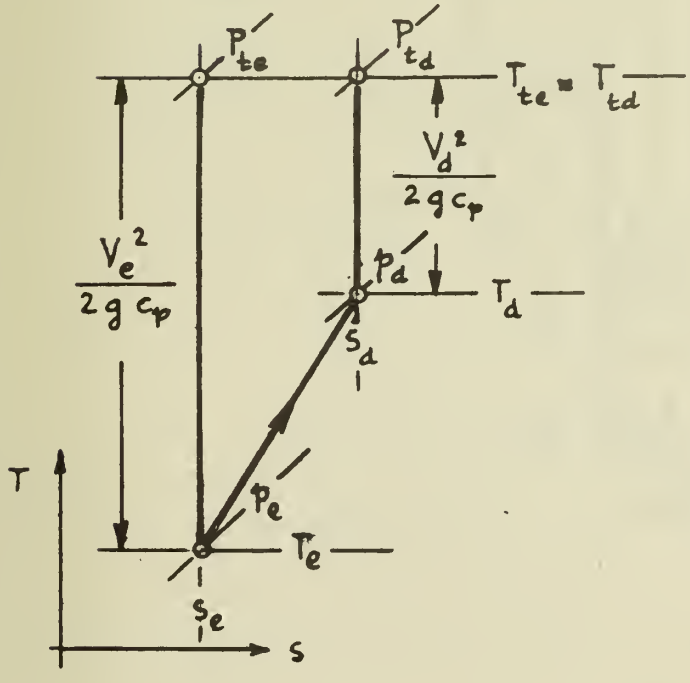

FIG 10 c. PROCESS IN ENTROPY DIAGRAM

MHV 1/21/72

FIG. 11 CONDITIONS IN FLOW STRAIGHTENER AND DISCHARGE DUCT

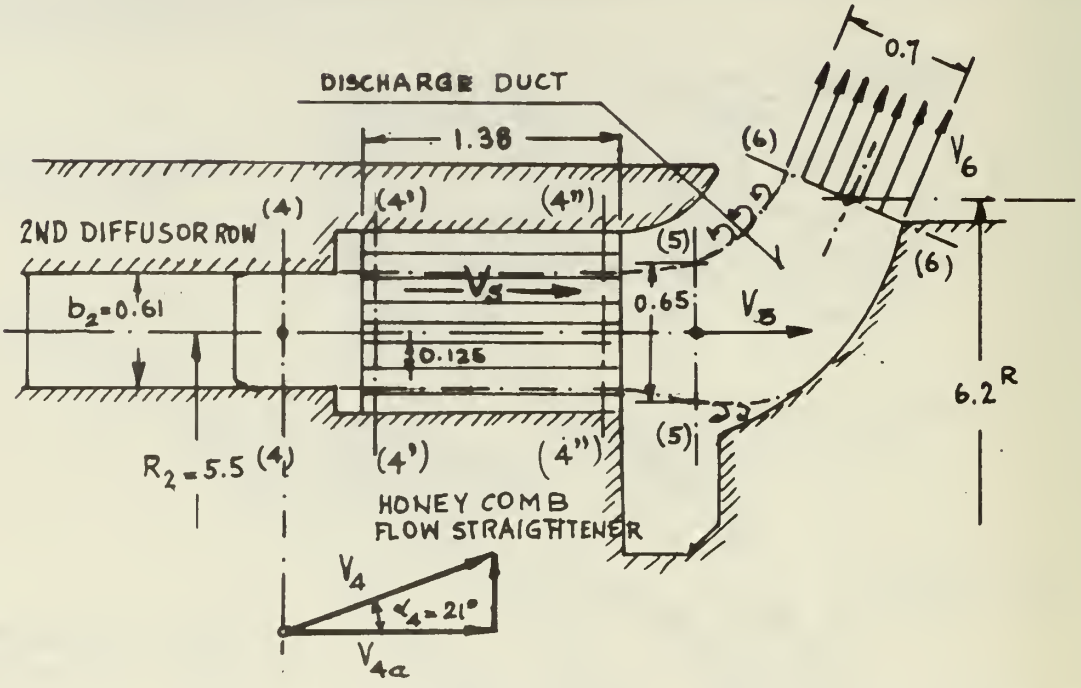

FIG. 11a FLOW STRAIGHTENER AND DISCHARGE DUCT GEOMETRY

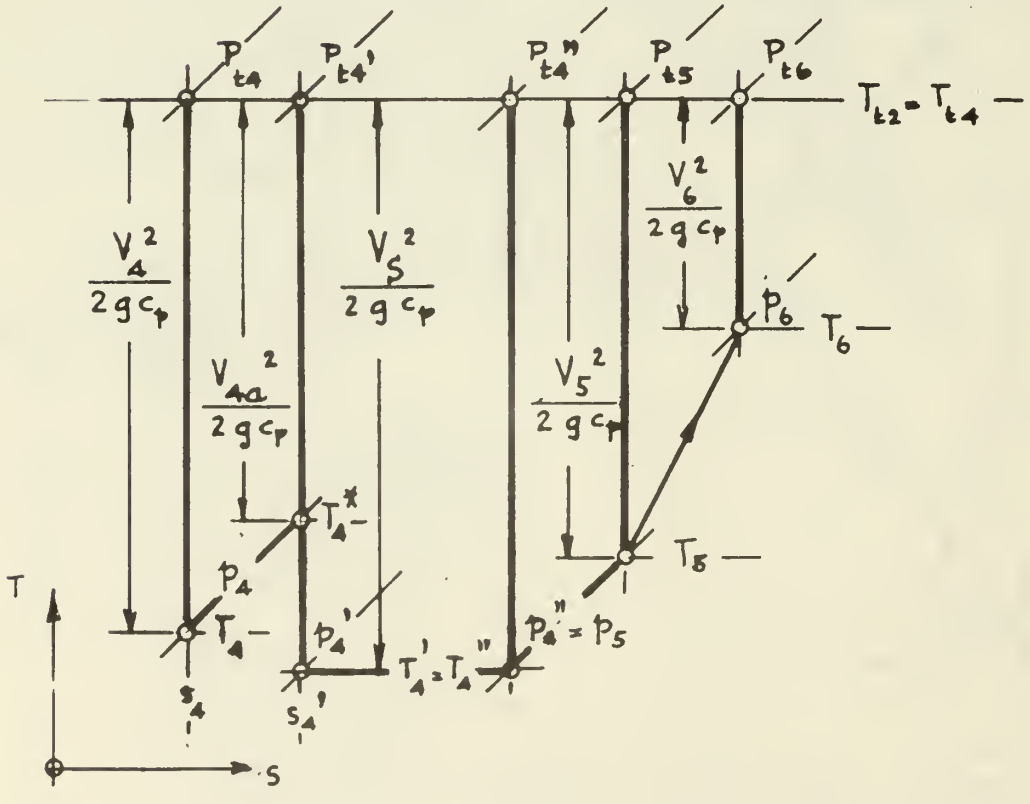

FIG. 11b FLOW PROCESS REPRESENTED IN ENTROPY DIAGRAM

MHV 1/21/1

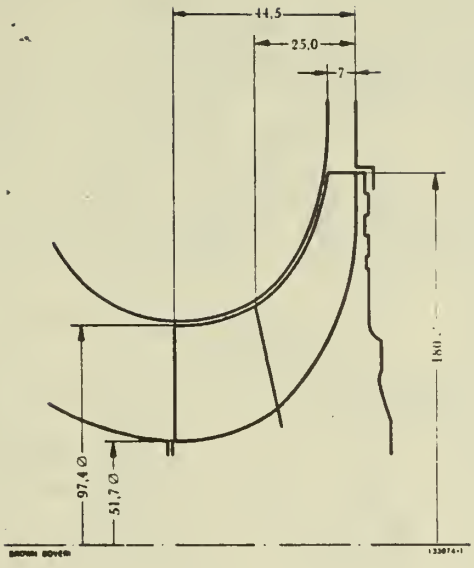

FIG. 12 ROTOR DIMENSIONS

Fig. 12 is identical with Fig. 2 of Ref. 10
(Dimensions are in millimeters)

$$R_{1o}/R_2 = 97.4/180 = 0.541$$

$$R_{1i}/R_2 = 51.7/180 = 0.287$$

$$b_2/R_2 = 7/90 = 0.078$$

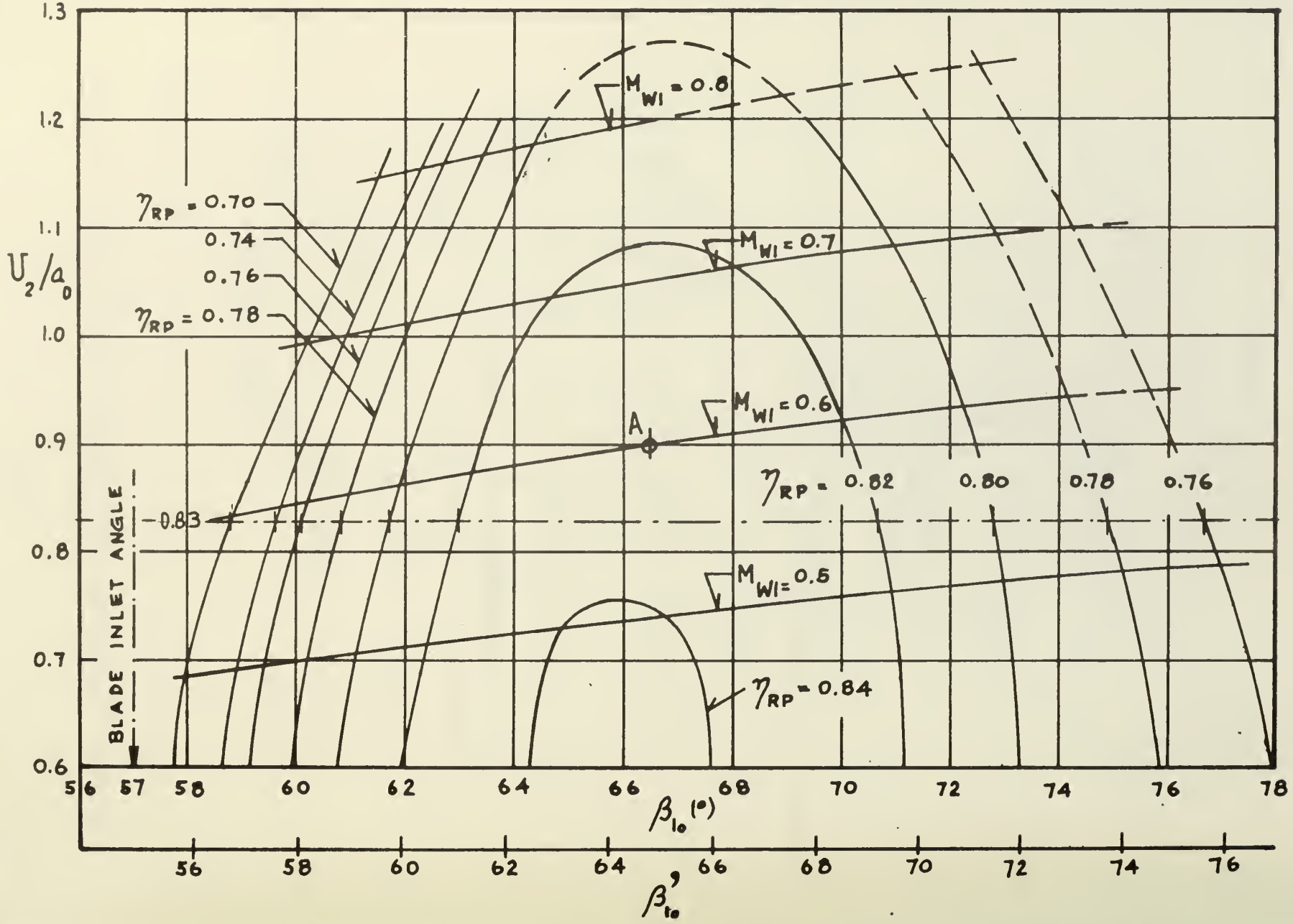

FIG. 13 POLYTROPIC ROTOR EFFICIENCY η_{RP} AS FUNCTION OF FLOW ANGLE β_{1o} AT INDUCER TIP RADIUS AND SPEED RATIO U_2/a_0 (ADAPTED FROM FIG.4 of REF.10)

FIG. 14. ARC LENGTH OF PARABOLIC MEAN CAMBER LINE OF INDUCER BLADE OF AXIAL LENGTH L AND BLADE ANGLE β_B AT LEADING EDGE LE

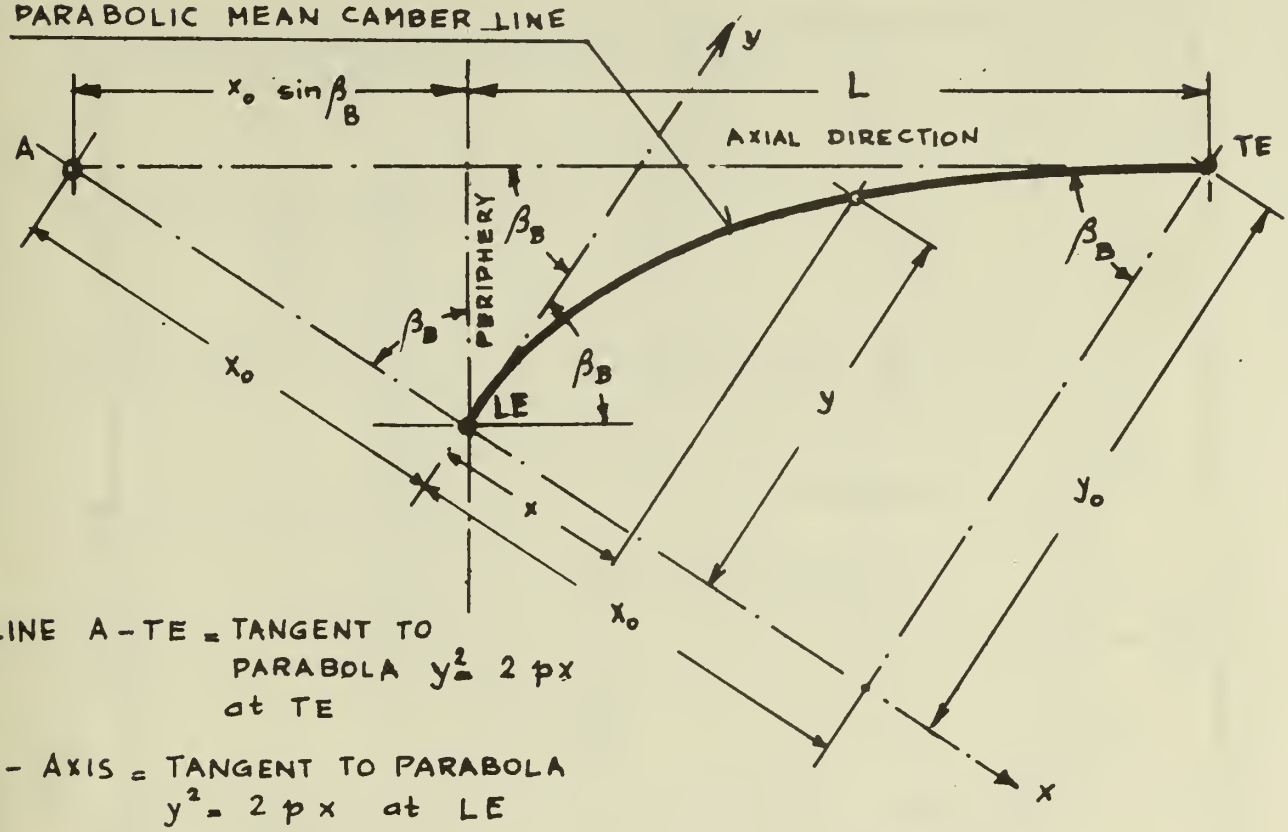

LINE A-TE = TANGENT TO PARABOLA $y^2 = 2px$ at TE

y- AXIS = TANGENT TO PARABOLA $y^2 = 2px$ at LE

$$\tan\beta_B = \frac{2x_o}{y_o} \rightarrow y_o = 2x_o \cot\beta_B$$

$$p = \frac{y_o^2}{2x_o} = 2x_o \cot^2\beta_B$$

$$(x_o \sin\beta_B + L)\sin\beta_B = 2x_o \rightarrow x_o = \frac{L}{(2/\sin\beta_B) - \sin\beta_B}$$

$$p = \frac{2L\cot^2\beta_B}{(2/\sin\beta_B) - \sin\beta_B}$$

m = ARC LENGTH OF CAMBER LINE FROM LE TO TE

$$m = \frac{p}{2}\left\{\sqrt{\frac{2x_o}{p}\left(1+\frac{2x_o}{p}\right)} + \ln\left(\sqrt{\frac{2x_o}{p}} + \sqrt{\left(1+\frac{2x_o}{p}\right)}\right)\right\}$$

EXAMPLE : $\beta_B = 57°$, $L = 19.5$

$x_o = 12.61$ $\quad y_o = 16.38$ $\quad p = 10.64$ $\quad m = 21.51$

M.H.V. 2/7/72

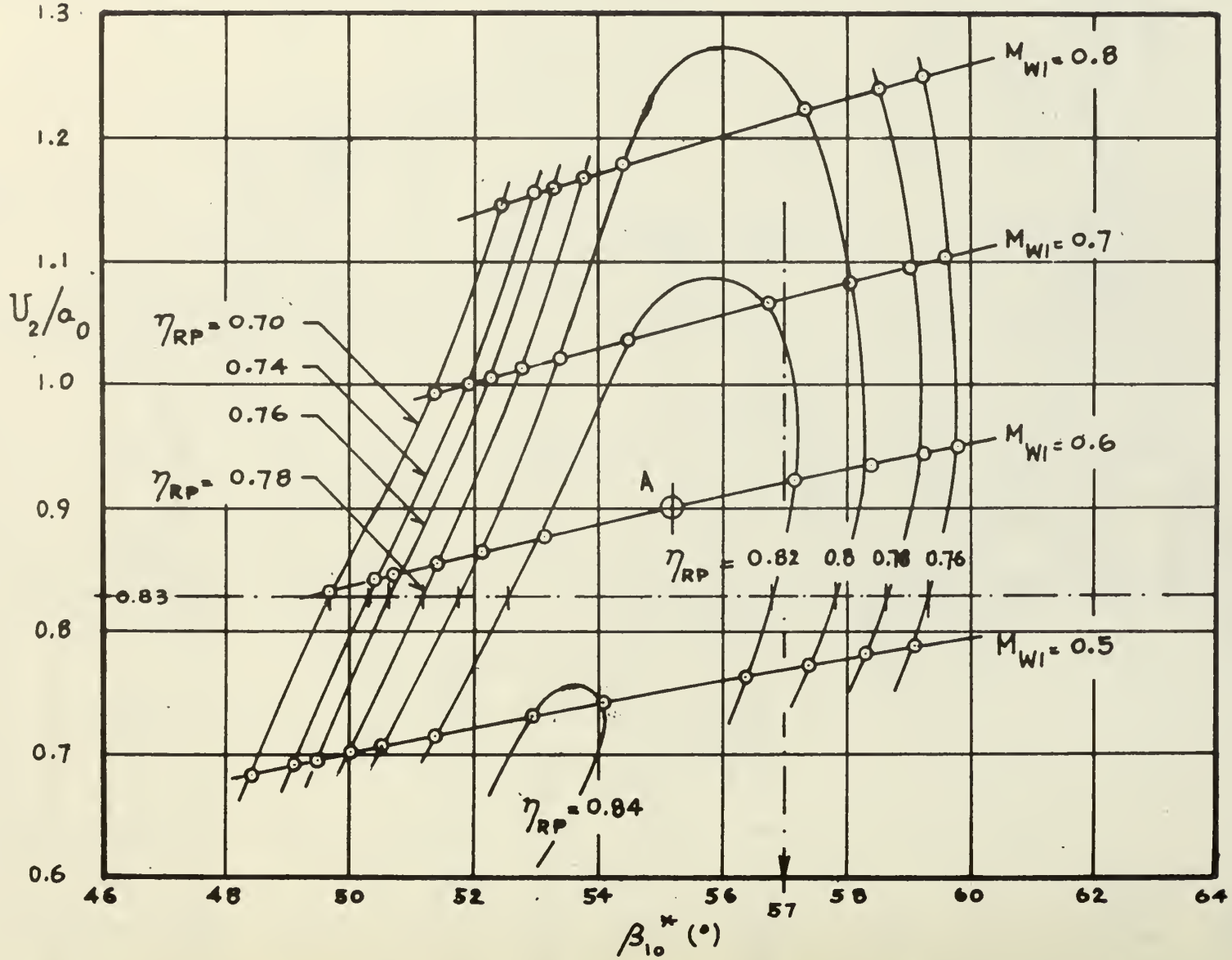

FIG. 15 FLOW ANGLE β_{1o}^* CALCULATED FROM EQ.C(4) FOR VALUES OF U_2/a_0 AND M_{W1} OF FIG. 13 FOR R_{1o}/R_2 = 97.4/180 = 0.541 IN ACCORDANCE WITH FIG. 12

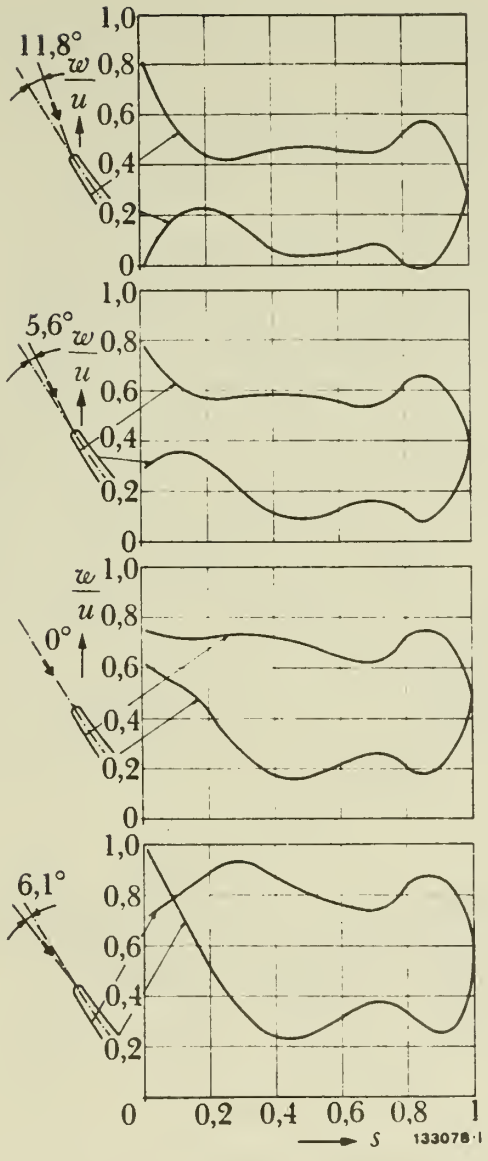

FIG. 16 VELOCITY DISTRIBUTIONS AT INDUCER TIP AT DIFFERENT INCIDENCE ANGLES

w = Relative velocity on blade surface

u = Peripheral speed

s = Distance along parabolic camber line of inducer

(Fig. 16 is identical with Fig. 5 of Ref. 10 and presents velocity distributions that are calculated by ignoring blade thickness, compressibility effects, and friction)

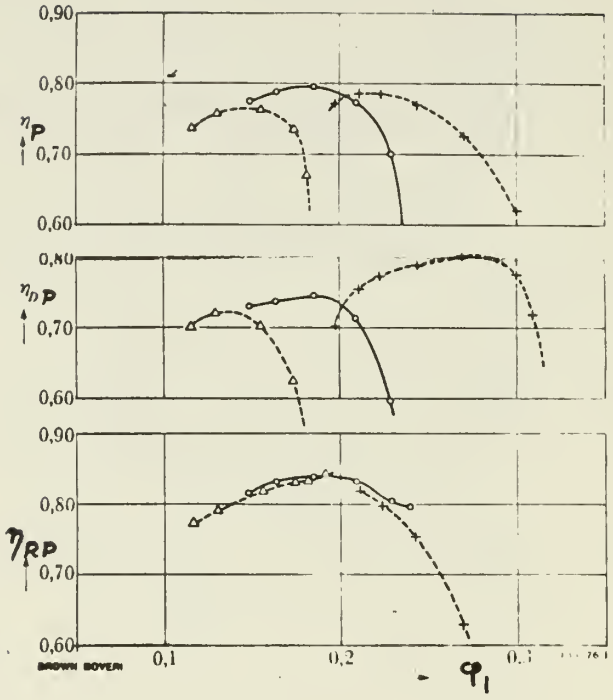

FIG. 17 COMPRESSOR PERFORMANCE AT U_2/a_0 = 0.83 OF ROTOR OF FIG. 12 WITH THREE DIFFERENT DIFFUSORS
(Adapted from Fig. 3 of Ref. 10)

η_{RP} = Polytropic Rotor Efficiency

η_{DP} = Polytropic Diffusor Efficiency

η_P = Polytropic Compressor Efficiency

$\varphi_1 = Q_1/(U_2 R_2^2)$

Q_1 = Volume Flow Rate at Inducer Inlet

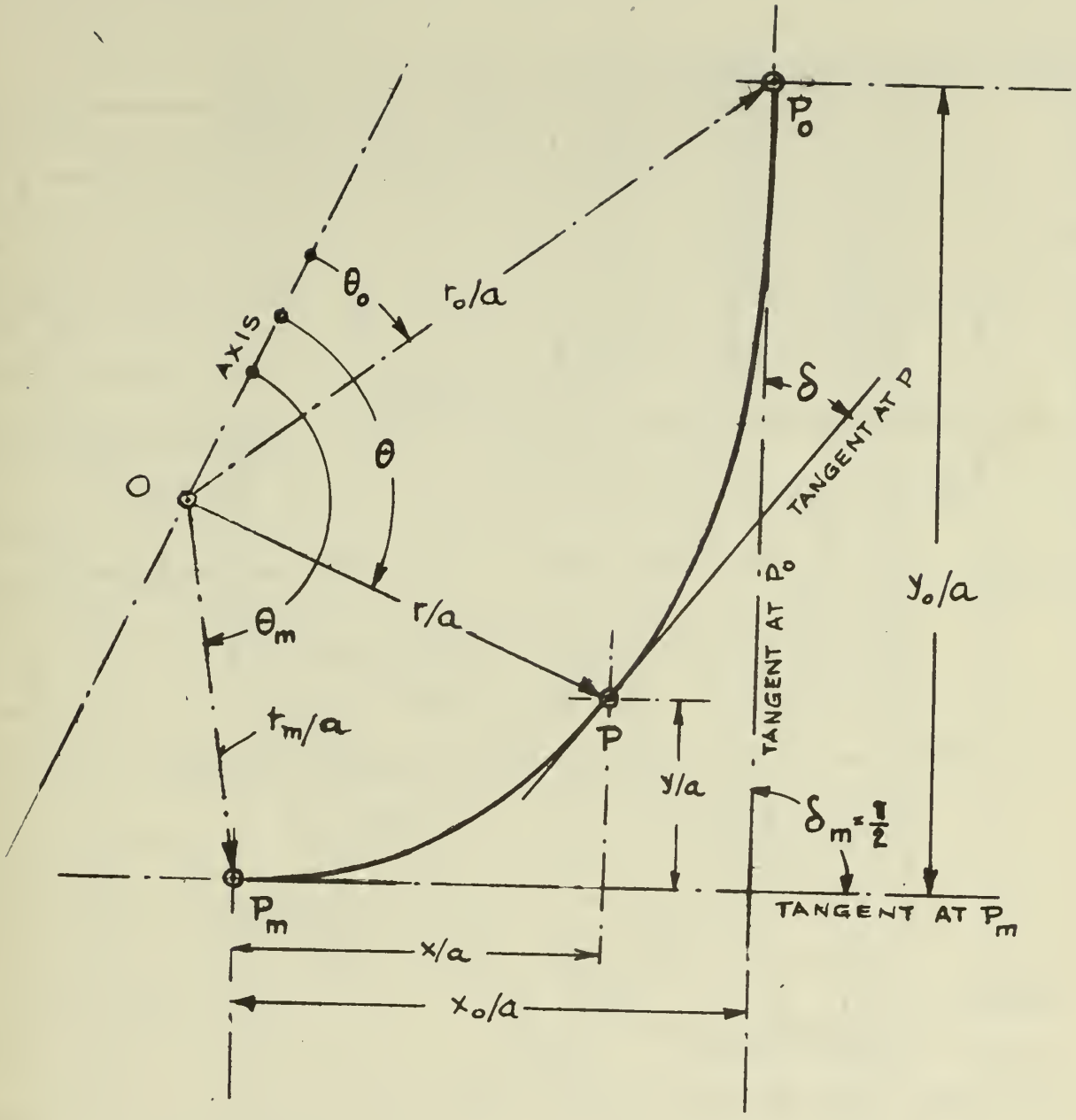

FIG. 18 MERIDIAN CURVE $r/a = \theta^{-b}$ with $\delta_m = \pi/2$

M.H.V. 3/10/42

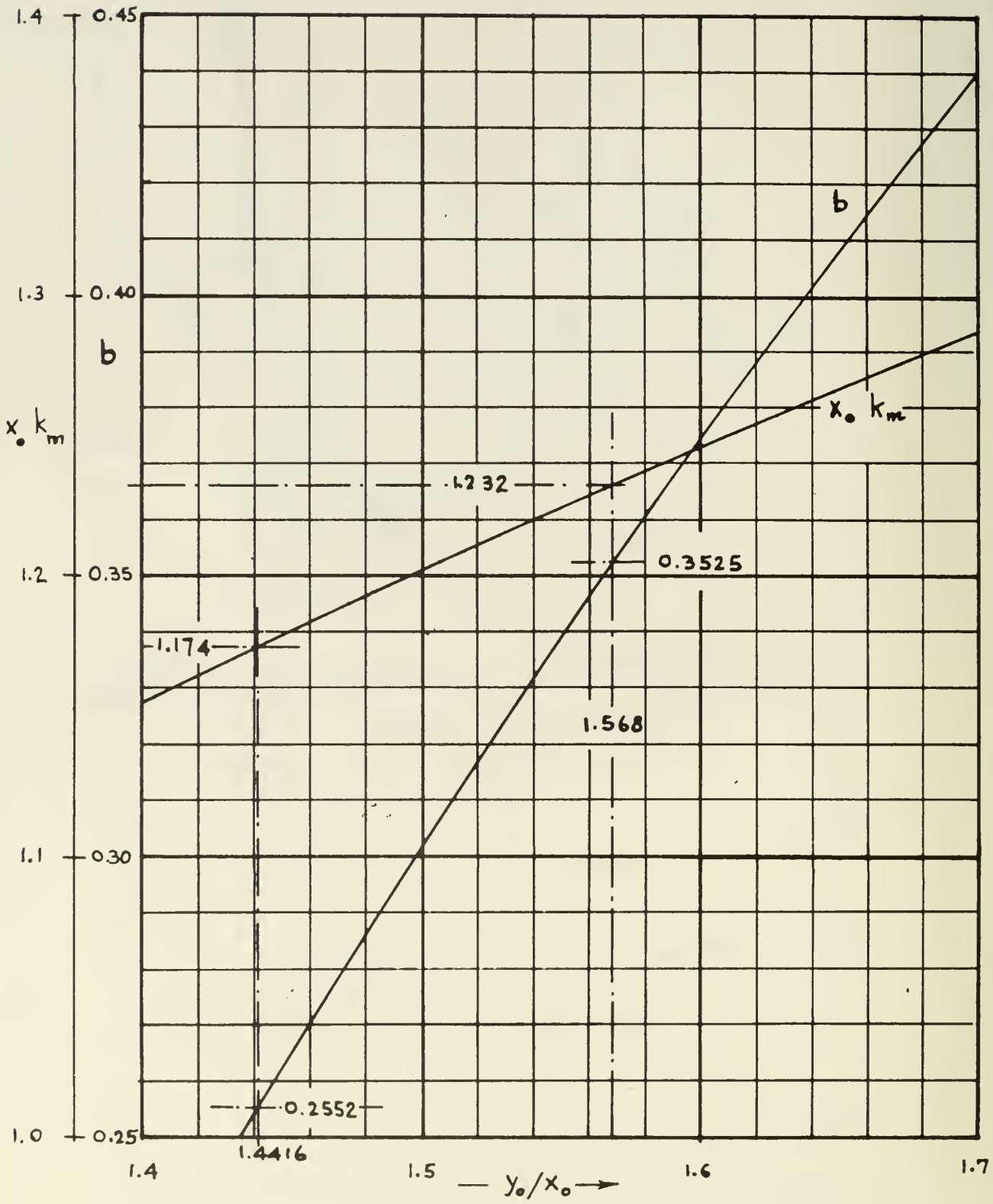

FIG. 19 RELATIONSHIP BETWEEN y_o/x_o, $x_o\ k_m$ AND y_o/x_o FOR MERIDIAN CURVE OF FIG. 18 CALCULATED WITH PROGRAM No. 110 OF APPENDIX D

M.H.V. 3/14/72

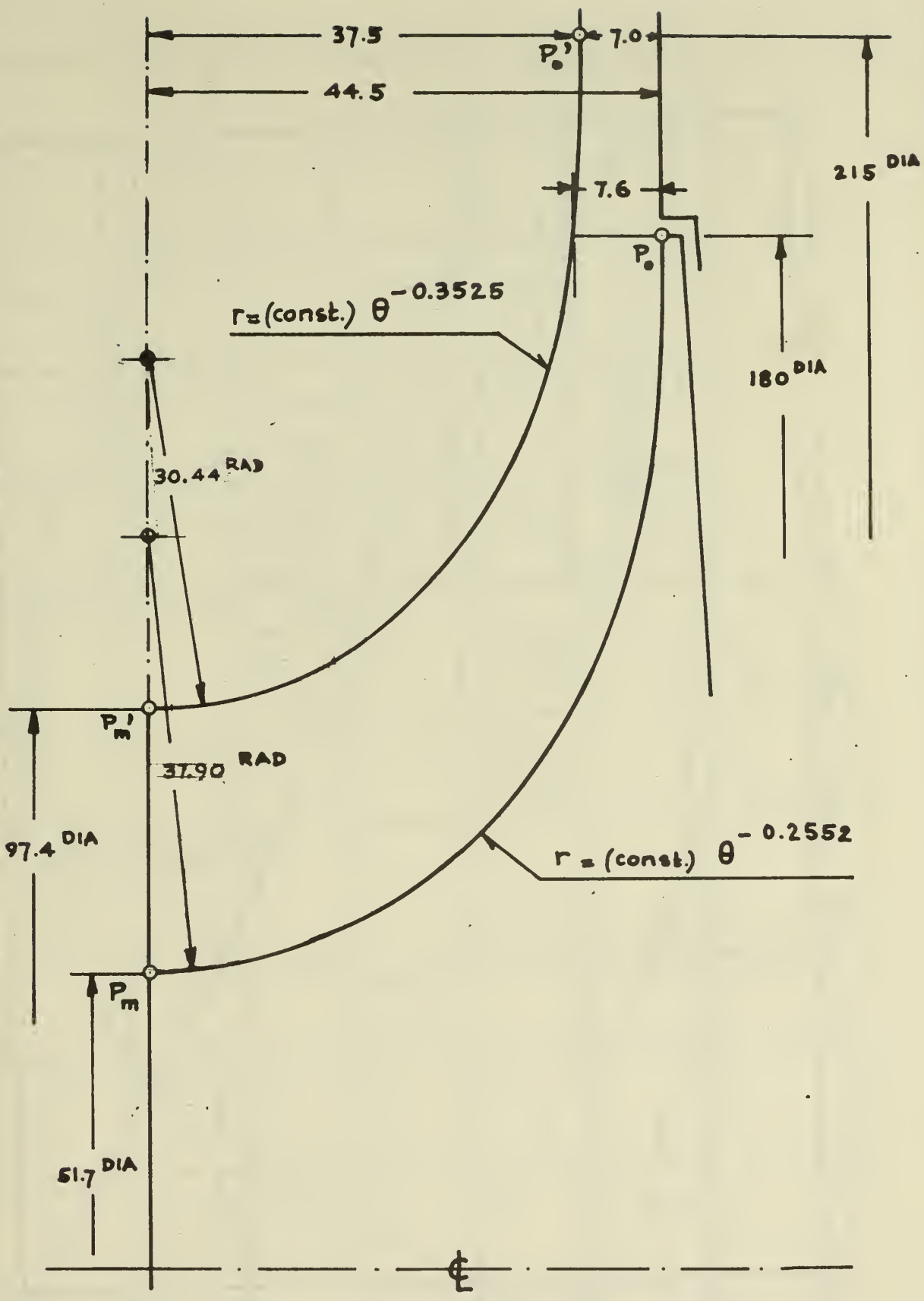

FIG. 20 SCALE DRAWING (2:1) OF MERIDIAN CONTOURS WITH $r/a=\theta^{-b}$ OF IMPELLER OF FIG. 12 THROUGH POINTS P_o, P_m, P_o', P_m'.

(Dimensions are in Millimeters)

M.H.V. 3/15/72

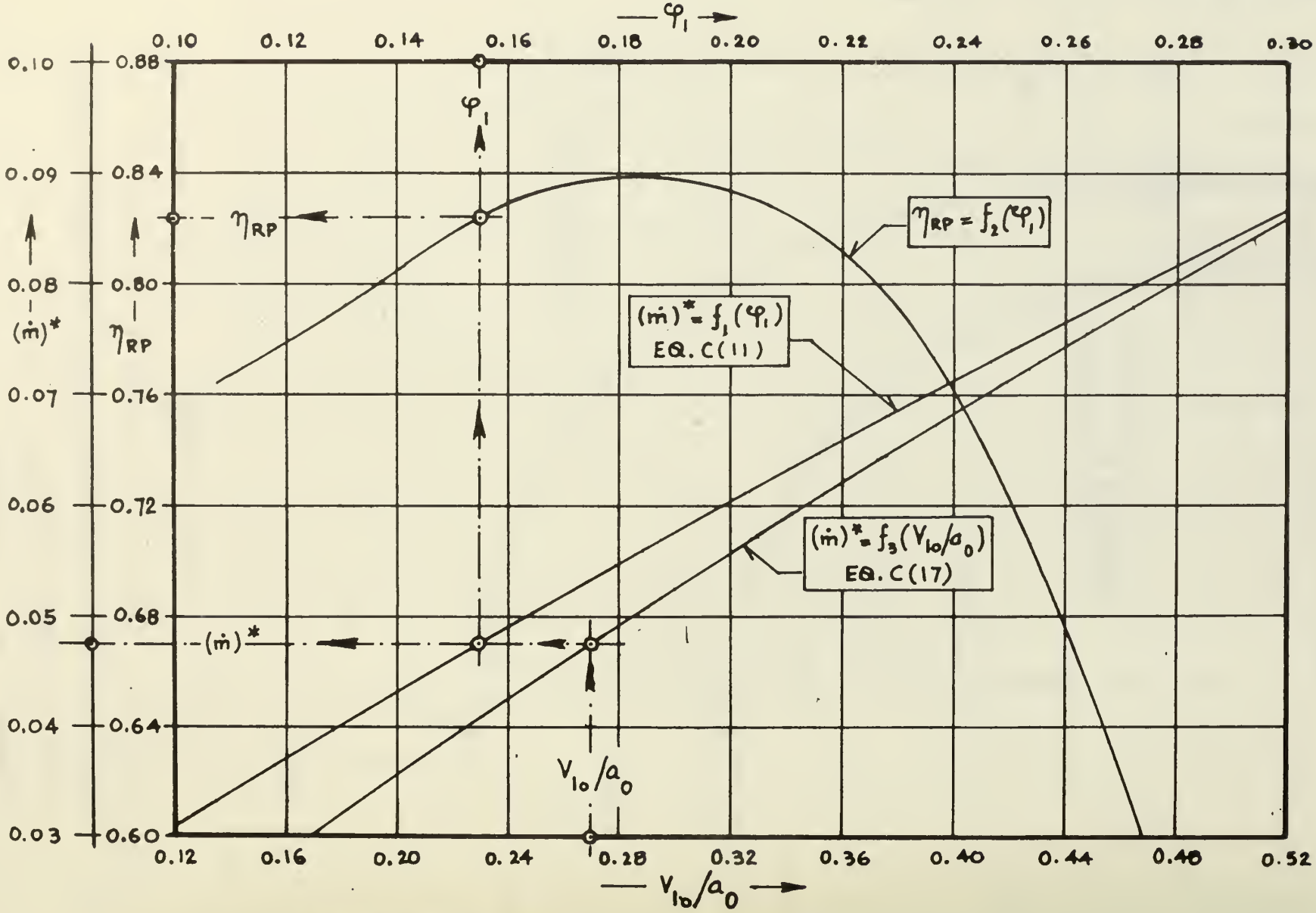

FIG. 21 DIMENSIONLESS MASS FLOW RATE $(\dot{m})^*$ AS FUNCTIONS OF FLOW FUNCTION φ_1 OF FIG. 17, AND V_{1o}/a_0 CALCULATED FROM EQ. C(17), WITH POLYTROPIC ROTOR EFFICIENCY η_{RP} FROM FIG. 17 FOR $U_2/a_2 = 0.83$.

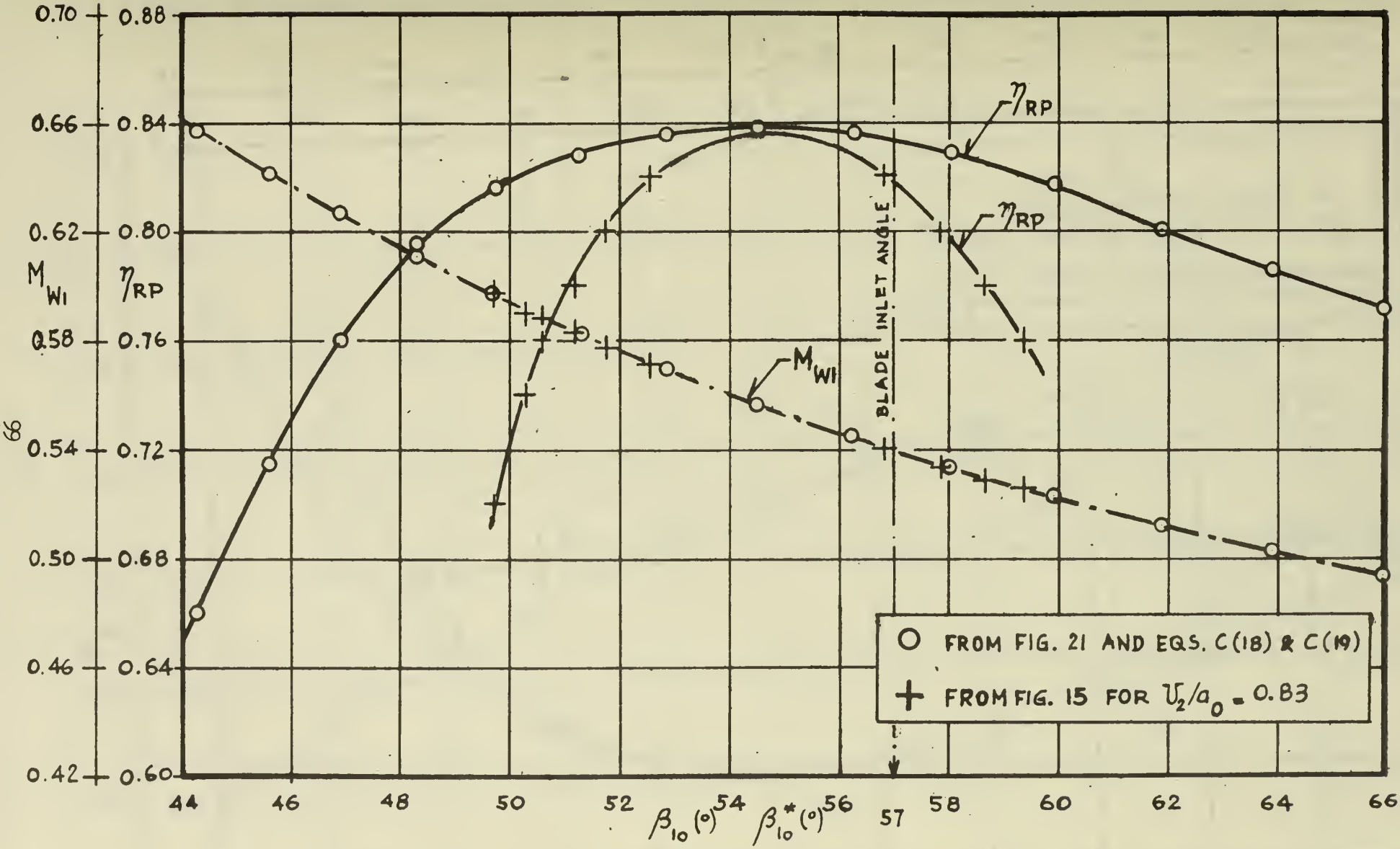

FIG. 22 POLYTROPIC ROTOR EFFICIENCY η_{RP} AND MACH NUMBER M_{W1} FROM FIGS. 21 AND 15, AS FUNCTIONS OF FLOW ANGLE β_{1o}, FOR $U_2/a_0 = 0.83$

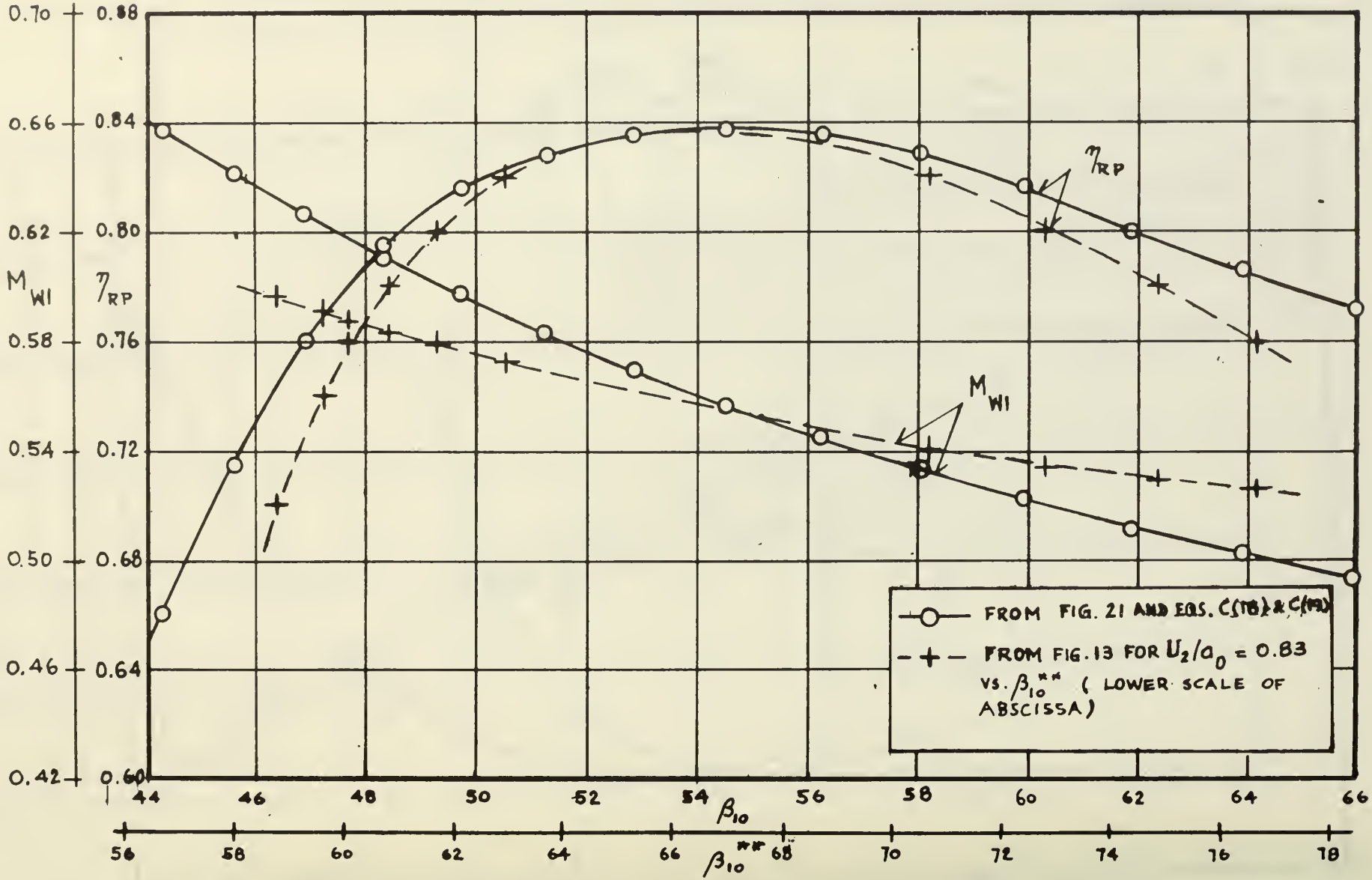

FIG. 23 POLYTROPIC ROTOR EFFICIENCY η_{RP} AND MACH NUMBER M_{W1} AS FUNCTION OF FLOW ANGLE FROM FIG. 21 (UPPER SCALE FOR β_{10}) AND FIG. 13 FOR $U_2/a_0 = 0.83$ (LOWER SCALE FOR β_{10}^{**})

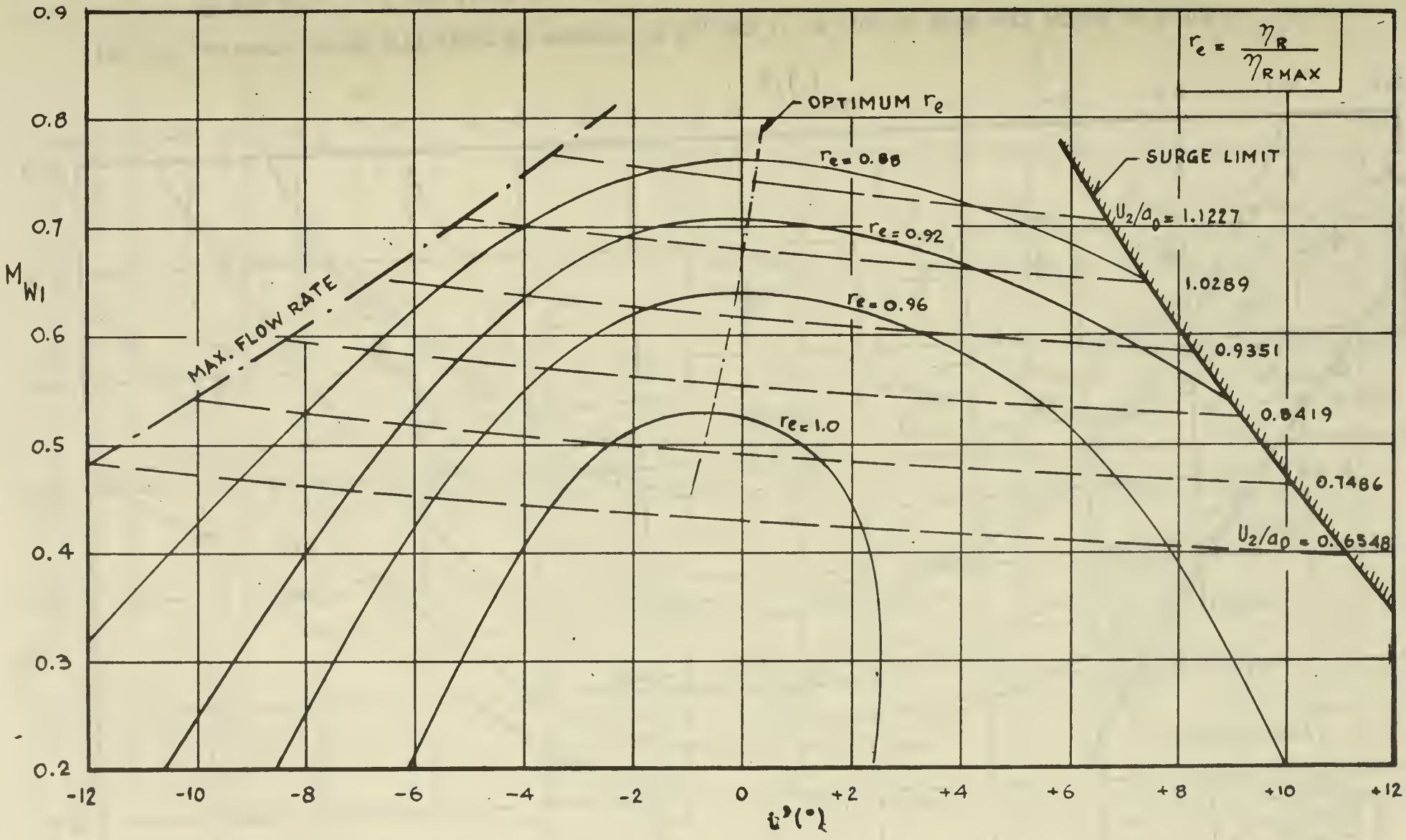

FIG. 24 ADIABATIC ROTOR EFFICIENCY η_R AS FUNCTION OF MACH NUMBER M_{W1}, PERIPHERAL SPEED RATIO U_2/a_0, AND INCIDENCE ANGLE i' (ADAPTED FROM FIG. 23b OF REF. 2)

– – – Curves for U_2/a_0 = constant

η_{RMAX} = Maximum Adiabatic Rotor Efficiency

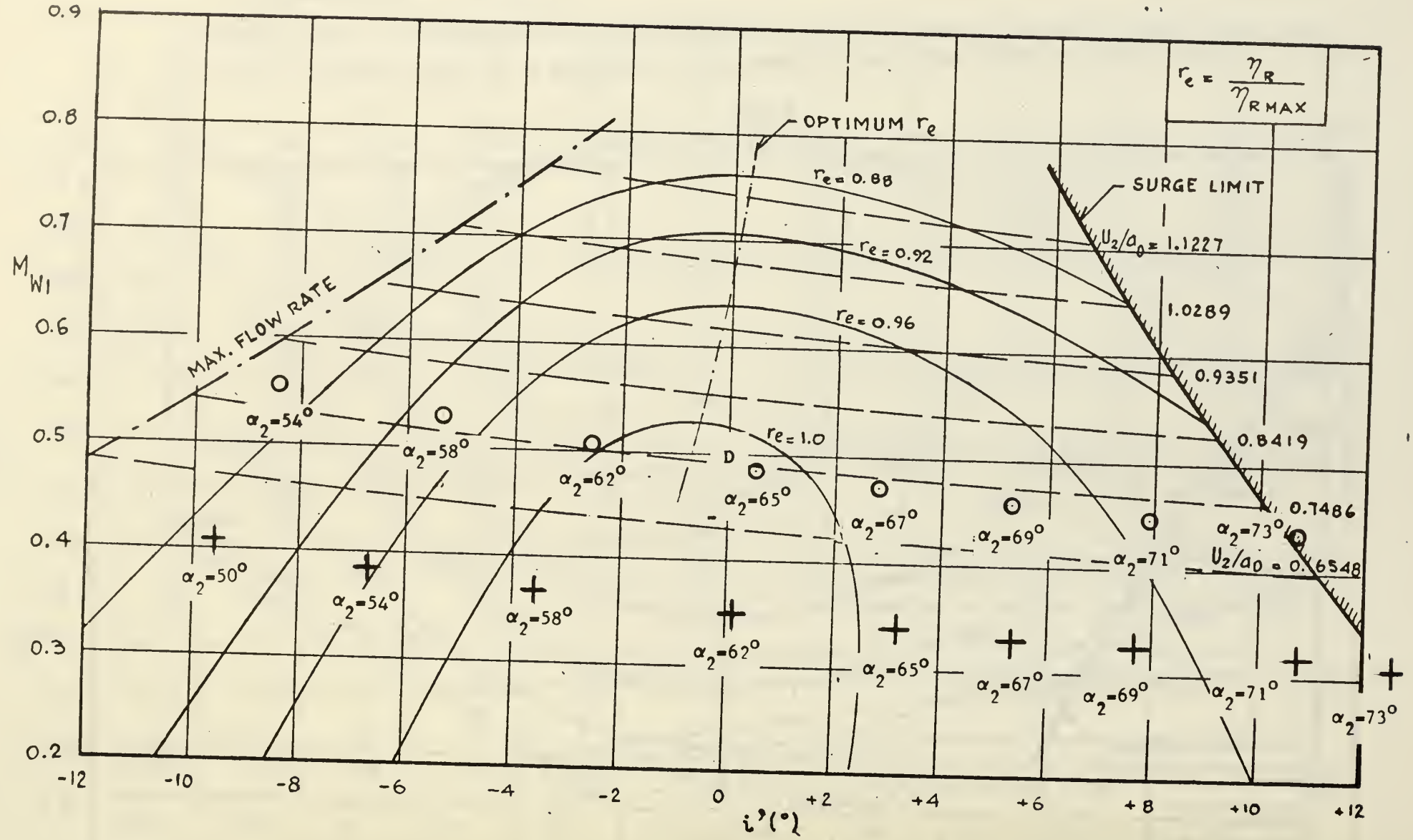

FIG. 25 ADIABATIC ROTOR EFFICIENCY AS FUNCTION OF M_{W1} AND i' OF FIG. 24 WITH DATA POINTS OF TABLE X

⊙ FOR U_2/a_0 = 0.7156 (TABLE X, SHEET 1)

\+ FOR U_2/a_0 = 0.516 (TABLE X, SHEET 2)

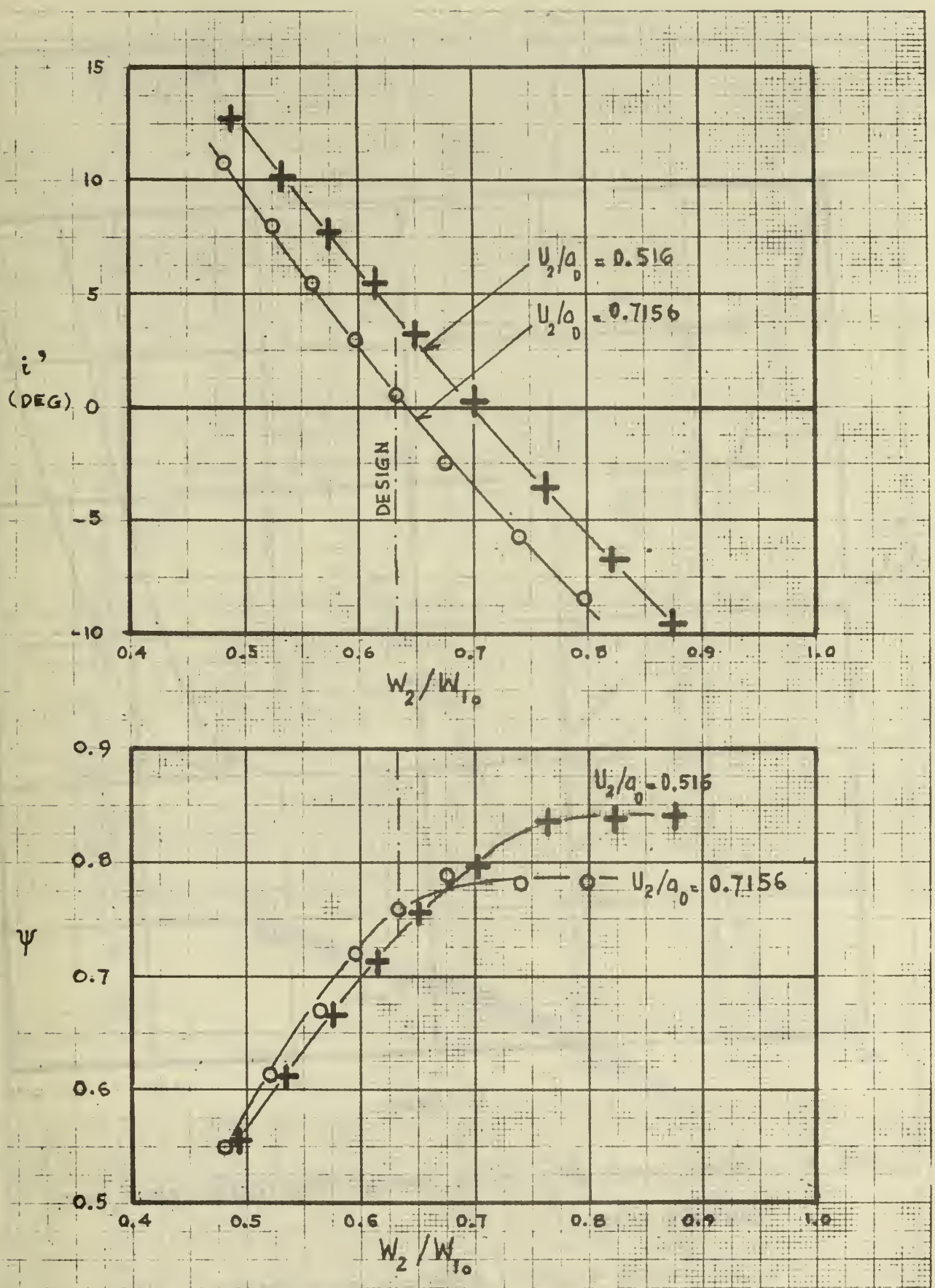

FIG. 26 VELOCITY COEFFICIENT Ψ AND INCIDENCE ANGLE i' OF HYBRID COMPRESSOR ROTOR AS FUNCTION OF DECELERATION RATIO W_2/W_{1o} OF RELATIVE VELOCITIES FROM DATA OF TABLE X

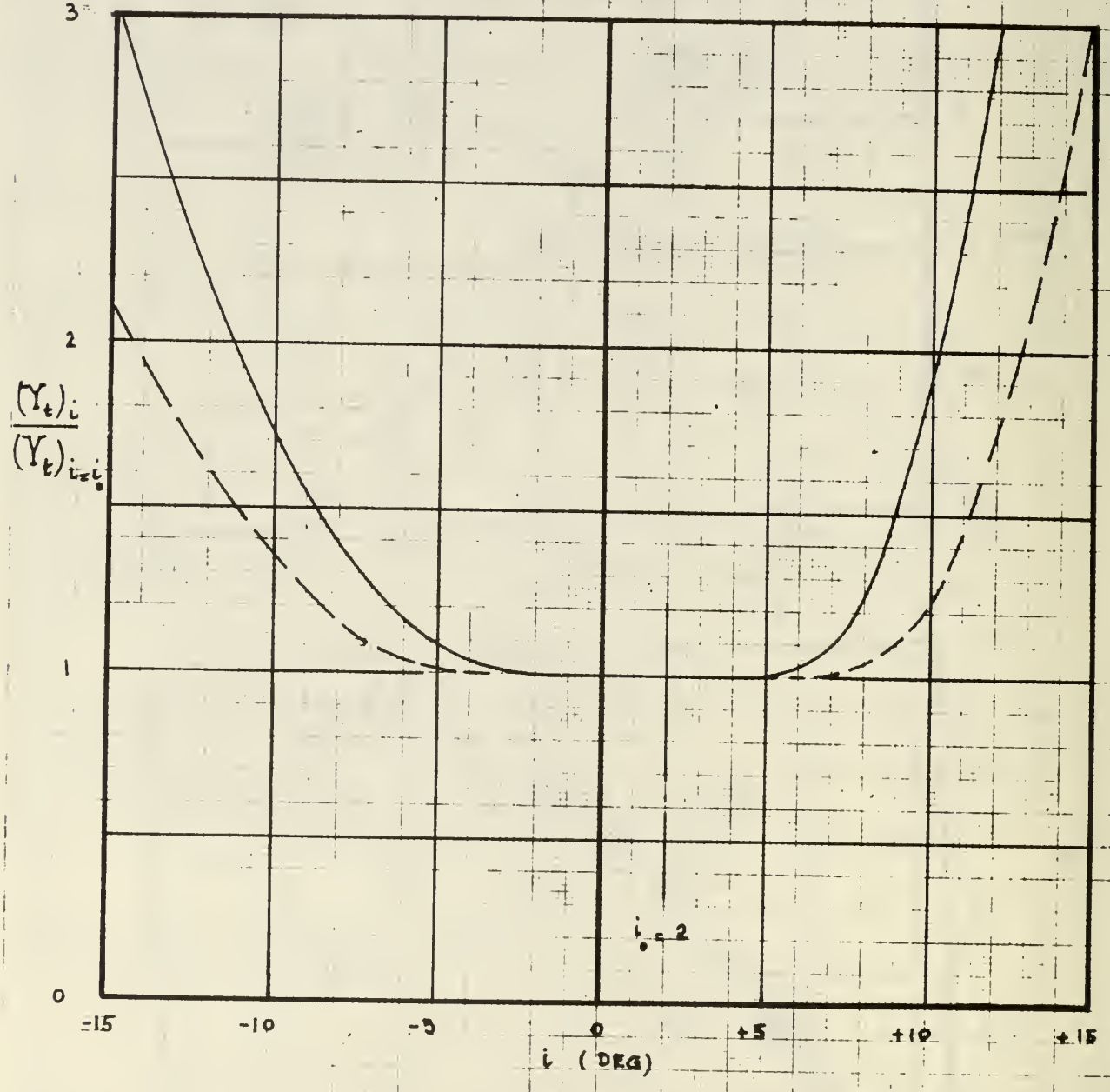

FIG. 27 ASSUMED CHANGE OF DIFFUSOR PRESSURE LOSS COEFFICIENT Y_t WITH INCIDENCE ANGLE i

——— $U_2/a_0 = 0.7156$; $0.641 \leq M_{V2} \leq 0.672$

– – – $U_2/a_0 = 0.516$; $0.472 \leq M_{V2} \leq 0.504$

P_{t4}/P_0 = Pressure Ratio; HP = Drive Power; η_T = Total-Total Efficiency; $\dot{w}$ = Flow Rate; N = Speed

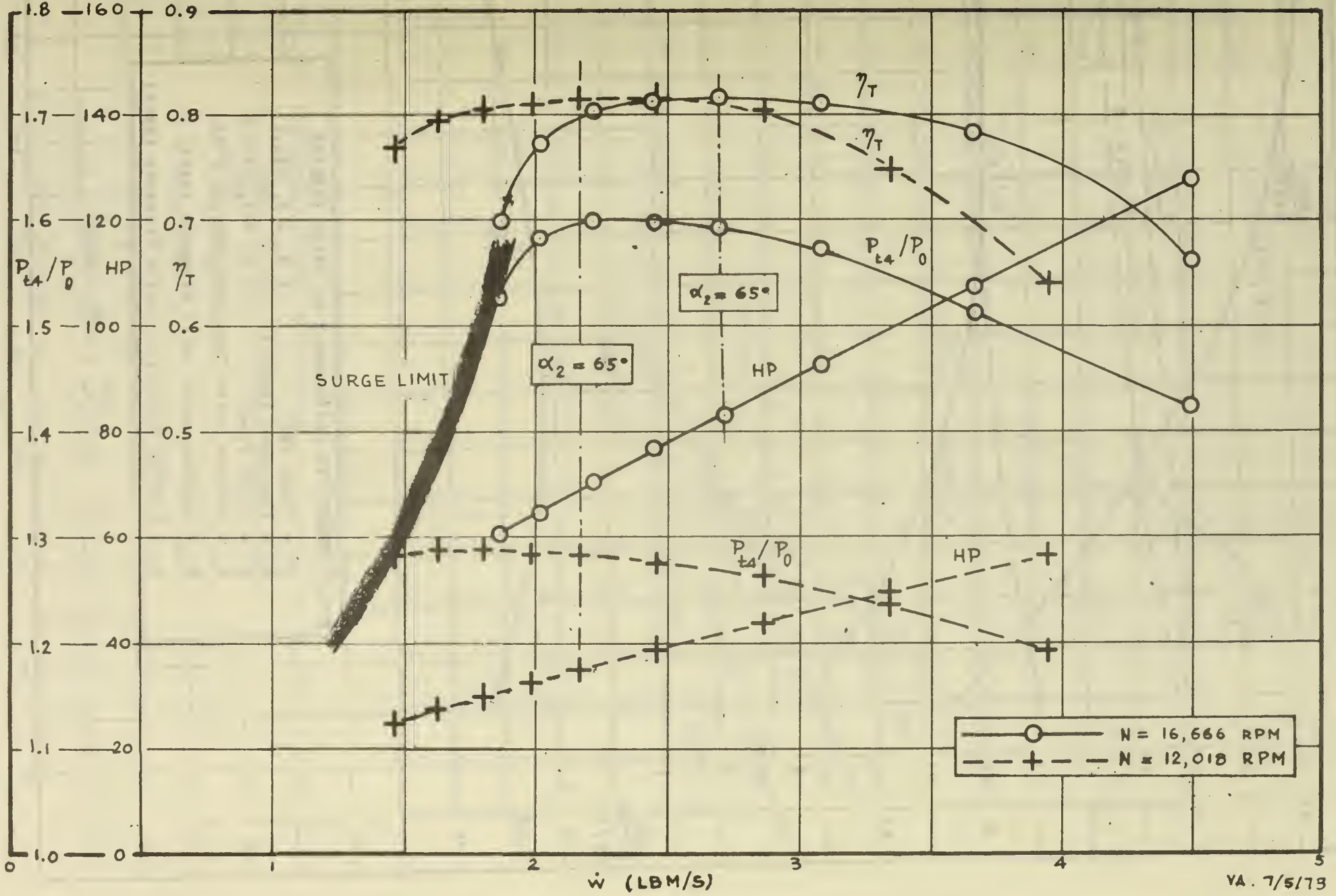

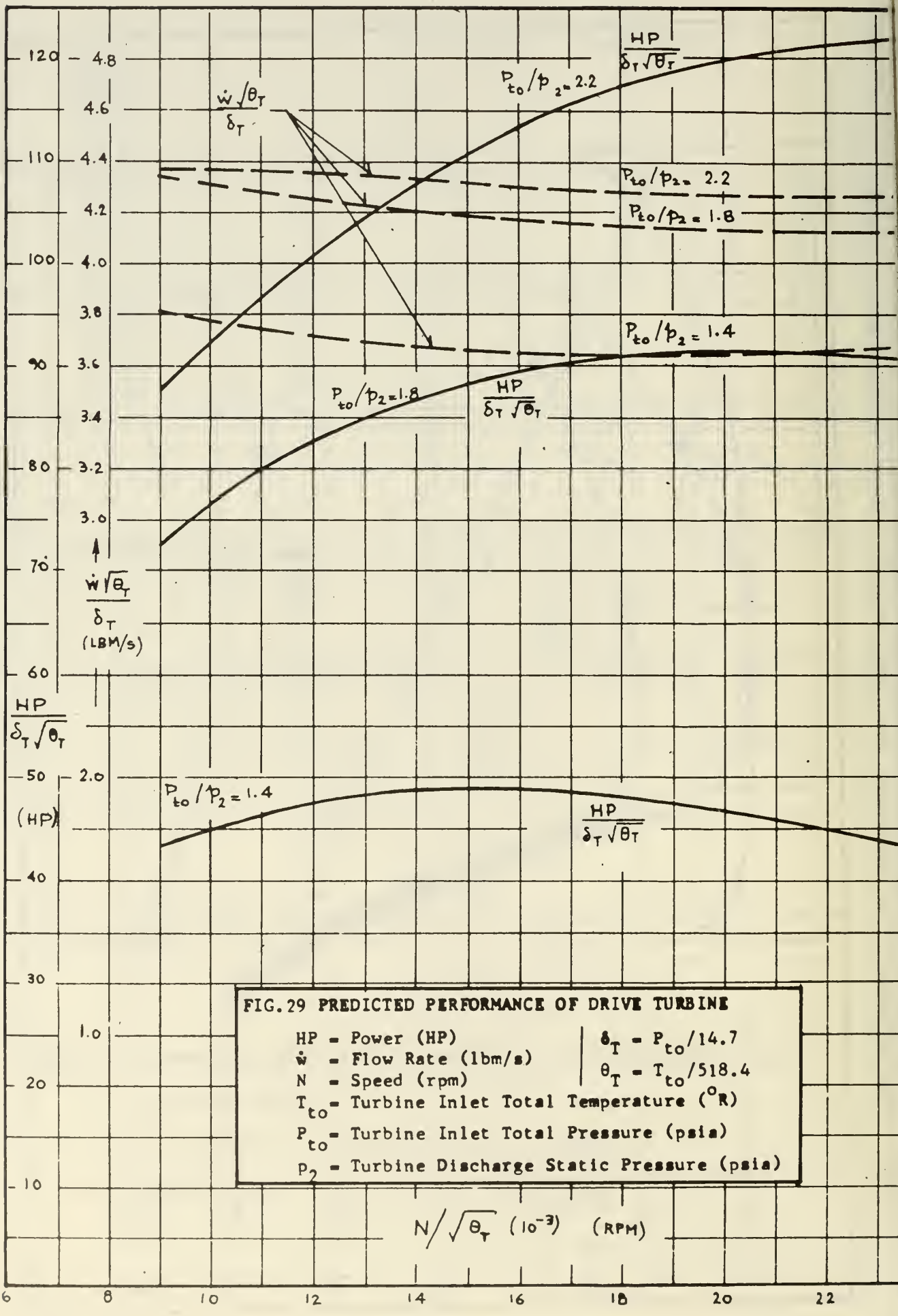

FIG. 29 PREDICTED PERFORMANCE OF DRIVE TURBINE

HP = Power (HP)
$\dot{w}$ = Flow Rate (lbm/s)
N = Speed (rpm)
T_{to} = Turbine Inlet Total Temperature (^{o}R)
P_{to} = Turbine Inlet Total Pressure (psia)
p_2 = Turbine Discharge Static Pressure (psia)

$\delta_T = P_{to}/14.7$
$\theta_T = T_{to}/518.4$

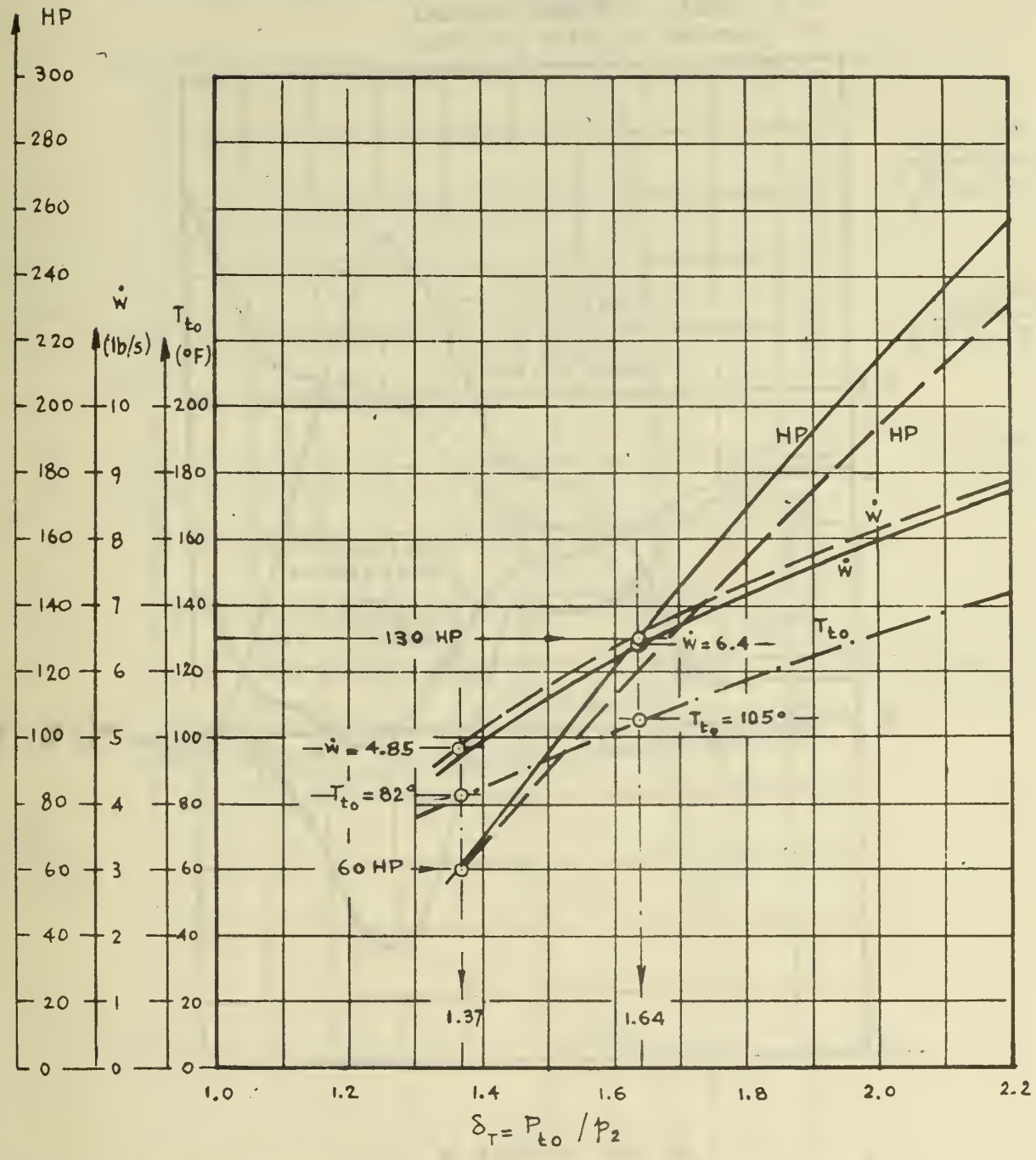

FIG. 30 PREDICTED TURBINE PERFORMANCE

$\delta_T = P_{to}/p_2$ = Total-to-Static Pressure Ratio

$\dot{w}$ = Flow Rate (lbm/s)

HP = Horse Power

T_{to} = Turbine Inlet Temperature (^{o}F)

——— N = 16,666 rpm

– – – N = 12,018 rpm

FIG. 31 STRESS DISTRIBUTION IN HYBRID ROTOR
(Method of Schilhansl, Ref. 17)

σ_{RADIAL} = Radial Stress; σ_{HOOP} = Tangential Stress

ρ = Density of Blade Material
ω = Angular Velocity of Rotor

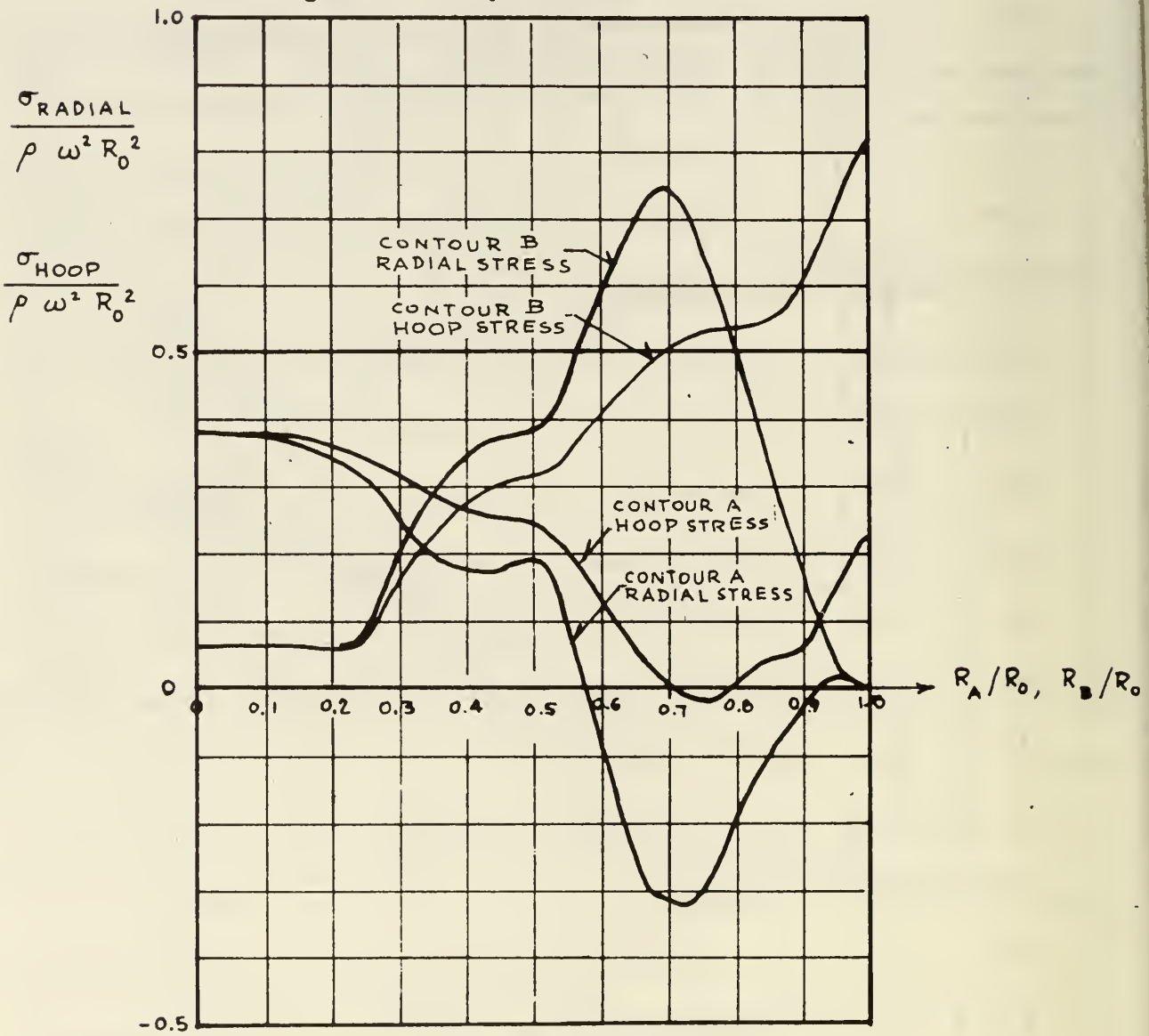

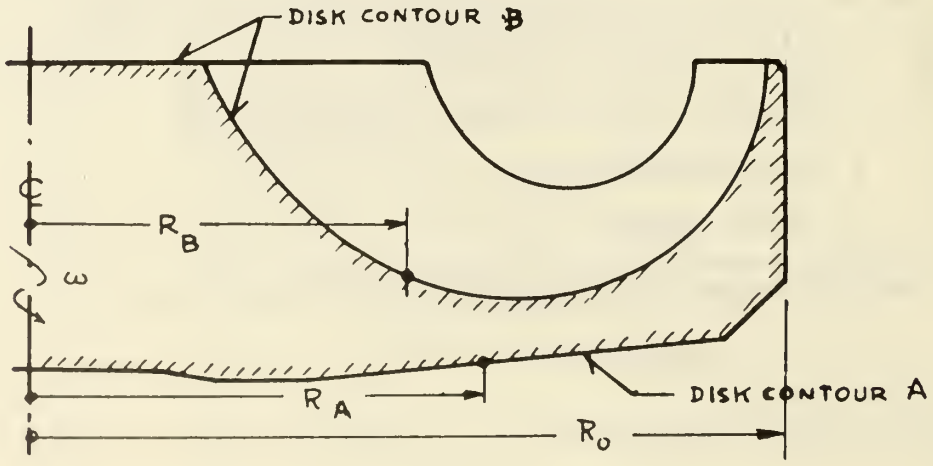

FIG. 32 BLADE STRESSES OF HYBRID ROTOR

(Method of Schilhansl, Ref. 17)

σ_B = Blade Stress

(For other symbols, see Fig. 31)

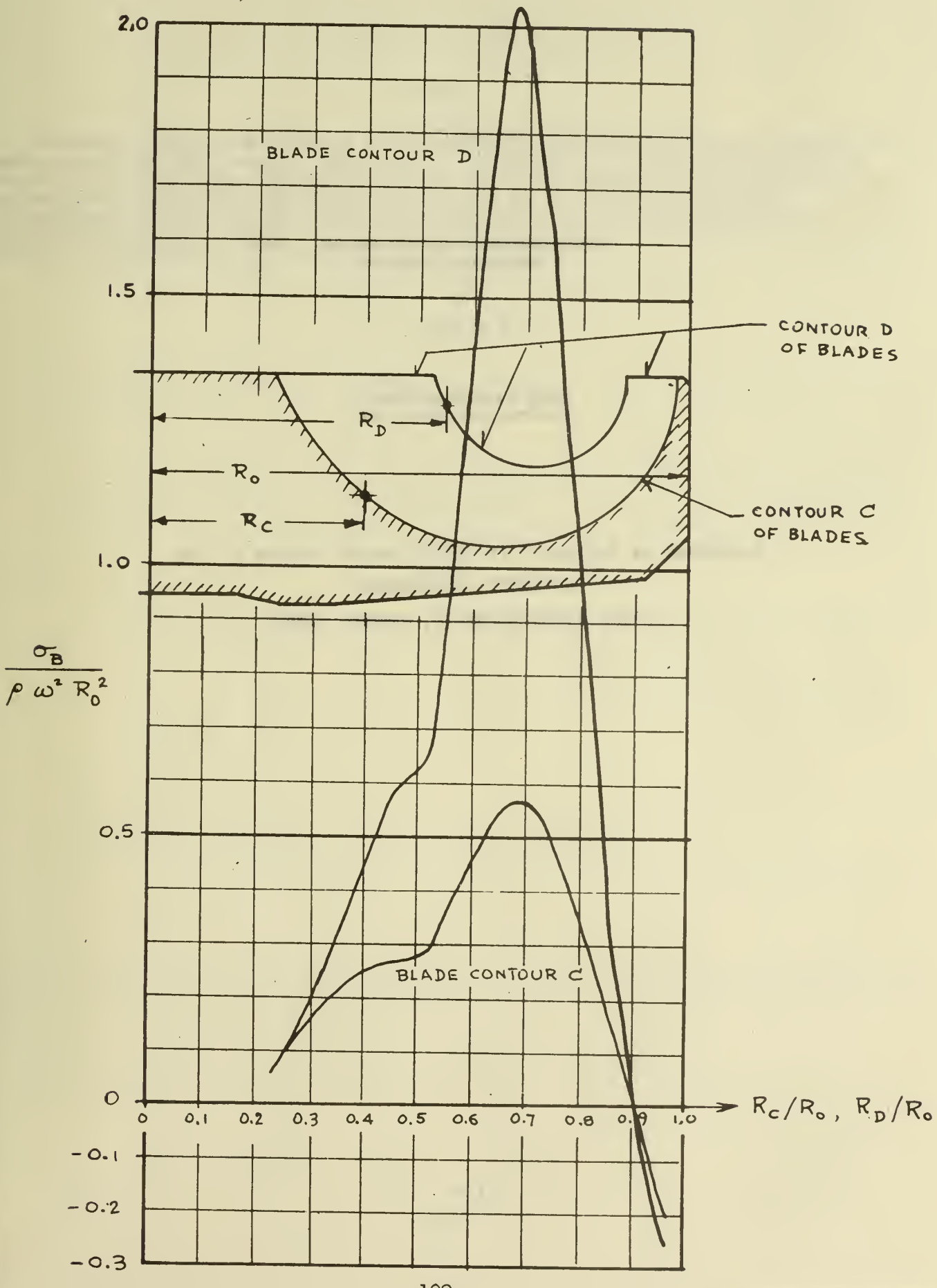

APPENDIX A

BASIC ELEMENTS FOR ADVANCED DESIGNS OF RADIAL-FLOW COMPRESSORS

by

M. H. Vavra

Naval Postgraduate School
Monterey, California 93940

Published as Article 6 in AGARD Lecture Series No. 39
"ADVANCED COMPRESSORS"
NATO, AGARD-LS-39-70, London 1970

SUMMARY

Dimensionless parameters are presented for the design of compressors with axial inlet velocities and radial blades at the rotor discharge. These parameters take account of the compressibility of the flow and hold for arbitrary fluids. They permit to evaluate the effect of changes of the design variables on the conditions of state of the fluid at different locations, and on the geometry of the design. Loss relationships are discussed and their effects on performance are shown. The design parameters are compared with the so-called specific speed criteria to show that the latter do not satisfy the laws of similarity if compressibility effects are taken into account.

BASIC ELEMENTS FOR ADVANCED DESIGN OF RADIAL-FLOW COMPRESSORS

M. H. Vavra

1. INTRODUCTION

Under consideration are high-speed centrifugal compressors with rotors of the type shown in Fig. 1 that have radial blades at the discharge and where the absolute inlet velocities are in axial direction. With a straight annular inlet duct these inlet velocities will be uniform between the radii R_{1i} and R_{1o} of the impeller eye. For a particular relative flow angle β_{1o} and the relative velocity W_{1o} at R_{1o}, there is then known the peripheral speed U_{1o}, which, for chosen radius ratios R_2/R_{1o}, establishes the peripheral rotor speed U_2 at R_2. The average relative velocity W_2 at the discharge of a rotor with radial blades is not radial, but has an average angle β_2. With the slip factor μ there is

$$\beta_2 = \tan^{-1} \frac{(1-\mu)\, U_2}{V_{m2}} \tag{1}$$

where V_{m2} is the average meridional velocity at the rotor discharge. Equation 1 is a consequence of the definition of the slip factor

$$\mu = \frac{V_{u2}}{U_2} \tag{2}$$

For a simplified analysis of the compressor performance that assumes uniform conditions at the rotor discharge not only in peripheral but also in axial direction, across the blade width b_2, and for axial absolute velocities V_1 at the rotor inlet, the specific work ΔH_w necessary to drive the compressor is from moment of momentum consideration, for an assumed adiabatic process,

$$\Delta H_w = \mu\, U_2^2 \qquad \left(\frac{\text{ft-lb}}{\text{slug}}\right) \tag{3}$$

For a perfect gas with $\gamma = c_p/c_v$ = constant, the actual rise in total temperature ΔT_w in the rotor is

$$\Delta T_w = \frac{\Delta H_w}{c_p} = \frac{\mu\, U_2^2}{c_p}$$

With the gas constant R_G there is

$$c_p = R_G\, \frac{\gamma}{\gamma-1} \tag{4}$$

Let

$$a_0 = \sqrt{\gamma\, R_G\, T_{t1}} \qquad = \sqrt{\gamma\, R_G\, T_0} \tag{5}$$

be the velocity of sound at the total inlet temperature $T_{t1} = T_0$. Then

$$\frac{\Delta T_w}{T_0} = \mu\, (\gamma-1)\, \left(\frac{U_2}{a_0}\right)^2 \tag{6}$$

For an isentropic compression process from the total inlet pressure $P_0 = P_{t0} = P_{t1}$ to the discharge pressure P_{t4}, the necessary work required would be $c_p\, \Delta\, T_{is}$, where

$$\Delta T_{is} = T_0 \left[\left(\frac{P_{t4}}{P_0}\right)^{\frac{\gamma-1}{\gamma}} - 1 \right] \tag{7}$$

The compressor efficiency η_c is defined by

$$\eta_c = \frac{\Delta T_{is}}{\Delta T_w} = \frac{\left(\frac{P_{t4}}{P_0}\right)^{\frac{\gamma-1}{\gamma}} - 1}{\mu(\gamma-1)\, \left(\frac{U_2}{a_0}\right)^2} \tag{8}$$

For a particular design the following data are usually prescribed:

$\dot{m}$ - mass flow rate (slug/s)

P_0 - total inlet pressure (psia)

T_0 - total inlet temperature ($^\circ$R)

P_{t4} - discharge pressure (psia)

γ - ratio of specific heats c_p and c_v

R_G - gas constant $(\frac{\text{ft-lb}}{\text{slug}, ^\circ\text{R}})$

With the indicated units, which are frequently used for engineering purposes, a quantity of mass is in slugs which is derived from the chosen units of force, length, and time. However, the relations which are going to be established hold for any consistent system of units, hence also for one where the primary units are mass, length and time, and where forces are in derived units.

For the given conditions there are to be found the following data for an optimum design:

U_2 - peripheral rotor speed at R_2

b_2/R_2 - $\frac{\text{ratio of axial impeller width at discharge}}{\text{outer radius of impeller}}$

R_{1o}/R_2 - $\frac{\text{outer radius at rotor inlet}}{\text{outer radius of impeller}}$

R_{1i}/R_{1o} - $\frac{\text{inner radius at rotor inlet}}{\text{outer radius at rotor inlet}}$

ω - angular velocity of impeller (radians/s)

β_{1o} - relative flow angle at R_{1o}

α_2 - absolute flow angle at R_2

R_3/R_2 - $\frac{\text{radius at inlet lip of diffusor blades}}{\text{outer radius of impeller}}$

R_4/R_2 - $\frac{\text{radius at discharge of diffusor}}{\text{outer radius of impeller}}$

Important design criteria are also:

$M_{W1} = \frac{W_{1o}}{a_1}$ - Mach number of relative velocity W_{1o} at outer radius R_{1o} at impeller inlet

$M_{V2} = \frac{V_2}{a_2}$ - Mach number of absolute velocity V_2 at impeller discharge

Mechanical and fluid dynamics considerations impose design limits of:

a) U_2, because of permissible rotor stresses
b) R_{1o}/R_2, which cannot exceed about 0.70 to 0.75 to obtain an outer rotor contour with acceptably small curvatures in the meridinal plane
c) R_{1i}/R_{1o}, which, if too small, does not permit the arrangement of a sufficiently large number of rotor blades Z_R with reasonable thickness
d) β_{1o}, which cannot be larger than about 70° for manufacturing reasons
e) b_2/R_2, which cannot be smaller than certain limits to obtain good efficiencies
f) α_2, which cannot exceed 70° to 80° because of manufacturing reasons and because of poor diffusor performance, especially if M_{V2} is larger than unity.

2. COMPRESSION PROCESS

Figure 2 is a temperature-entropy diagram showing the thermodynamic process in the compressor of Fig. 1. The temperature differences in Fig. 2 correspond roughly to the velocities of the triangles of Fig. 1 to obtain a realistic representation. Since by Eq. 6 the work input ΔT_w is also $\Delta T_w = \mu\,(U_2^2/c_p)$, the temperature rise $T_2 - T_1$ in the rotor is roughly one-half of ΔT_w. Later on the so-called degree of reaction r* will be introduced to determine this ratio more precisely.

Station (1) in Fig. 2 corresponds to the static condition at the rotor inlet, given by the static pressure p_1 and the static temperature T_1. The total pressure and total temperature at this station are $P_{t1} = P_0$ and $T_{t1} = T_0$. For the isentropic process between (0) and (1).

$$\frac{T_{t1}}{T_1} = \frac{T_0}{T_1} = 1 + \frac{\gamma-1}{2} M_{V1}^2 \qquad (9)$$

and

$$\frac{P_{t1}}{p_1} = \frac{P_0}{p_1} = \left(\frac{T_0}{T_1}\right)^{\frac{\gamma}{\gamma-1}}$$

where

$$M_{V1} = \frac{V_1}{a_1} = \frac{V_1}{[\gamma R_G T_1]^{\frac{1}{2}}}$$

is the Mach number of the absolute velocity V_1 at the rotor inlet.

The conditions of state at all locations can be expressed with the parameters U_2/a_0, R_{1o}/R_2, M_{W1}, β_{1o}, α_2, μ, and loss coefficients that establish the entropy increments between the different stations, if it is assumed that the flow process along the outer contour of the rotor between the radii R_{1o} and R_2 is representative of the rotor flow in general. The later assumption is made because the relative velocity W_1 and the relative flow angle β_1 are higher at R_{1o} than at other radii R_1. Hence along the outer rotor contour from R_{1o} to R_2 there occur the highest deceleration ratio W_{1o}/W_2 and the largest flow deflection $\Delta\beta = \beta_{1o} + \beta_2$. Moreover since the path travelled by a fluid particle along the outer rotor contour is shorter than that travelled by a particle entering at other radii R_1, the conditions along the outer rotor contour will establish design limitations and have a critical influence on the rotor losses.

With the chosen parameters, Eq. 9 can be rewritten

$$\frac{T_1}{T_0} = \frac{1}{1 + \frac{\gamma-1}{2} M_{W1}^2 \cos^2\beta_{1o}}$$

This formula is also given by Eq. I(5) of Table I. This table has been arranged to list the pertinent relations for the determination of the flow properties in the compressor for ready reference. In the following only the main steps will be indicated that led to these formulas without going into the details of their derivations. Some of the equations, for instance Eq. I(6), can be obtained directly from Fig. 2. It can be noted that all temperatures are given as multiples of the total inlet temperature $T_0 = T_{t1}$, and pressures are listed as ratios with respect to $P_0 = P_{t1}$. The static temperature T_2 of the rotor discharge [Eq. I(7)] is equal to the difference of the total temperature T_{t2} at the rotor exit and $V_2^2/2c_p$, where V_2 is given by Eq. I(3). The temperature T_2' is necessary to calculate the pressure ratio p_2/P_0 by Eq. I(20). Evidently T_2' depends on the entropy increase $s_2 - s_1$ in the rotor.

The process between stations (1) and (2) from the rotor inlet to its discharge can be formulated by

$$T_1 - \frac{W_{1o}^2}{2c_p} - \frac{U_{1o}^2}{2c_p} = T_2 + \frac{W_2^2}{2c_p} - \frac{U_2^2}{2c_p} \qquad (10)$$

which is a fundamental relation obtained from the energy equation for steady, adiabatic flows along streamlines in rotors, as shown in Art. 7.5 of Ref. 1.

The following discussion uses a relation which is obtained from Eq. 10 for incompressible flows (See Eq. 7(44) of Ref. 1). At a particular radius R along the outer rotor contour where the peripheral and relative velocities are U and W, respectively, the static pressure p is

$$p = p_1 + \frac{\rho}{2}(U^2 - U_{1o}^2) + \frac{\rho}{2}(W_{1o}^2 - W)^2 - \Delta p_f \qquad (11)$$

where ρ is the constant mass density of the fluid, and Δp_f the pressure loss due to frictional effects in the rotor. At the rotor inlet, where $U = U_{1o}$ and $W = W_{1o}$, the static pressure is evidently equal to p_1, the static pressure in the absolute flow just ahead of the rotor at R_{1o}. Equation 11 shows that, independently of the values of W and Δp_f, there will always occur a pressure increase $\rho/2(U^2-U_{1o}^2)$ if a fluid particle moves from R_{1o} to R. An additional pressure rise is produced by decelerating the relative velocity from W_{1o} to W. A flow that moves in a direction where the static pressure increases is more susceptible to separations than an accelerated flow, but the frictional pressure loss between neighboring stations is proportional to the dynamic head $(\rho/2)\,W^2$ in both flows. In view of Eq. 11 however there exist differences between flows that pass through stationary channels and those in rotating impellers. If a relative flow is decelerated in a rotating channel, whose distance from the axis of rotation increases in flow direction, it will not necessarily separate even though it moves against rapidly increasing static pressures, provided these pressure gradients are produced by the centrifugal force field and not by large reductions in relative velocity. If the same static pressure rise would have to be produced in a stationary channel of the same length as the rotating one, the deceleration of the flow per unit length would very likely become excessive and could be associated with considerably increased losses because of flow separations. On the other hand, if it were possible to ignore the effects due to Coriolis accelerations, it could be stated that the pressure losses in a stationary and in a rotating channel of equal length and shape would have to be equal for the same velocity heads and equal flow decelerations, except for influences due to Reynolds number differences. Moreover, for different velocity heads the pressure losses would be directly proportional to the velocity heads at corresponding locations in the two channels. However if the respective performance of the two channels were evaluated by a loss coefficient ζ_R that relates the frictional pressure drop Δp_f to the actual static pressure rise in the channel, its value would be lower for the rotating channel than for the stationary one because of the additional pressure rise $(\rho/2)(U^2 - U_{1o}^2)$. The performance of the channels can be compared only by means of a loss coefficient ζ_W that is defined as the ratio of the pressure drop Δp_f and

the pressure rise $(\rho/2)(W_{1o}^2 - W_1^2)$ due to the flow deceleration, irrespective of whether additional pressure rise is produced by the centrifugal force field or not.

These elementary considerations have not been presented here to imply that the loss coefficients ζ_W in a rotating and in a stationary channel of the same geometry are equal. In Ref. 1, Art. 8.5, it is shown that flows in stationary and rotating channels have fundamental differences as far as their rotational characteristics are concerned, and consequences of these conditions are described in Arts. 10.5 and 12.2 of Ref. 1. The intent of the above discussion is to draw attention to the fact that frequently used formulations for the efficiency of impellers for centrifugal turbines and compressors cannot serve as a measure for the performance of these rotors, and that some of the separation criteria applied to flows in centrifugal rotors have no physical meaning.

A commonly used definition for the efficiency of a centrifugal compressor rotor is

$$\eta_R = \frac{T_2' - T_1}{T_2 - T_1} \tag{12}$$

The significance of the temperatures is evident from Fig. 2. Equation 12 holds for the compressible flow of fluids with a constant value of $\gamma = c_p/c_v$. Similar to the preceding discussion that delt with incompressible flows, part of the temperature rise in the rotor is due to the increase in peripheral speed from station (1) to station (2). Equation 10, rewritten as

$$T_2 - T_1 = \frac{U_2^2 - U_{1o}^2}{2c_p} + \frac{W_{1o}^2 - W_2^2}{2c_p} = T_u - T_1 + \frac{W_{1o}^2 - W_2^2}{2c_p} \tag{13}$$

shows that the static temperature rise $T_u - T_1$ due to the centrifugal force field is equal to the first term on the right-hand side of Eq. 13. It occurs in rotors with and without flow losses, hence it is independent of the entropy increase $s_2 - s_1$. Thus the compression corresponding to $(U_2^2 - U_{1o})^2/2\,c_p$ occurs along the isentropic line s_1 = constant from T_1 to T_u, from station (1) to station (u) in Fig. 2, producing the static pressure rise $p_u - p_1$, where

$$\frac{p_u}{p_1} = \left(\frac{T_u}{T_1}\right)^{\frac{\gamma}{\gamma-1}} = \left(1 + \frac{(U_2^2 - U_{1o}^2)}{2\,c_p\,T_1}\right)^{\frac{\gamma}{\gamma-1}} = \left(1 + \frac{\gamma-1}{2}\,\frac{U_2^2 - U_{1o}^2}{\gamma\,R_G\,T_1}\right)^{\frac{\gamma}{\gamma-1}}$$

The deceleration of the relative velocity from W_{1o} to W_2 produces the temperature rise

$$T_2 - T_u = \frac{W_{1o}^2 - W_2^2}{2\,c_p} \tag{14}$$

with an entropy increase from s_1 to s_2, due to the flow losses, which in turn affect the pressure rise $p_2 - p_u$. The efficiency of the process from (u) to (2) can be defined by the so-called wheel efficiency η_W

$$\eta_W = \frac{T_2' - T_u}{T_2 - T_u} = \frac{T_2' - T_u}{(W_{1o}^2 - W_2^2)/2\,c_p} \tag{15}$$

giving

$$\frac{T_2'}{T_u} = \eta_W\,\frac{T_2}{T_u} + 1 - \eta_W$$

and

$$\frac{p_2}{p_u} = \left(\frac{T_2'}{T_u}\right)^{\frac{\gamma}{\gamma-1}}$$

From a fluid dynamics view point only the efficiency η_W is a measure for the quality of the rotor performance. In particular, low measured values of η_W are indications for the existence of flow separations, although η_W will be affected also by the tip clearance losses, the so-called scrubbing losses produced by the rotating blades in the wall boundary layer at the fixed shroud, and the mixing losses after the rotor. However, low efficiencies η_W are only partly reflected in the rotor efficiency η_R of Eq 12 because of the temperature rise $T_u - T_1$ which is produced without entropy increases. If the entropy diagram of Fig. 2 were to represent the actual conditions in the compressor of Fig. 1, there would be, by measuring the temperature differences in Fig. 2,

$$\eta_R = 0.84$$

and

$$\eta_W = 0.57$$

Although the value of $\eta_R = 0.84$ seems to indicate that the flow in the rotor is reasonably good, the low value of $\eta_W = 0.57$ shows clearly that it should be possible to improve the rotor considerably with a redesign. Such improvement should be undertaken not only to increase the overall efficienty of the compressor by reducing the entropy rise $s_2 - s_1$ in the rotor, but also to produce more uniform flow conditions at the

rotor discharge since it might then be possible to reduce the diffusor losses also.

The process in the rotor that involves the relative velocity changes can be considered also from a different view point. Equation 10 may be written as

$$T_E = T_1 + \frac{W_{1o}^2}{2\,c_p} + \frac{U_2^2 - U_{1o}^2}{2\,c_p} = T_u + \frac{W_{1o}^2}{2\,c_p} = T_2 + \frac{W_2^2}{2\,c_p} \tag{16}$$

where T_E is the so-called equivalent total temperature of the rotor flow. Equation 16 has the same form as the energy equation for an adiabatic process of an absolute flow if T_E is replaced by the constant absolute total temperature T_t and W_2 by the absolute velocity V. The temperature T_E is constant for a process in a particular rotor having a fixed radius ratio R_{1o}/R_2 and turning at a specified speed. Thus, for given inlet conditions, Eq. 16 can be used also for an isentropic process along s_1 = constant from (u) to (2') to give, in accordance with Fig. 2,

$$T_E = T_2' + \frac{W_{2is}^2}{2\,c_p} \tag{17}$$

for the same pressure rise $p_2 - p_u$ as produced by the process with friction, and W_{2is} is the theoretical velocity available at the pressure p_2. In turbine calculations it is customary to express the rotor losses by so-called velocity coefficients ψ

$$\psi = \frac{W_2}{W_{2is}} \tag{18}$$

If this formulation is used for compressors also, there is from Eq. 17,

$$T_2' = T_E - \frac{1}{\psi^2}\frac{W_2^2}{2\,c_p} \tag{19}$$

Introduced into Eq. 15

$$\eta_W = \frac{W_{1o}^2 - W_2^2/\psi^2}{W_{1o}^2 - W_2^2} = \frac{1 - \frac{1}{\psi^2}\left(\frac{W_2}{W_{1o}}\right)^2}{1 - \left(\frac{W_2}{W_{1o}}\right)^2} \tag{20}$$

or

$$\psi = \frac{W_2/W_{1o}}{\left[1 - \eta_W + \eta_W \left(\frac{W_2}{W_{1o}}\right)^2\right]^{\frac{1}{2}}} \tag{21}$$

The reason for introducing ψ as an alternate for η_W is that η_W equals $-\infty$ for the special condition where $W_2 = W_{1o}$, or $T_2 = T_u$. In this case, and if W_2 is larger than W_{1o}, the velocity coefficient ψ can however still be applied. On the other hand, for usual designs where W_2 is smaller than W_{1o}, the velocity coefficient is not a good measure for the rotor performance since ψ can be increased by simply making the velocity W_2 smaller, and it is then more appropriate to use the wheel efficiency η_W for the loss evaluation. Since the same difficulties in expressing the losses occur in turbines also, an additional formulation is sometimes used which establishes the drop in total pressure that is associated with the entropy increase $s_2 - s_1$. For radial compressor rotors these formulation are either

$$Y_1 = \frac{P_{E1} - P_{E2}}{P_{E1} - p_u} \tag{22}$$

or

$$Y_2 = \frac{P_{E1} - P_{E2}}{P_{E2} - p_2} \tag{23}$$

depending on whether the pressure drop $P_{E1} - P_{E2}$ is referred to the inlet or the exit conditions. Although these total pressure loss coefficients are useful at small Mach numbers, or for incompressible flows where $P_{E1} - p_u = (\rho/2)\,W_{1o}^2$ and $P_{E2} - p_2 = (\rho/2)W_2$, it can be shown that the corresponding coefficients which relate the losses to the kinetic energy of the flow (in the same manner as η_W of Eq. 15, or ψ of Eq. 18) become smaller for constant values of Y_1 or Y_2 if the Mach number of the inlet or discharge flow increases.[2] Although the actual energy losses tend to increase with increasing flow Mach numbers, an indiscriminate application of Eqs. 22 or 23 with values of Y from low-speed tests can be used as a wrong argument that the opposite is true.

To simplify the relations for the determination of the conditions of state in the compressor the velocity coefficients ψ will be used in the equations of Table I. To compare two rotors with different radius ratios and different deceleration ratios W_2/W_{1o}, the efficiency η_W of Eq. 15 should be used as a

measure for their performance. Equations 20 and 21 relate ψ and η_W to each other. Paragraph 5 contains a discussion that deals with the magnitudes of η_W. With the formulas of Table I it is possible also to establish a relation for the determination of η_W for known values of η_R of Eq. 12, or vice versa. From

$$\eta_R = \frac{\eta_W \left[\left(\frac{W_{1o}}{U_2}\right)^2 - \left(\frac{W_2}{U_2}\right)^2\right] + 1 - \left(\frac{R_{1o}}{R_2}\right)^2}{\left(\frac{W_{1o}}{U_2}\right)^2 - \left(\frac{W_2}{U_2}\right)^2 + 1 - \left(\frac{R_{1o}}{R_2}\right)^2} \tag{24}$$

and with

$$C = \frac{1 - \left(\frac{R_{1o}}{R_2}\right)^2}{\left(\frac{R_{1o}}{R_2}\right)^2 \cot^2\beta_{1o} + 2\mu \left(1 - \frac{\mu}{2\sin^2\alpha_2}\right)} \tag{25}$$

there are

$$\eta_R = \eta_W + C\,(1 - \eta_W) \tag{26}$$

and

$$\eta_W = \frac{\eta_R - C}{1 - C} \tag{27}$$

High performance compressors with high pressure ratios cannot be equipped with diffusors that are circular cascades with airfoil shaped blades. Figure 1 is a realistic sketch of a high speed compressor operating with an average discharge velocity V_2 that is supersonic. To obtain reasonably large axial blade widths b_2 as well as acceptable shapes of the meridinal rotor contours, it is necessary to resort to large angles α_2 at the rotor discharge. At large angles α_2, practical consideration dictate a limited number of diffusor channels, say, about 8 to 10 for angles α_2 of about 75°, and the permissible diffusion in these individual channels produces configurations similar to that depicted in Fig. 1. One of the most critical problem areas is the design of the flow passages from the rotor discharge to the entrance of the diffusor channels proper. The absolute flow leaving the rotor is not only non-uniform but also non-steady, because the relative velocity at the rotor discharge must by necessity vary between the suction and the pressure sides of the rotor blades at R_2. Designs where the radius R_3 is very much larger than the outer rotor radius R_2, or compressors with vaneless diffusor for large angles α_2, were found to be inferior to machines with small radial gaps $R_3 - R_2$, especially for high subsonic or supersonic velocities V_2. If it were not for the excessive noise the diffusor lips would preferably be arranged even closer to R_2 as shown in Fig. 1.

Theoretical attempts were made in Refs. 3 and 4 to evaluate the losses in the space between R_2 and R_3, and in vaneless diffusors, that are due to mixing and frictional effects. The results of these investigations do not agree with reality if M_{V2} and/or α_2 are large. These inconsistencies are due to the assumption that equal flow angles are supposed to occur across the axial width b_z of the flow channel after the rotor, a condition which is created by assuming that the frictional forces along the walls act equally on all particles between them. In actuality the flow angles α (measured with respect to the radial direction) decrease radically in the wall boundary layers in the direction from the mid-section of the channel toward the wall. The particles inside the boundary layers then move more rapidly to larger radii into zones of higher pressure than those outside of the boundary layers and very easily cause flow separations from the walls, thereby impairing the effectiveness of such diffusors.

In the writer's opinion it is incorrect to state that in efficient diffusors the vanes must not be too close to the impeller, or that the velocity at their entrance must be subsonic in all cases. For the reason mentioned above, it is equally wrong to maintain that vaneless diffusors must be arranged for supersonic absolute velocities at the rotor discharge.

Because of the inability to separate the losses that exist between the radii R_2 and R_4 of Fig. 1 an overall diffusor efficiency η_D will be introduced. With the symbols of Fig. 2

$$\eta_D = \frac{T_4' - T_2}{T_4 - T_2} \tag{28}$$

where

$$T_4 - T_2 = \frac{V_2^2 - V_4^2}{2\,c_p} \tag{29}$$

The velocity V_4 exists at the diffusor discharge at the radius R_4, and is taken as

$$V_4 = \lambda\, V_2 \tag{30}$$

With small values of λ the radius ratios R_4/R_2 become large because of the limited amount of diffusion that is possible per unit length in flow direction to avoid separations in the diffusor channels. Values of λ of about 0.20 to 0.30 are common to limit R_4/R_2 to about 2. With designs of the type shown in Fig. 1 the kinetic energy $V_4/2\,c_p$ cannot be converted into pressure rise, since the flow from the individual diffusors is dumped into a receiver surrounding them. As indicated by station (d) in Fig. 2 the total pressure P_{t4} at the compressor discharge is then equal to the static pressure p_4 at the diffusor exit, and

the total temperature at the compressor discharge is $T_{t4} = T_{t2}$ for adiabatic processes. The dumping of the kinetic energy $V_4^2/2\ c_p$ is reflected in the overall diffusor efficiency η_D^* between rotor and compressor discharge

$$\eta_D^* = \eta_D\ (1 - \lambda^2) \tag{40}$$

Diffusor design criteria and approximate methods to evaluate the diffusor losses are given in paragraph 5.

Since

$$T_4 = T_{t2} - \frac{V_4^2}{2\ c_p} = T_{t4} - \lambda^2\ \frac{V_2^2}{2\ c_p}$$

and with Eq. 28 there is then obtained the temperature T_4 , as given by Eq. I(11) of Table I. The pressure $p_4 = P_{t4}$ is determined from

$$\frac{p_4}{p_2} = \left(\frac{T_4'}{T_2}\right)^{\frac{\gamma}{\gamma-1}}$$

for the isentropic process along the line s_2 = constant. Because the isentropic temperature differences between lines of constant pressure are proportional to the initial temperatures of the processes, there is, with the symbols of Fig. 2,

$$\frac{T_4'' - T_2'}{T_4' - T_2} = \frac{T_2'}{T_2}$$

and

$$\frac{T_4''}{T_0} = \frac{(T_4'/T_0)(T_2'/T_0)}{T_2/T_0}$$

As shown in Table I the ratio T_4''/T_0 can be expressed by Eq. I(13) which has the form

$$\frac{T_4''}{T_0} = \frac{1 + A(X_1 + A\ X_2)}{1 + A\ B} \tag{41}$$

where X_1 and X_2 are given by Eqs. I(14) and I(15), and

$$A = (\gamma-1)\ \mu\ \left(\frac{U_2}{a_0}\right)^2 \tag{42}$$

$$B = 1 - \frac{\mu}{2\ \sin^2\alpha_2} \tag{43}$$

The temperature rise ΔT_{is} for an isentropic compression from the total conditions P_0, T_0 at the compressor inlet, to the discharge pressure P_{t4} is, with Eq. 41,

$$\frac{\Delta T_{is}}{T_0} = \frac{T_4''}{T_0} - 1 = \frac{A[X_1 - B + A\ X_2]}{1 + A\ B} \tag{44}$$

Eq. 44 is identical with Eq. I(16) of Table I.

As shown in Table I the pressures at the different stations can be determined from the established temperatures by using the pressure-temperature relation for isentropic processes of perfect gases.

3. PERFORMANCE AND DESIGN PARAMETERS

The overall compressor efficiency defined by Eq. 8 is, with Eqs. 6, 42, and 44,

$$\eta_c = \frac{\Delta T_{is}}{\Delta T_w} = \frac{X_1 - B + A\ X_2}{1 + A\ B}$$

With Eqs. 42 and 43 the above relation establishes Eq. II(1) of Table II. This table lists the equations necessary to determine the performance and the geometry of the compressor. Only the principal steps that led to the equations of Table II are described in the following, the details of the derivations are omitted. The symbols of Table II are those of Figs. 1 and 2, with additional ones that are defined in this paragraph.

The degree of reaction r* is defined as the ratio of the isentropic temperature rise $T_2' - T_0$ in the rotor to that corresponding to the pressure ratio P_{t4}/P_o . Equation II(2) of Table II shows that for $\eta_c = 1$ and $\psi = 1$, the degree of reaction is

$$r^* = r_o^* = \left[1 - \frac{\mu}{2 \sin^2 \alpha_2}\right]$$

For a slip factor $\mu = 0.85$, r_o^* changes from about 0.544 to 0.433 if the angle α_2 is reduced from 75° to 60°. For low degrees of reaction a large part of the overall pressure rise must be produced in the diffusor. Since this energy conversion is associated with greater losses than the pressure rise produced in the rotor, high degrees of reaction are desirable. This condition is used in hydraulic pumps which usually have backward-bent rotor blades to produce most, if not all, of the pressure rise in the rotor. However, if such rotors were employed for light gases, such as air, the pressure rise would be too small for most applications, not only because of the reduced specific work input but also because such rotors would not be able to operate at high speeds on account of the high bending stresses in the blades. In rotors with radial blades it seems beneficial to use large angles α_2 to increase r*. At a fixed peripheral speed U_2 the velocities V_2 decrease if α_2 is increased, but difficulties occur then because of the geometry of the passages from the wheel to the diffusor inlet. The deceleration ratio W_2/W_{1o} becomes smaller also, as shown by Eq. II(5), and the increased losses caused by larger flow decelerations in the rotor may off-set the gain that would be obtained from the increased degree of reaction if other conditions would remain unchanged. The choice of these design parameters to obtain the best possible solution must usually be based on experience because of the interactions between rotor and diffusor that are greatly influenced by their designs.

The slip factor μ appears in most of the equations of Tables I and II. More has been written on this subject than on any other in the field of radial pumps and compressors, primarily because it is of great importance to know exactly how much energy a wheel will absorb. If wrong values of μ are used in a design the desired pressure ratio will not be obtained even though the expected efficiency is reached. Reference 7 is a recent paper where tests obtained with one particular wheel are compared with data obtained from experiments, and with slip factor formulas, by other authors. As is frequently the case in many studies on the subject, test data from a single wheel obtained at off-design conditions are used to establish design point data for other impellers. Moreover, the highest ratio U_2/a_0 was only about 0.51 in the tests of Ref. 7. The bibliography of Ref. 7 fails to mention the investigations of Refs. 5 and 6 which were undertaken at Daimler-Benz A. G. by systematically testing ten high-performance impellers of different shapes up to values of U_2/a_0 of about 1.1. In the writer's opinion, the data published in Refs. 5 and 6 are extremely valuable to the designer and the original curves of the article have been replotted in Fig. 3 to give wider publicity to this important contribution to the state of the art.

With the slip factor known from Fig. 3 the compressor efficiency of a particular design can be determined from Eq. II(1) for known losses. Equation II(3) is plotted in Fig. 4 for $\gamma = 1.4$, and different values of $\mu\eta_c$, to show the magnitudes of U_2/a_0 necessary to produce particular pressure ratios. For advanced gas turbine applications it would be desirable to operate at pressure ratios of between 8 and 10. For $\eta_c = 0.8$ and $\mu = 0.875$, Fig. 3 shows that values of U_2/a_0 of about 1.8 are necessary to reach this goal. Thus, at an inlet temperature of 60°F, where $a_0 = 1120$ ft/s, the rotor of such a compressor has to operate with a peripheral speed U_2 of about 2000 ft/s, requiring special materials and careful rotor designs for the resulting high stresses.

By Eq. I(6) the rise of the total temperature in the compressor is $T_{t2} - T_0 = T_0(\gamma-1)\mu(U_2/a_0)^2 = 590°F$, or about 600°F, for $\mu = 0.875$ and $T_0 = 520°R$. Since the degree of reaction is around 0.5, the static temperature T_2 at the rotor discharge is then about 60 + 600/2 = 360°F. At this temperature, high-strength aluminum alloys have rupture stresses, and stresses for specified creep rates, which are less than one-half of the allowable stresses at room temperature. Hence it is necessary to use titanium alloys, for instance those with about 6 percent aluminum and 4 percent vanadium. At 360°F the design criterion for these materials is the yield stress since no appreciable creep effects occur even for operating times of 100,000 hours. Their 0.2 percent offset yield strength at 360°F is about 120 kpsi, with an ultimate strength of about 150 kpsi. As shown in chapter C of Ref. 8, the tangential stress in a non-supported ring of small radial thickness rotating with the peripheral speed U_2 is ρU_2^2. For titanium with a specific gravity of 4.43, this value is about 240 kpsi at $U_2 = 2000$ ft/s. Figures C.27 and C.29 of Ref. 8 show the so-called equivalent centrifugal stresses σ_e in rotors with radial blades as multiples of $\rho U2^2 = \rho\omega^2 R_2^2$, for a design where the disk extends to the outer tip of the blades at R_2, and another which has so-called scallops between the blades, similar to the rotor design shown in Fig. 1. Not counting the stress peaks at the central bore, which are more of the nature of stress concentrations that will be relieved by plastic deformations, because titanium has high ductility on account of its 20 percent elongation, the maximum stress ratios $\sigma_e/(\rho U_2^2)$ are about 0.25 and 0.16 for the rotors without and with scallops, respectively. Hence the maximum stresses at 2000 ft/s will be about 60 kpsi for one and about 40 kpsi for the other rotor. This discussion shows that compressor rotors operating at tip speeds of 2000 ft/s are feasible and that by arranging scallops, and using 75 percent of the 0.2 percent offset yield stress, or 90 kpsi, as design criterion, the maximum tip speed could be as high as 3000 ft/s or over 900 m/s. The latter speeds would give velocity ratios U_2/a_0 of about 2.68 at $T_0 = 60°F$ and $\gamma = 1.4$. For $U_2/a_0 = 2.68$, $\mu = 0.85$, $\eta_c = 0.80$, pressure ratios P_{t4}/P_o of about 43 could be reached in a single stage for gases with $\gamma = 1.4$. The extreme difficulties that would be associated with such a design, in particular those arising because of the large volume flow reductions, will not be discussed here. The intent of the fore-going deliberations is to show that pressure ratios in centrifugal compressors for air are not restricted because of rotor stresses.

Important advances are being made in nuclear gas turbines with helium as working fluid, as described in a recent article by Bammert and Bohm[9]. The main difficulties in the design of the turbomachines for this plant are the low pressure ratios that can be produced with helium in a conventional compressor stage, since the molecular weight of helium is only about 4 and $\gamma = 1.659$. At 60°F the velocity of sound in helium is 3275 ft/s. For a rotor with $U_2 = 3000$ ft/s, a speed ratio $U_2/a_0 = 0.916$ would be obtained in a radial compressor. All velocities in the compressor would be subsonic and design point efficiencies of about $\eta_c = 0.85$ seem feasible. For μ=0.90, $\eta_c = 0.85$, $U_2/a_0 = 0.916$, at $\gamma = 1.659$, the resulting pressure ratio P_{t4}/P_0 would be 2.43 in accordance with Eq. 8.

In Ref. 9 a 25 MW_e closed-cycle helium gas turbine plant is described that operates with a turbine pressure ratio of 2.55. The pressure ratio of the compressors will have to be about 2.7 to overcome the pressure losses in the reactor and heat exchangers, of which no values are given in the paper. Reference 9 shows however that the plant has three axial compressors in series, each consisting of 9 stages. Since intercoolers are arranged between the three compressors each will produce a pressure ratio of about 1.4. If the three axial compressors were replaced by two single-stage radial compressors, of the type described with an intercooler between them, it would be possible to obtain an overall pressure ratio of about six which would be of advantage for the cycle. The writer does not want to minimize the difficulties that would be connected with the development of radial compressors and radial turbines for such applications, in addition to those connected with the bearings, seals and gear drives, but it is felt that they might be the ultimate solution for these highly interesting power plants.

Equation I(1) will be used in an example to show the influence of the diffusor losses on the compressor efficiency at different speed ratios U_2a_0, for absolute flow angles α_2 of 60° and 75°. The velocity coefficients ψ will be determined by assuming a wheel efficiency η_W of Eq. 15 of 0.7 for both impellers. Equations 21 and 24 were used to establish Fig. 5. The deceleration ratios W_2/W_{1o} are 0.68 for $\alpha_2 = 60°$ and 0.366 for $\alpha_2 = 75°$ by Eq. I(5) for the data listed in Fig. 5. This difference makes the choice of equal efficiencies η_W for both cases somewhat dubious. It is seen from Fig. 5 that the rotor efficiencies η_R are 0.89 and 0.855 for $\alpha_2 = 60°$ and $\alpha_2 = 75°$, respectively. The corresponding values of ψ, which will be used in Eq. I(1), are 0.865 and 0.585. It is assumed further that the velocity V_4 at the diffusor discharge is 0.2 V_2, or $\lambda = 0.2$, so that $\eta_D^* = 0.96\ \eta_D$ by Eq. I(12). Figure 6 shows the large effect of the diffusor losses on the compressor efficiency. To obtain $\eta_c = 0.85$, the diffusor efficiency must be about 0.9 for all speed ratios U_2/a_0. If η_D were 0.7 instead of 0.9, the compressor efficiency would only be 0.75. At $U_2/a_0 = 1.6$, this decreased diffusor efficiency would reduce the pressure ratio of the compressor from about 7 to 5.8, which in a gas turbine plant would produce a mismatch between turbine and compressor, with additional adverse effects on the thermal efficiency of the plant. Figure 6 shows also that the diffusor has a larger influence on η_c at the higher flow angle α_2. On the other hand, the Mach number M_{V2} of the rotor discharge velocity will be lower at $\alpha_2 = 75°$ than at $\alpha_2 = 60°$. The respective values can be obtained from Eq. II(6) which has been represented in Fig. 7 for $\gamma = 1.4$. At $U_2/a_0 = 1.6$, the values of M_{V2} are 1.16 and 1.24 for α_2 of 75° and 60°, respectively, for the design parameters listed in Fig. 5.

Figure 7 shows that the Mach number M_{V2} becomes unity for values of U_2/a_0 between 1.1 and 1.3, depending on the choice of α_2. From Fig. 8, which is a representation of Eq. II(4), it can be noted that for a speed ratio $U_2/a_0 = 1.2$ and at a radius ratio R_{1o}/R_2 of about 0.67, which represents an average design value, the relative velocity W_{1o} at the rotor inlet has a Mach number M_{W1} of about 0.9 at an inlet angle β_{1o} of 65°. Figures 8 and 4 show that the Mach number M_{W1} for air compressors will not have to be larger than about 1.3 to produce pressure ratios up to about ten. Some sources state that no efficient inducers can be built for values of M_{W1} larger than 0.8 because of "shock losses". It seems to the writer that such statements are not different from those made some years ago, which predicted that it would be impossible for an airplane to break the "sonic barrier", or others which maintained that an axial compressor has to operate at subsonic velocities to be efficient. Advances in transonic axial-flow compressor stages have shown that human ingenuity can overcome these so-called barriers. Reference 10 is cited as an example, where a transonic boost stage ahead of the inlet of a centrifugal compressor is described, which produces a pressure ratio of 1.43 for air at an efficiency of 90 percent with a tip Mach number of 1.05.

The flow in an inducer of an impeller with radial blades is different from that in an axial-flow rotor. In the latter, particles that have been moving along the suction and the pressure sides of the blades are mixed at essentially constant static pressure after the trailing edges at the discharge, whereas no such mixing occurs in the flow channels where the inducer joins the radial blades of the impeller. Hence the pressure distributions along the walls of the inducer blades must be radically different from those along the surfaces of an axial rotor blade, and separation criteria that are based on the diffusion factor of axial cascades cannot be applied. Similar to the conditions in transonic axial stages the supersonic relative velocity at the tip of an inducer becomes sonic at a particular radius R_{1c}, and subsonic at radii R_{1x} smaller than R_{1c}. Denoting the Mach number of W_1 at R_{1x} by M_{1x}, and that at R_{1o} by M_{W1} as previously defined, there is

$$\frac{R_{1x}}{R_{1o}} = \frac{1}{\sin\beta_{1o}}\left[\left(\frac{M_{1x}}{M_{W1}}\right)^2 + \sin^2\beta_{1o} - 1\right]^{\frac{1}{2}} \qquad (45)$$

Figure 10 shows the values of R_{1x}/R_{1o} obtained from Eq. 45 for $M_{W1} = 1.3$, at different relative flow angles β_{1o} at the inducer tip, and for particular values of the Mach number M_{1x}. This graph is presented to show that it is non-sensical to state that M_{W1} cannot exceed particular values without specifying at what angle β_{1o} and at what ratio R_{1i}/R_{1o} this limitation holds. Whereas at $\beta_{1o} = 75°$ a Mach number of unity occurs at $R_{1x}/R_{1o} = 0.75$, the whole inlet annulus will have supersonic relative velocities at $\beta_{1o} = 50°$, for the same Mach number $M_{W1} = 1.3$ at the tip. Moreover, if at $\beta_{1o} = 75°$ the hub/tip ratio R_{1i}/R_{1o} of the inlet eye is 0.75 in one machine and, say, 0.3 in another the losses due to compressibility effects will certainly be different. Figure 10 also shows the Mach numbers M_{V1} of the absolute velocity V_1 ahead of the impeller which, as indicated earlier, has been assumed to remain constant in radial direction. They have values of 0.336 and 0.919, respectively, for $\beta_{1o} = 75°$ and $\beta_{1o} = 55°$ at $M_{W1} = 1.3$, and it is inconceivable to the writer that the losses will remain constant independent of M_{V1}. Clearly, if M_{V1} becomes larger than unity very special conditions occur since the flow in the annulus becomes choked at $M_{V1} = 1$ as has been discussed in Art. 9.9 of Ref. 1. Some of the peculiarities associated with cascades at supersonic inlet velocities are mentioned in Art. 9.10 of the same reference.

The writer believes that the, by now, almost classical view points of flows through turbomachines have outlived their usefulness. They may even be a hindrance for future developments and if accepted without questioning, may prevent original thinking and could make people believe that all problems have been or will be solved by their use. This classical method assumes that the fluid particles in a turbomachine move on axisymmetric stream surfaces of shapes which are either assumed a priori, or obtained

by simplified theoretical methods. Further, it is assumed that the flow through a turbomachine can be replaced by the flows through a multiplicity of annular channels bounded by neighboring stream surfaces, which are closely spaced between the meridional contours of the flow channel of the machine at hub and tip. The stream surfaces are actually considered to be thin, solid walls that do not create disturbances, and it is assumed that the flows in these individual channels do not interact with each other. In each one of the channels there exists then a so-called quasi two-dimensional flow of the type described in Art. 12 of Ref. 1. The performances of the different cascades, which are now arranged in the various flow channels to produce the specified flow deflection, are taken to be those of two-dimensional cascades obtained either in cascade test rigs or by theoretical methods. With the latter, one can at best attempt a solution for the special relative flows W in rotors that satisfy the condition $\nabla \times \vec{W} = -2\vec{\omega}$; that is, where the curl of the velocity function is a constant, since ω is the angular velocity vector of the rotor. Such flows are isentropic but can be compressible. However, disturbances due to shocks cannot occur. This condition limits the theoretical evaluation to flows where the local Mach numbers must be less than or, at the most, equal to unity. More general solutions of the so-called blade-to-blade problem on axisymmetric stream surfaces have not yet been obtained and are very difficult to formulate.

So-called quasi two-dimensional flows with $\nabla \times \vec{W} = -2\vec{\omega}$ are discussed in Art. 12 of Ref. 1. By introducing a stream function ψ there is obtained a second order partial differential equation of the form (see Eq. 12(9), p. 307, Ref. 1)

$$\frac{1}{R^2}\psi_{,,\theta} + \psi_{,,m} - \frac{1}{R^2}\left[(\ln\rho)_{,\theta}\right]\psi_{,\theta}$$

$$+ \left[(\ln R)_{,m} - [\ln(\Delta h\rho)]_{,m}\right]\psi_{,m} = -2(\Delta h)\,\rho\omega\sin\lambda \qquad (46)$$

The commas denote partial differentions with respect to the coordinates listed after them, where ϑ is the angle in peripheral direction and m the length along the generatrix of the stream surface. The mass density is denoted by ρ, R is the radius from the axis, Δh is the varying distance between neighboring stream surfaces, ω is the angular rotor velocity, and λ is the angle of the tangent to the generatrix with the axis of rotation. For $\lambda = 0$ the particles move on cylindrical stream surfaces, and $\lambda = 90^\circ$ covers flows in radial compressor wheels with stream surfaces that are planes perpendicular to the axis. For the latter case, and for conical stream surfaces, Eq. 46 has been solved by Stanitz for thin blades.[3] For cascades with airfoil-shaped blades, that are arranged on an arbitrary surface of revolution, computer programs are described in Ref. 11 for solutions with relaxation methods that need high-speed computers with large storage capacities. As interesting and useful these theoretical attempts are, one must be critical to evaluate what they really produce in form of results, and whether or how these data will help to improve present designs, and to create the turbomachinery which is to be built in the future.

The mere fact that modern computers can solve differential equations with complicated boundary conditions which, hitherto, could not be tackled by hand calculations is no assurance that the results must be correct from a physical point of view. Computers can only perform mathematical manipulations as they are told to do, and no result is better than the assumptions that were used to formulate the problem that is solved by these apparently sophisticated, but inherently stupid, machines.

Two of the necessary boundary conditions for solving Eq. 46 with the programs of Ref. 11 require that the flows upstream and downstream of the blades are uniform, and that the flow angles at these stations be specified. These conditions imply that the tangential deflection through the cascade is known a priori, whereas in actuality the possible deflection depends on the attitude of the blades in the cascade and the upstream conditions only. Whereas in turbine cascades it is possible to calculate the discharge angle from the geometry of the cascade with approximate methods, such predictions are not possible in axial compressor cascades, in fact one of the major problems is to find out what the discharge angles are for imposed incidence angles. Actually then, Ref. 11 produces pressure distributions about blades for specified locations of the rear stagnation points, and if they have been chosen wrongly the pressure pattern will be wrong also. As in most theoretical cascade flow investigations the effects of upstream or downstream cascades cannot be taken into account; the row investigated constitutes in actuality a disturbance located between two flow fields that extend to infinity far upstream and far downstream without being disturbed by other cascades.

A major drawback of all methods that are based on Eq. 46 is however that the right-hand side of this relation becomes zero if either ω is zero, or if λ is zero. If the angular velocity is zero the cascade is stationary and instead of the pattern of the relative velocity W one deals with the absolute velocity V in a stator whose curl $\nabla \times \vec{V}$ is now zero because of the initial condition that $\nabla \times \vec{W} = -2\vec{\omega}$. The velocities V of such flows must be gradients of a potential function φ, and Eq. 46 can be modified to

$$\nabla^2\varphi = \frac{\nabla\varphi}{a^2} \cdot \nabla\left(\frac{V^2}{2}\right) \qquad (47)$$

where "a" is the variable velocity of sound at the different locations in the flow field. As before it is necessary that $M = V/a$ is everywhere smaller than unity. For incompressible flows, where the velocity of sound "a" is tending toward infinity, Eq. 47 reduces to Laplace's equation $\nabla^2\varphi = 0$. Equation 47 is a partial differential equation of the Poisson type and the term on its right-hand side can be interpreted mathematically to be the result of sources in the flow field. Expressed differently, the curl of $\vec{V}$ is zero, but its divergence $\nabla \cdot \vec{V}$ is not; which means that flow must be generated somewhere in the field, and sources judiciously arranged therein can take care of this situation. Reference 12 develops calculating methods that are based on this idea by using the principles of superposition, but again for assumed axisymmetric stream surfaces, namely, cones in particular.

It can be noticed also, that Eq. 46 changes into Eq. 47 if $\lambda = 0$; that is, if cylindrical stream surfaces are assumed to exist. Thus, as far as axial machines with cylindrical stream surfaces are concerned, the flow through a rotor is not different from the flow through a stator, if the cascades have the same geometries and if the flow angles of the relative and absolute flows are equal. On the other hand it can be proved without a shadow of a doubt, e.g., by Art. 8.5 of Ref. 1, that even isentropic relative flows in rotors must be fundamentally different in character from absolute flows. From Eq. 8(23) of Ref. 1 it can be seen clearly that the simplest relative flow must have $\nabla \times \vec{W} = -2\vec{\omega}$, and if Kelvin's theorem is extended to relative flows (Eq. 8 (22) of Ref. 1), and applied to isentropic conditions, one sees that the change of the circulation Γ_R around a moving fluid curve C in a relative flow is not zero but equal to

$$\frac{D\Gamma_R}{dt} = -2 \oint_{(C)} d\vec{r}_R \cdot \vec{\omega} \times \vec{W} \tag{48}$$

In an absolute isentropic flow, however, the change of the circulation around a moving fluid is indeed zero. Equation 48 indicates that $D\Gamma_R/dt$ is zero only if the relative flow vectors $\vec{W}$ are everywhere parallel with $\vec{\omega}$, hence parallel with the axis of rotation. Rotors of this type are not capable of changing the energy of fluids and have no practical interest. That the condition $\nabla \times \vec{W} = -2\vec{\omega}$ is not in conflict with Eq. 48 can be proved with simple means.

It can be stated therefore that the stream surfaces in a rotating cascade must differ from those that would occur if the same cascade were stationary. More precisely, the stream surface in a stationary cascade, whose flow satisfies $\nabla \times \vec{V} = 0$, must change to a pattern that satisfies $\nabla \times \vec{W} = -2\vec{\omega}$, and it is not possible that the relative flow in the rotating cascade has the same stream surfaces as the absolute flow. In particular, the relative stream surfaces cannot be axisymmetric, if those of the absolute have this character. More about these conditions has been described in Art. 10.5 of Ref. 1, but it is evident from the above discussion that results obtained by solving Eqs. 46 and 47 must be of approximate nature even for the idealized flows that are investigated, and they must be interpreted in the proper perspective of their initial assumptions.

Such results, or data from stationary cascade test rigs which basically are obtained with the same assumptions as those of the above-mentioned theories, are now used to establish the blading elements in the individual flow channels between the solid stream surfaces. The classical method consists in designing the actual blade surfaces through the profiles of these blade elements. The "solid" stream surfaces are then, so to say, removed and it is assumed that the originally calculated or assumed stream surfaces will also exist for the flow about these three-dimensional blades. It is quite clear that there are many possibilities of arranging an actual blading with the profile sections that are obtained from the flows through the individual flow channels, depending, for instance, on how the leading edge of the blade is arranged. In the inducer of Fig. 1 the leading edge of the blade could be pulled forward in flow direction to obtain a blade surface that is leaning more away from a meridional plane than if the leading edge were to slant backward, although at the different radii the blade angles would be exactly equal. Without a doubt these two blades would exert different forces on the flow, one could tend to push the flow toward the tip, the other toward the hub, and it is inconceivable that the flow pattern in the meridian channel would remain unchanged. In Ref. 2 (Table C-2, p. 26) an investigation dealing with the blading of an axial-flow machine has been carried out to check whether it is possible to build a rotor with a very large number of thin blades that produces the idealized relative flow with $\nabla \times \vec{W} = -2\vec{\omega}$ near its cylindrical hub. This flow condition establishes a particular change of the flow angle in radial direction, and requires that the blade surface consists of radial lines. Since for a large number of blades the flow and the blade angles must be identical, the last mentioned requirement establishes the change of the flow angle along the radius by itself. It can be seen that the two values differ, primarily because from $\nabla \times \vec{W} = -2\vec{\omega}$ the necessary blade angle change depends on the ratio of ω and the axial component of $\vec{W}$, whereas this is not the case for the other. Hence, it is evident that the condition $\nabla \times \vec{W} = -2\vec{\omega}$ cannot be maintained in a blading with a finite axial length, and that the actual blade shapes as a whole will have an influence on the flow through them. These examples show that the flow patterns in a machine can be influenced by particular arrangements of the profiles in direction of the blade height and that they will have a bearing on the meridional flow. The classical approach, so to say, linearizes the problem, and does not take account of the interactions that occur between the flows through the different elementary channels from the hub to the tip. It further tries to explain all phenomena with a two-dimensional model, at best with one on stream surfaces that are surfaces of revolution, and looses sight of the actual three-dimensional effects that occur in reality. These limiting view points seem to be particularly harmful if supersonic flows occur in a relative flow field where, as discussed earlier in connection with the inducer inlet, the absolute flow is subsonic. Stationary cascade test data cannot give a true picture of the conditions since they replace again the relative flows by an absolute flow between "solid" stream surfaces, where in particular the condition that the flow component perpendicular to the cascade axis, which is in reality the actual absolute flow, has no special significance. In a supersonic cascade test rig it will hardly be possible to determine cascade performance at different incidence angles nor establish design data for blades where only parts of the blades have supersonic velocities. For inducers of radial compressors which are followed by radial blades it does not seem possible to use cascade data with any degree of realism, and only experimental work with actual rotating wheels will show what detrimental effects high relative flow Mach numbers have on the performance.

There seem to exist a number of design variables that should be examined for supersonic inducers. The possibility of influencing the flow pattern near the tip by appropriate blade shapes to produce, say, greater mass flow rates per unit area near the hub, has been mentioned. These designs could be extended to produce swept-wing effects, similar to what has become the standard design of wings for high-speed airplanes. It is well known that in supersonic flows the velocity parallel with the leading edge of a swept-back wing with infinite span cannot produce variations in pressure, hence only the component of velocity perpendicular to the leading edge can create losses that are caused by compressibility effects. Peculiar conditions could however occur at the outer wall, if this principle were applied to the design of the inducer inlet edges, but it might be possible to obtain considerable improvements. The writer is surprised that such designs

have not been tried for axial compressor stages, especially for those with large blade heights. Swept-back blades would not necessarily have greatly increased bending stresses, since the maximum section modulus of an airfoil profile is a large multiple of the minimum modulus about the outer principal axis. If the centers of gravity of the profiles along the blade height were displaced backward along this axis of the hub profile, it should be possible to minimize the stresses that are caused by the additional bending moment about the other principal axis.

The writer believes that it is possible to build inducers at supersonic relative inlet velocities for absolute inlet Mach numbers M_{V1} of about 0.5 to 0.6 with good efficiency and minimum flow disturbances. Converging-diverging passages in the inducer seem unnecessary, especially if only part of the rotating channel has supersonic velocities. Leading edge radii must be as small as possible, but large enough to avoid damage by flutter, and great care must be taken to properly design the suction side of the blade to provide a good transition into the actual blade channel. It is not believed however that the blades must be designed for incidence angles if the proper blockage factor is used for the flow area calculations at the inlet. This statement contradicts the data of Ref. 13, where the optimum rotor efficiency η_R is shown to occur at positive incidence angles of about 10^o at R_{1o} for blade angles of 57^o. The inlet channel ahead of the eye of the wheel that was tested, has curved meridinal contours, hence the inlet velocity V_1 is not uniform from R_{1i} to R_{1o}. Although it is stated in Ref. 13 that the distribution of V_1 was determined by probes, slight inaccuracies of the measurements, or a location of the probe at some distance forward of the leading edges of the rotor could easily be responsible for these unusually large incidence angles. By means of theoretical methods, which are not described in detail, the velocity distributions along the inducer were determined also in Ref. 13 to verify the test data. However, as shown by Fig. 5 of Ref. 13, the inducer has simply been replaced by a cascade, since at its discharge the velocities on either sides of the blade are shown to be equal, a situation which cannot exist in reality, and which gives questionable value to the argumentation based on it.

Design criteria for the whole rotor passages from the inlet to the discharge are often given in terms of the deceleration ratio W_2/W_{1o} of the relative rotor velocities. From earlier discussions with regard to rotor losses it is evident that not all losses in a rotating impeller depend exclusively on this ratio. They will also be greatly influenced by the performance of the inducer, in particular, on the velocity distribution that exists at the station where the inducer blades join the radial impeller blades. It is necessary to have a good appreciation of the complexities of flows in rotating impellers to avoid over-simplifications and the setting up of design criteria that are based on wrong models. An invaluable contribution to investigating the real flow phenomena in rotating impellers has been made by Fowler[14], who actually measured the velocity distribution in the passages of a large compressor with probes from a platform inside the hub that was rotating with the wheel. Figure 11 has been adapted from a personal communication of Mr. Fowler to the writer. It shows the velocity profiles at seven cross sections of the rotor flow channel of an unshrouded wheel with radial blades at the discharge, when operating at a peripheral speed $U_2 = 17$ ft/s. The meridional flow channel has the smoothly changing contours used for modern designs. Plane 1 of Fig. 11 is at the inlet section of the inducer blades, extending from the leading edge of one blade to the back of a neighboring one, and the blades become radial near plane 3. The zones with reduced velocities at the blade tips that are due to the blade gap and the scrubbing effects along the outside wall, remain almost equal from plane 3 to the discharge plane 7. It is of interest to compare these measured velocity distributions with the theoretical solutions of Eq. 47 for radial blades and incompressible flows. The pattern of the streamlines obtained by Stanitz for a radial impeller with 20 blades is shown in Fig. 3.5.2 of Ref. 3. The velocities are inversely proportional to the distance between neighboring streamlines. The leading surface of a blade will be called the pressure side, the trailing surface of the same blade is its suction side. Hence the direction in a blade channel from the pressure side of one blade to the suction side of the neighboring one, is in direction of rotation of the wheel.

At the outer radius of the wheel (R = 1 in Fig. 3.5.2 of Ref. 3) the theoretical analysis predicts that the velocity in a blade channel increases in direction of rotation, whereas exactly the opposite trend is seen to occur in plane 7 of Fig. 11. However in planes 3 and 4, and to a lesser degree in plane 5, the measured velocity changes agree in the main with the theoretical ones which predict a velocity increase in direction of rotation at all radii. This situation occurs because the theoretical method shows, or is based on the assumption, that at radii smaller than about 70 percent of R_2 the relative velocities are everywhere radial. Then, as determined in Art. 10.6 of Ref. 1, and as shown in Fig. 10(5a), they will increase linearly with the angle along the periphery in direction of rotation. The measured reversal of this behavior, starting from plane 5 to the discharge plane 7, cannot be due to viscous effects only, which are neglected in the theoretical treatment, but must occur because of flow peculiarities that a simplified theory cannot take into account. In his personal communication to the writer, Mr. Fowler also remarked that the directions of the relative velocities at the discharge did not have as large a deviation from the radial direction as Fig. 3.5.3 of Ref. 3 shows. The measured flow distributions suggest that considerable mixing of the different flow strata must occur while they pass through the compressor and it is very unlikely that there exist axisymmetric surfaces. Reference 15 describes tests of single, straight diffusors that were arranged radially and rotated in the test rig of Ref. 14, to examine the effects of centrifugal and Coriolis forces on decelerated flows that move radially outward. Diffusors with different divergence angles where investigated, first while stationary and then while rotating. It was found that considerable differences occur if a diffusor is rotated. Static tests with a two-dimensional diffusor with an included angle of 10^o showed the well-known peaked velocity distributions that occur for these angles. If rotating, the peaks flatten out and the flow becomes more stable. These results agree with the conclusions reached earlier about the beneficial effects of a centrifugal force field on decelerated flows, but they show also that boundary layers along rotating walls, where the fluid particles are also affected by Coriolis forces, exhibit different characteristics than those along stationary walls. Similar results have been obtained in Ref. 16 which describes tests of flows through a channel with constant cross section that is rotated about an axis. Because of these conditions, different separation criteria for boundary layers must be applied if they occur on stationary walls or on surfaces that rotate about an axis.

For this reason it is not possible to use conventional boundary layer theories as a means to find permissible deceleration ratio W_2/W_{1o} for the relative flows in impellers, nor can attempts be successful that try to relate this ratio to the NASA diffusion factor, which has proved to be a satisfactory separation criterion for axial compressor bladings which have small flow deflections, hence, where the changes of the

Coriolis forces are small if the blading rotates. Much more fundamental work dealing with boundary layers on rotating walls and investigations with modern flow visualization methods must be carried out before it is possible to establish satisfactory design limits for flows in radial impellers. Recent endeavors that use holography with Pulse-Lasers for investigations of flows in rotating wheels might open entirely new ways to study actual flows in high-speed machines where the effects of centrifugal and Coriolos forces are large.

If the above-mentioned peculiarities of rotor flows are not taken into account one might come to the conclusion, as some sources do, that flow separations will occur in an impeller if W_2/W_{1o} equals 0.6, and that a ratio of 0.62 should be used for design purposes to avoid excessive losses. Such values are obtained from analogies with stationary diffusors or oversimplified boundary layer considerations for, say, linearly changing velocities along a surface, as is the case on the suction side of a blade in an axial compressor cascade. Figure 9 is a diagram for the determination of the deceleration ratio W_2/W_{1o} in accordance with Eq. II(5) of Table II. If, for instance, the limit for this ratio were set at 0.65, the discharge angle α_2 could not be larger than about 60° for a radius ratio R_{1o}/R_2 of 0.7 and $\beta_{1o} = 60°$. For larger discharge angle α_2 the radius ratio R_{1o}/R_2 would have to be decreased. Figure 12 is presented to show these conditions more precisely if the lower limit of W_2/W_{1o} is assumed to equal 0.6 and if the slip factor μ is 0.85. For these conditions and at $\alpha_2 = 75°$, the maximum radius ratio R_{1o}/R_2 could not exceed 0.42 at a relative flow angle $\beta_{1o} = 70°$. Experience with high performance compressors shows however that impellers with radius ratio in accordance with the dashed curve have operated successfully. At $\alpha_2 = 75°$, for instance, and at a radius ratio R_{1o}/R_2 of 0.68 the deceleration ratio is of the order of 0.35 to 0.3, depending on β_{1o}, as shown in Fig. 9 by following path "b" in the diagram. Therefore, if the deceleration ratio W_2/W_{1o} is used as a preliminary design criterion it is permissible to apply minimum values of about 0.3 or even somewhat lower, say, about 0.26. A unique relationship between W_2/W_{1o} and the wheel efficiency η_W cannot be established because of lack of test data but in Paragraph 5 some test results are plotted to show the order of magnitude of η_W. A correlation between W_2/W_{1o} and η_W can probably never be obtained because of the additional rotor losses that depend on a number of additional factors.

For known values of M_{W1}, β_{1o}, and U_2/a_o it is possible to calculate the wheel radius R_2 with Eq. II(9) of Table II, if the ratio R_{1i}/R_{1o} were known. The quantity k_{B1} is a blockage factor which is primarily depending on the number of inducer blades and their thickness at the inlet throat, although excessively thick boundary layers on the walls of the inlet annulus can affect k_{B1} also. Evidently if U_2/a_o is known the angular velocity ω is known also, if R_2 has been determined. However ω can be determined directly by Eq. II(10) of Table II, for known or chosen quantities M_{W1} and β_{1o}. Eq. II(10) is useful to establish the necessary rotative speed to handle particular flow rates. If ω is given, because of the prime mover that drives the compressor, Eq. II(10) makes it possible to verify whether a particular flow rate can be handled at this speed. The ratio of axial blade width b_2 and R_2 is obtained by Eq. II(11). The blockage factor k_{B2} is the ratio of the actual flow area at the wheel discharge and the area $2\pi R_2 b_2$, multiplied by an experience factor that depends on the boundary layer thickness on the side walls.

The necessary diffusor exit area A_4 at the radius R_4 is obtained from Eq. II(14) for specified values $\lambda = V_4/V_2$ and known efficiencies η_c. A blockage factor k_{B4} takes account of the displacement thickness of the boundary layers which reduce the actual flow area at the discharge of the diffusor. Section x-x of Fig. 1 is taken to be either the throat of the diffusor where the flow is choked if the absolute velocity V_2 after the rotor is supersonic, or the entrance section of the actual diffusor if V_2 is subsonic. The necessary total flow area of all diffusor channels is denoted by A_x, and k_{Bx} is again an area blockage factor. The area A_x can be determined for both cases if the ratio of the total pressures P_{tx} at station x and P_{t2} at the rotor discharge is known. Although P_{t2}/P_0 could be expressed by Eq. I(19) of Table I and then introduced into Eqs. II(13) and II(14), it is better to use these relations as listed, since it is possible to judge approximately what values the ratio P_{tx}/P_{t2} will have for particular diffusor designs. If V_2 is supersonic the throat area is obtained with the dimensionless critical flow function Φ_c of Eq. II(14) which has a value $\Phi_c = 0.6847$ for $\gamma = 1.4$. For subsonic velocities V_2 the diffusor inlet area can be determined only if the velocity V_x at station x is specified, by assuming a value $\xi = V_x/V_2$. Usually this ratio is taken to be about 1.02 to 1.05 because a slight acceleration between stations (2) and (x) will produce more uniform flow conditions at the diffusor inlet. For a chosen number of diffusor flow channels, usually arranged between parallel walls, the diffusor widths at inlet and discharge can be determined from A_x and A_4, and the methods described in Paragraph 5 establish the necessary length of the diffusor channels. With this length and the chosen diffusor arrangement it is possible to establish the outer radius R_4 of the diffusor.

4. SIMILARITY CONSIDERATIONS

If effects due to gravity, surface tension, and heat conductivity can be ignored, which is permissible for most flows in turbomachines, the laws of dynamic similarity establish that flow processes of perfect gases in geometrically similar channels are equal in performance if the Reynolds numbers R_e and the velocity ratios $V/\sqrt{R_G T}$ are respectively equal at corresponding stations in the channels. As derived for instance by Ackeret et. al., in Ref. 17, the latter condition can be expressed in terms of equal Mach numbers M, with the additional requirement that the fluids passing through the geometrically similar channels have equal specific heat ratios γ. Reference 17 shows also that the effects of different values of γ are small only if the Mach numbers are less than about 0.6. The reason is that gases with different heat ratios γ produce different relative changes in density if passing through a channel with particular area ratios. Hence the values $V/\sqrt{R_G T}$ cannot remain equal in geometrically similar channels.

Assuming then that gases with equal values of γ are considered only, and that the Reynolds numbers of the flows in the compressors to be compared are in a range where they can vary considerably without largely changing the frictional coefficients; that is, if they are moderately large and if the flow surfaces are rough, dynamic similarity is achieved in geometrically similar machines at equal Mach numbers.

In hydraulic machines, similarity considerations that are based on the so-called specific speed have been used with success and it will now be examined whether it is possible to apply this method also to the compressors considered here that operate at high speed ratios U_2/a_o. Attempts to obtain design limits and to establish the optimum operating range of radial compressors with this means are described in Refs.

18 and 19. In both reference there is used the specific speed N_s (see Eq. III(1) of Table III)

$$N_S = \frac{N\, Q^{\frac{1}{2}}}{H_{is}^{3/4}}$$

similar to the practice in hydraulic pump design. In the latter application, Q, which is the volume flow rate through the machine, is everywhere constant. In a compressor for gases however, where the volume flow rate will change considerably from inlet to discharge, a choice must be made whether Q at station (1), or at, say, station (2) is to be used in Eq. 50. In both references the quantity Q is taken to be the inlet flow rate Q_1 without giving reasons for this choice. As in Refs. 18 and 19, and as shown in Table III by Eq. III(1), the value of N_S depends on the system of units which is used. In the two cited references N_S has the dimension rpm $ft^{3/4}$ $sec^{-1/2}$, which is awkward for purposes of comparison with similar coefficients in other systems of units, and such formulations are not in keeping with the general and very desirable tendency to use dimensionless quantities throughout. For this reason it is more appropriate to use the dimensionless speed n_S, with units as defined by Eq. III(3) of Table III, which for particular conditions has the same value in all consistent systems of units. The quantity n_S is obtained by dividing the value of N_S in the given English units by 129.

Whereas Ref. 18 (Fig. 2.8) simply presents a graph showing a direct correlation of the efficiency of different compressor types with N_S, Ref. 19 uses the so-called specific diameter D_S as an additional parameter, which is defined by (see Eq. III(2) of Table III)

$$D_S = \frac{D\, H_{is}^{1/4}}{Q_1^{1/2}}$$

This quantity is also not dimensionless. However Eq. III(4) defines a dimensionless specific diameter d_S that is obtained from D_S in English units by division with 0.42.

The coefficient ξ_1 of Eq. III(5) represents the ratio of the area of the flow annulus at the compressor inlet and the area πR_{1o}^2, where R_{1o} is the outer radius of the rotor inlet eye. As shown in Table III the quantities n_S and d_S can be expressed also with the chosen parameters of Tables I and II, to obtain Eqs. III(6) and III(7). Both contain ξ_1, so that this ratio can be obtained from either of these relations as shown by Eqs. III(8) and III(9). By equating these expressions there is obtained Eq. III(10), or

$$n_S\, d_S = \frac{2}{(\mu\, \eta_c)^{1/2}}$$

where μ is the slip factor and η_c the compressor efficiency. Since μ is a known quantity for a particular compressor design, and because η_c can be determined with Eq. II(1), the specific diameter d_S is directly related to n_S and there is no reason why both n_S and d_S should be specified for a design with radial blades. Equation III(11) shows that by specifying n_S there can be obtained the radius ratio R_{1i}/R_{1o} for particular values of β_{1o} and R_{1o}/R_2 which are usually chosen on the basis of other considerations, as explained earlier, Equations II(9) and II(10) of Table II, with the known ratios R_{1i}/R_{1o}, would then give directly the necessary radius R_2 or the angular velocity ω for given operating conditions. If the optimum efficiency of a compressor were a unique function of n_S, and if R_{1i}/R_{1o} and/or the other parameters could be adjusted to meet the optimum value, the designer would have a simple criterion for the optimization of compressors.

From Ref. 18 (Fig. 2.8, p. 38) it appears that radial compressors should have the best efficiency for values of N_S between 75 and 85, or for n_S between 0.58 and 0.66. Table III gives an example for design parameters that have been used successfully. In one case, a radius ratio R_{1o}/R_2 of 0.56, in another a ratio $R_{1o}/R_2 = 0.7$ was chosen. For the smaller value of R_{1o}/R_2 it is not possible to design for $N_S = 80$, since the hub/tip ratio at the inlet becomes zero at $N_S = 71$. In an actual design of a compressor that had efficiencies higher than 80 percent, the hub/tip ratio at the inlet was about 0.46 for $R_{1o}/R_2 = 0.56$, hence it operated at $N_S = 60$ and did not have the much lower efficiency predicted by Ref. 18. For the example in Table III with the higher ratio $R_{1o}/R_2 = 0.7$ the ratio R_{1i}/R_{1o} becomes zero at $N_S = 99.4$, and an actual high-performance machine is known to the writer that has an inlet hub/tip ratio of 0.34, hence it operates at $n_S = 0.725$ or $N_S = 93.5$. Thus, the sharp optimum for N_S in Ref. 18 does not occur in reality and $N_S = 80$ or $n_S = 0.62$ is not a design criterion.

It is obvious from Eq. III(6) that all radial compressors have values of N_S between, say, 60 and 110. Lower and higher values would lead to impossible designs which would never be built anyway. The only merit of the specific speed is to find out whether a radial compressor can be built at all for given values of N, Q_1, and H_{is}. If N_S is outside the range of 60 to 110, and if the above-mentioned design conditions cannot be changed, another type of compressor has to be chosen. However, if the relations of Table II were applied, the same conclusions would also be reached immediately even if the specific speed concept had never been invented. In fact its use can also be dangerous if, as might be the case for the example of Table III with $R_{1o}/R_2 = 0.56$, the designer would try to reach the highest possible N_S by making the radius ratio R_{1i}/R_o excessively small or choosing too high a value of R_{1i}/R_o to reduce N_S for $R_{1o}/R_2 = 0.7$. The example also shows that large changes of R_{1i}/R_{1o} have a small influence of N_S except, near the maximum possible value of N_S where R_{1i}/R_o tends toward zero. Further, if $N_S = 80$ would be considered necessary, a large number of high-performance radial compressors would never have been built, much to the detriment of the development of these promising machines, where a better physical understanding of the complicated flow phenomena can still lead to considerably improved performance.

Unfortunately there always exists the tendency in engineering to try to set up simple rules or criteria which make it possible to judge whether or not a design is feasible, without having to go through the strenuous mental processes to try to understand the phenomena that actually occur and to relate them to the fundamental laws of nature. If our only task were to build the same machines over and over again, sometimes

a little smaller, all would be well with this kind of handbook engineering. However, if an engineer believes that improvements are possible,aand if he reflects on what has happened during the past years he cannot doubt that this will be the case, he must not accept the barriers that have been set up by past experience, and be impressed by the achievements that have been made. With a critical mind he has to evaluate what is true and what is false with accepted methods, and his aim must be to try to understand, to search, and to improve. Too often engineers are handlers of formulas or recipes, and there is the tendency to accept their results as correct without much questioning, especially if they are ground out by a computer, without finding out what sort of basic principles and assumptions led to the numbers. In the near future our modern computers may well be the biggest obstacle to imaginative original thinking and the use of new concepts, since for every problem there will very soon exist some sort of a program that can show that everything is known, and that nothing new needs to be added. All one has to know is the necessary format for the input to obtain the desired result, in print, in graphs, even in drawings. The inventive and critical engineer however must take the trouble to find out how the program was established and what basic principles and assumption were made, and must then evaluate the obtained numbers in the light of these conditions.

The biggest objection to the specific speed criteria is however that they do not satisfy the laws of dynamic similarity, even not for the limiting conditions that were assumed earlier. Equation III(6) shows that n_S is independent of the pressure ratio that is produced by a compressor. If all factors in Eq. III(6) are equal for two compressors, they can have different values of U_2/a_0 and therefore widely different blade width b_2 at the rotor discharge. One compressor could operate with subsonic, the other with supersonic velocities at the diffusor inlet. Figure 13 is an adaptation of Fig. 4 of Ref. 19. The curves of constant efficiency $\eta_c = 0.7$ and $\eta_c = 0.8$ and the curves labeled $N_{W1} = 1.0$ and $N_{W1} = 1.2$ for P_{t4}/P_0 were taken from Ref. 19 and redrawn in a bigger scale. Although labeled as lines of constant Mach number in Ref. 19 the curves for N_{W1} = constant are for constant ratios of relative inlet and critical velocity for the total inlet temperature. Equation III(14) of Table III shows how these ratios are related to the actual Mach numbers M_{W1}. Although the differences between N_{W1} and M_{W1} are small at low Mach numbers, the values of M_{W1} vary from 0.94 to 1.01 for $N_{w1} = 1.0$ if β_{1o} changes from 50° to 75°. According to the author of Ref. 19 the curves for $N_{W1} = 1.0$ and 1.2 represent design limits for higher pressure ratios. It is stated that maximum efficiencies will occur for impellers with backward bent blades operating at specific speeds N_S between 90 and 130, and specific diameters D_S between 1.3 and 1.7. The straight lines labeled $\mu\eta_c$ = constant which the present writer drew into the original diagram of Ref. 19 represent Eq. III(10), and relate D_S to N_S for wheels with radial blades at the discharge. Average values for $\mu\eta_c$ for such impellers are 0.7, hence all radial compressor of this type must lie in the vicinity of this curve for $\mu\eta_c$ in Fig. 13. The points labeled (1) to (7) in Fig. 13 represent design points for some actual compressors known to the writer, operating with U_2/a_0 of about unity, and inlet Mach numbers of 0.9 and higher. It is of interest to note that all these points lie on the curve $\eta_c = 0.70$ of Ref. 19 whereas all compressors, even those having N_S-values between 60 and 70, have efficiencies of 80 percent and higher. This situation shows again that the specific speed concept is a highly unsatisfactory design criterion, especially for radially-bladed compressor wheels, since it is impossible to design such machines with operating points that fall inside the closed curve, labeled $\eta = 0.8$ in Fig. 13. It is pointed out in Ref. 19 that the data presented in its Fig. 4 were calculated on the basis of loss considerations. It can be concluded therefore that this loss evaluation is in error or unsuitable for compressors with rotors that have radial blades at the discharge.

What seems more crucial to the writer is the fact that on the basis of Fig. 4 of Ref. 19 (or Fig. 13 of the present article) one might come to the conclusion that it is not possible to build high-speed compressors of the type discussed here with high efficiencies, for instance, as required for gas turbines, and that further developments of these machines might not be undertaken because of "proof" that improvements are not possible. This is again a case which shows that an analysis is no better than its assumption. Since the specific speed has no real physical meaning, unlike the actual similarity parameters such as Reynolds number, Mach number and others, the writer deplores the tendency to express everything in flow machines with N_S, also phenomena on which N_S has really no primary influence. Because of the definition of N_S it is always possible to do so because either rotative speeds and flow velocities, or lengths, can be related to it, and since in all these expressions there then appears N_S in one form or another, depending on what simplifying assumptions were made, the reader is given to believe that N_S has a governing influence on the performance, and that manipulating N_S is all that needs to be done to create an optimum design. Everyone who has observed actual flows in turbomachines in test rigs, and has tried to understand the complexities of these processes will agree that nature just is not so simple that it can be explained by a set of convenient numbers.

5. LOSSES IN RADIAL COMPRESSORS

It has been stated earlier that the wheel efficiency η_W of Eq. 15 is the best measure for the quality of a rotor wheel. As indicated, a number of factors influence η_W, but it will be examined now whether the deceleration ratio W_2/W_{1o} has an overriding effect on η_W, as has been suggested by some sources which state that W_2/W_{1o} should not be smaller than about 0.6 to avoid flow separations. It has already been shown in Fig. 12 that such a limit cannot be used for compressors that operate at high speed ratios U_2/a_0 because the radius ratios R_{1o}/R_2 become too small, and it is then not possible to handle the large changes in volume flow rate from rotor inlet to rotor discharge, that occur at high pressure ratios, with acceptable ratios of axial blade width b_2 and R_2. The example of paragraph 6 demonstrates this condition clearly. If $W_2/W_{1o} \geqq 0.6$ were a realistic criterion, the losses in rotors with high speed ratios would be large and it would be difficult to obtain high efficiencies. Figure 14 is presented to show that many compressors have deceleration ratios that are smaller than 0.6 without a drastic decrease in η_W. The circles in Fig. 14 represent design point data of some of the compressors of Ref. 6, and others that are known to the writer. The points indicated by × and + were calculated from the data given in Ref. 13, and the curves drawn through them represent the change of η_W with operating conditions of a particular wheel at values of U_2/a_0 of 0.83 and 1.02, respectively. All data points are for impellers with radial blades at the rotor discharge, and all compressors operate at high speed ratios, having overall efficiencies in excess of 80 percent.

In contrast to the expected trend that η_W decreases with decreasing values of W_2/W_{1o}, the opposite

could be deduced from Fig. 14, since wheel No. 1 with $W_2/W_{1o} = 0.265$ has the highest efficiency $\eta_W = 0.77$. For each data point in Fig. 14 are also given the ratios R_{1o}/R_2, R_{1i}/R_{1o}, b_2/R_2 and $\Delta x/\Delta R$ of the rotor. The latter ratio establishes the general shape of the meridional channel and the values show that the contours of the meridional flow paths of all compressors must have small curvatures with the exception, maybe, of wheel No. 11. Definite reasons for the higher values of η_W in some designs cannot be given, probably because of the effect of the design of the inducers on the wheel performance. However, it is recognizable from Fig. 14 that high efficiencies η_W are reached either for high ratios R_{1i}/R_{1o} or high values of b_2/R_2. The influence of R_{1o}/R_2 seems small, although most good wheels have values of R_{1o}/R_2 between 0.6 and 0.7. Large ratios R_{1i}/R_{1o} require high relative Mach numbers M_{W1} to pass the flow rate through the eye of the impeller, and high ratios b_2/R_2 are obtained if the absolute flow angles α_2 are large. For high values of M_{W1} the inducer becomes critical, and with large angles α_2 the design of the diffusor, especially the transition between wheel and diffusor throat, becomes a difficult task. It is felt that high performance compressors can be developed if more attention is given to these two problem areas.

From the curves in Fig. 14 it is quite evident that the range in which η_W remains constant for off-design operation becomes smaller the higher the speed ratio U_2/a_0 is, a condition which is, at least in part, responsible for the steeper characteristics of compressors operating at high speed ratios.

The ratio of b_2/R_2 also has an effect on the disk friction loss of an impeller. Assuming that the disk extends to the outer radius R_2; that is, if no scallops are arranged, a frictional moment M_{DF} acts on the back side of the impeller which can be determined by [20]

$$M_{DF} = c_M \rho_2 D_2^3 U_2^2 \tag{49}$$

where c_M depends on the Reynolds number

$$Re = \frac{U_2 D_2}{\nu} \tag{50}$$

and the axial gap δ_a between the rotating disk and the stationary wall. The influence of the ratio δ_a/R_2, and the effect of disk roughness, which have been investigated by Refs. 21, 22, 23, and 24 are discussed in Ref. 8. Figure 15 has been established from the results of the quoted references, but experience has shown that the values of c_M can be a multiple of those of Fig. 15 if the flow in the region between the disk and the wall has radial velocity components pointing away from or toward the axis of the impeller. For compressors pumping ambient air the Reynolds number of Eq. 50 varies between about (10^6) and $3(10^7)$ for peripheral speeds between 1000 and 1600 ft/s, and rotor diameters between 3 and 20 inches. Although the average value of c_M from Fig. 15 is then about $1.5\ (10^{-4})$, it has been shown by experience that $c_M = 2.5(10^{-4})$ is more realistic for actual compressor wheels. For a mass flow rate $\dot{m}$ the power absorbed by an impeller is $\dot{m}\ \mu\ U_2^2$ in accordance with Eq. 3, which is also equal to $M\omega$, where M is the driving moment, and

$$M = \frac{\dot{m}\ \mu\ U_2^2}{\omega} = \dot{m}\ R_2\ \mu\ U_2$$

However

$$\dot{m} = 2\pi\ R_2\ b_2\ k_{B2}\ V_{m2}\ \rho_2$$

and, with the relations of Table I,

$$M = 2\pi\ R_2^3 \left(\frac{b_2}{R_2}\right) k_{B2}\ \mu^2\ U_2^3\ \rho_2\ \cot\alpha_2 \tag{51}$$

The total moment which has to be overcome by the driving source is then $M + M_{DF}$ and if the efficiency of the compressor is η_c, without taking the disk friction moment into account, the actual compressor efficiency η of the machine is $\xi_{DF}\ \eta_c$, and

$$\xi_{DF} = \frac{M}{M + M_{DF}} = \frac{1}{1 + (M_{DF}/M)}$$

Then by Eqs. 49 and 51

$$\xi_{DF} = \frac{1}{1 + \dfrac{(4/\pi)\ c_M \tan\alpha_2}{(b_2/R_2)\ \mu^2\ k_{B2}}} \tag{52}$$

It can be noted that ξ_{DF} is independent of the mass density ρ_2 and R_2 since both M and M_{DF} are proportional to these quantities. Hence Eq. 51 holds for all impellers with radial blades the outer radius R_2. Equation

52 is plotted in Fig. 16. This figure shows that with small ratios b_2/R_2 there can occur a considerable reduction in efficiency, which is the greater the larger the angle α_2 is. For $\alpha_2 = 75^\circ$ the ratio (b_2/R_2) $k_{B2}\,\mu^2$ should not be less than about 0.06 to limit ξ_{DF} to 0.98. Then, with $k_{B2} = 0.95$ and $\mu = 0.90$, the ratio of b_2/R_2 must not be smaller than 0.08 to avoid efficiency reductions because of disk friction moments.

Although the above limit for b_2/R_2 has been obtained by considering the frictional moment at the back side of the impeller, it is very probably that the so-called scrubbing loss of the blade tips at the outer contour of the meridional flow path produces frictional moments which are of similar nature and of the same order of magnitude as the disk friction moments. Moreover, as shown in Fig. 15 for the latter, these moments will also not be greatly influenced by the ratio of tip clearance and R_2 if it is of the order of 0.05, which constitutes a normal to lower limit for most designs. The scrubbing loss is similar to the loss due to disk friction because the boundary layer along the stationary outer wall is rotated by the blade tips. If the losses at the blade tip would be taken to be those due to the flow of the fluid from the pressure side to the pressure side of the blade across the blade clearance, it would be inconceivable that the reductions in compressor efficiency with increased tip clearance are as small as shown by the measurements of Ref. 25. The same behavior has been found in radial turbines[8] where an increase of the ratio of tip clearance and axial blade width b from 4 percent to 10 percent produced practically no drop in efficiency, but if 10 percent was exceeded there occured a radical efficiency reduction. The sudden drop beyond the 10 percent clearance ratio could occur because of massively increased leakage flows across the blade tips once they are outside the wall boundary layer.

Experience has also shown that the ratio of blade width b_2/R_2 should not be less than 8 percent. The value of c_M in Eq. 51 for the representation in Fig. 16 has actually been increased from the average value for disk friction ($\sim 1.5\ (10^{-4})$) to $2.5(10^{-4})$ to demonstrate that this limit is very likely due to the combined effects of disk friction and scrubbing loss. For this ratio of b_2/R_2 and for properly designed inducer sections of an impeller, with meridional contours having small and smoothly changing curvatures, it should be possible to obtain wheel efficiencies η_W of between 0.75 and 0.80 for $b_2/R_2 = 0.08$ if the ratios R_{1i}/R_{1o} are not less than about 0.5.

A large portion of the total losses in radial compressors occurs between the discharge of the wheel and the diffusor throat. The non-uniform distribution of the relative velocities at the rotor discharge produces a non-steady and greatly irregular absolute flow at this station which must be directed toward the diffusor inlet, preferably in a manner that provides uniform flow conditions at this station. If this uniformity is not achieved it is very unlikely that the diffusor proper can perform its function with minimum losses. Very limited data are available for the design of and the losses in these transition sections. Figure 17 shows a typical distribution of the static pressures along the side walls of such a diffusor inlet for a machine that has a value of M_{V2} of about 1.18. Firstly it is clear that the absolute flow is irregular, judging from the change of the pressures in peripheral direction at the wheel discharge. Secondly, the design of the diffusor inlet is not as good as it is desirable because fluid particles undergo compressions and expansions before they reach the diffusor throat. Moreover, Fig. 17 also shows the futility of trying to apply simplified calculating method for this part of the process in the compressor.

Of particular importance is the design of the leading edge of the diffusor blade since the slightest misorientation will produce major disturbances usually with the effect that the flow rate at which the compressor surges is too close to its design flow rate. This condition occurs if the mean angle of the lip section with respect to the radial direction is too large or too small, and since the optimum angle depends on the performance of the rotor, it is not possible to indicate exactly how the transition section must be designed. Experiences have made it obvious, however, that theoretical methods which prescribe a logarithmic spiral or other shapes for the curved part of the transition section overlook the fact that the flows to be handled are so far from being uniform that is almost impossible to obtain optimum solutions without extensive experimental work that investigate the performance of different shapes, not only with respect to optimum efficiency but also to obtain the necessary surge margin. One of the major problems with experiments however is the accurate measurement of the static pressures in these irregular flows. In most cases it is found that Pitot-static pressure probes with even the smallest possible tube diameters are sufficient to change the flow pattern, in fact they usually throw the compressor into surge if it is operating near the design point, so that one has to rely on static wall pressure taps to investigate the effectiveness of different designs. Schlieren pictures for supersonic conditions do also not give information that can be interpreted with ease because of the three-dimensional character of the flow, not to mention the difficulties associated with the arrangement of the necessary optical system. It is therefore quite difficult to measure the true average static pressure after a compressor wheel, and because of the uncertainties that arise if the average static wall pressures at R_2 is identified with it, the separation of the losses into those originating in the wheel, and those occuring in the transition section to the diffusor, is equally difficult. For this reason the evaluation of the actual wheel efficiency η_W may be associated with errors and this could be the reason why it is often impossible to correlate experimental data from different sources. Laser systems were mentioned earlier as an experimental tool to investigate flows in turbomachines, and if the so-called velocimeter, using two laser beams for the determination of the actual magnitude and direction of the velocity in the vicinity of a particular station has been perfected, this instrumentation would be the best possible means to observe the true flow patterns in machines, not only qualitatively but also quantitatively.

In accordance with a limited amount of test data with a compressor operating at $U_2/a_0 = 1.4$, with $M_{V2} = 1.18$, the approximate ratio of the total pressure P_{t2} at the rotor discharge and P_{tx} at the throat of the diffusor was found to be about 1.14, giving an efficiency of the transition section of 0.63. This efficiency is defined as the ratio of the actual static temperature rise to obtain sonic velocity at the throat to that of an isentropic compression for the same pressure ratio. The average discharge flow angle α_2 was about 75°. It seems however that the transition section of the compressor in question could be improved, so that the numbers given above represent only orders of magnitude and not values that cannot improved.

Although a large number of tests have been carried out with subsonic diffusors by many sources, these data cannot be applied directly to the diffusors of compressors with high speed ratios, especially if the

Mach numbers at the diffusor inlet are close to unity. Moreover, it has almost become standard procedure to apply the so-called equivalent cone angle of straight, round diffusors to decelerating flow channels with other cross sections. This procedure converts the inlet and discharge flow areas of a diffusor with arbitrary cross sections into circular ones, either with equal areas or by means of the hydraulic diameter, and then determines the equivalent cone angle with these diameters and the actual length of the diffusor. Either of the two methods for the determination of the equivalent cone angle breaks down for particular designs, or gives results that are in disagreement with actual test data.

An attempt to establish a more rigorous calculating method for arbitrary channels has been made by Traupel[26], primarily for incompressible flows and approximations for the compressible case, but it is then suggested that the equivalent cone angle be used again as a criterion for the permissible deceleration. A different approach is possible, however, which has a minimum of simplifying assumption and has proved to be valid for diffusors of arbitrary geometry, even axisymmetric ones with curved meridian channels and annular cross sections, for instance those arranged after turbomachines to deflect the flow from the axial to the radial direction. The derivation and the use of the equations are given in Table IV. From the laws of conservation of momentum, mass, and energy, combined with the first law of thermodynamics, there is obtained Eq. IV(10) which relates the frictional heat $T\,ds$ to the work necessary to overcome the action of the shear stresses along the channel walls. With the so-called referred mass flow rate $\dot{m}_{r3}$ at the diffusor inlet, which is a dimensionless quantity defined by Eq. IV(14), there is then obtained the principal equation IV(15). This equation is of the form $dX_1 = dX_2$, where dX_1 contains the properties of state ρ, p, and s, at the stations along the channel length, and dX_2 is depending only on the channel geometry and the skin friction coefficient c_f. Actually, for a given diffusor the variables in dX_1 are not independent of the changes of the channel geometry along its length L that occur in dX_2. However, if one were to adjust the flow areas A and the wetted perimeter C of the sections between the inlet and the exit in such a manner that the thermodynamic process of the fluid in the channel would follow a polytropic law, it would be possible to integrate dX_1 independently from dX_2 since s, and ρ are then unique functions of the pressure p for a constant polytropic efficiency η_p or a constant loss coefficient $\zeta = 1 - \eta_p$. Conversely, if an average skin friction coefficient $\bar{c}_f$ is introduced, the value of X_2 is obtained by integrating the quantity $d\Omega$ from diffusor inlet to diffusor discharge, establishing the so-called diffusor shape factor Ω which is identical with the value Φ of Ref. 26. The diffusor shape factor is a dimensionless quantity which depends only on the area and perimeter changes along the length L of the diffusor.

From the integration of dX_1 there is obtained the quantity X_1 as a unique function of the static pressure ratio in the diffusor, γ, and the polytropic loss coefficient ζ. For $\gamma = 1.4$ the function X_1 is plotted in Fig. 18 for different values of ζ, as function of the pressure ratio p_4/p_3. Obviously the conditions of state change monotonously during the polytropic process from p_3 to p_4 in Fig. IV(2), and the function X_1 only holds for such changes. Hence if the area changes in the diffusor would be such that compressions in one part would be followed by expansions in another part, the function X_1 could not take care of the situation, since for an expansion the polytropic law established by Eq. IV(7) would produce an entropy decrease in violation of the second law of thermodynamics. However, even for smoothly changing areas in the diffusor, which it will have in any case, the thermodynamic process in the T-s diagram of Fig. IV(2) might not follow the isentropic line which is shown there, but one which curves either upward or downward from it. It must be recognized however that the value of the function X_1 will not be greatly changed by different distribution of p along L, similar to the integral of Tds which is about equal to $(T_3 + T_4)(s_4 - s_3)/2$ almost independent of how the process proceeds from station (3) to station (4), provided it goes along a smooth and fairly regular curve in the T-s diagram.

Moreover, the polytropic loss coefficient ζ is not assumed a priori, but adjusted to satisfy the equation of continuity at the diffusor discharge for a specified average skin friction coefficient. The necessary iteration to solve this problem is explained in Table IV. The method employs the dimensionless flow function Φ which is plotted in Fig. 18 also, with the ratio of total and static pressure that correspond to an isentropic process as variable. Blockage factors for the diffusor areas are introduced to take account of the boundary layer thickness.

For small pressure ratios p_4/p_3; that is, for low Mach numbers at the diffusor inlet, the method leads to relations that are identical with those commonly applied for the loss evaluation for incompressible diffusor flows. In particular, the average skin friction coefficient is equal to

$$\bar{c}_f = \frac{C_{PRi} - C_{PR}}{\Omega} \tag{53}$$

where C_{PRi} and C_{PR} are the so-called ideal and actual recovery factors, which express the increase in static pressure as percentage of the kinetic energy of the flow at the diffusor inlet. The quantity Ω is the diffusor shape factor defined by Eq. IV(19).

Figure 19 shows the skin friction coefficients $\bar{c}_f$ obtained with Eq. 53 from the experimental data of Ref. 27 for two-dimensional diffusors. Except for the diffusor with $L_o/a_i = 48$, which is unduly long, the data lie within a relatively small band, with the test data for a thin displacement thickness of the boundary layer at the inlet near its lower boundary. It is of interest to note that for large values of Ω the skin friction coefficients are very nearly equal to those of fully developed turbulent flows along moderately rough surfaces in pipes or along plates, as shown by Ref. 20 (p. 587, and p. 611). The results of Ref. 28 which were obtained, in part, at high subsonic speeds give values of $\bar{c}_f$ that lie in the same band as in Fig. 19, indicating that the skin friction coefficients $\bar{c}_f$ are directly related to Ω for different types of cross sections, and at speeds where compressibility effects cannot be disregarded.

This product is shown in Fig 20

From Eq. IV(18) of Table IV it is seen that X_2 is directly proportional to $\bar{c}_f\,\Omega$, for the same data points of Ref. 27 as plotted in Fig. 19. Hence it appears that a diffusor with a shape factor Ω equal to 10 represents an optimum solution. If Ω is smaller the efficiency decreases radically and for values of Ω larger than 10 a diffusor does not make full use of the possible adverse pressure gradient that a boundary layer can sustain without flow separations. The criterion $\Omega = 10$ has been used by the writer with

success for a number of diffusor designs, and a variety of different diffusor shapes is now being tested at NPGS to verify the validity of the criterion at high inlet velocities and with inlet flow distortions.

As shown also in Ref. 26, the shape factor of a round conical diffusor with inlet radius R_i, length L, and the half-angle ϵ of its divergence is

$$\Omega = \frac{1}{2 \tan \epsilon} \left[1 - \frac{1}{(1 + 2(L/R_i) \tan \epsilon)^4}\right] \qquad (54)$$

For conical diffusors where L is large with respect to R_i, Eq. 54 gives a divergence angle of $2\epsilon = 5^o45'$. The influence of the ratio L/R_i is small if L/R_i is larger than about 10. Two-dimensional straight diffusors with constant depth b, and widths a_i at the inlet and a_d at the discharge, determined by $a_d = a_i + 2\ L \tan \epsilon$, where ϵ is again the half-angle of the channel, have shape factors

$$\Omega = \frac{L/a_i}{1 + 2(L/a_i) \tan \epsilon} \left[1 + \frac{1}{1 + 2(L/a_i \tan \epsilon} + \frac{2\ a_i}{b}\right] \qquad (55)$$

If the diffusor of Fig. 17 had a ratio $a_i/b = 2.4$, the value of Ω for $\epsilon = 5^o$ and $L/a_i = 10$, is about equal 22.4, which appears to be excessive. Hence the diffusor should have a divergence perpendicular to the plane of drawing also to increase b_i at the inlet to b_d at the discharge. For shapes of this type the expression of Eq. IV(19) for Ω leads to complicated integrals. However with a simple graphical integration for a half-angle of divergence of about 2^o that produces a ratio $b_d/b_i = 2.4$ with the widths a_i and a_d remaining unchanged, the diffusor form factor is reduced to about 11.2. A diffusor channel for this value of Ω for compressors is very likely very close to the optimum possible solution because of then non-uniform flow conditions that exist at its inlet.

Because of these disturbances, the values of $\Omega\ \bar{c}_f$ presented in Fig. 20 should also be increased, say, from 0.10 to about 0.15, or 0.20, for Ω of about 10. How these values affect the diffusor efficiency will be shown with a simplified approach of the diffusor design method of Table IV. It is assumed that the Mach number M_{V3} at the throat is unity, but the method is not restricted to this value. The flow function Φ_3 of Eq. IV(22) is then equal to 0.6847 in accordance with Fig. 18, and $P_{t3}/p_3 = 1.8929$. From Eq. IV(28) for for $M_{V3} = 1$, $\gamma = 1.4$,

$$\dot{m}_{r3} = (0.6847)\ (1.2)^3 = 1.1832$$

From Eq. IV(18)

$$X_2 = \frac{1.1832^2}{2}\ \bar{c}_f\ \Omega = 0.7\ \bar{c}_f\ \Omega$$

Hence, $X_2 = 0.07$ for $\bar{c}_f\ \Omega = 0.1$, $X_2 = 0.14$ for $\bar{c}_f\ \Omega = 0.2$, and these values are equal to the values of the function X_1 which is plotted in Fig. 18. It will now be assumed that the area ratio A_3/A_4 of the diffusor is $1/6.6 = 0.151$ as is the case for the design of Fig. 17 with a half-angle of divergence of 2^o to increase the depth b also. With blockage factors $k_{B3} = 0.96$ and $k_{B4} = 0.90$, by Eq. IV(29)

$$\Phi_4 = (0.6847)\ (0.151)\ (0.96/0.9)\ (P_{t3}/P_{t4}) = 0.11\ (P_{t3}/P_{t4})$$

Assuming that P_{t3}/P_{t4} is about 1.05, the value of Φ_4 is 0.115. From the plot of Φ vs P_t/p_t it can be seen that for $\Phi_4 = 0.115$, or slight changes of it on account of a wrongly chosen value of P_{t3}/P_{t4}, the value of P_{t4}/p_4 will not be higher than 1.02 because of the large change of Φ with P_t/p_t close to unity. Then,

$$\frac{p_4}{p_3} = \frac{P_{t3}/p_3}{P_{t4}/p_4} \frac{P_{t4}}{P_{t3}} = \frac{1.8929}{1.02} \left(\frac{1}{1.05}\right) = 1.77$$

The approximate values of ζ can then be read from Fig. 18 at the intersection of the lines for the known values of X_1 and for $p_4/p_3 = 1.77$. For $\bar{c}_f\ \Omega = 0.1$, or $X_1 = 0.07$, there is $\zeta = 0.070$, and for $\bar{c}_f\ \Omega = 0.2$, or $X_1 = 0.14$, one finds $\zeta = 0.130$, giving approximate values of the diffusor efficiency of 0.93 and 0.87, respectively, without taking account of the reheat effects that are reflected in Eq. IV(35). The values of ζ thus obtained can then be used to determine the pressure ratio p_4/p_3 more precisely, by taking the pressure ratio P_{t3}/P_{t4} to be that obtained from Eq. IV(33) with the approximate pressure ratio $p_4/p_3 = 1.77$.

6. SAMPLE CALCULATIONS

To demonstrate the effectiveness of the developed performance parameters, and the help of the figures, the dimensions of an impeller for an air compressor with a pressure ratio of eight will be established for the following conditions:

$$\dot{m} = 2.5 \text{ lbm/s} = (2.5/32.174) \text{ slug/s}$$

$$P_0 = 14.7 \text{ psia};\ T_0 = 520^o\text{R}$$

$$P_{t4}/P_0 = 8$$

$$R_G = 1716.48 \frac{\text{ft-lb}}{\text{slug, }^\circ R}\ ;\ \gamma = 1.4$$

From Eq. 5

$$a_0 = 1117.8 \text{ ft/s}$$

Assuming $\mu = 0.9$; $\eta_c = 0.82$, from Eq. II(3), or Fig. 4,

$$U_2/a_0 = 1.658$$

hence

$$U_2 = 1853.4 \text{ ft/s}$$

Figure 8 clearly shows that for this U_2/a_0 and reasonable ratios R_{1o}/R_2 the relative inlet velocity M_{W1} must be supersonic. For $M_{W1} = 1.15$ and $\beta_{1o} = 70^\circ$ there is from Fig. 8, or Eq. II(4),

$$\frac{R_{1o}}{R_2} = 0.642$$

Judging from Fig. 4 it is necessary to choose $\alpha_2 = 74^\circ$ to obtain a value of W_2/W_{1o} of about 0.4. More precisely from Eq. II(5)

$$\frac{W_2}{W_{1o}} = 0.405$$

For a chosen value of the wheel efficiency η_W of 0.7, there are from Eq. 21

$$\Psi = 0.629;\ \Psi^2 = 0,394$$

and the usual rotor efficiency η_R defined by Eq. 12, in accordance with Eq. 24, is

$$\eta_R = 0.88$$

With these values by Eq. II(9)

$$\left[1 - \left(\frac{R_{1i}}{R_{1o}}\right)^2\right] k_{B1} = \frac{\dot{m}\sqrt{R_G T_0}}{\pi R_2^2 P_0} \quad (5.7138)$$

and from Eq. II(11)

$$\frac{b_2}{R_2} k_{B2} = \frac{\dot{m}\sqrt{R_G T_0}}{\pi R_2^2 P_0} \quad (0.4127)$$

and, for approximate values $k_{B1} = 0.85$, $k_{B2} = 0.95$, by division of two above-listed relations,

$$\frac{b_2/R_2}{1 - (R_{1i}/R_{1o})^2} = 0.0646$$

Evidently this ratio holds for all compressors for the chosen conditions, irrespective of the flow rate and the inlet pressure. For chosen radius ratios R_{1i}/R_{1o} there are:

R_{1i}/R_{1o} =	0.2	0.3	0.4	0.5
b_2/R_2 =	0.062	0.059	0.054	0.048

All these ratios are too small to obtain the desired efficiency. They were obtained because R_{1o}/R_2 was chosen too small and the angle β_{1o} is too large, and both these values were taken to maintain a low Mach number M_{W1}. For a second try, let:

$$R_{1o}/R_2 = 0.7;\ \beta_{1o} = 60^\circ;\ \alpha_2 = 75^\circ$$

Then, from the inverse of Eq. II(4), expressing M_{W1} as function of R_{1o}/R_2 and β_{1o},

$$M_{W1} = 1.3198$$

From Eq. II(5)

$$\frac{W_2}{W_{1o}} = 0.360$$

The latter value seems acceptable in view of Fig. 14, and by proper rotor dimensioning a wheel efficiency $\eta_W = 0.7$ should still be reached. By Eq. 21.

$$\Psi = 0.576; \quad \Psi^2 = 0.332$$

By Eq. II(9)

$$\left[1 - \left(\frac{R_{1i}}{R_{1o}}\right)^2\right] k_{B1} = \frac{\dot{m}\sqrt{R_G T_0}}{\pi R_2^2 P_0} \quad (3.7063)$$

and, from Eq. II(11)

$$\frac{b_2}{R_2} k_{B2} = \frac{m\sqrt{R_G T_0}}{\pi R_2^2 P_0} \quad (0.4494)$$

With $k_{B1} = 0.85$, $k_{B2} = 0.95$

$$\frac{b_2/R_2}{1 - (R_{1i}/R_{1o})^2} = 0.1074$$

For the chosen value $b_2/R_2 = 0.08$ the radius ratio R_{1o}/R_2 can be 0.5, which makes it possible to design a meridional flow path that has an acceptable shape.

From the inlet conditions and the design flow rate:

$$\frac{m\sqrt{R_G T_0}}{P_0} = \frac{2.5}{32.174} \frac{\sqrt{(1716.48)(520)}}{14.7} = 4.994 \text{ in.}^2$$

because the pressure P_0 was introduced in pound per sq. in.. Then, from the previous data,

$$\pi R_2^2 = \frac{(4.994)(3.7063)}{(1 - 0.25)(0.85)} = 29.034 \text{ in.}^2$$

Hence

$$R_2 = 3.04 \text{ in.} \; ; \; D_2 = 6.08 \text{ in.}$$

$$R_{1o} = 2.125 \text{ in.} \; ; \; D_{1o} = 4.25 \text{ in.}$$

$$R_{1i} = 1.062 \text{ in.} \; ; \; D_{1i} = 2.125 \text{ in.}$$

$$b_2 = 0.243 \text{ in.}$$

For the chosen data, from Eq. II(6),

$$M_{V2} = 1.256$$

The rotative speed N can be determined from Eq. II(10), or directly from

$$N = \frac{30}{\pi} \omega = \frac{30}{\pi} \frac{U_2}{R_2} = \frac{(30)(1853.4)}{\pi(3.04/12)} = 69{,}860 \text{ rpm}$$

REFERENCES

1. Vavra, M. H. — Aerothermodynamics and Flow in Turbomachines, Wiley Bros, New York, 1960.

2. Vavra, M. H. — Axial Flow Turbines, Von Karman Institute for Fluid Dynamics, Lecture Series 15, pp. 99/100, April 1969.

3. Traupel, W. — Die Theorie der Stroemung durch Radialmaschinen, Braun, Karlsruhe, 1962.

4. Johnston, J. P.; Dean, R. C., Jr. — J. Engg. for Power, Trans. ASME, pp. 49-62, January 1966.

5. Stiefel, W. — "Experimental Investigations on Radial Compressors ...", Course Note 53b, Von Karman Institute, March 1965.

6. Stiefel, W. — "Undersuchung an Radialen Verdichterlauefern," AVA Forschungsbericht 63-01, Triebwerksaerodynamik der Turbomaschinen, Teil II, Goettingen, 1963.

7. Sakai, T.; Watanabe, I., et al. — "On the Slip Factor of Centrifugal and Mixed-Flow Impellers", ASME Paper 67-WA/GT-10.

8. Vavra, M. H. — "Radial Turbines", Part 4 of AGARD-VKI Lecture Series 6 on Flow in Turbines", Von Karman Institute, March 1968.

9. Bammert, K.; Bohm, E. — "Nuclear Plants with High-Temperature Reactor and Helium Turbine," ASME Paper 69-GT-43, March 1969.

10. Groh, F. W.; Robb, W. L. — "High Efficiency Can Be Achieved in Small Size Transonic Compressor Rotors," SAE Paper 820C, January 1964.

11. Katsanis, T.; McNally, W. D. — "Programs for Computation of Velocities and Streamlines on a Blade-to-Blade Surface of a Turbomachine" ASME Paper 69-GT-48, March 1969.

12. Jmbach, H. E. — "Die Berechnung der kompressiblen, reibungsfreien Unterschallstroemung durch rauemliche Gitter aus Schaufeln auch grosser Dicke und starker Woelbung" Mittlg No 8, Inst. Thermische Turbomaschinen, ETH, Juris Verlag, Zurich, 1964.

13. Linsi, U. — Brown Boveri Review, Vol. 53, No. 3, p. 161, March 1965.

14. Fowler, H. S. — "Some Measurements of the Flow Patterns in a Centrifugal Compressor Impeller," ASME Paper 65-WA/FTP-7, April 1965.

15. Fowler, H. S. — "The Distribution and Stability of Flow in a Rotating Channel," ASME Paper 68-GT-1, March 1968.

16. Halleen, R. M.; Johnson, J. P. — "The Influence of Rotation on Flow in a Long Rectangular Channel" Stanford University, Report MD-18, May 1967.

17. Ackeret, J.; Keller, C.; Salzmann, F. — Schweizer Bauzeitung, No. 23, December 1934.

18. Shepherd, D. G. — "Principles of Turbomachinery", Macmillan; New York, 1956.

19. Baljé, O. E. — J. Engg for Power, Trans. ASME Series A, Vol. 84, No. 1, pp. 83-114, Jan 1962.

20. Schlichting, H. — Boundary-Layer Theory, 6th ed., p. 606, McGraw-Hill, N. Y., 1968.

21. Daily, J. W.; Nece, R. E. — J. of Basic Engg., Trans. ASME, p. 217, March 1960.

22. Nece, R. E.; Daily, J. R. — J. of Basic Engg., Trans. ASME, p. 553, Sept. 1960.

23. Pantel, K. — Forschung, Vol. 16, p. 97, 1950.

24. Moroti, L. A.; Deak, G.; Kreith, F. — J. of Basic Engg., Trans. ASME, p. 539, Sept. 1960.

25. Schmidt-Theuner, P.; Mattern, J. — Brown Boveri Review, Vol. 55, No. 8, p. 453, 1968.

26. Traupel, W. — Thermische Turbomaschinen, Bd. I., p. 308, Springer, Berlin, 1962.

27. Waitman, B. A.
Reneau, L. R.
Kline, S. J. — J. of Basic Engg., Trans. ASME, Vol. 83, Series D., No. 3, p. 349, Sept. 1961.

28. Sovran, G.
Klomp, E. D. — "Experimentally Determined Optimum Geometries for Rectinlinear Diffusors with Rectangular, Conical or Annular Cross Sections," Symposium on Fluid Mechanics of Internal Flow, General Motors Research Laboratories, Sept. 1965.

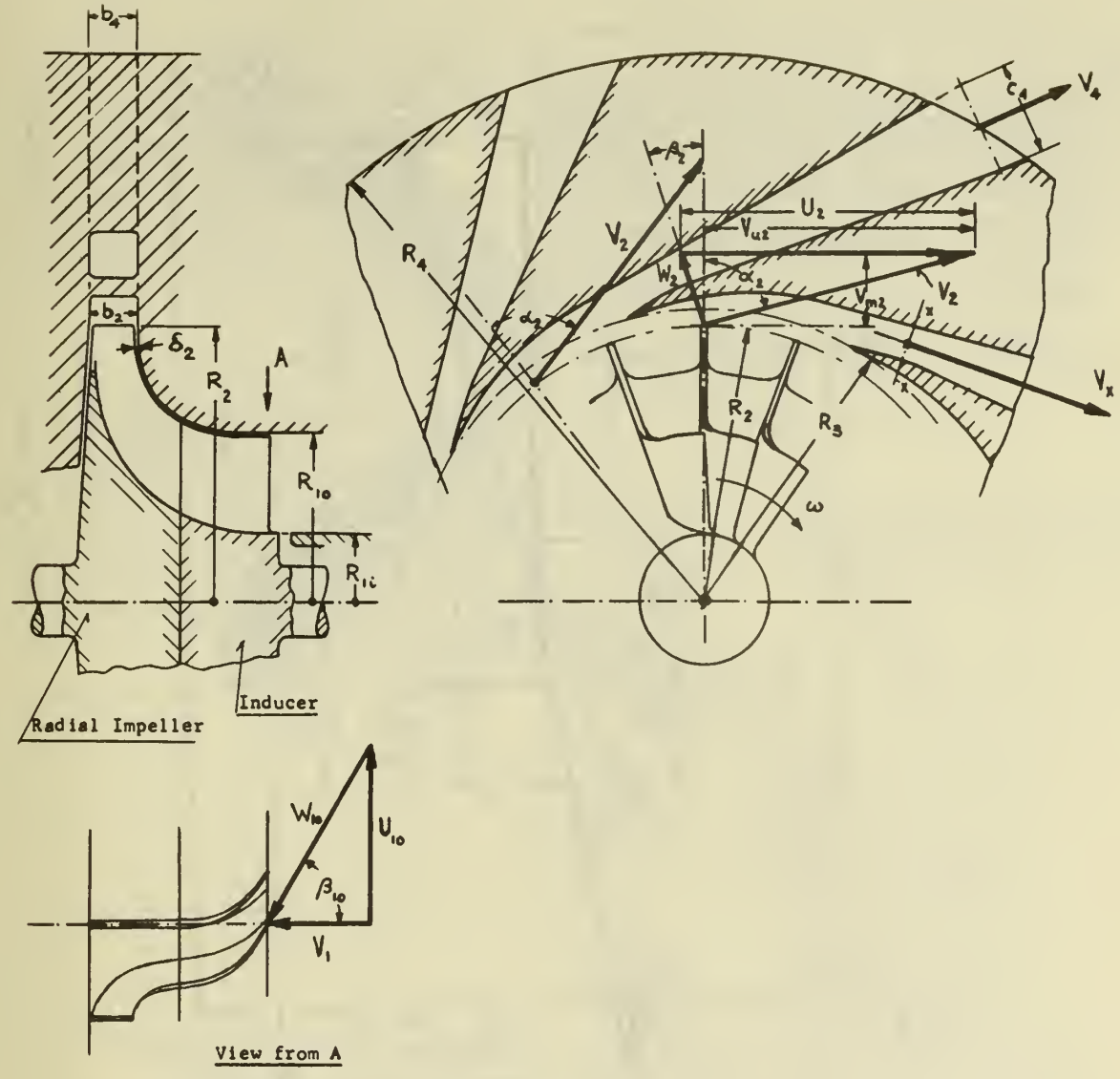

FIG. 1 RADIAL - FLOW COMPRESSOR

R - Radius
V - Absolute Velocity
W - Relative Velocity
U - Peripheral Speed
α - Absolute Flow Angle
β - Relative Flow Angle
b - Axial Channel Width
c - Height of Diffusor Channel

Subscripts:
1 - refers to rotor inlet
2 - refers to rotor discharge
3 - refers to inlet lip of diffusor blades
x - refers to throat of diffusor channel
4 - refers to discharge of diffusor channel

m - refers to meridional direction
u - refers to peripheral direction
i - refers to inner radius at compressor inlet
o - refers to outer radius at compressor inlet

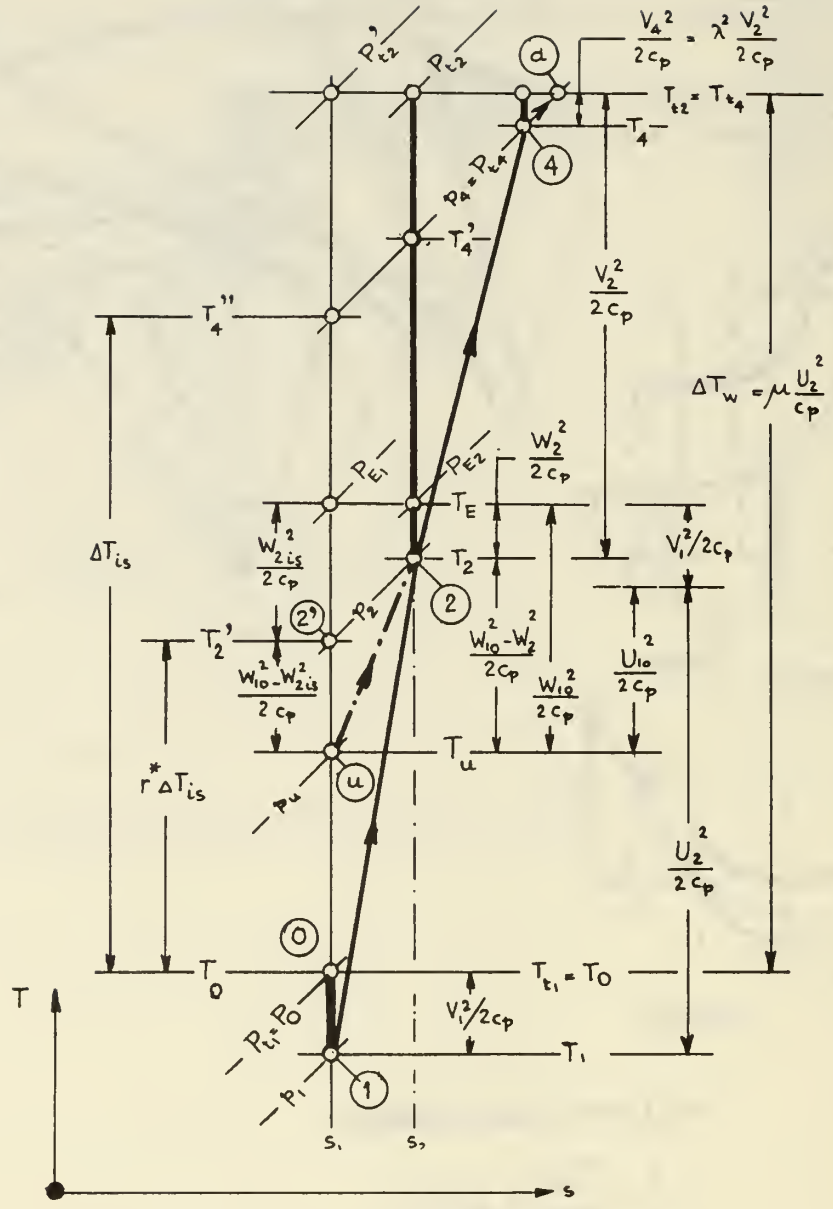

FIG.2 TEMPERATURE-ENTROPY DIAGRAM OF COMPRESSION PROCESS IN COMPRESSOR OF FIG. 1

- c_p - Specific Heat at constant Pressure
- p - Static Pressure
- P_t - Total Pressure
- T - Static Temperature
- T_t - Total Temperature
- s - Entropy
- $\lambda = V_4 / V_2$

(For other symbols and station designation see Fig.1)

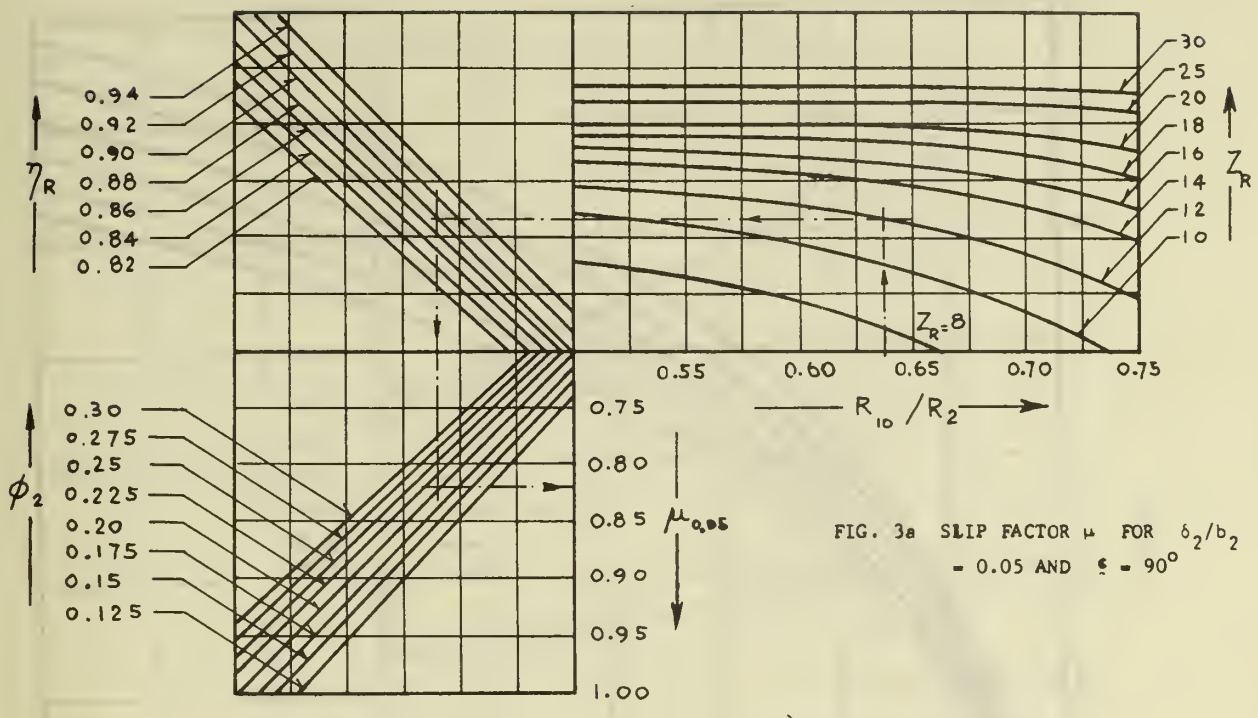

FIG. 3a SLIP FACTOR μ FOR δ_2/b_2 = 0.05 AND ε = 90°

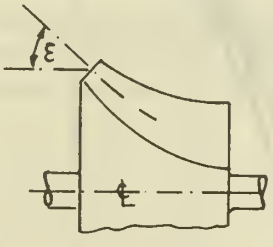

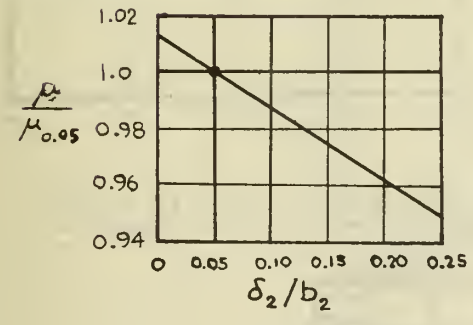

FIG. 3b CORRECTION FACTOR FOR RATIOS OF TIP CLEARANCE δ_2 AND AXIAL BLADE WIDTH b_2 DIFFERENT FROM 0.05

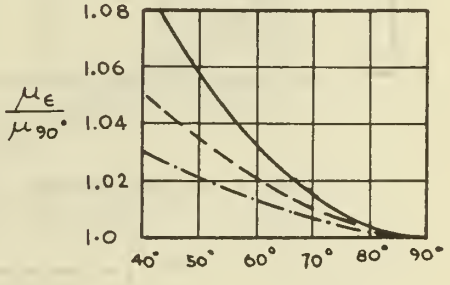

FIG. 3c CORRECTION FACTOR FOR MIXED-FLOW IMPELLERS

FIG. 3 SLIP FACTOR FOR RADIAL COMPRESSOR IMPELLERS WITH RADIAL BLADES AT DISCHARGE

(Figures were adapted from Refs. 5 and 6)

ϕ_2 - $\frac{V_{m2}}{U_2}$ (see Eq. II(8) of Table II)

η_R - Rotor Efficiency (see Eq. 12)

Z_R - Number of Rotor Blades

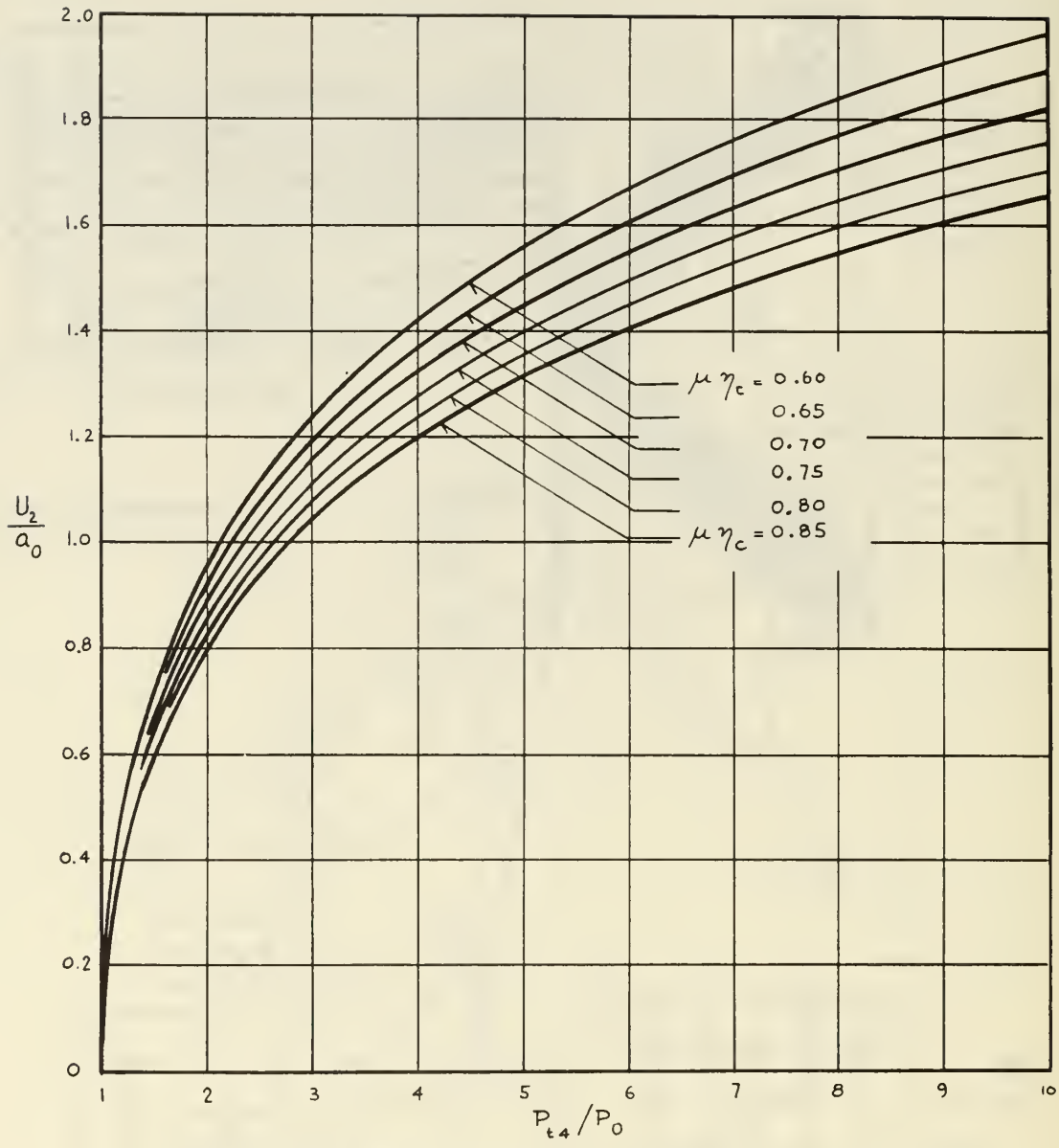

FIG. 4 RELATION BETWEEN PRESSURE RATIO AND U_2/a_0 FOR $\nu = 1.4$ (Eq. II(3))

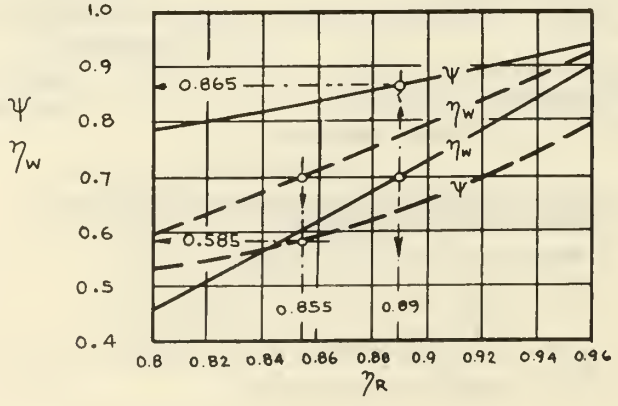

FIG. 5 RELATION BETWEEN ROTOR LOSS FORMULATIONS WITH η_R, η_W AND ψ(Eos. 22 and 24)

——— $\alpha_2 = 60^\circ$
– – – $\alpha_2 = 75^\circ$
} $\beta_{1o} = 70^\circ$, $R_{1o}/R_2 = 0.7$, $\mu = 0.85$

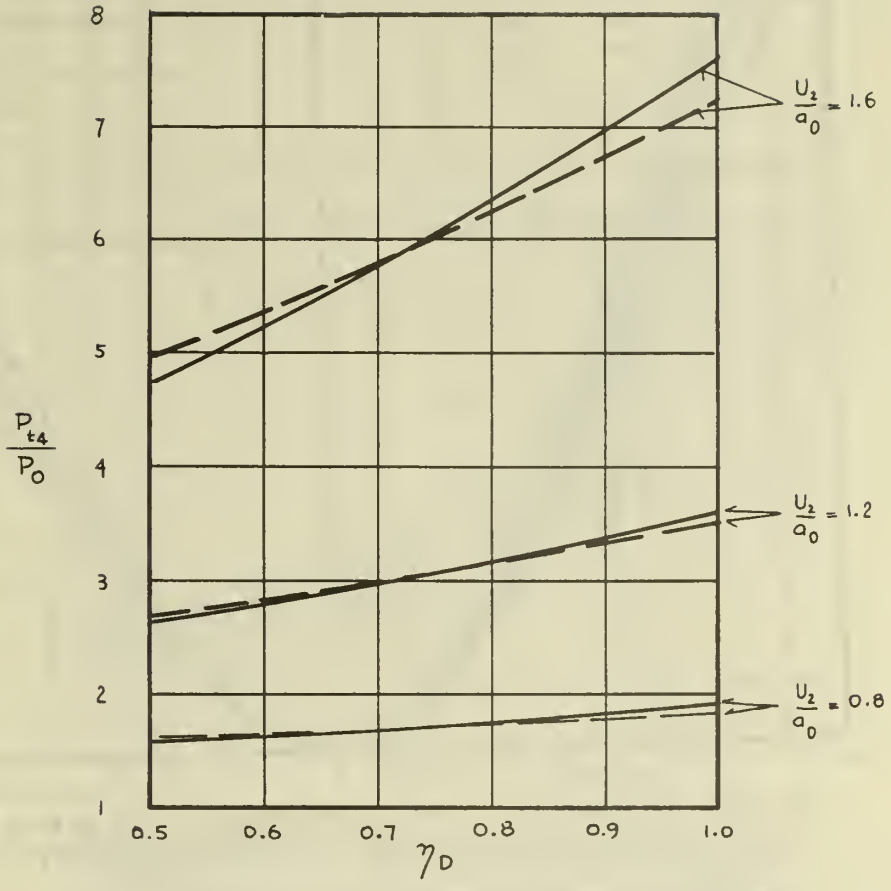

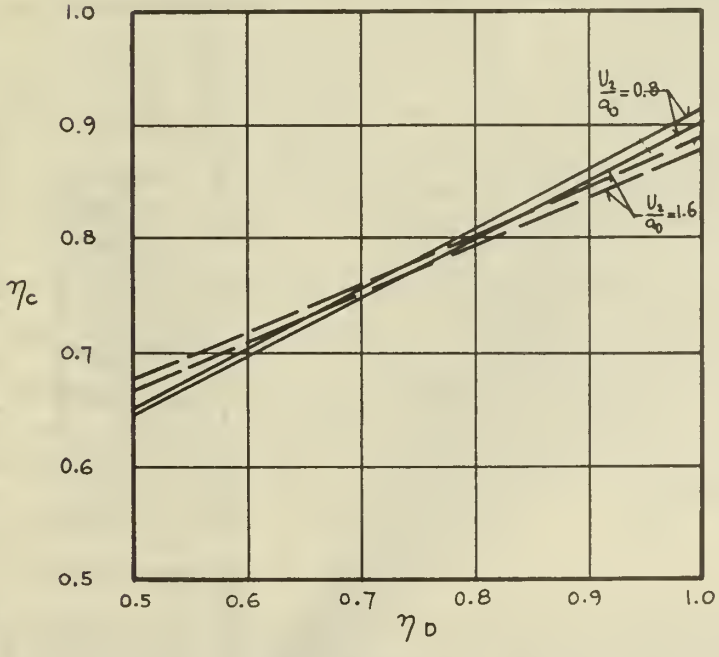

FIG.6 INFLUENCE OF DIFFUSOR EFFICIENCY η_D ON EFFICIENCY η_c AND PRESSURE RATIO P_{t4}/P_0 OF COMPRESSORS AT DIFFERENT SPEED RATIOS U_2/a_0

$\beta_{1o} = 70^\circ$; $R_{1o}/R_2 = 0.7$; $\lambda = V_4/V_2 = 0.2$

——— $\alpha_2 = 60^\circ$; $\eta_W = 0.7$; $\eta_R = 0.89$; $\psi = 0.865$

— — — $\alpha_2 = 75^\circ$; $\eta_W = 0.7$; $\eta_R = 0.855$; $\psi = 0.585$

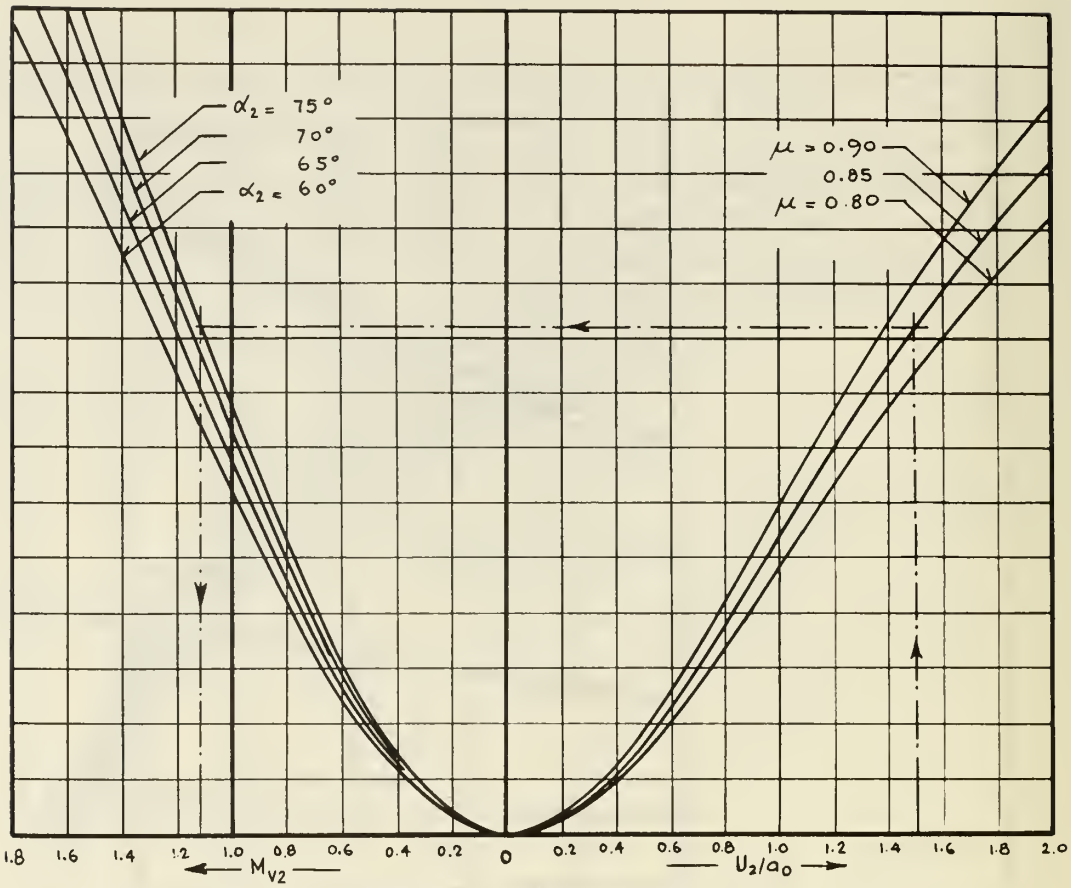

FIG.7 RELATION BETWEEN MACH NUMBER M_{V2} OF ABSOLUTE VELOCITY AT ROTOR DISCHARGE AND SPEED RATIO U_2/a_0 , FOR γ = 1.4 (Eq. II(6) of Table II)

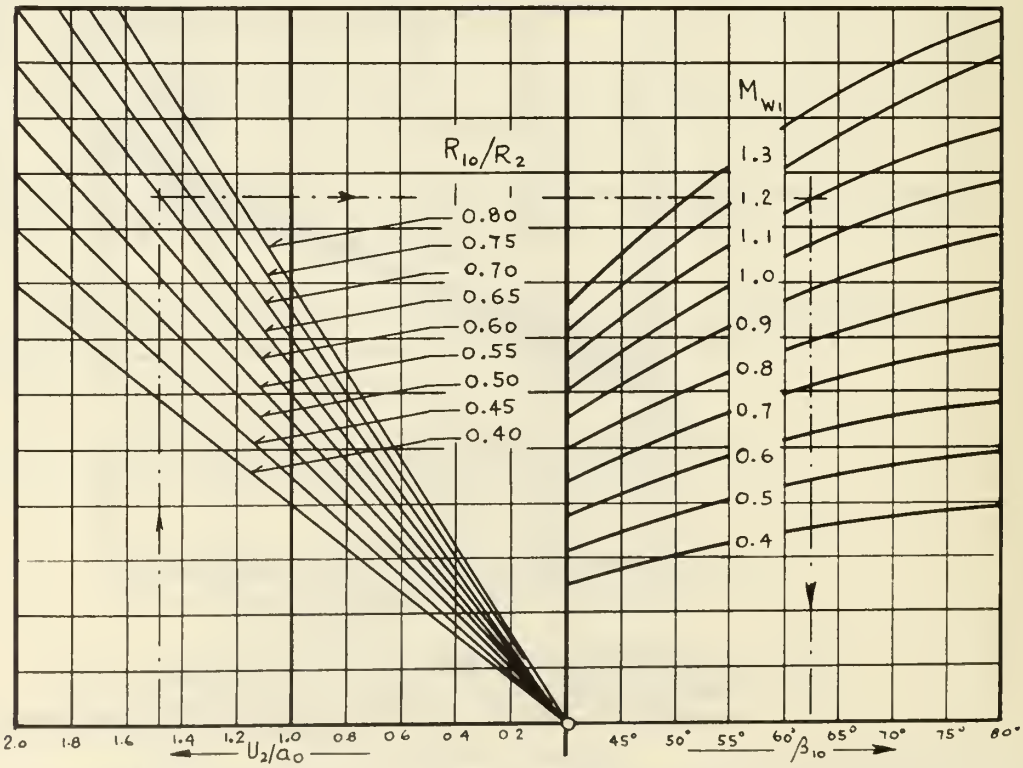

FIG.8 RELATION BETWEEN SPEED RATIO U_2/a_0 ,RADIUS RATIO R_{1o}/R_2, VS. MACH NUMBER $M_{W1} = W_{1o}/a_1$ AND RELATIVE FLOW ANGLE β_{1o} AT OUTER RADIUS R_{1o} OF COMPRESSOR INLET, FOR γ =1.4. (Eq. II(4) of Table II)

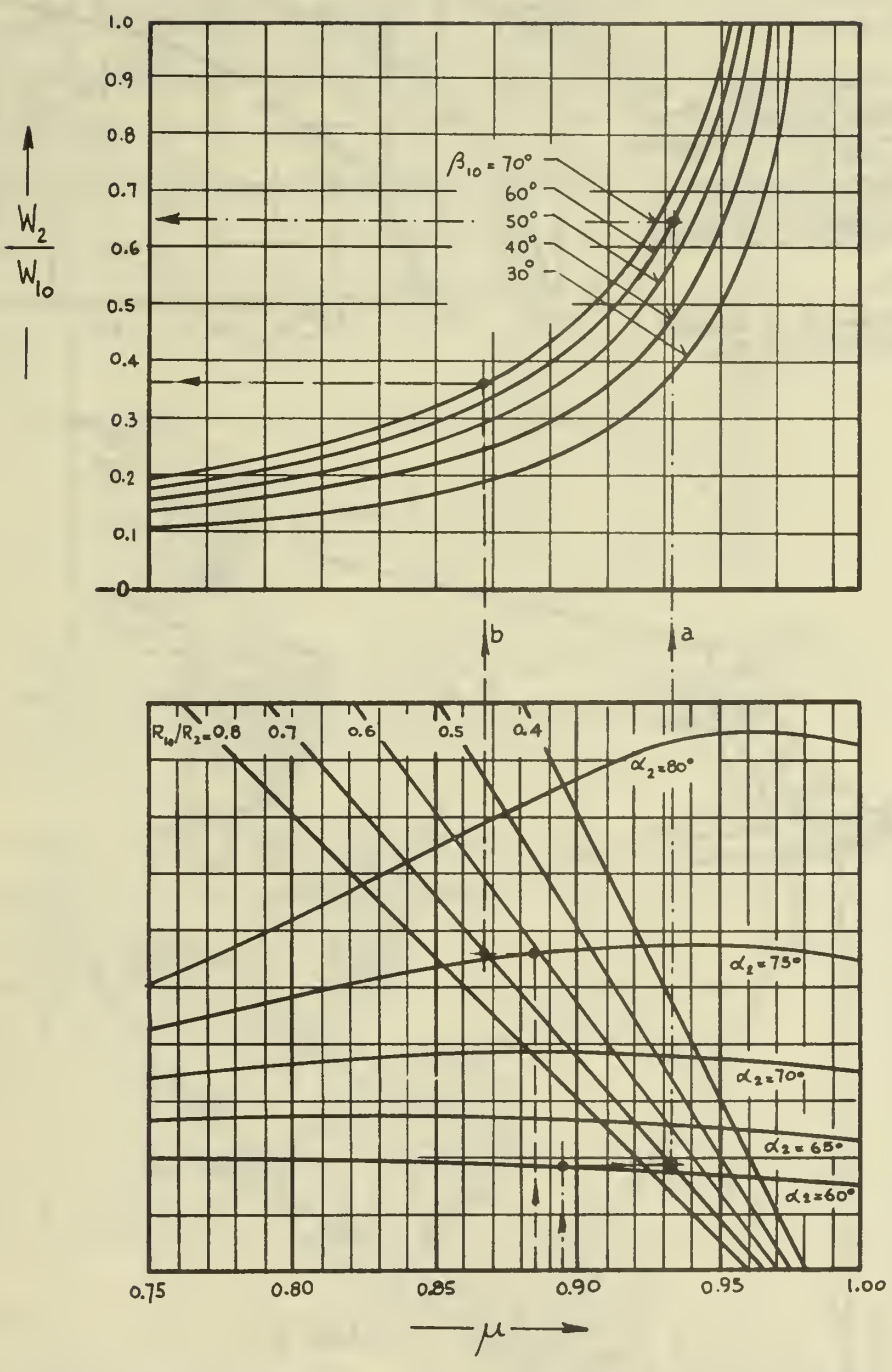

FIG.9 DIAGRAM REPRESENTING EQUATION II(5) OF TABLE II, SHOWING RELATIONSHIP BETWEEN DECELERATION RATIO W_2/W_{1o} OF RELATIVE ROTOR VELOCITIES, RADIUS RATIO R_{1o}/R_2, RELATIVE INLET FLOW ANGLE β_{1o}, ABSOLUTE ROTOR DISCHARGE ANGLE α_2, AND SLIP FACTOR μ.

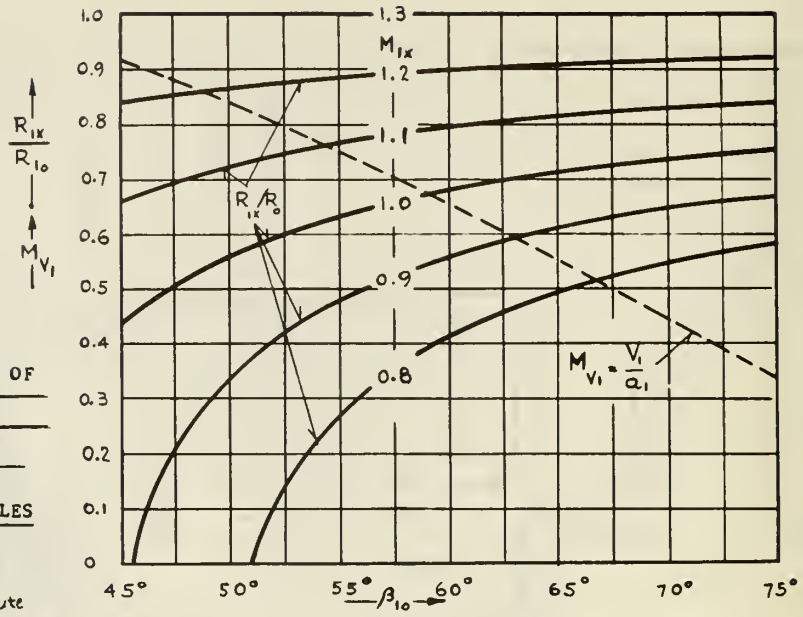

FIG. 10 MACH NUMBER M_{1x} OF RELATIVE INLET VELOCITY AT RADIUS R_{1x} FOR $M_{W1} = 1.3$ AT OUTER RADIUS R_{1o} OF WHEEL INLET, AT DIFFERENT FLOW ANGLES β_{1o} AT R_{1o}

M_{V1} = Mach number of Absolute Velocity V_1 at Inlet

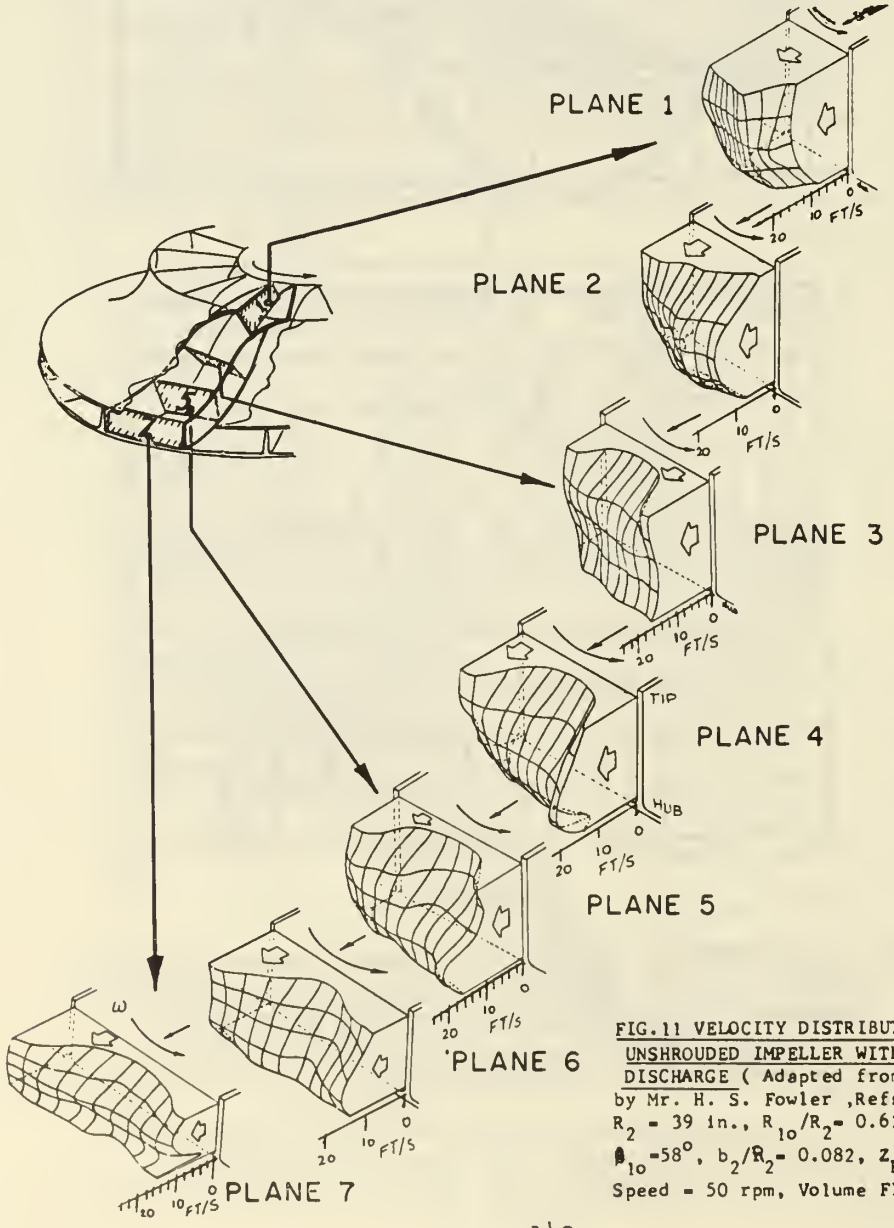

FIG. 11 VELOCITY DISTRIBUTIONS MEASURED IN UNSHROUDED IMPELLER WITH RADIAL BLADES AT THE DISCHARGE (Adapted from Personal Communication by Mr. H. S. Fowler ,Refs. 14 and 15)
R_2 = 39 in., R_{1o}/R_2 = 0.629, R_{11}/R_{1o} = 0.752
β_{1o} = 58°, b_2/R_2 = 0.082, Z_R = 26, δ_2/R_2 = 0.005
Speed = 50 rpm, Volume Flow = 64.2 ft^3/s

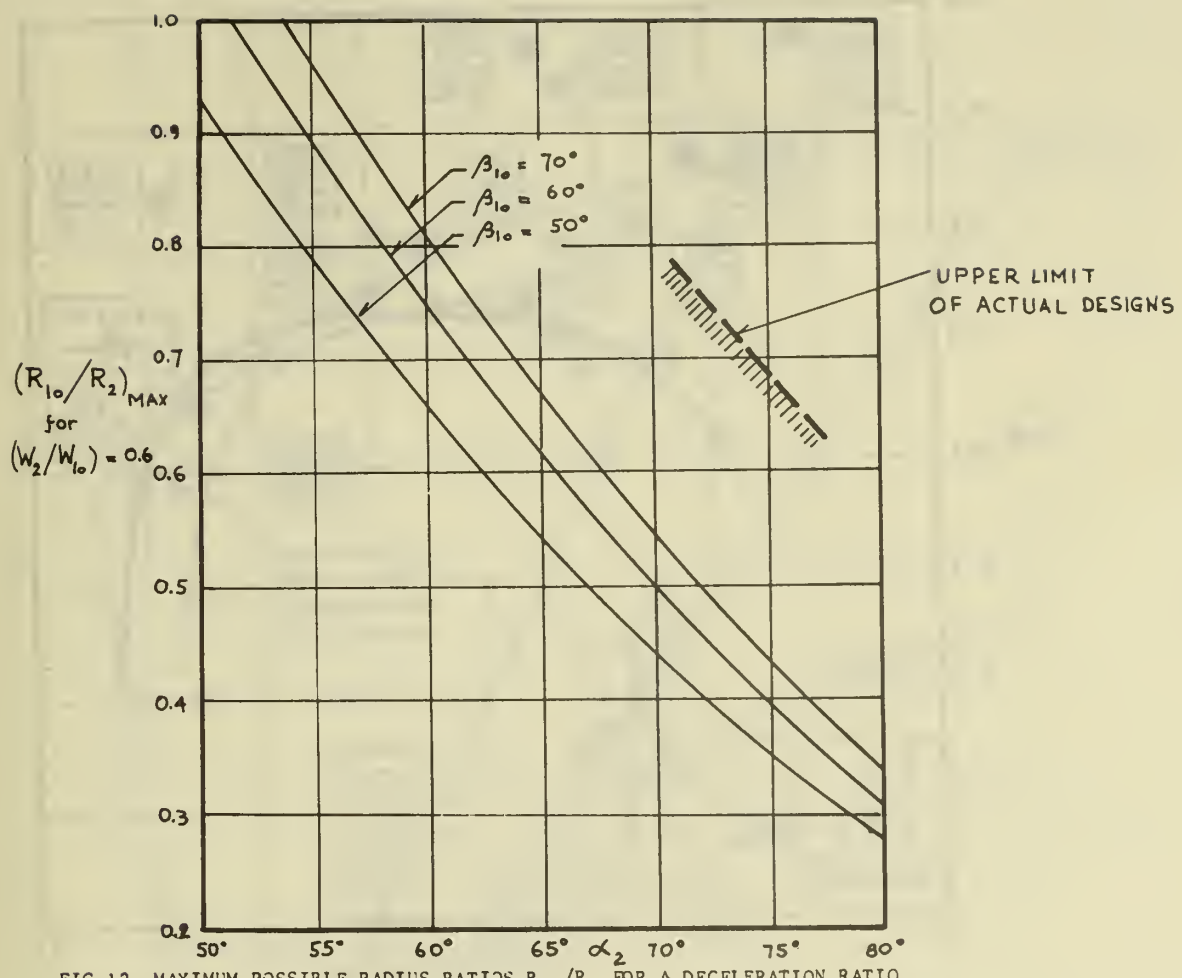

FIG.12 MAXIMUM POSSIBLE RADIUS RATIOS R_{1o}/R_2 FOR A DECELERATION RATIO $W_2/W_{1o} = 0.6$ FOR A SLIP FACTOR $\mu = 0.85$

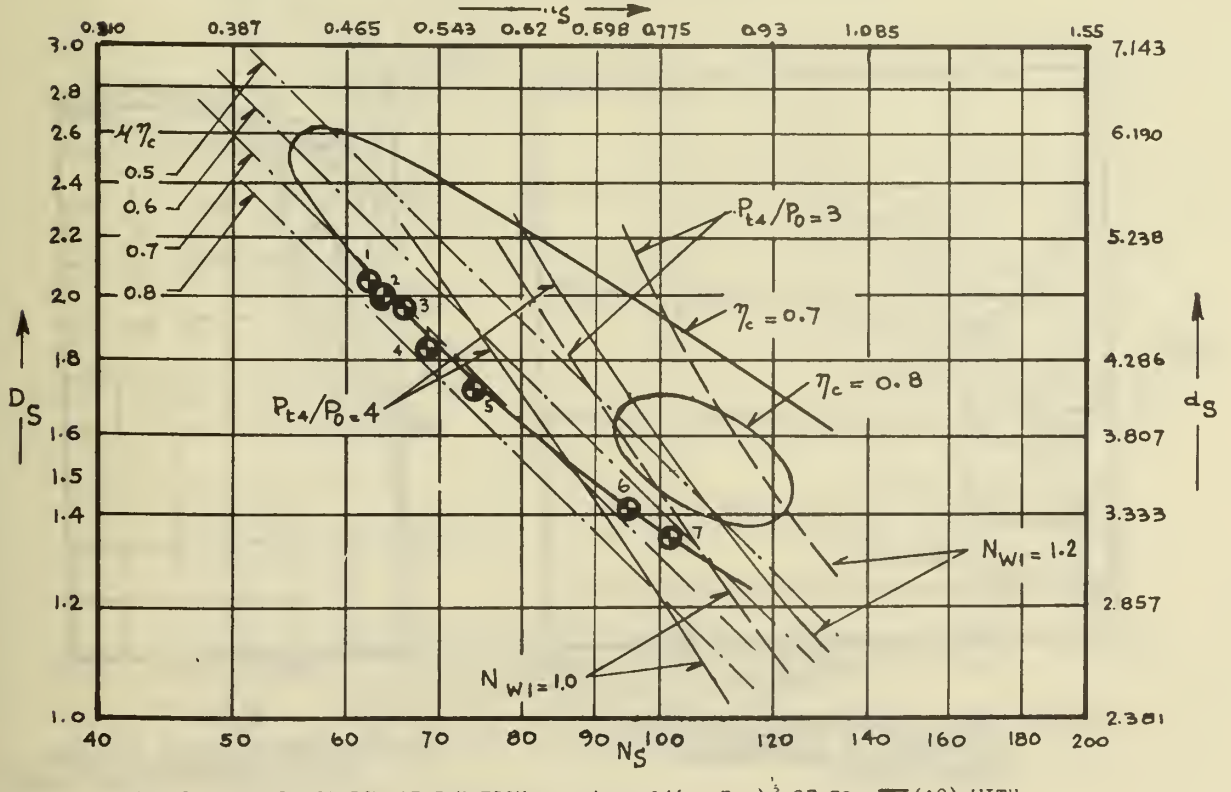

FIG.13 REPRESENTATION OF EQUATION $n_S d_S = 2/(\mu\eta_c)^{\frac{1}{2}}$ OF EQ. III(10) WITH DESIGN DATA POINTS OF ACTUAL COMPRESSORS

(Other Curves adapted from Fig. 4 of Ref. 19)

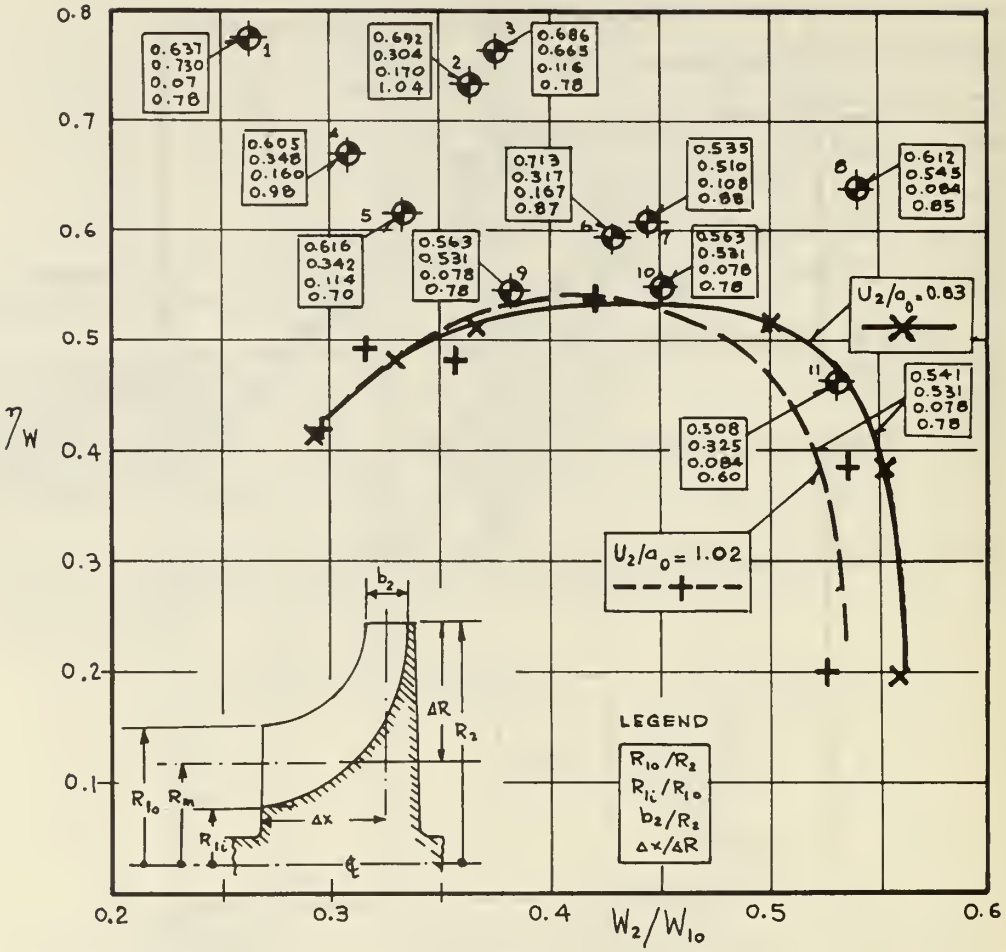

FIG. 14 WHEEL EFFICIENY η_W AS FUNCTION OF THE DECELERATION RATIO W_2/W_{10} OF DIFFERENT RADIAL IMPELLERS

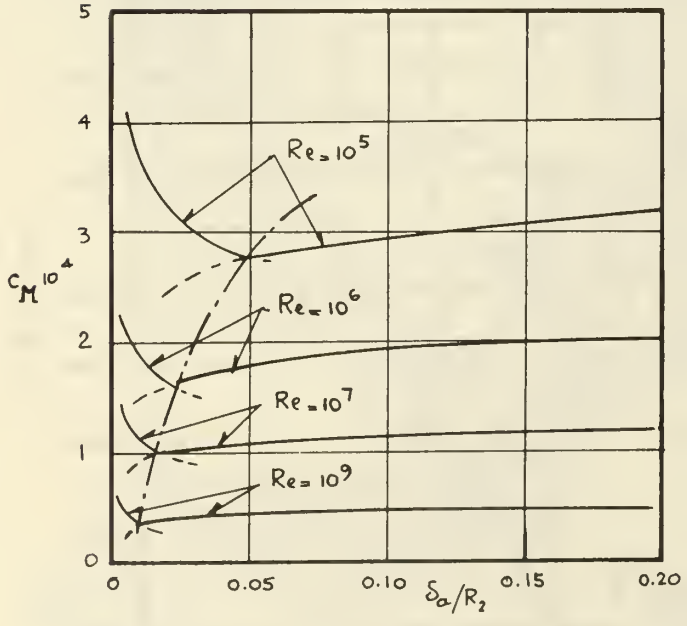

FIG. 15 DISK FRICTION MOMENT COEFFICIENT AS FUNCTION OF CLEARANCE AND REYNOLDS NUMBER

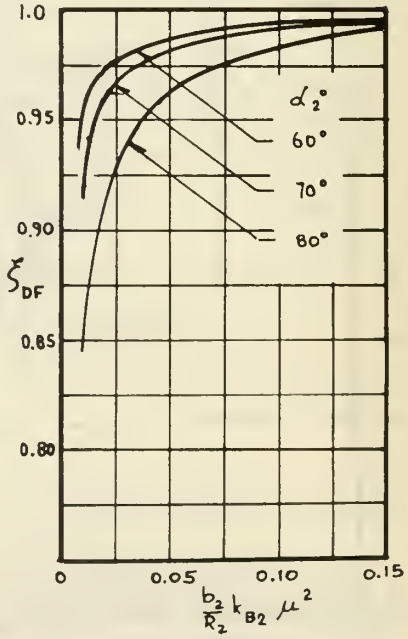

FIG. 16 INFLUENCE OF DISK FRICTION MOMENT ON COMPRESSOR EFFICIENCY

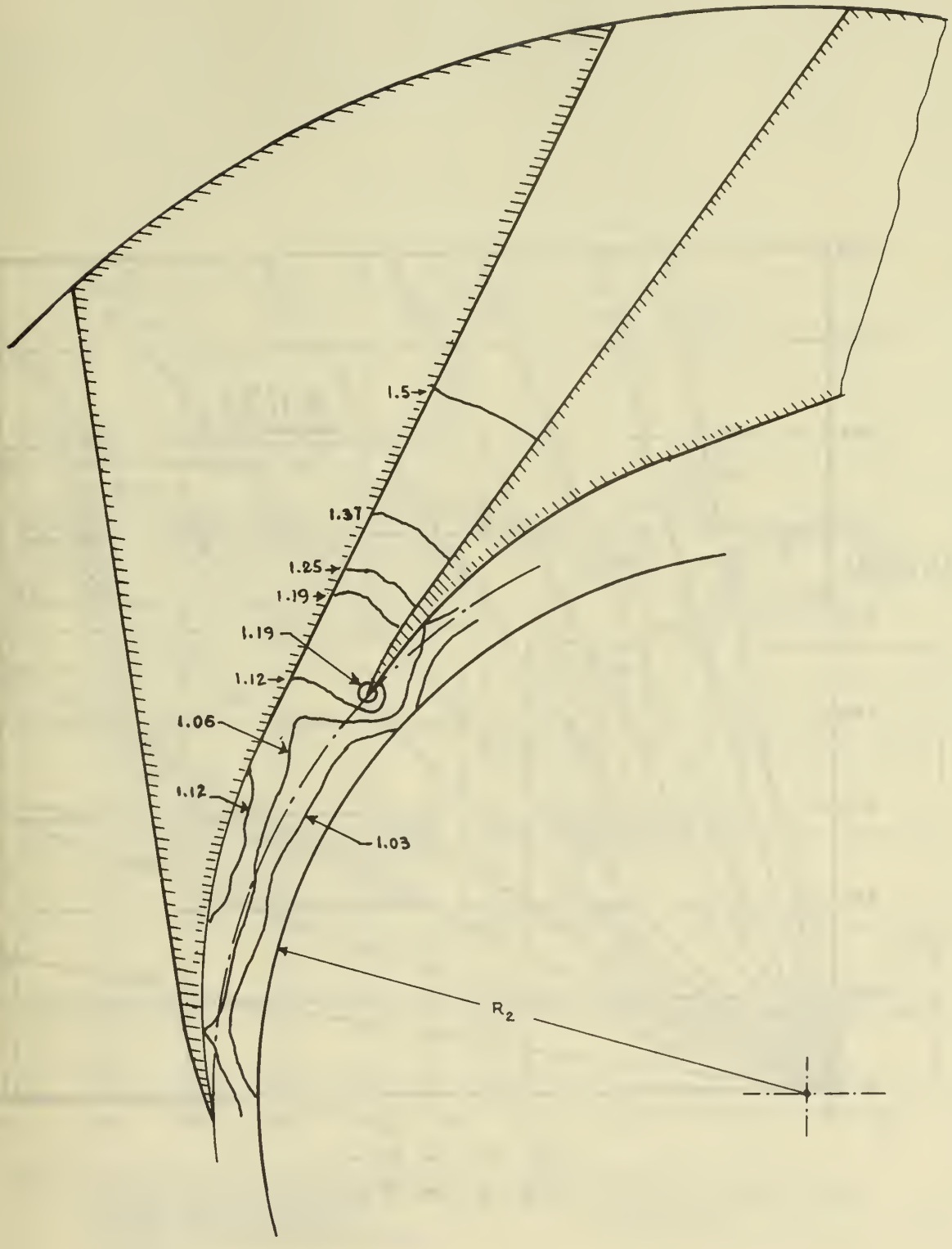

FIG. 17 TYPICAL DISTRIBUTION OF STATIC PRESSURES IN TRANSITION SECTION AND DIFFUSOR OF HIGH SPEED COMPRESSOR

(Numbers represent approximate ratios of static pressures and average pressure p_2)

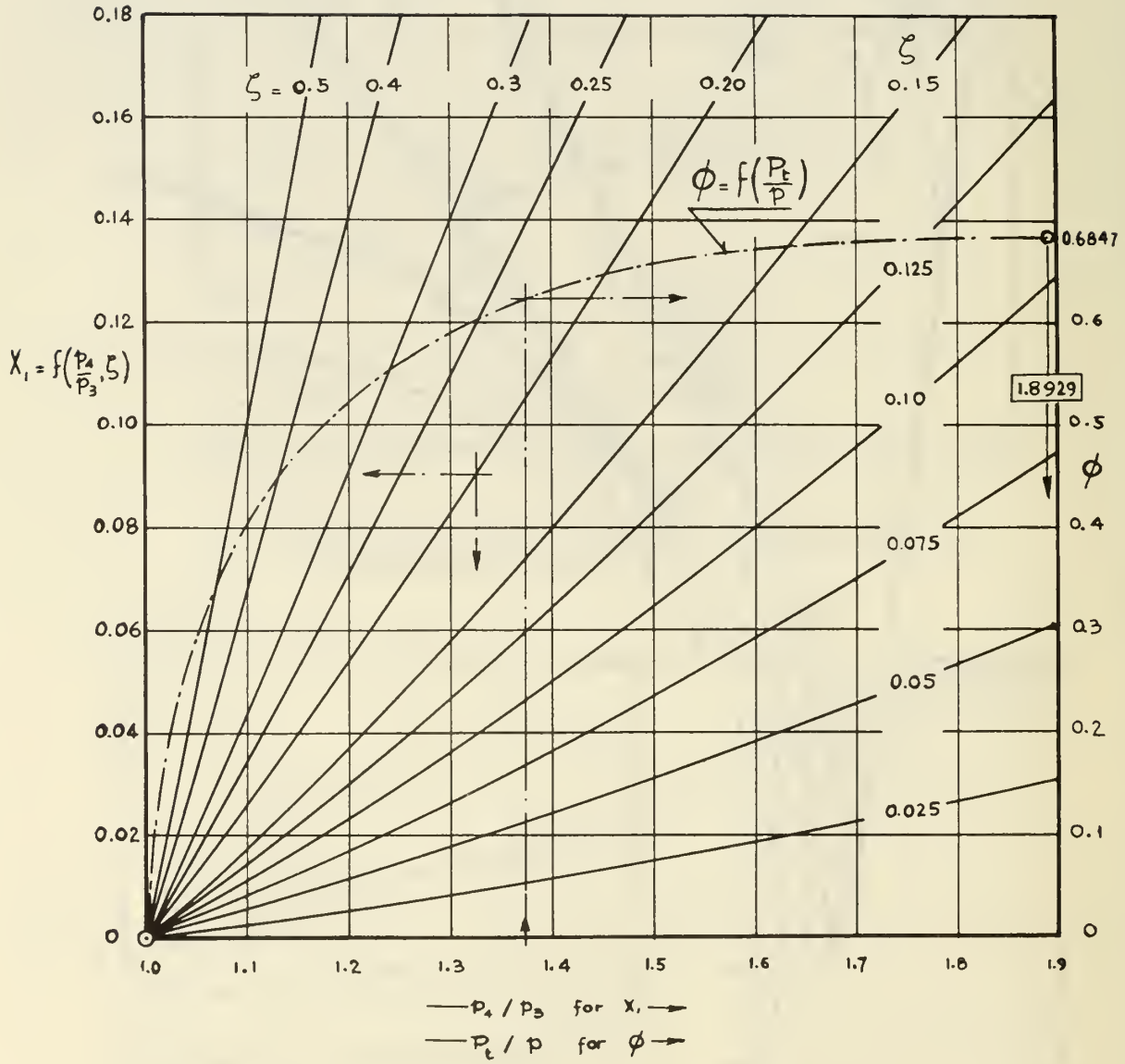

FIG. 18 FUNCTION X_1 OF EQ. IV(16) OF TABLE IV FOR DIFFUSOR CALCULATION AND DIMENSIONLESS FLOW FUNCTION OF EQ. IV(22) AND IV(29) OF TABLE IV

$(\gamma = 1.4)$

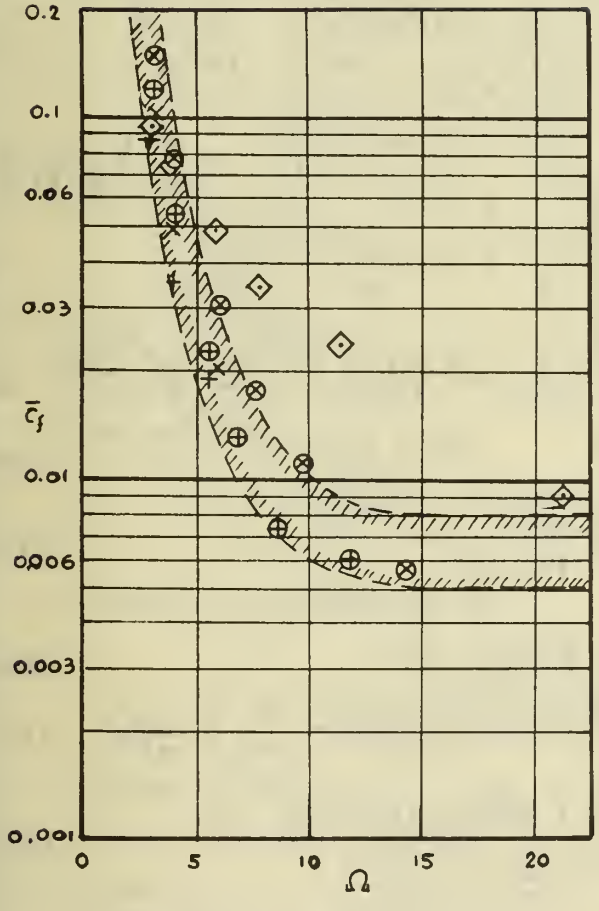

FIG.19 AVERAGE SKIN FRICTION COEFFICIENTS $\bar{c}_f$ OBTAINED FROM TWO-DIMENSIONAL DIFFUSOR TEST DATA OF REF.27 AS FUNCTION OF THE DIFFUSOR SHAPE FACTOR Ω

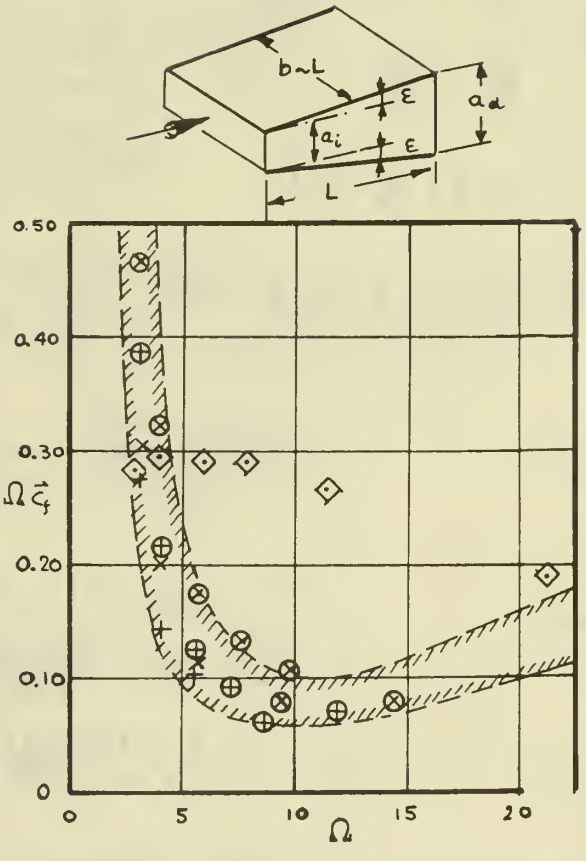

FIG.20 VALUES OF Ω $\bar{c}_f$ FROM FIG.19 AS FUNCTION OF Ω

SYMBOLS IN FIGS. 19 AND 20:

⊕	$L/a_i = 8$, $2\delta^*/a_i \simeq 0.017$	+	$L/a_i = 8$, $\delta^*/a_i \simeq 0$
⊗	$L/a_i = 12$, $2\delta^*/a_i \simeq 0.025$	×	$L/a_i = 12$, $\delta^*/a_i \simeq 0$
◇	$L/a_i = 48$, $2\delta^*/a_i \simeq 0.018$		

δ^* = Displacement Thickness of Boundary Layer on Top and Bottom Wall

TABLE I FLOW PROPERTIES IN COMPRESSOR

(For Symbols see Figs. 1 and 2)

VELOCITIES

$$\frac{V_1}{U_2} = \frac{R_{10}}{R_2}\cot\beta_{10} \qquad I(1)$$

$$\frac{W_{10}}{U_2} = \frac{R_{10}}{R_2}\frac{1}{\sin\beta_{10}} \qquad I(2)$$

$$\frac{V_2}{U_2} = \frac{\mu}{\sin\alpha_2} \qquad I(3)$$

$$\frac{W_2}{U_2} = \left[1 - 2\mu\left(1 - \frac{\mu}{2\sin^2\alpha_2}\right)\right]^{\frac{1}{2}} \qquad I(4)$$

$$\frac{V_{u2}}{U_2} = \mu$$

$$\frac{W_{u2}}{U_2} = 1 - \mu$$

$$\frac{V_{m2}}{U_2} = \mu\cot\alpha_2$$

$$V_4 = \lambda V_2$$

$$W_2 = \psi W_{2is}$$

TEMPERATURES

$$\frac{T_{t1}}{T_0} = 1$$

$$\frac{T_1}{T_0} = \frac{1}{1 + \frac{\gamma-1}{2} M_{w1}^2 \cos^2\beta_{10}} = \frac{1 + \frac{\gamma-1}{2}\left(\frac{U_2}{a_0}\right)^2\left(\frac{R_{10}}{R_2}\right)^2}{1 + \frac{\gamma-1}{2} M_{w1}^2} \qquad I(5)$$

$$\frac{T_{t2}}{T_0} = 1 + (\gamma-1)\mu\left(\frac{U_2}{a_0}\right)^2 \qquad I(6)$$

$$\frac{T_2}{T_0} = 1 + (\gamma-1)\mu\left(\frac{U_2}{a_0}\right)^2\left[1 - \frac{\mu}{2\sin^2\alpha_2}\right] \qquad I(7)$$

$$\frac{T_{t4}}{T_0} = \frac{T_{t2}}{T_0}$$

$$\frac{T_2'}{T_0} = 1 + (\gamma-1)\mu\left(\frac{U_2}{a_0}\right)^2\left[\frac{1}{\psi^2}\left(1 - \frac{\mu}{2\sin^2\alpha_2}\right) - \frac{1}{2\mu}\left(\frac{1}{\psi^2} - 1\right)\right] \qquad I(8)$$

$$a_0 = \left[\gamma R_G T_0\right]^{\frac{1}{2}}$$

$$\frac{T_4}{T_0} = 1 + (\gamma-1)\mu\left(\frac{U_2}{a_0}\right)^2\left[1 - \frac{\lambda^2\mu}{2\sin^2\alpha_2}\right] \qquad I(9)$$

$$\frac{T_E}{T_0} = 1 + \frac{\gamma-1}{2}\left(\frac{U_2}{a_0}\right)^2 \qquad I(10)$$

$$\frac{T_4'}{T_0} = 1 + (\gamma-1)\mu\left(\frac{U_2}{a_0}\right)^2\left[1 - \frac{\mu}{2\sin^2\alpha_2}\left(1 - \eta_D^*\right)\right] \qquad I(11)$$

$$\eta_D^* = \eta_D\left(1 - \lambda^2\right) \qquad I(12)$$

$$\frac{T_4''}{T_0} = \frac{(T_4'/T_0)(T_2'/T_0)}{T_2/T_0} = \frac{1 + (\gamma-1)\mu\left(\frac{U_2}{a_0}\right)^2\left[X_1 + (\gamma-1)\mu\left(\frac{U_2}{a_0}\right)^2 X_2\right]}{1 + (\gamma-1)\mu\left(\frac{U_2}{a_0}\right)^2\left[1 - \frac{\mu}{2\sin^2\alpha_2}\right]} \qquad I(13)$$

$$X_1 = \eta_D^* - \frac{1}{2\mu}\left(\frac{1}{\psi^2} - 1\right) + \left(1 - \frac{\mu}{2\sin^2\alpha_2}\right)\left(1 + \frac{1}{\psi^2} - \eta_D^*\right) \qquad I(14)$$

$$X_2 = \frac{\eta_D^*}{2\mu}\left(1 - \frac{1}{\psi^2}\right) + \left(1 - \frac{\mu}{2\sin^2\alpha_2}\right)\left(\frac{\eta_D^*}{\psi^2} - \frac{[1-\eta_D^*]}{2\mu}\left[\frac{1}{\psi^2} - 1\right]\right) + \left(1 - \frac{\mu}{2\sin^2\alpha_2}\right)^2\left(\frac{1-\eta_D^*}{\psi^2}\right) \qquad I(15)$$

$$\frac{\Delta T_{is}}{T_0} = \frac{T_4'' - T_0}{T_0} = \frac{(\gamma-1)\mu\left(\frac{U_2}{a_0}\right)^2\left[X_1 - \left(1 - \frac{\mu}{2\sin^2\alpha_2}\right) + (\gamma-1)\mu\left(\frac{U_2}{a_0}\right)^2 X_2\right]}{1 + (\gamma-1)\mu\left(\frac{U_2}{a_0}\right)^2\left[1 - \frac{\mu}{2\sin^2\alpha_2}\right]} \qquad I(16)$$

PRESSURES

$$\frac{P_{t2}'}{P_0} = \left(T_{t2}/T_0\right)^{\frac{\gamma}{\gamma-1}} \qquad I(17)$$

$$\frac{P_1}{P_0} = \left(T_1/T_0\right)^{\frac{\gamma}{\gamma-1}} \qquad I(18)$$

$$\frac{P_{t2}}{P_0} = \frac{p_2}{P_0}\frac{P_{t2}}{p_2} = \left[\frac{(T_2'/T_0)(T_{t2}/T_0)}{T_2/T_0}\right]^{\frac{\gamma}{\gamma-1}} \qquad I(19)$$

$$\frac{p_2}{P_0} = \left(T_2'/T_0\right)^{\frac{\gamma}{\gamma-1}} \qquad I(20)$$

$$\frac{P_{t4}}{P_0} = \frac{p_4}{P_0} = \left(T_4''/T_0\right)^{\frac{\gamma}{\gamma-1}} \qquad I(21)$$

$$\frac{p_4}{p_2} = \left(T_4'/T_2\right)^{\frac{\gamma}{\gamma-1}} = \left(\frac{T_4'/T_0}{T_2/T_0}\right)^{\frac{\gamma}{\gamma-1}} \qquad I(22)$$

$$\frac{P_{E1}}{P_0} = \left(T_E/T_0\right)^{\frac{\gamma}{\gamma-1}} \qquad I(23)$$

$$\frac{P_{E2}}{P_0} = \frac{p_2}{P_0}\frac{P_{E2}}{p_2} = \left[\frac{(T_2'/T_0)(T_E/T_0)}{T_2/T_0}\right]^{\frac{\gamma}{\gamma-1}} \qquad I(24)$$

TABLE II PERFORMANCE AND DESIGN PARAMETERS

$$\eta_c = \frac{\Delta T_{is}}{\Delta T_w} = \frac{X_1 - \left(1 - \frac{\mu}{2\sin^2\alpha_2}\right) + (\gamma-1)\mu\left(\frac{U_2}{a_0}\right)^2 X_2}{1 + (\gamma-1)\mu\left(\frac{U_2}{a_0}\right)^2\left[1 - \frac{\mu}{2\sin^2\alpha_2}\right]} \qquad \text{II(1)}$$

(X_1 and X_2 are given by Eqs. I(14) and I(15) of Table I)

$$r^* = \frac{T_2' - T_0}{\Delta T_{is}} = \frac{\frac{1}{\psi^2}\left(1 - \frac{\mu}{2\sin^2\alpha_2}\right) - \frac{1}{2\mu}\left(\frac{1}{\psi^2} - 1\right)}{\eta_c} \qquad \text{II(2)}$$

$$\frac{U_2}{a_0} = \left[\frac{\left(P_{t4}/P_0\right)^{\frac{\gamma-1}{\gamma}} - 1}{(\gamma-1)\mu\,\eta_c}\right]^{\frac{1}{2}} \qquad \text{II(3)}$$

$$\frac{R_{10}}{R_2} = \frac{M_{w1}\sin\beta_{10}}{\frac{U_2}{a_0}\left[1 + \frac{\gamma-1}{2}M_{w1}^2\cos^2\beta_{10}\right]^{\frac{1}{2}}} \qquad \text{II(4)}$$

$$\frac{W_2}{W_{10}} = \frac{\left[1 - 2\mu\left(1 - \frac{\mu}{2\sin^2\alpha_2}\right)\right]^{\frac{1}{2}}\sin\beta_{10}}{\left(R_{10}/R_2\right)} \qquad \text{II(5)}$$

$$M_{V2} = \frac{V_2}{a_2} = \frac{\mu\frac{U_2}{a_0}}{\sin\alpha_2\left[1 + (\gamma-1)\mu\left(\frac{U_2}{a_0}\right)^2\left(1 - \frac{\mu}{2\sin^2\alpha_2}\right)\right]^{\frac{1}{2}}} \qquad \text{II(6)}$$

$$\phi_1 = \frac{V_1}{U_2} = \frac{M_{w1}\cos\beta_{10}}{\frac{U_2}{a_0}\left[1 + \frac{\gamma-1}{2}M_{w1}^2\cos^2\beta_{10}\right]^{\frac{1}{2}}} \qquad \text{II(7)}$$

$$\phi_2 = \frac{V_{m2}}{U_2} = \mu\cot\alpha_2 \qquad \text{II(8)}$$

$$\pi R_2^2\left[1 - \left(\frac{R_{1i}}{R_{10}}\right)^2\right]k_{B1} = \left(\frac{\dot m\sqrt{R_G T_0}}{P_0}\right)\left(\frac{U_2}{a_0}\right)^2\frac{\left[1 + \frac{\gamma-1}{2}M_{w1}^2\cos^2\beta_{10}\right]^{\frac{3\gamma-1}{2(\gamma-1)}}}{\sqrt{\gamma}\,M_{w1}^3\cos\beta_{10}\sin^2\beta_{10}} \qquad \text{II(9)}$$

$$\frac{\omega}{\left[1 - \left(\frac{R_{1i}}{R_{10}}\right)^2\right]k_{B1}} = \left[\frac{a_0 P_0}{\dot m}\right]^{\frac{1}{2}}\frac{\sin\beta_{10}\left[\pi\gamma\cos\beta_{10}\right]^{\frac{1}{2}}}{\left[1 + \frac{\gamma-1}{2}M_{w1}^2\cos^2\beta_{10}\right]^{\frac{3\gamma-1}{4(\gamma-1)}}} \qquad \text{II(10)}$$

$$\left(\frac{b_2}{R_2}\right)k_{B2} = \left(\frac{\dot m\sqrt{R_G T_0}}{\pi R_2^2 P_0}\right)\frac{1 + (\gamma-1)\mu\left(\frac{U_2}{a_0}\right)^2\left(1 - \frac{\mu}{2\sin^2\alpha_2}\right)}{2\mu\sqrt{\gamma}\cot\alpha_2\left(\frac{U_2}{a_0}\right)\left\{1 + (\gamma-1)\mu\left(\frac{U_2}{a_0}\right)^2\left[\frac{1}{\psi^2}\left(1 - \frac{\mu}{2\sin^2\alpha_2}\right) - \frac{1}{2\mu}\left(\frac{1}{\psi^2} - 1\right)\right]\right\}^{\frac{\gamma}{\gamma-1}}} \qquad \text{II(11)}$$

Diffusor Exit Area A_4:

$$A_4 k_{B4} = \left(\frac{\dot m\sqrt{R_G T_0}}{P_0}\right)\frac{\sin\alpha_2}{\lambda\mu\sqrt{\gamma}\left(\frac{U_2}{a_0}\right)}\frac{\left[1 + (\gamma-1)\mu\left(\frac{U_2}{a_0}\right)^2\left(1 - \frac{\lambda^2\mu}{2\sin^2\alpha_2}\right)\right]}{\left[1 + \eta_c(\gamma-1)\mu\left(\frac{U_2}{a_0}\right)^2\right]^{\frac{\gamma}{\gamma-1}}} \qquad \text{II(12)}$$

Diffusor Throat Area A_x if $M_{V2} > 1$:

$$A_x k_{Bx} = \frac{\left(\frac{\dot m\sqrt{R_G T_0}}{P_0}\right)}{\phi_c\left(\frac{P_{tx}}{P_{t2}}\right)\left[1 + (\gamma-1)\mu\left(\frac{U_2}{a_0}\right)^2\right]^{\frac{\gamma+1}{2(\gamma-1)}}}\gamma^{\frac{\gamma}{\gamma-1}} \qquad \text{II(13)}$$

where

$$\phi_c = \left\{\frac{2\gamma}{\gamma-1}\left[\left(\frac{2}{\gamma+1}\right)^{\frac{2}{\gamma-1}} - \left(\frac{2}{\gamma+1}\right)^{\frac{\gamma+1}{\gamma-1}}\right]\right\}^{\frac{1}{2}} \qquad \text{II(14)}$$

and

$$\gamma = \frac{T_2/T_0}{T_2'/T_0} = \frac{1 + (\gamma-1)\mu\left(\frac{U_2}{a_0}\right)^2\left[1 - \frac{\mu}{2\sin^2\alpha_2}\right]}{1 + (\gamma-1)\mu\left(\frac{U_2}{a_0}\right)^2\left[\frac{1}{\psi^2}\left(1 - \frac{\mu}{2\sin^2\alpha_2}\right) - \frac{1}{2\mu}\left(\frac{1}{\psi^2} - 1\right)\right]} \qquad \text{II(15)}$$

Diffusor Throat Area A_x if $M_{V2} \leqq 1$, and $V_x = \xi V_2$:

$$A_x k_{Bx} = \frac{\sin\alpha_2\left(\frac{\dot m\sqrt{R_G T_0}}{P_0}\right)}{\xi\mu\sqrt{\gamma}\left(\frac{U_2}{a_0}\right)\left(\frac{P_{tx}}{P_{t2}}\right)\left[1 + (\gamma-1)\mu\left(\frac{U_2}{a_0}\right)^2\left(1 - \frac{\xi^2\mu}{2\sin^2\alpha_2}\right)\right]^{\frac{1}{\gamma-1}}}\gamma^{\frac{\gamma}{\gamma-1}} \qquad \text{II(16)}$$

TABLE III SPECIFIC SPEED RELATIONS

DEFINITIONS WITH ENGLISCH UNITS

(see Refs. 18 and 19)

SPECIFIC SPEED

$$N_S = \frac{N\ Q_1^{1/2}}{H_{is}^{3/4}} \qquad \text{III(1)}$$

SPECIFIC DIAMETER

$$D_S = \frac{D\ H_{is}^{1/4}}{Q_1^{1/2}} \qquad \text{III(2)}$$

DEFINITIONS IN DIMENSIONLESS FORM

$$n_S = \frac{N_S}{129} = \frac{\omega\ Q_1^{1/2}}{(c_p\ \Delta T_{is})^{3/4}} \qquad \text{III(3)}$$

$$d_S = \frac{D_S}{0.42} = \frac{D\ (c_p\ \Delta T_{is})^{1/4}}{Q_1^{1/2}} \qquad \text{III(4)}$$

N - Rotative Speed (rpm)
ω - Angular Velocity (radians/s)
Q_1 - Inlet Volume Flow Rate (cuft/s)
$H_{is} = g_o\ c_p\ \Delta T_{is}$ - Isentropic Head (ft-lb/lbm)
g_o - Gravitational Constant = 32.174 ft/s^2
c_p - Specific Heat at Constant Pressure $\left(\frac{\text{ft-lb}}{\text{slug, deg.R}}\right)$
ΔT_{is} - Isentropic Temperature Rise in Compressor (deg. R)
D - Rotor Diameter (ft)

RELATIONS WITH SYMBOLS OF TABLES I AND II

$$\xi_1 = 1 - \left(\frac{R_{1i}}{R_{1o}}\right)^2 \qquad \text{III(5)}$$

$$Q_1 = \pi R_{1o}^2\ \xi_1\ k_{B1}\ V_1$$
$$V_1 = U_{1o} \cot \beta_{1o}$$
$$c_p\ \Delta T_{is} = \mu\ \eta_c\ U_2^2$$
$$\omega = U_2/R_2$$
$$D = 2\ R_2 = 2\ U_2/\omega$$

$$n_S^2 = \pi\left(\frac{R_{1o}}{R_2}\right)^3 k_{B1}\ \frac{\cot \beta_{1o}\ \xi_1}{(\mu\ \eta_c)^{3/2}} \qquad \text{III(6)}$$

$$d_S^2 = \frac{4}{\pi}\ \frac{(\mu\ \eta_c)^{1/2}}{(R_{1o}/R_2)^3\ k_{B1} \cot \beta_{1o}\ \xi_1} \qquad \text{III(7)}$$

and

$$\xi_1 = \frac{n_S^2}{\pi}\ \frac{(\mu\ \eta_c)^{3/2} \tan \beta_{1o}}{k_{B1}\ (R_{1o}/R_2)^3} \qquad \text{III(8)}$$

$$\xi_1 = \frac{4}{\pi\ d_S^2}\ \frac{(\mu\ \eta_c)^{1/2} \tan \beta_{1o}}{k_{B1}\ (R_{1o}/R_2)^3} \qquad \text{III(9)}$$

Equating Eqs. 8 and 9:

$$n_S\ d_S = \frac{2}{(\mu\ \eta_c)^{1/2}} \qquad \text{III(10)}$$

From Eq.8

$$\frac{R_{1i}}{R_{1o}} = \left[1 - \frac{n_S^2}{\pi}\ \frac{(\mu\ \eta_c)^{3/2} \tan \beta_{1o}}{k_{B1}\ (R_{1o}/R_2)^3}\right]^{1/2} \qquad \text{III(11)}$$

EXAMPLE: For μ= 0.88 , η_c= 0.83 , k_{B1}= 0.85 , and β_{1o}= 68° , find R_{1i}/R_{1o} for different values of N_s for the two radius ratios R_{1o}/R_2 = 0.56 and R_{1o}/R_2 = 0.70

For R_{1o}/R_2 = 0.56; from Eq.11

$$\frac{R_{1i}}{R_{1o}} = \left[1 - n_S^2(3.288)\right]^{1/2} \qquad \text{III(12)}$$

R_{1i}/R_{1o} is zero for $n_{S\,max}$=0.552,or N_{Smax}=71
For values of N_S lower than 71:

N_S	60	65	70
n_S	0.465	0.504	0.543
R_{1i}/R_{1o}	0.537	0.406	0.178

For R_{1o}/R_2 = 0.70; from Eq.11

$$\frac{R_{1i}}{R_{1o}} = \left[1 - n_S^2(1.683)\right]^{1/2} \qquad \text{III(13)}$$

R_{1i}/R_{1o} is zero for n_{Smax} = 0.771,or N_{Smax}=99.4
For values of N_S lower than 99.4:

N_S	70	80	90	98
n_S	0.543	0.620	0.698	0.760
R_{1i}/R_{1o}	0.710	0.594	0.424	0.169

Relation between so-called Mach Number $N_{W1} = W_{1o} / \sqrt{\frac{2\gamma}{\gamma+1} R_G T_0}$ and actual Mach Number $M_{W1} = W_{1o}/a_1$:

$$N_{W1}^2 = \left[\frac{\gamma+1}{2}\ M_{W1}^2\right] \Big/ \left[1 + \frac{\gamma-1}{2} M_{W1}^2 \cos^2 \beta_{1o}\right] \qquad \text{III(14)}$$

TABLE IV ANALYSIS OF FLOWS IN DIFFUSORS

ONE-DIMENSIONAL FLOW IN CHANNEL

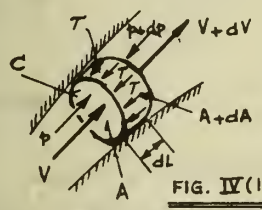

FIG. IV(1)

A - Flow Area
C - Wetted Perimeter
L - Channel Length
$\dot{m}$ - Mass Flow Rate
p - Static Pressure
T - Wall Shear Stresses
ρ - Mass Density

From Momentum Theorem:

$$\frac{1}{\rho} dp + d\left(\frac{V^2}{2}\right) = -\frac{\tau}{\rho}\frac{C}{A} dL \qquad \text{IV (1)}$$

From Equation of Continuity:

$$\dot{m} = A \rho V \qquad \text{IV (2)}$$

Derivation:

Eq. IV(4) into Eq. IV(1)

$$c_p dT - Tds + d\left(\frac{V^2}{2}\right) = -\frac{\tau}{\rho}\frac{C}{A} dL$$

$$d\left(c_p dT + \frac{V^2}{2}\right) - Tds = -\frac{\tau}{\rho}\frac{C}{A} dL$$

From Eq. 3

$$dT_t = 0 = d\left(T + \frac{V^2}{2c_p}\right)$$

$$Tds = \frac{\tau}{\rho}\frac{C}{A} dL \qquad \text{IV (10)}$$

From Frictional Law with Eq. 2:

$$\tau = c_f \frac{\rho}{2} V^2 = \frac{c_f}{2}\frac{\dot{m}^2}{\rho A^2} \qquad \text{IV (12)}$$

Into Eq. 10

$$Tds = \frac{c_f}{2}\frac{\dot{m}^2}{\rho^2 A^3} C\, dL \qquad \text{IV (13)}$$

THERMODYNAMIC CONDITIONS

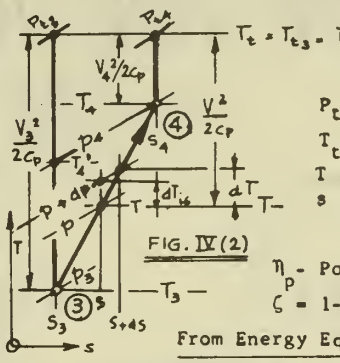

FIG. IV(2)

$T_t = T_{t3} = T_{t4}$

P_t - Total Pressure
T_t - Total Temperature
T - Static Temperature
s - Entropy

η_p - Polytropic Efficiency
$\zeta = 1 - \eta_p$ - Loss Coefficient

From Energy Equation:

$$T_t = T_{t3} = T_{t4} = T + \frac{V^2}{2c_p} = T_3 + \frac{V_3^2}{2c_p} = T_4 + \frac{V_4^2}{2c_p} \qquad \text{IV (3)}$$

From First Law of Thermodynamics: IV (4)

$$T\,ds = c_p\, dT - \frac{1}{\rho} dp = R_G \frac{\gamma}{\gamma-1} dT - \frac{1}{\rho} dp$$

$$ds = R_G\left[\frac{\gamma}{\gamma-1}\frac{dT}{T} - \frac{dp}{p}\right] \qquad \text{IV (5)}$$

For Adiabatic Polytropic Process

$$\eta_p = \frac{dT_{is}}{dT} = \frac{T\left[\left(\frac{p+dp}{p}\right)^{\frac{\gamma-1}{\gamma}} - 1\right]}{dT} = \frac{T}{dT}\frac{\gamma-1}{\gamma}\frac{dp}{p} \qquad \text{IV (6)}$$

$$\frac{dT}{T} = \frac{\gamma-1}{\eta_p \gamma}\frac{dp}{p} \qquad \text{IV (7)}$$

$$T = \text{constant}\; p^{\frac{\gamma-1}{\eta_p \gamma}} \qquad \text{IV (8)}$$

$$\rho = \text{constant}\; p^{1-\frac{\gamma-1}{\eta_p \gamma}} \qquad \text{IV (9)}$$

From Eqs. 5 and 7

$$\frac{ds}{R_G} = \left(\frac{1}{\eta_p} - 1\right)\frac{dp}{p} = \frac{\zeta}{1-\zeta}\frac{dp}{p} \qquad \text{IV (11)}$$

Dimensionless Referred Mass Flow Rate

$$\dot{m}_{r3} = \frac{\dot{m}\sqrt{R_a T_3}}{p_3 A_3} \qquad \text{IV (14)}$$

PRINCIPAL EQUATION obtained from Eqs. 13 and 14, and $\rho = \frac{p}{R_G T}$

$$dX_1 = \frac{\rho}{\rho_3}\frac{p}{p_3} d\left(\frac{s}{R_G}\right) = \frac{c_f}{2}\left(\dot{m}_{r3}\right)^2 \left(\frac{A_3}{A}\right)^3 \frac{C\, dL}{A_3} = \frac{c_f}{2}\left(\dot{m}_{r3}\right)^2 d\Omega = dX_2 \qquad \text{IV (15)}$$

$$X_1 = \int_3^4 dX_1 = \int_3^4 \frac{\rho}{\rho_3}\frac{p}{p_3} d\left(\frac{s}{R_G}\right) \qquad \text{IV (16)}$$

With Eqs. 11 and 9

$$dX_1 = \left(\frac{1}{\eta_p} - 1\right)\frac{\rho}{\rho_3}\frac{p}{p_3}\frac{dp}{p} = \left(\frac{1}{\eta_p} - 1\right)\frac{\rho}{\rho_3} d\left(\frac{p}{p_3}\right)$$

$$dX_1 = \left(\frac{1}{\eta_p} - 1\right)\left(\frac{p}{p_3}\right)^{1-\frac{\gamma-1}{\eta_p\gamma}} d\left(\frac{p}{p_3}\right)$$

$$X_1 = \int_1^{(p_3/p_4)} dX_1 = \frac{\frac{1}{\eta_p} - 1}{2 - \frac{\gamma-1}{\eta_p\gamma}}\left[\left(\frac{p_4}{p_3}\right)^{2-\frac{\gamma-1}{\eta_p\gamma}} - 1\right]$$

and

$$X_1 = \frac{\zeta\gamma}{\gamma+1-2\zeta\gamma}\left[\left(\frac{p_4}{p_3}\right)^{\frac{\gamma+1-2\zeta\gamma}{(1-\zeta)\gamma}} - 1\right] \qquad \text{IV (20)}$$

$$X_2 = \frac{1}{2}\left(\dot{m}_{r3}\right)^2 \int_0^L c_f\, d\Omega = \frac{\bar{c}_f}{2}\left(\dot{m}_{r3}\right)^2 \int_0^L d\Omega \qquad \text{IV (17)}$$

$$X_2 = \frac{\bar{c}_f}{2}\left(\dot{m}_{r3}\right)^2 \Omega \qquad \text{IV (18)}$$

$$\Omega = \int_0^L \left(\frac{A_3}{A}\right)^3 \frac{C\, dL}{A_3} \qquad \text{IV (19)}$$

Ω will be denoted as Diffusor Shape Factor

From Eq. 20

$$\frac{p_4}{p_3} = \left[\frac{X_1(\gamma+1-2\zeta\gamma)}{\zeta\gamma} + 1\right]^{\frac{(1-\zeta)\gamma}{\gamma+1-2\zeta\gamma}} \qquad \text{IV (21)}$$

TABLE IV (CONTD.) METHODS OF SOLUTION

For Effective Flow Area $A_3^* = k_{B3} A_3$ (k_{B3} = Blockage Factor, A_3 = Actual Area at Diffusor Inlet)

$$\frac{\dot m \sqrt{R_G T_{t3}}}{A_3^* P_{t3}} = \sqrt{\frac{2\gamma}{\gamma-1}\left[\left(\frac{p_3}{P_{t3}}\right)^{\frac{2}{\gamma}} - \left(\frac{p_3}{P_{t3}}\right)^{\frac{\gamma+1}{\gamma}}\right]} = \phi_3 = f\left(\frac{P_{t3}}{p_3}, \gamma\right) \qquad \text{IV (22)}$$

From Eq. 14

$$\bar{\dot m}_{r3} = \frac{\dot m \sqrt{R_G T_3}}{A_3^* p_3} = \phi_3 \frac{\sqrt{(T_3/T_{t3})}}{p_3/P_{t3}} \qquad \text{IV (23)}$$

If p_3 is known,

$$\frac{T_3}{T_{t3}} = \left(\frac{p_3}{P_{t3}}\right)^{\frac{\gamma-1}{\gamma}} \qquad \text{IV (25)}$$

Into Eq. 23

$$\dot m_{r3} = \phi_3 \left(\frac{P_{t3}}{p_3}\right)^{\frac{\gamma+1}{2\gamma}} \qquad \text{IV (27)}$$

If $M_{V3} = V_3/\sqrt{\gamma R_G T_3}$ is known, with $c_p = R_G \frac{\gamma}{\gamma-1}$,

$$\frac{T_{t3}}{T_3} = 1 + \frac{V_3^2}{2 c_p T_3} = 1 + \frac{\gamma-1}{2}\frac{V_3^2}{\gamma R_G T_3} = 1 + \frac{\gamma-1}{2} M_{V3}^2 \qquad \text{IV (24)}$$

$$\frac{P_{t3}}{p_3} = \left[1 + \frac{\gamma-1}{2} M_{V3}^2\right]^{\frac{\gamma}{\gamma-1}} \qquad \text{IV (26)}$$

Into Eq. 23

$$\dot m_{r3} = \phi_3 \left[1 + \frac{\gamma-1}{2} M_{V3}^2\right]^{\frac{\gamma+1}{2(\gamma-1)}} \qquad \text{IV (28)}$$

For known Ω and $\bar c_f$, i.e. X_2 from Eq. 18, and $X_1 = X_2$, the Loss Coefficient ζ must be obtained with an iteration to satisfy the Equation of Continuity at Diffusor Discharge. For Effective Flow Area $A_4^* = k_{B4} A_4$ (k_{B4} = Blockage Factor, A_4 = Actual Diffusor Discharge Area), since $T_{t4} = T_{t3}$,

$$\frac{\dot m \sqrt{R_G T_{t3}}}{A_4^* P_{t4}} = \sqrt{\frac{2\gamma}{\gamma-1}\left[\left(\frac{p_4}{P_{t4}}\right)^{\frac{2}{\gamma}} - \left(\frac{p_4}{P_{t4}}\right)^{\frac{\gamma+1}{\gamma}}\right]} = \phi_4 = f\left(\frac{P_{t4}}{p_4}, \gamma\right) = \phi_3 \frac{A_3^*}{A_4^*} \frac{P_{t3}}{P_{t4}} \qquad \text{IV (29)}$$

Since P_{t3}/P_{t4} is as yet unknown, it is not possible to determine P_{t4}/p_4 from function ϕ_4 to obtain $p_4/p_3 = (P_{t3}/p_3)/(P_{t4}/p_4)$. Additional relation is obtained by calculating entropy increase $\Delta s = s_4 - s_3$ for polytropic process from p_3 to p_4 with Eq. 11, and for T_t = constant from P_{t3} to P_{t4} with Eq. 5.

For Polytropic Process:

$$\frac{\Delta s}{R_G} = \frac{\zeta}{1-\zeta} \ln\left(\frac{p_4}{p_3}\right) = \ln\left[\left(\frac{p_4}{p_3}\right)^{\frac{\zeta}{1-\zeta}}\right] \qquad \text{IV (30)}$$

Along Line $T_{t3} = T_{t4}$ = Constant:

$$\frac{\Delta s}{R_G} = -\ln\left[\frac{P_{t4}}{P_{t3}}\right] = \ln\left[\frac{P_{t3}}{P_{t4}}\right] \qquad \text{IV (31)}$$

Equating Eqs. 30 and 31

$$\frac{p_4}{p_3} = \left(\frac{P_{t3}}{P_{t4}}\right)^{\frac{1-\zeta}{\zeta}} \qquad \text{IV (32)}$$

$$\frac{P_{t3}}{P_{t4}} = \left(\frac{p_4}{p_3}\right)^{\frac{\zeta}{1-\zeta}} \qquad \text{IV (33)}$$

With Eq. 33

$$\frac{P_{t4}}{p_4} = \left(\frac{P_{t4}}{P_{t3}}\right)\left(\frac{P_{t3}}{p_3}\right)\left(\frac{p_3}{p_4}\right) = \frac{(P_{t3}/p_3)}{(P_{t3}/P_{t4})(p_4/p_3)} = \frac{(P_{t3}/p_3)}{\left(\frac{p_4}{p_3}\right)^{\frac{1}{1-\zeta}}} \qquad \text{IV (34)}$$

ITERATION PROCEDURE

(1) For given values of Ω and $\bar c_f$ calculate X_2 from Eq. 18 with Eq. 27 or 28. $X_1 = X_2$

(2) Choose initial value of ζ

(3) Calculate $p_4/p_3 = p_4'/p_3$ by Eq. 21 for X_1 and ζ

(4) Calculate $P_{t3}/P_{t4} = P_{t3}/P_{t4}'$ from Eq. 33 for p_4'/p_3

(5) Calculate $\phi_4' = \phi_3 (A_3^*/A_4^*)(P_{t3}/P_{t4}')$ (Eq. 29)

(6) Calculate P_{t4}'/p_4' from Eq. 34 for p_4'/p_3

(7) Calculate $\phi_4 - \phi_4''$ from Flow Function (Eq. 29) for $P_{t4}/p_4 = P_{t4}'/p_4'$

$\phi_4'' = \phi_4'$?

No → Change Value of ζ → (3)

Yes → ζ ; $(p_4/p_3) = (p_4'/p_3)$; $(P_{t4}/P_{t3}) = (P_{t4}'/P_{t3})$

Diffusor Efficiency η_{D3-4} between Stations (3) and (4)

$$\eta_{D3-4} = \frac{T_4' - T_3}{T_4 - T_3} = \frac{T_4'/T_3 - 1}{T_4/T_3 - 1} = \frac{(p_4/p_3)^{\frac{\gamma-1}{\gamma}} - 1}{T_4/T_3 - 1}$$

With Eq. 8

$$\eta_{D3-4} = \frac{(p_4/p_3)^{\frac{\gamma-1}{\gamma}} - 1}{(p_4/p_3)^{\frac{\gamma-1}{\gamma(1-\zeta)}} - 1} < (1-\zeta) \qquad \text{IV (35)}$$

APPENDIX B: MANUFACTURING DRAWINGS

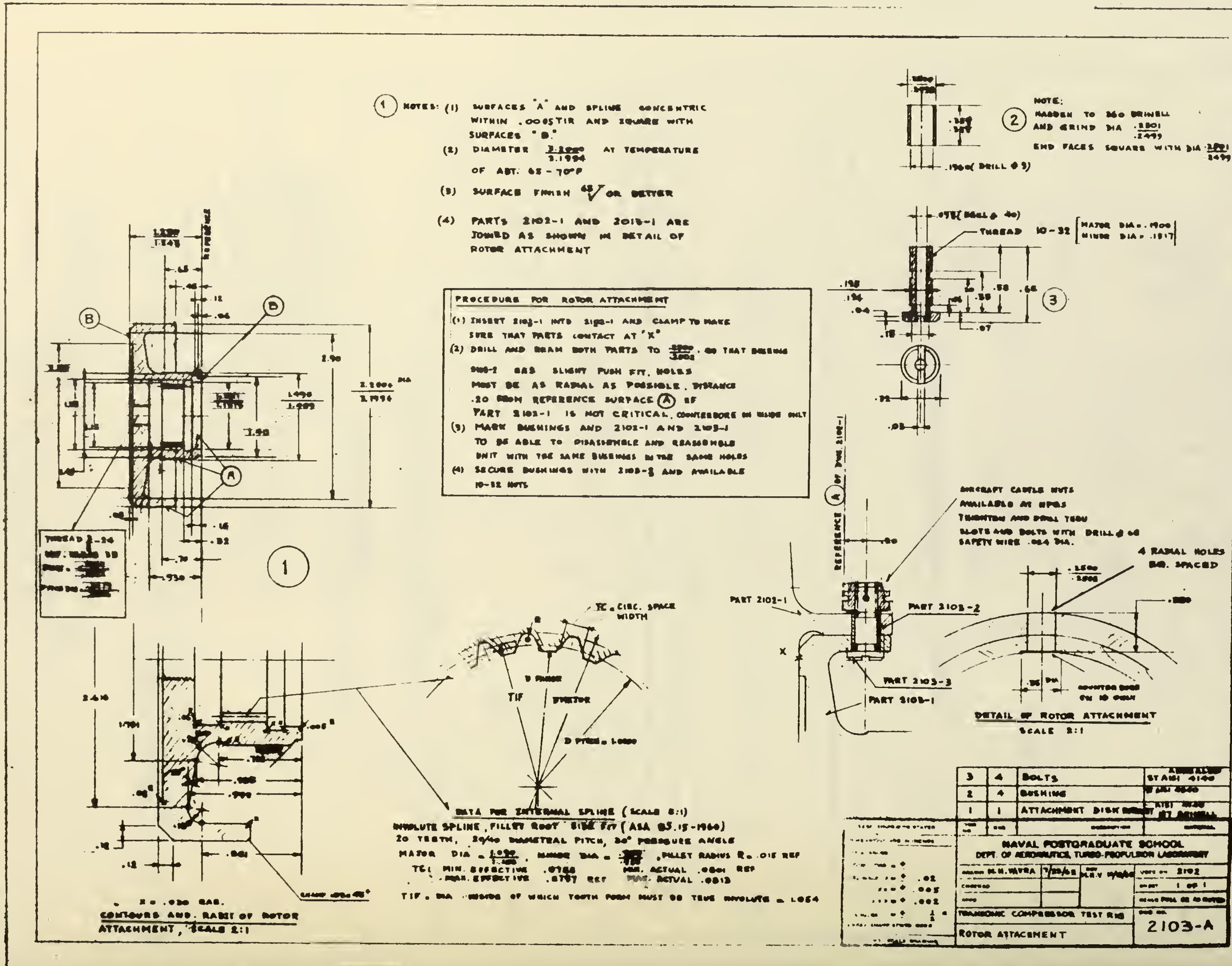

1 NOTES: (1) SURFACES "A" AND SPLINE CONCENTRIC WITHIN .0005TIR AND SQUARE WITH SURFACES "B."
(2) DIAMETER 2.2000/2.1994 AT TEMPERATURE OF ABT. 65 - 70°F
(3) SURFACE FINISH 63 OR BETTER
(4) PARTS 2102-1 AND 2013-1 ARE JOINED AS SHOWN IN DETAIL OF ROTOR ATTACHMENT
PROCEDURE FOR ROTOR ATTACHMENT
(1) INSERT 2103-1 INTO 2102-1 AND CLAMP TO MAKE SURE THAT PARTS CONTACT AT "X"
(3) MARK BUSHINGS AND 2102-1 AND 2103-1 TO BE ABLE TO DISASSEMBLE AND REASSEMBLE UNIT WITH THE SAME BUSHINGS IN THE SAME HOLES
(4) SECURE BUSHINGS WITH 2103-3 AND AVAILABLE 10-32 NUTS
NOTE:
2 HARDEN TO 360 BRINELL AND GRIND DIA .2501/.2499
END FACES SQUARE WITH DIA
THREAD 10-32
3
1
AIRCRAFT CASTLE NUTS AVAILABLE AT NPGS
SAFETY WIRE .064 DIA.
4 RADIAL HOLES EQ. SPACED
PART 2102-1
PART 2103-2
PART 2103-3
PART 2103-1
DETAIL OF ROTOR ATTACHMENT
SCALE 2:1
DATA FOR INTERNAL SPLINE (SCALE 8:1)
INVOLUTE SPLINE, FILLET ROOT SIDE FIT (ASA B5.15-1960)
20 TEETH, 20/40 DIAMETRAL PITCH, 30° PRESSURE ANGLE
TIF
CONTOURS AND RADII OF ROTOR ATTACHMENT, SCALE 2:1
3 4 BOLTS
2 4 BUSHING
1 1 ATTACHMENT DISK
NAVAL POSTGRADUATE SCHOOL
DEPT. OF AERONAUTICS, TURBO-PROPULSION LABORATORY
TRANSONIC COMPRESSOR TEST RIG
ROTOR ATTACHMENT
2103-A

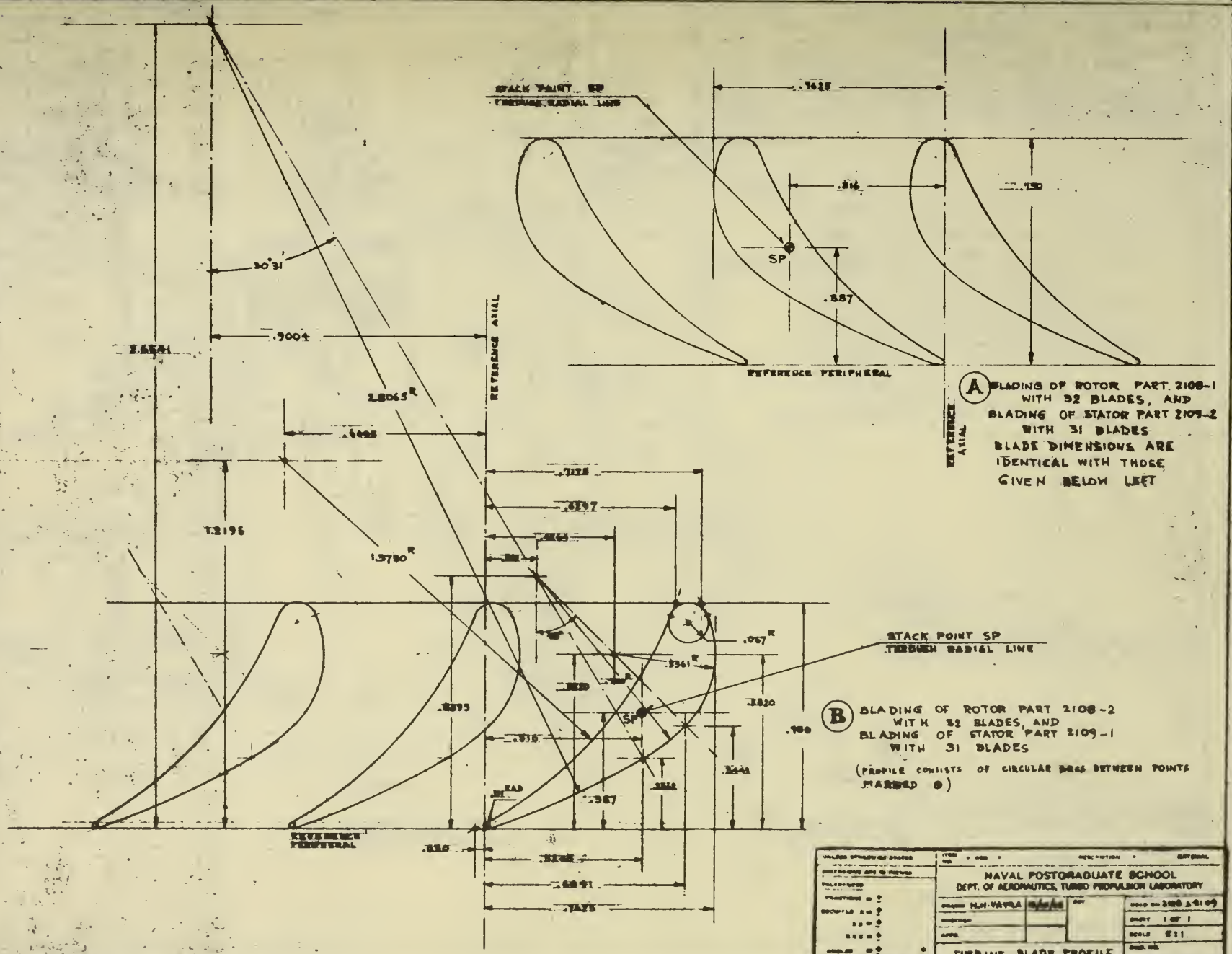

A BLADING OF ROTOR PART 2108-1 WITH 32 BLADES, AND BLADING OF STATOR PART 2109-2 WITH 31 BLADES BLADE DIMENSIONS ARE IDENTICAL WITH THOSE GIVEN BELOW LEFT

B BLADING OF ROTOR PART 2108-2 WITH 32 BLADES, AND BLADING OF STATOR PART 2109-1 WITH 31 BLADES

(PROFILE CONSISTS OF CIRCULAR ARCS BETWEEN POINTS MARKED ●)

NAVAL POSTGRADUATE SCHOOL
DEPT. OF AERONAUTICS, TURBO PROPULSION LABORATORY

TURBINE BLADE PROFILE
TRANSONIC COMPRESSOR TEST

2107

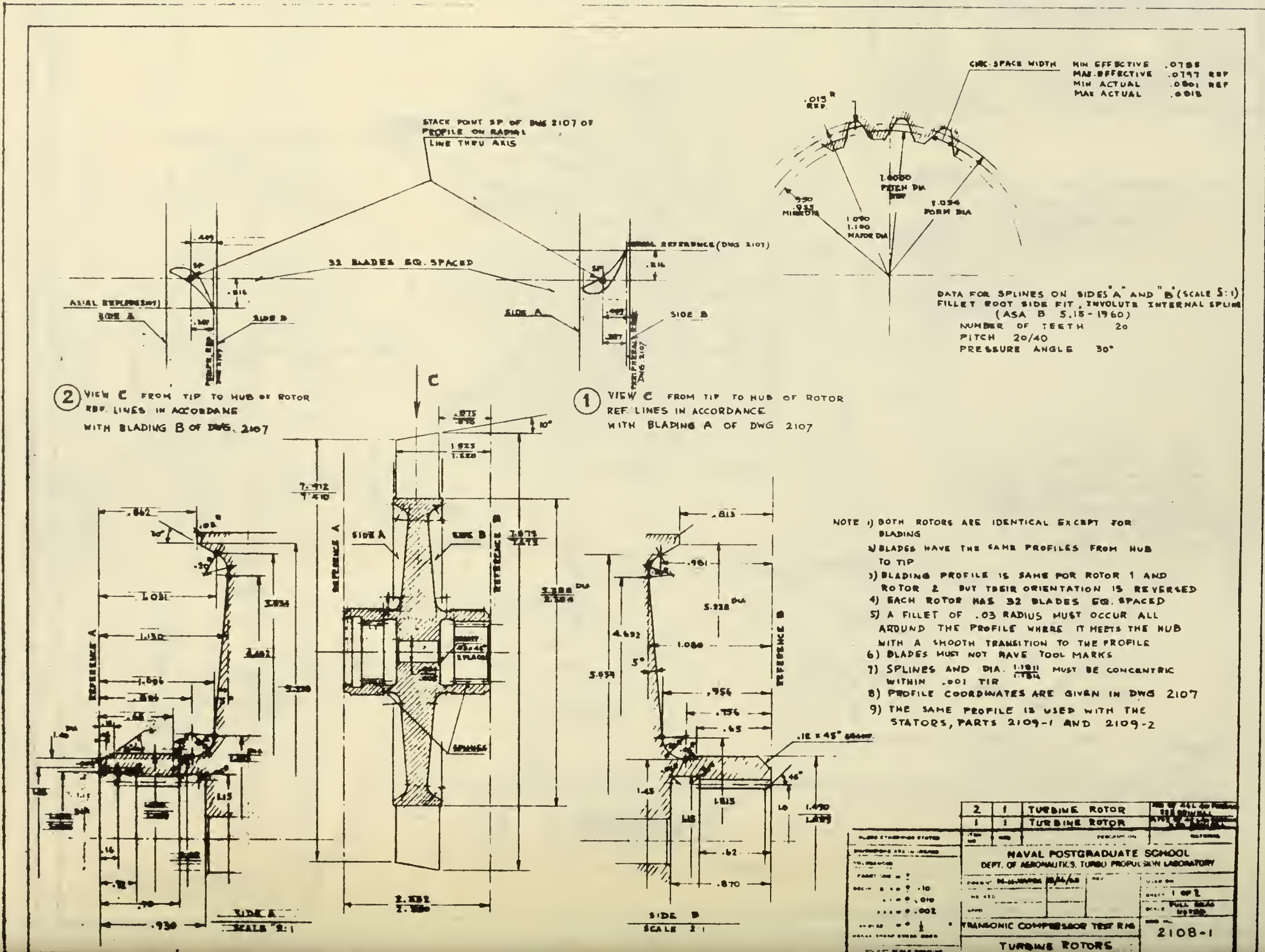

CIRC. SPACE WIDTH
MIN EFFECTIVE .0788
MAX EFFECTIVE .0797 REF
MIN ACTUAL .0801 REF
MAX ACTUAL .0818
.015 R REF.
1.0000 PITCH DIA
1.054 FORM DIA
1.090 1.100 MAJOR DIA
STACK POINT SP OF DWG 2107 OF PROFILE ON RADIAL LINE THRU AXIS
32 BLADES EQ. SPACED
SIDE A
SIDE B
DATA FOR SPLINES ON SIDES "A" AND "B" (SCALE 5:1)
FILLET ROOT SIDE FIT, INVOLUTE INTERNAL SPLINE
(ASA B 5.15-1960)
NUMBER OF TEETH 20
PITCH 20/40
PRESSURE ANGLE 30°
2 VIEW C FROM TIP TO HUB OF ROTOR REF. LINES IN ACCORDANE WITH BLADING B OF DWG. 2107
1 VIEW C FROM TIP TO HUB OF ROTOR REF. LINES IN ACCORDANCE WITH BLADING A OF DWG 2107
C
REFERENCE A
REFERENCE B
SPLINES
NOTE 1) BOTH ROTORS ARE IDENTICAL EXCEPT FOR BLADING
2) BLADES HAVE THE SAME PROFILES FROM HUB TO TIP
3) BLADING PROFILE IS SAME FOR ROTOR 1 AND ROTOR 2 BUT THEIR ORIENTATION IS REVERSED
4) EACH ROTOR HAS 32 BLADES EQ. SPACED
5) A FILLET OF .03 RADIUS MUST OCCUR ALL AROUND THE PROFILE WHERE IT MEETS THE HUB WITH A SMOOTH TRANSITION TO THE PROFILE
6) BLADES MUST NOT HAVE TOOL MARKS
7) SPLINES AND DIA. 1.1811 / 1.1814 MUST BE CONCENTRIC WITHIN .001 TIR
8) PROFILE COORDINATES ARE GIVEN IN DWG 2107
9) THE SAME PROFILE IS USED WITH THE STATORS, PARTS 2109-1 AND 2109-2
SIDE A SCALE 2:1
SIDE B SCALE 2:1
2 1 TURBINE ROTOR
1 1 TURBINE ROTOR
NAVAL POSTGRADUATE SCHOOL
DEPT. OF AERONAUTICS, TURBO PROPULSION LABORATORY
TRANSONIC COMPRESSOR TEST RIG
TURBINE ROTORS
1 OF 2
FULL SIZE NOTED
2108-1

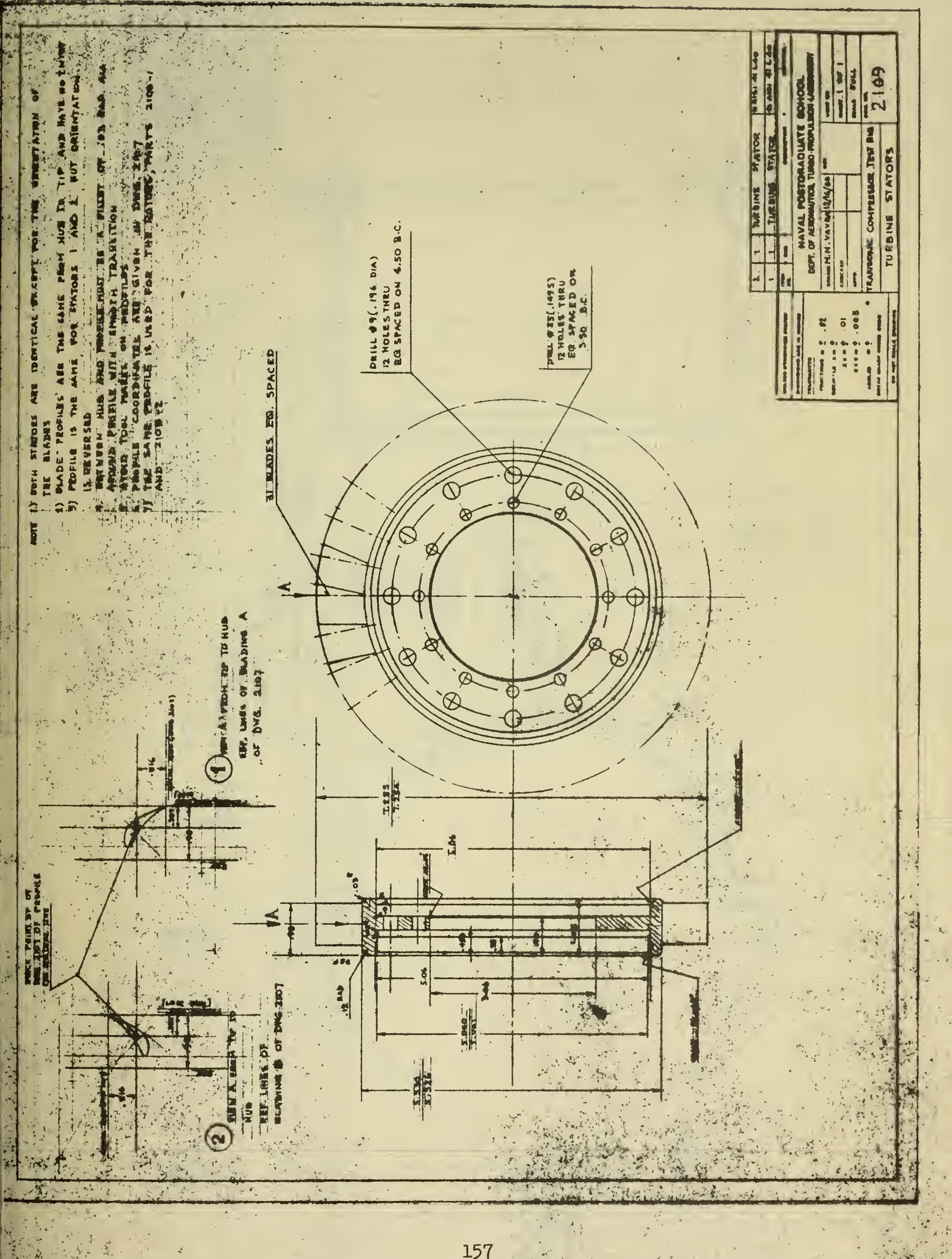
31 BLADES EQ. SPACED
DRILL #9 (.196 DIA)
12 HOLES THRU
EQ SPACED ON 4.50 B.C.
12 HOLES THRU
EQ. SPACED ON
3.50 B.C.
TURBINE STATOR
NAVAL POSTGRADUATE SCHOOL
TRANSONIC COMPRESSOR TEST RIG
TURBINE STATORS
2109

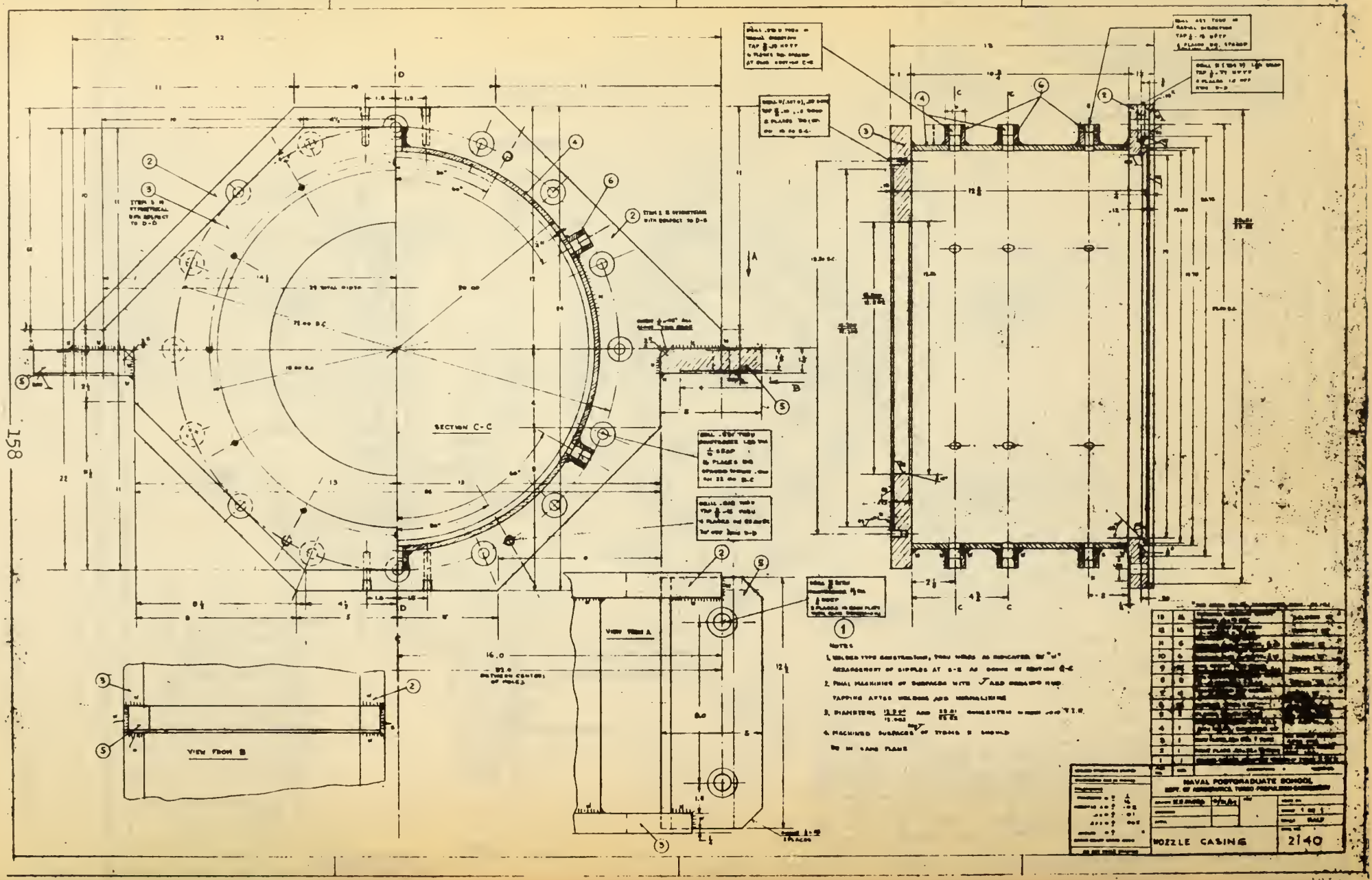
SECTION C-C
VIEW FROM B
VIEW FROM A
NOTES
NOZZLE CASING
2140

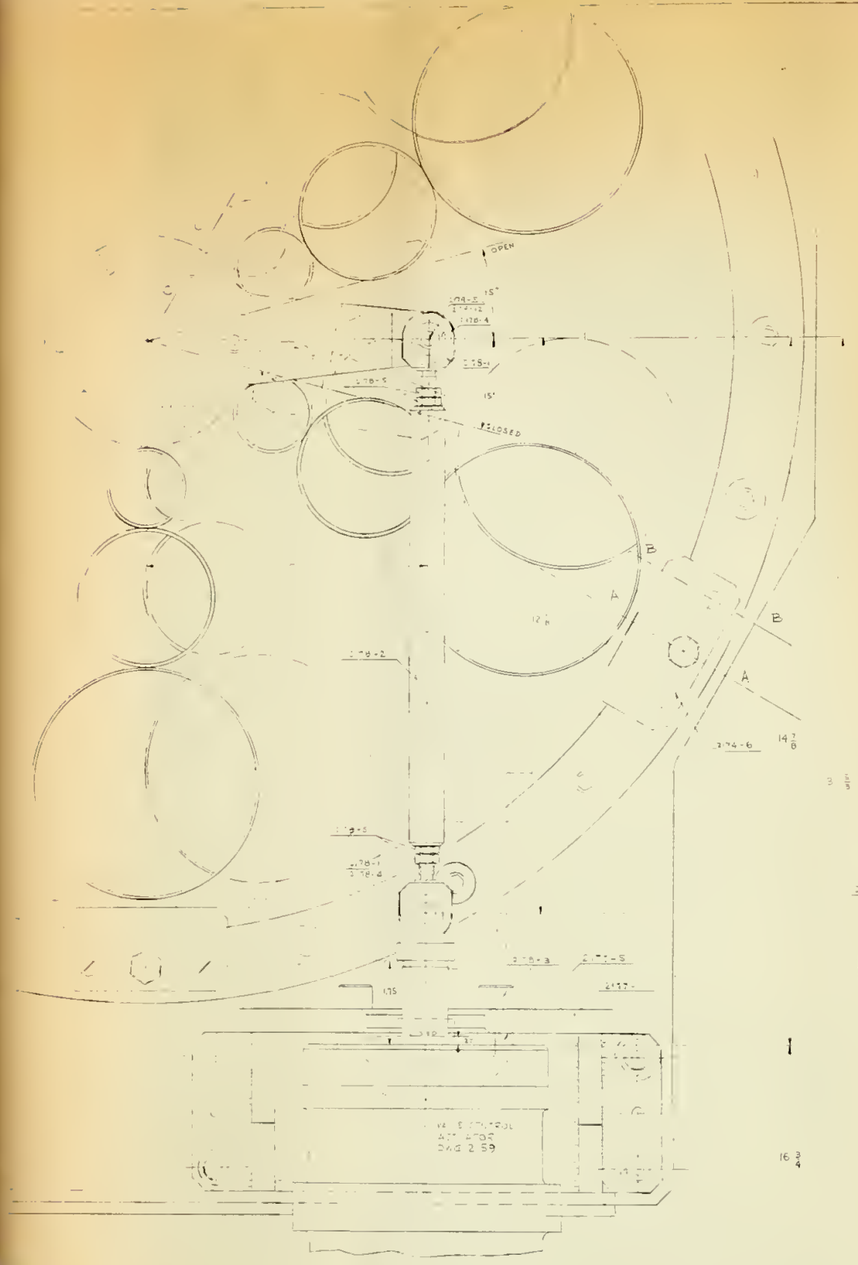

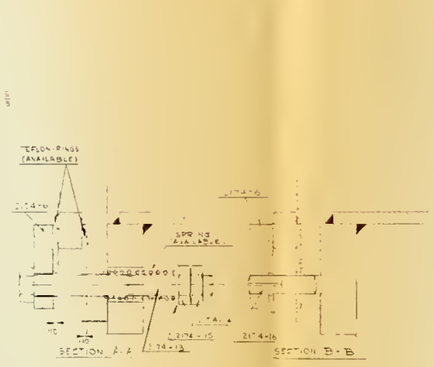

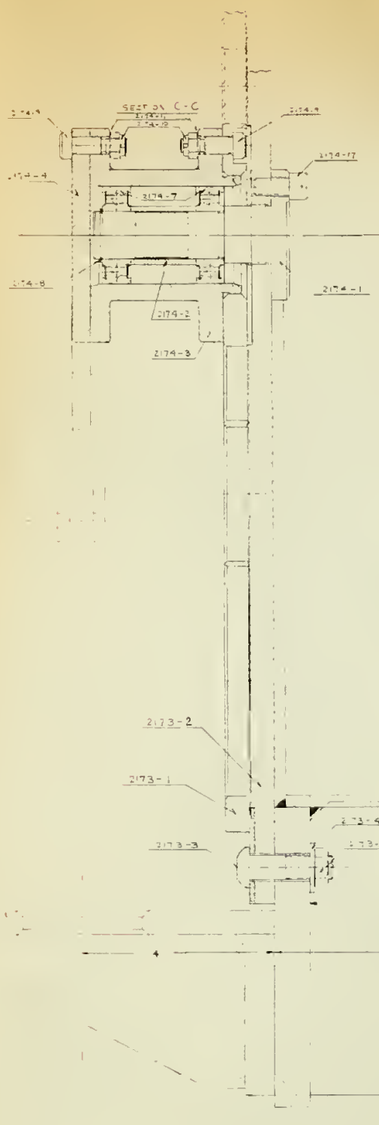

INLET THROTTLE VALVE ASSEMBLY 2.58

BODINE ELECTRIC MOTOR
TYPE KCI-23A2AI
115V, 75WATT, 67RPM

SECTION B-B

SECTION A-A

PACKING .03 THICK

2166-1
2166-2
2166-3
2166-4
2166-5

2167-1
2167-2
2167-3
2167-4
2167-5
2167-6
2167-7
2167-8
2167-9

2168-1
2168-2
2168-3
2168-4
2168-5
2168-6
2168-7
2168-8
2168-9
2168-10
2168-11
2168-12
2168-13
2168-14
2168-15
2168-16
2168-17
2168-18
2168-19
2168-20
2168-21
2168-22
2168-23
2168-24
2168-25
2168-26
2168-27
2168-28
2168-29
2168-30
2168-31
2168-32
2168-33
2168-34
2168-35
2168-36
2168-37
2168-38
2168-39
2168-40

UNLESS OTHERWISE STATED	ITEM NO.	# REQ.	DESCRIPTION / MATERIAL
DIMENSIONS ARE IN INCHES			
FRACTIONS ±			
DECIMALS .XX ±			
.X ±			
.XXX ±			
ANGLES ± °			
BREAK SHARP EDGES .005R			
DO NOT SCALE DRAWING			

NAVAL POSTGRADUATE SCHOOL
DEPT. OF AERONAUTICS, TURBO PROPULSION LABORATORY

DRAWN	M H VAVRA	5/14/70	REV
CHECKED			
APPD			

USED ON 2158
SHEET 1 OF 1
SCALE FULL

TRANSONIC COMPRESSOR TEST RIG
CONTROL VALVE ACTUATOR
DWG NO 2159

24 HOLES $\frac{3}{16}$ EQ SPACED ON $34\frac{1}{2}$ B.C., USE PART 16 AS TEMPLATE

24 HOLES $\frac{7}{16}$ EQ. SPACED ON $34\frac{1}{2}$ B.C., USE PART 17 AS TEMPLATE

.1345 (10 GA.)

INTERMITTENT 10° FILLET WELD 2"x 2" ALL PARTS 5

1 x 1 x 45° 4 PLACES

1 x 1 x 45° (2 PLACES)

SECTION C-C

SECTION D-D

SECTION B-B

DETAIL II (FULL SCALE)

DETAIL I (FULL SCALE)

MINIMUM CLEARANCE SO THAT ITEMS 3 CAN BE LOCATED EVERYWHERE ALONG ITEMS 5

DRILL $\frac{7}{16}$ THRU

DRILL $\frac{5}{16}$ THRU
TAP $\frac{3}{8}$ - 16 UNC
18 PLACES AT 2" CENTERS IN EACH ITEM 5

8 HOLES $\frac{7}{16}$ DIA EQ. SPACED ON $7\frac{1}{2}$ B.C.

DRILL $\frac{25}{64}$ DIA THRU
TAP $\frac{3}{8}$ - 18 NPTF

VIEW FROM A

DRILL $\frac{27}{64}$ THRU
TAP $\frac{1}{2}$ - 13 UNC THRU
4 PLACES IN EACH PART 8

8 HOLES $\frac{7}{16}$ DIA EQ SPACED ON $7\frac{1}{2}$ B.C.
USE PART 12 AS TEMPLATE

FOR NOTES AND PARTS LIST SEE SHEET 2

UNLESS OTHERWISE STATED
DIMENSIONS ARE IN INCHES
TOLERANCES
FRACTIONS = ± 1/16
DECIMALS .X = ± .04
.XX = ± .02
.XXX = ±
ANGLES = ±
BREAK SHARP EDGES .005

DO NOT SCALE DRAWING

ITEM NO	QTY	DESCRIPTION	MATERIAL

NAVAL POSTGRADUATE SCHOOL
DEPT. OF AERONAUTICS, TURBO-PROPULSION LABORATORY

DRAWN MHVAVRA	8/12/70	REV	USED ON 2160
CHECKED			SHEET 1 OF 2
APPD.			SCALE 1/2 [3"/FT]

INLET PLENUM — DWG NO 2164-1

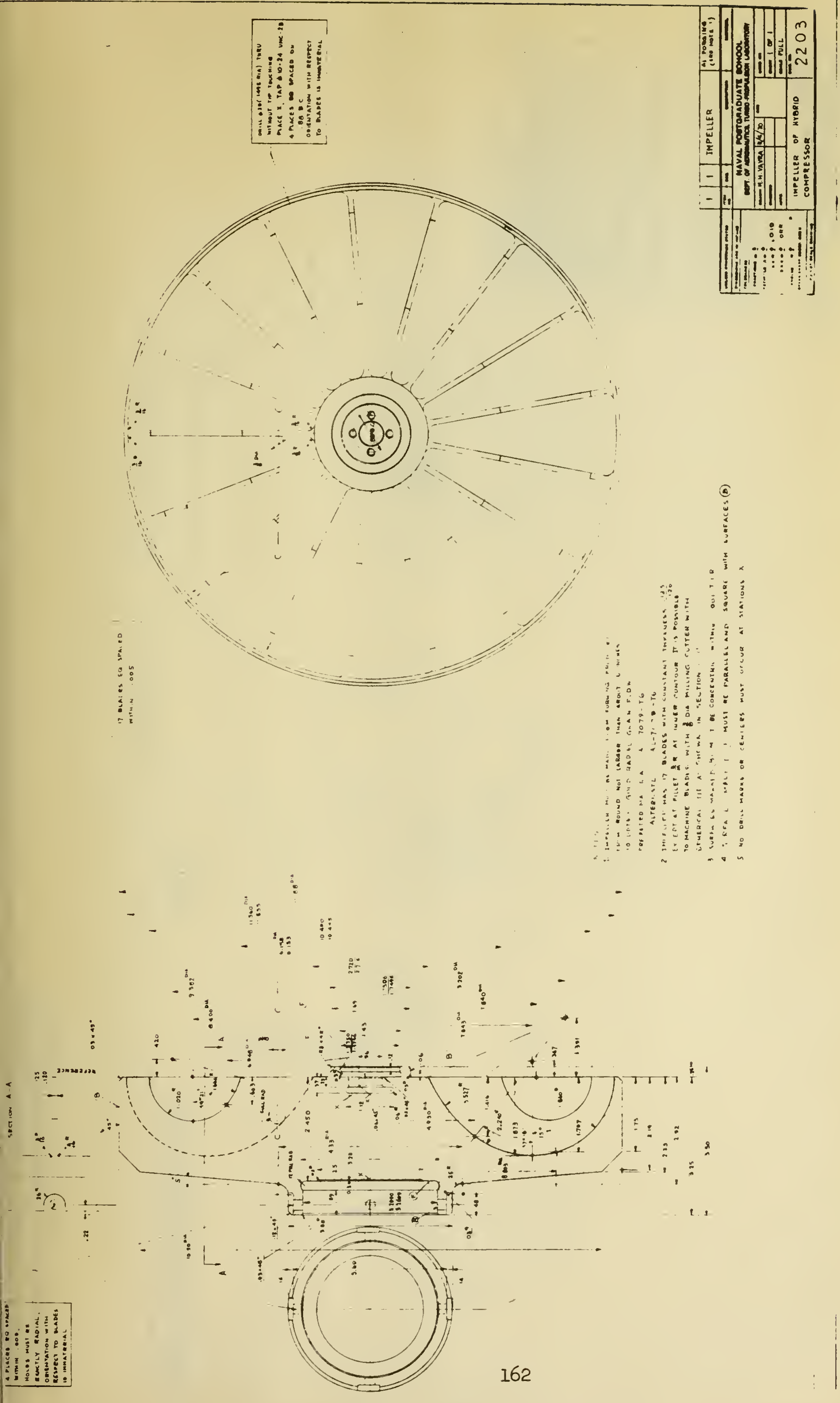
SECTION A-A
17 BLADES EQ SPACED
IMPELLER
NAVAL POSTGRADUATE SCHOOL
M.H. VAVRA
FULL
IMPELLER OF HYBRID COMPRESSOR
2203

COORDINATES X & Y OF BLADE PROFILES IN PLANES PERPENDICULAR TO RADIAL LINE THRU "A"

X	0	.200	.400	.600	.800	.900	1.000	1.100	1.200	1.300	1.400	1.500	1.550	1.600	1.650	1.700	1.750	1.800
Y	0	.004	.015	.035	.064	.082	.103	.128	.155	.187	.224	.265	.275	.320	.381	.386	.428	.480

COORDINATES R & Z OF SURFACE OF REVOLUTION THRU LEADING EDGES OF BLADES

R	2.088	2.800	2.600	2.400	2.200	2.000	1.800	1.600	1.500	1.400	1.300	1.200	1.144
Z	0	.015	.028	.047	.070	.102	.144	.200	.234	.275	.325	.384	.420

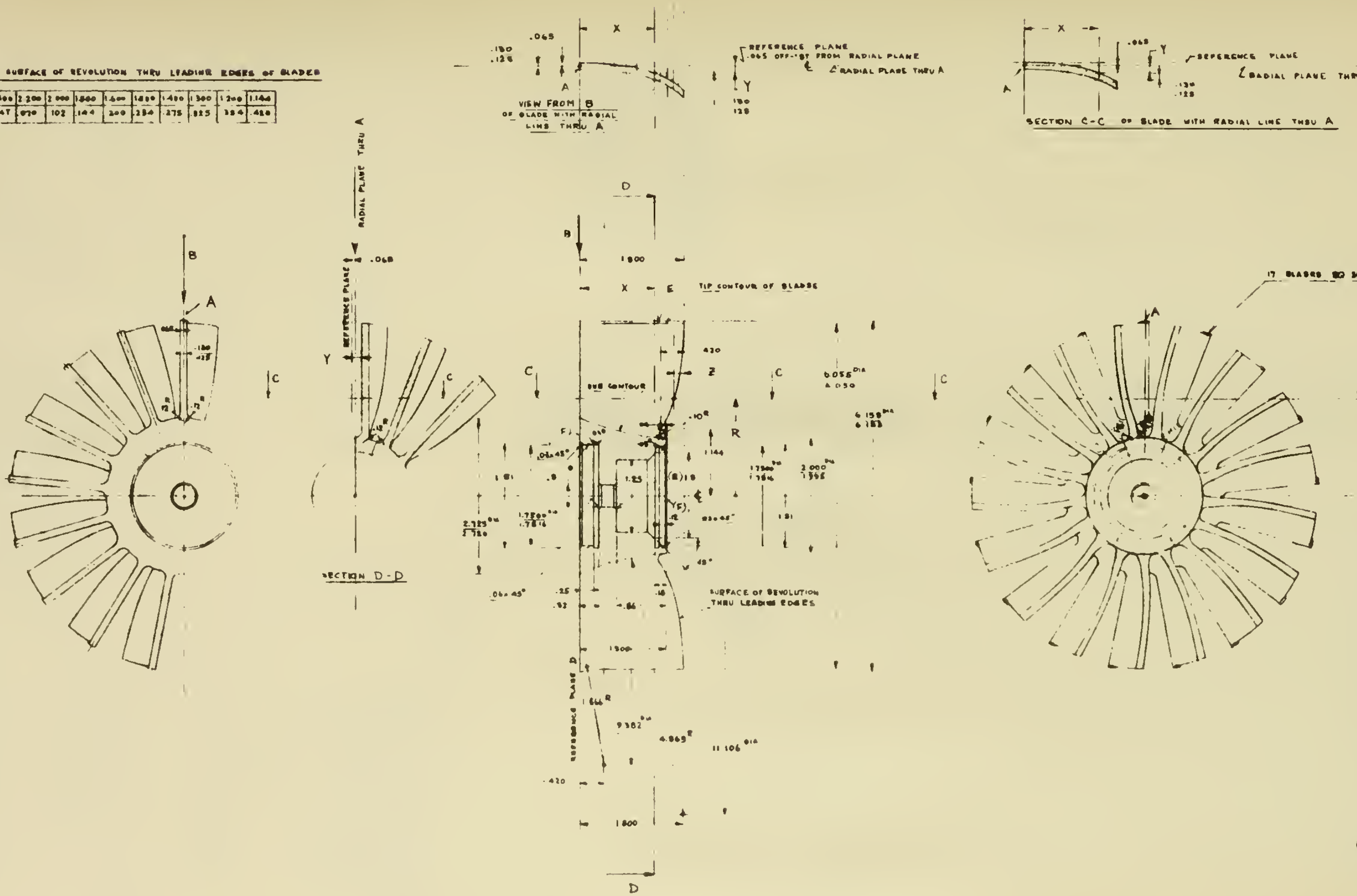

NOTES

1. FORGING MUST HAVE GOOD RADIAL GRAIN FLOW
   PREFERRED MATERIAL: AL-7079-T6
   ALTERNATE MATERIAL AL-7075-T6
2. THE BLADES ARE RADIAL IN REFERENCE PLANE D AS SHOWN IN VIEW AT LEFT. BLADES HAVE THE SAME PROFILE IN ALL PLANES PERPENDICULAR TO THE RADIAL LINE THRU THE POINTS A IN REFERENCE PLANE D. THE BLADE SURFACE CONSISTS OF STRAIGHT LINES THAT ARE PARALLEL WITH THE RADIAL LINE THRU POINT A (SEE SECTION D-D). THE GIVEN COORDINATES X, Y HOLD FOR THE CONVEX SIDE OF A BLADE. ITS CONCAVE SURFACE HAS THE COORDINATES X, (Y + .130/.125)
3. IF SPECIFIED HUB CONTOUR INCREASES MANUFACTURING COST CONSIDERABLY, IT CAN BE REPLACED BY A CONE BETWEEN THE DIAMETERS 2.725/2.720 AND 2.000/1.998.
4. BOTH SIDES OF THE BLADE SURFACE MUST HAVE A .12 RADIUS FILLET WITH THE HUB CONTOUR WITH A SMOOTH TRANSITION WITH THE BLADE SURFACE.
5. SURFACE OF REVOLUTION THRU LEADING EDGES WITH THE GIVEN COORDINATES R AND Z MUST ADJOIN HUB CONTOUR WITH .10 RADIUS FILLET AS SHOWN IN CROSS SECTION
6. SURFACES MARKED (E) MUST BE CONCENTRIC WITHIN .001 T.I.R.
7. SURFACES MARKED (F) MUST BE PARALLEL AND SQUARE WITH SURFACES (E)

1	1	INDUCER	AL. FORGING (SEE NOTE 1)

NAVAL POSTGRADUATE SCHOOL
DEPT. OF AERONAUTICS, TURBO PROPULSION LABORATORY

INDUCER OF HYBRID COMPRESSOR

2204

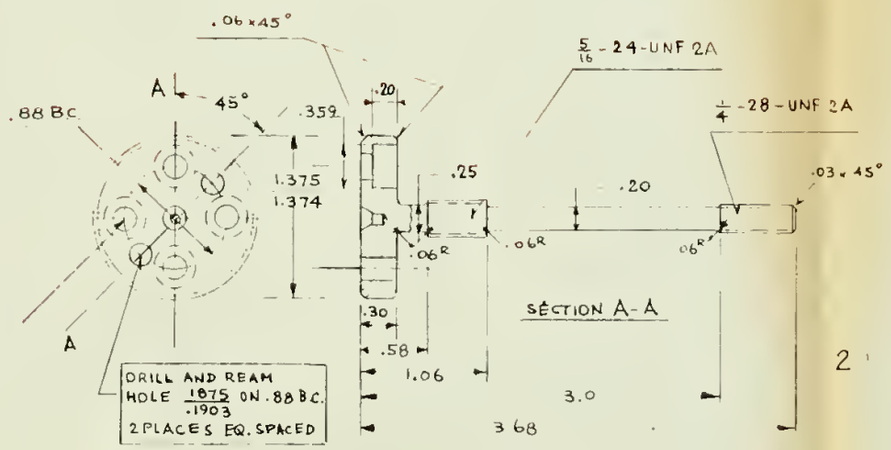

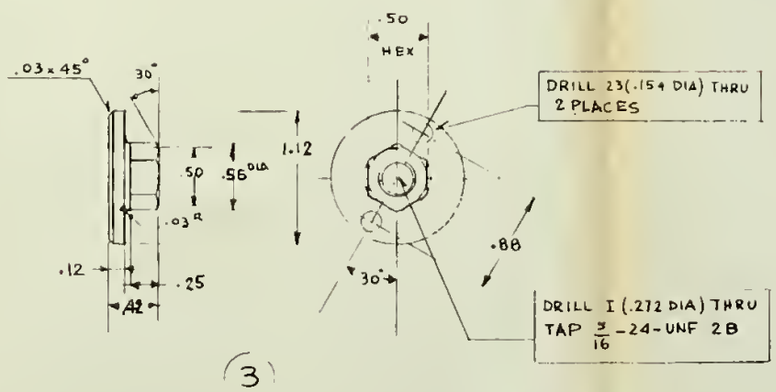

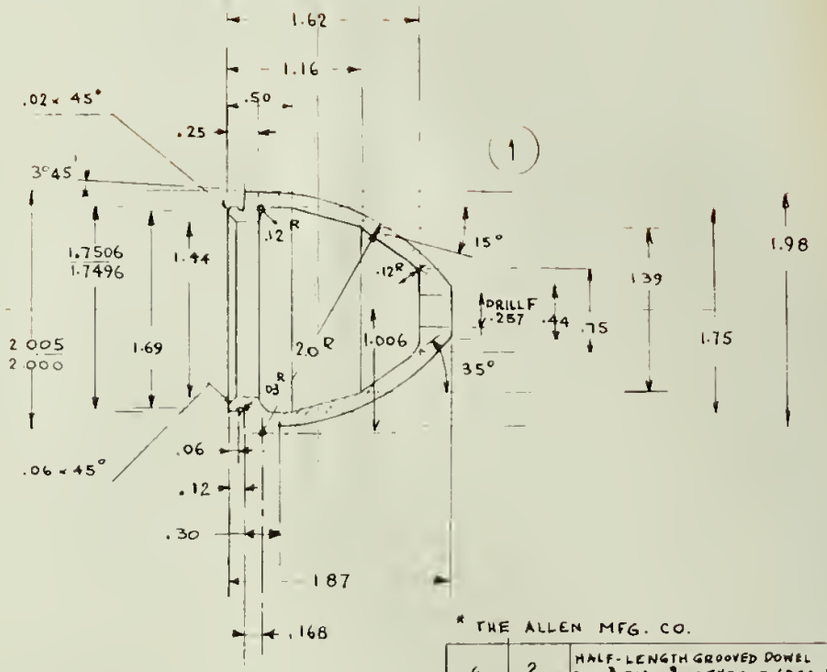

* THE ALLEN MFG. CO.

6	2	HALF-LENGTH GROOVED DOWEL PIN 3/16 DIA × 3/4 LG, TYPE B (ASA B. S. 20-1958)	STEEL
5	2	CROSS-DRILLED SOCK. HEAD CAP SCREWS # 6-32 × 3/8 LG.	ALLENOT ST. *
4	4	SOCK. HEAD CAP SCREWS # 10-24 × 3/8 LG.	ALLENOT ST. *
3	1	NUT	ST. AISI 4140
2	1	SUPPORT	ST. AISI 4140
1	1	HUB SPINNER	MAKE FROM AL. ROD 2024 - T4
NO.	REQ		MATERIAL

NAVAL POSTGRADUATE SCHOOL
DEPT. OF AERONAUTICS, [illegible] LABORATORY

DRAWN M.H. VAVRA | 11/5/70 | REV

DESCRIPTION

SHEET 1 OF 1

SCALE FULL

DWG NO. 2205

WHEEL ATTACHMENTS
HYBRID COMPRESSOR

TOLERANCES
FRACTIONS = ±
DECIMALS X.X = ± .02
X.XX = ± .01
X.XXX = ± .005
ANGLES = ± °
BREAK SHARP EDGES .005R
DO NOT SCALE DRAWING

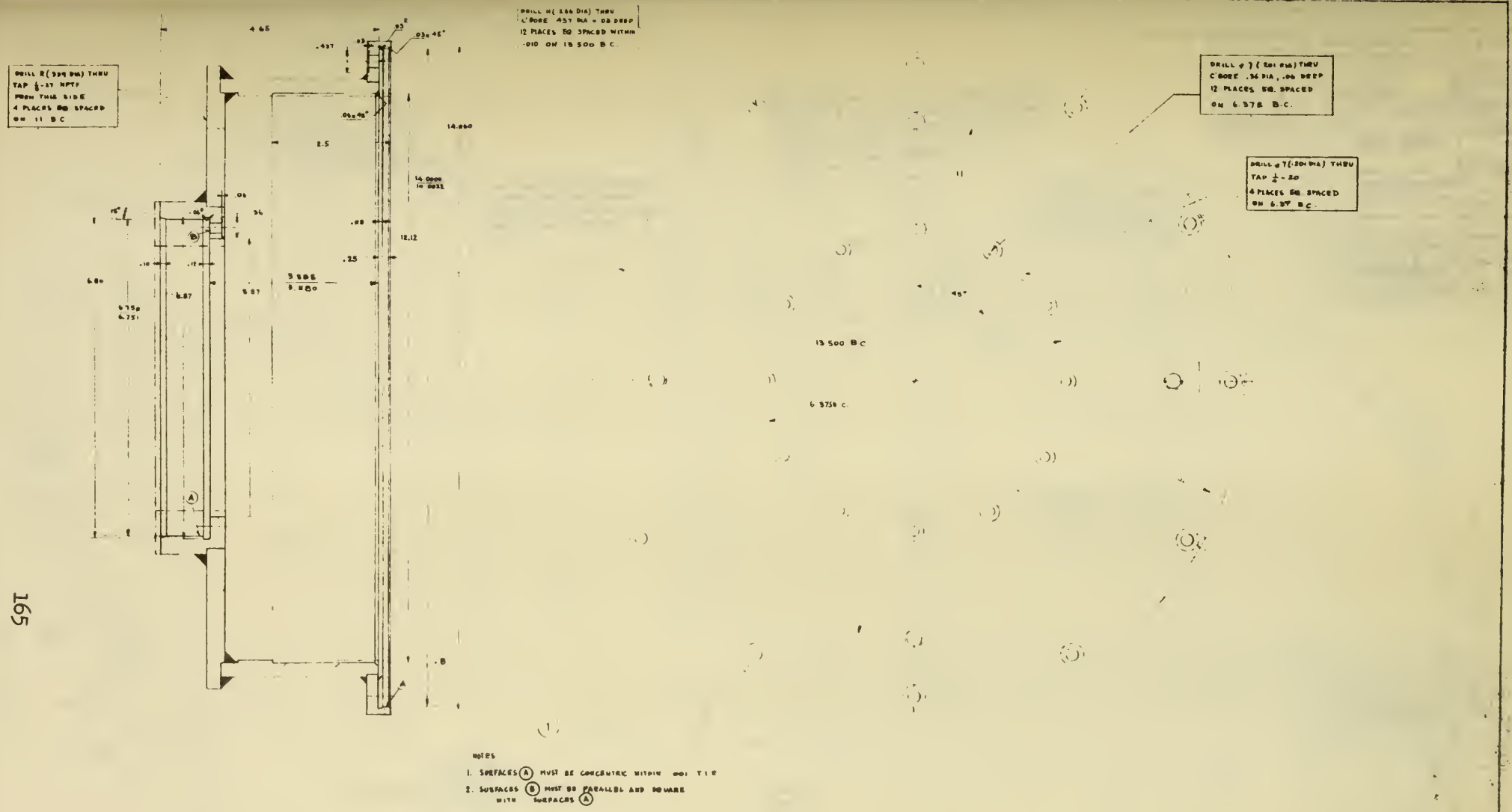
DRILL R (.339 DIA) THRU
TAP ⅜-27 NPTF
FROM THIS SIDE
4 PLACES EQ SPACED
ON 11 B.C.
DRILL H (.266 DIA) THRU
C'BORE .457 DIA x .03 DEEP
12 PLACES EQ SPACED WITHIN
.010 ON 13.500 B.C.
DRILL ø 7 (.201 DIA) THRU
C'BORE .36 DIA, .06 DEEP
12 PLACES EQ. SPACED
ON 6.378 B.C.
DRILL ø T (.201 DIA) THRU
TAP ¼-20
4 PLACES EQ. SPACED
ON 6.37 B.C.
13.500 B.C
6.3758 B.C.
NOTES
1. SURFACES (A) MUST BE CONCENTRIC WITHIN .001 T.I.R
2. SURFACES (B) MUST BE PARALLEL AND SQUARE WITH SURFACES (A)
NAVAL POSTGRADUATE SCHOOL
DEPT OF AERONAUTICS, TURBO PROPULSION LABORATORY
STATOR CASING
HYBRID COMPRESSOR
2207

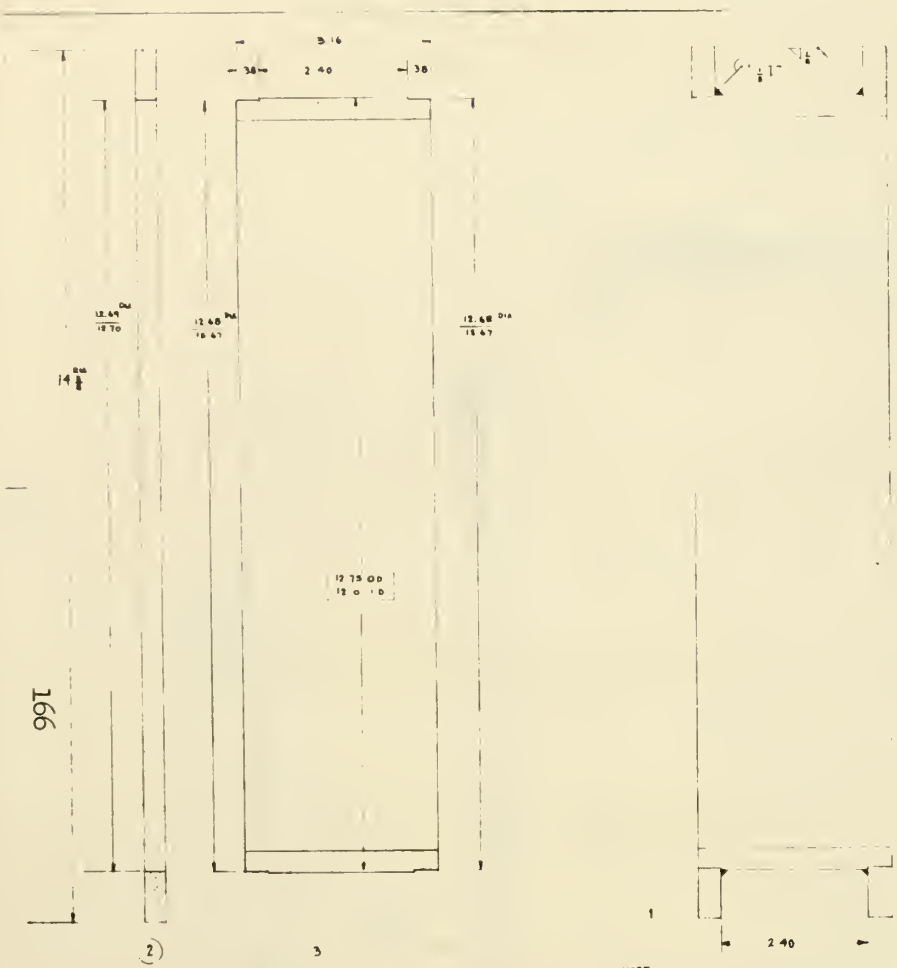

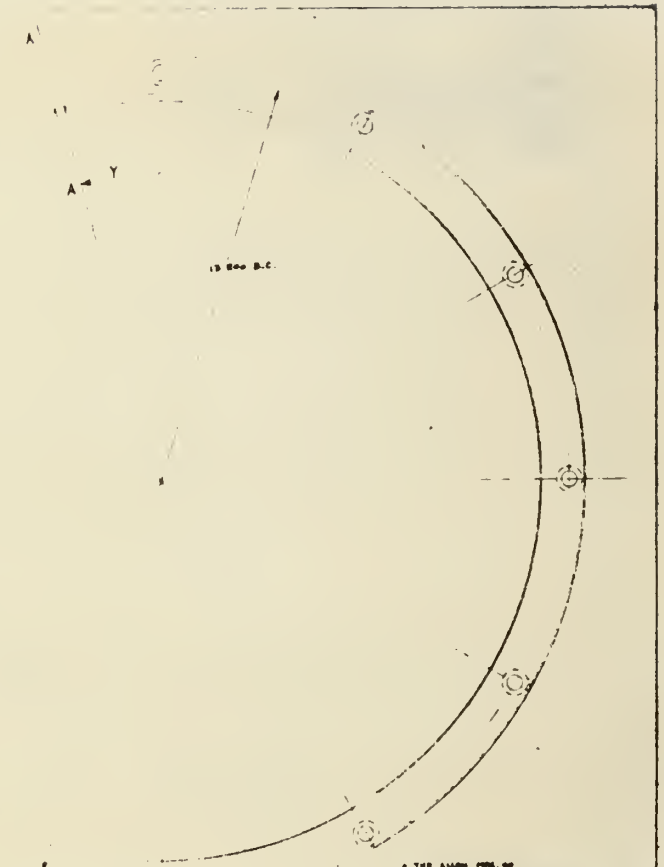

DRILL H (.266 DIA) THRU
C'BORE .42 DIA, .08 DEEP
72 PLACES EQ SPACED WITHIN
.01 OF 13.800 B.C. ON EACH
FLANGE

NOTES

1. SURFACES B MUST BE CONCENTRIC WITHIN .001 T.I.R
2. SURFACES C MUST BE PARALLEL AND SQUARE WITH SURFACES B
3. SCHEDULE FOR TAPS @ 10-32 IN SECTIONS A

ANGLE Y	18°	46°	76°	96°	136°	166°	186°
DISTANCE X1	.88	.45	.50	.46	.58	.86	.95
DISTANCE X2	1.05	1.17	1.27	1.80	1.69	1.78	1.90

7	14		ST.
6	24		ALLOY ST.
5	24		ALLOY ST.
4	1	DIFFUSER SLEEVE	MADE FROM ITEM 1
3	1		ST
2	2		
1	1		

NAVAL POSTGRADUATE SCHOOL
DEPT OF AERONAUTICS TURBO PROPULSION LABORATORY

DIFFUSER SLEEVE
HYBRID COMPRESSOR

2208

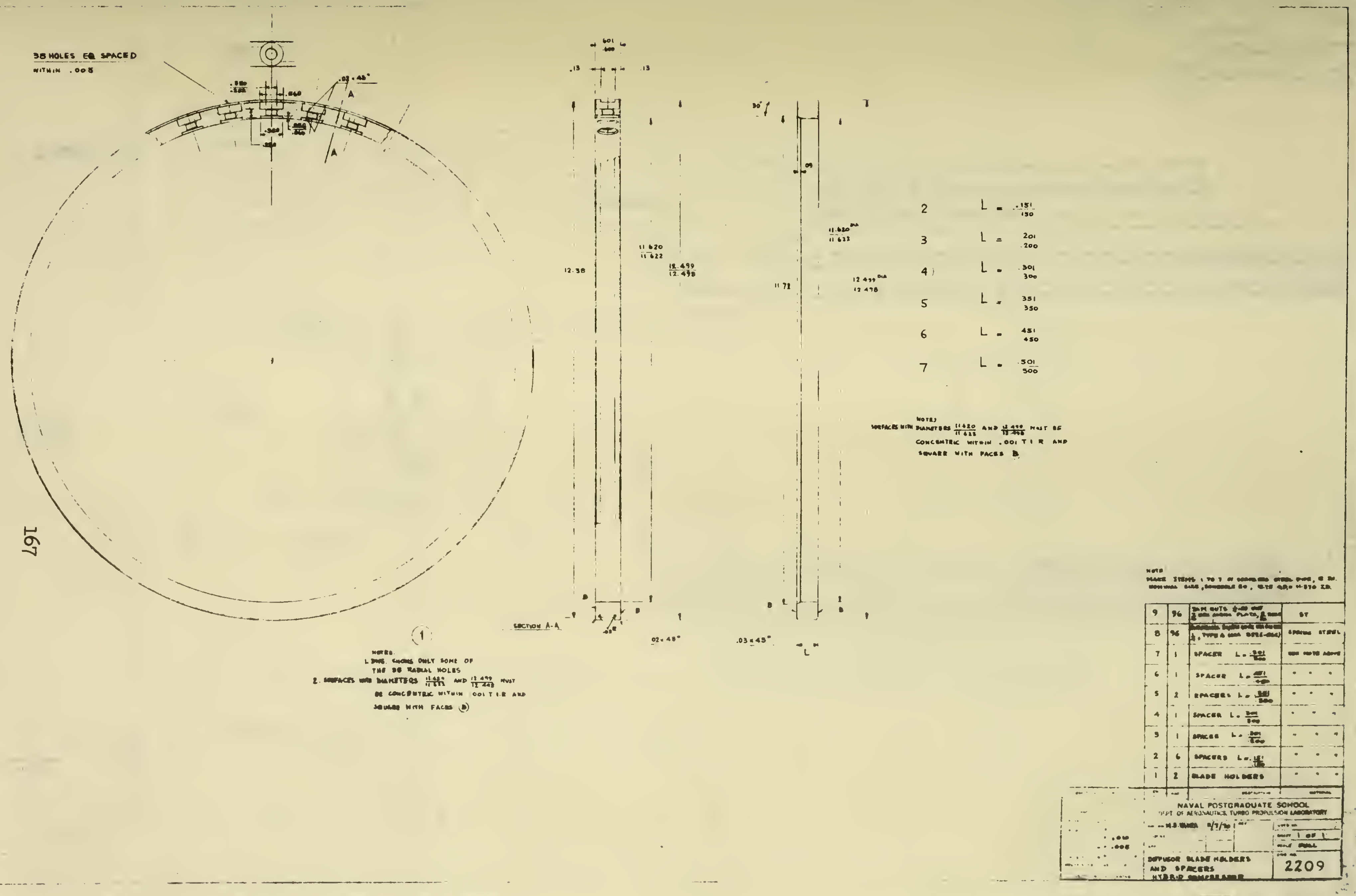

38 HOLES EQ SPACED
WITHIN .008
.02 x 45°
A
A
.13
.13
12.38
11.620
11.622
12.499
12.498
SECTION A-A
02 x 45°
.03 x 45°
30°
11.72
11.620 DIA
11.622
12.499 DIA
12.498
L
2 L = .151/.150
3 L = .201/.200
4 L = .301/.300
5 L = .351/.350
6 L = .451/.450
7 L = .501/.500
NOTES
SURFACES WITH DIAMETERS 11.620/11.622 AND 12.499/12.498 MUST BE CONCENTRIC WITHIN .001 T I R AND SQUARE WITH FACES B
1
NOTES
1. DWG. SHOWS ONLY SOME OF THE 38 RADIAL HOLES
2. SURFACES WITH DIAMETERS 11.620/11.622 AND 12.499/12.498 MUST BE CONCENTRIC WITHIN .001 T I R AND SQUARE WITH FACES (B)
9 96 ST
8 96 SPRING STEEL
7 1 SPACER SEE NOTE ABOVE
6 1 SPACER
5 2 SPACERS
4 1 SPACER
3 1 SPACER
2 6 SPACERS
1 2 BLADE HOLDERS
NAVAL POSTGRADUATE SCHOOL
DEPT OF AERONAUTICS TURBO PROPULSION LABORATORY
1 OF 1
FULL
DIFFUSOR BLADE HOLDERS
AND SPACERS
HYBRID COMPRESSOR
2209

PROFILE COORDINATES:

CONVEX SIDE	X1	0	005	010	017	034	070	106	143	212	288	361	434	507	581	646	727	801	874	947	1.020	1.093	1.166	1.238	1.311	1.347	1.383	1.400
	Y1	0	009	011	016	033	030	042	051	063	073	080	085	088	090	090	089	086	082	077	070	063	055	.046	031	.025	016	0
CONCAVE SIDE	X2	0	005	012	020	038	075	112	149	223	294	367	439	511	583	655	727	800	873	946	1.017	1.089	1.163	1.235	1.306	1.344	1.381	1.400
	Y2	0	-007	-008	-010	-012	-015	-016	-016	-015	-012	-008	-005	-001	001	004	006	008	009	010	010	009	008	006	.003	001	0	0

NOTES:

1. COORDINATE Y2 SHOWN IN FIGURE IS NEGATIVE. POSITIVE VALUES OF Y2 EXTEND UP FROM REFERENCE LINE
2. DISTANCES .03" AND .725" OF REFERENCE LINE TO CENTER OF FOOT .81/.80 DIA ARE NOT CRITICAL BUT SHOULD BE THE SAME FOR ALL BLADES
3. FILLETS .12 R ON BOTH SIDES OF BLADES WITH FOOT MUST EXTEND ALL ALONG SIDES AND HAVE TO BE CUT WITH CUTTER .25 DIA TO MEET DIA .81/.80 AND PROFILE PARTS THAT EXTEND OVER FOOT
4. VIEW FROM "A" IS A VIEW OF THE BLADE FROM ITS TIP TO THE BASE WITH .51/.50 DIA

1	42	DIFFUSOR BLADES TYPE A1	MADE FROM AL BAR 2024-T4

NAVAL POSTGRADUATE SCHOOL
DEPT OF AERONAUTICS, TURBO PROPULSION LABORATORY

M.G. PAVEA 10/5/70

±.005
±.002

SHEET 1 OF 4
SCALE 10:1

DIFFUSOR BLADES TYPE A1 | 2210-1

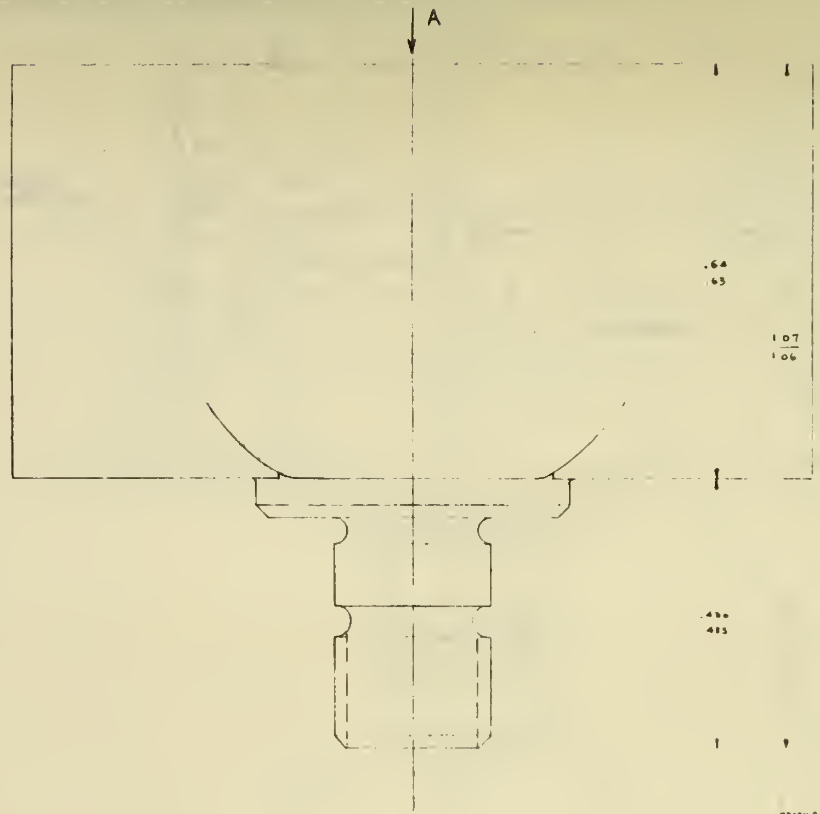

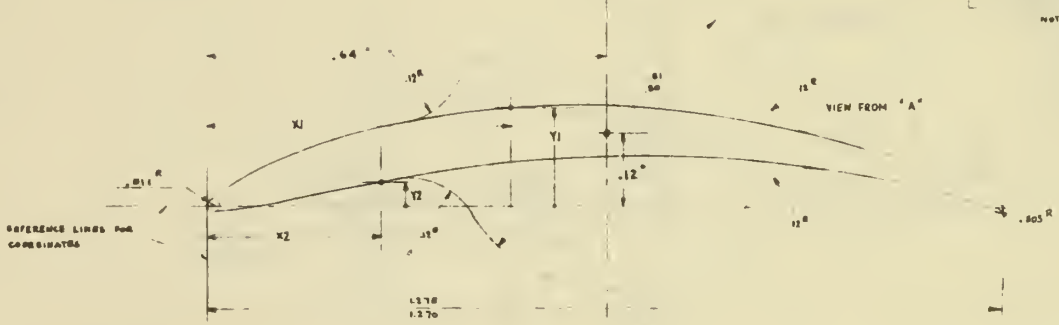

PROFILE COORDINATES:

CONVEX SIDE	X1	0	.053	.006	.011	.026	.056	.086	.117	.181	.245	.310	.376	.401	.507	.570	.637	.703	.768	.832	.890	.961	1.025	1.089	1.152	1.185	1.214	1.278
	Y1	0	.015	.013	.018	.028	.047	.065	.077	.152	.151	.157	.148	.107	.162	.165	.164	.161	.155	.146	.134	.119	.105	.082	.059	.047	.033	0
CONCAVE SIDE	X2	0	.009	.015	.020	.038	.072	.105	.137	.201	.264	.327	.385	.461	.515	.576	.637	.700	.765	.835	.896	.961	1.015	1.077	1.142	1.176	1.208	1.276
	Y2	0	-.008	-.010	-.006	-.003	.032	.006	.014	.027	.019	.050	.060	.069	.075	.080	.083	.084	.085	.080	.075	.065	.055	.046	.035	.024	.015	0

NOTES

1. COORDINATE Y2 AS SHOWN IN FIGURE IS POSITIVE, FOR NEGATIVE VALUES OF Y1 THE POINTS ARE BELOW THE REFERENCE LINE
2. DISTANCES .12" AND .64" ARE NOT CRITICAL BUT SHOULD BE EQUAL FOR ALL BLADES
3. FOR ALL MISSING DIMENSIONS SEE DWG 2210-1
4. FOR FILLETS BETWEEN BASE AND PROFILE (1 & 6) SEE NOTE 3 OF DWG 2210-1
5. VIEW FROM "A" IS A VIEW FROM BLADE TIP TO THE BASE WITH 51/50 DIA

2	42	DIFFUSOR BLADES TYPE A2	2024-T4

NAVAL POSTGRADUATE SCHOOL
DEPT OF AERONAUTICS TURBO PROPULSION LABORATORY

.005
.002

SHEET 3 OF 4
SCALE 10:1

DIFFUSOR BLADES TYPE A2 | 2210-2

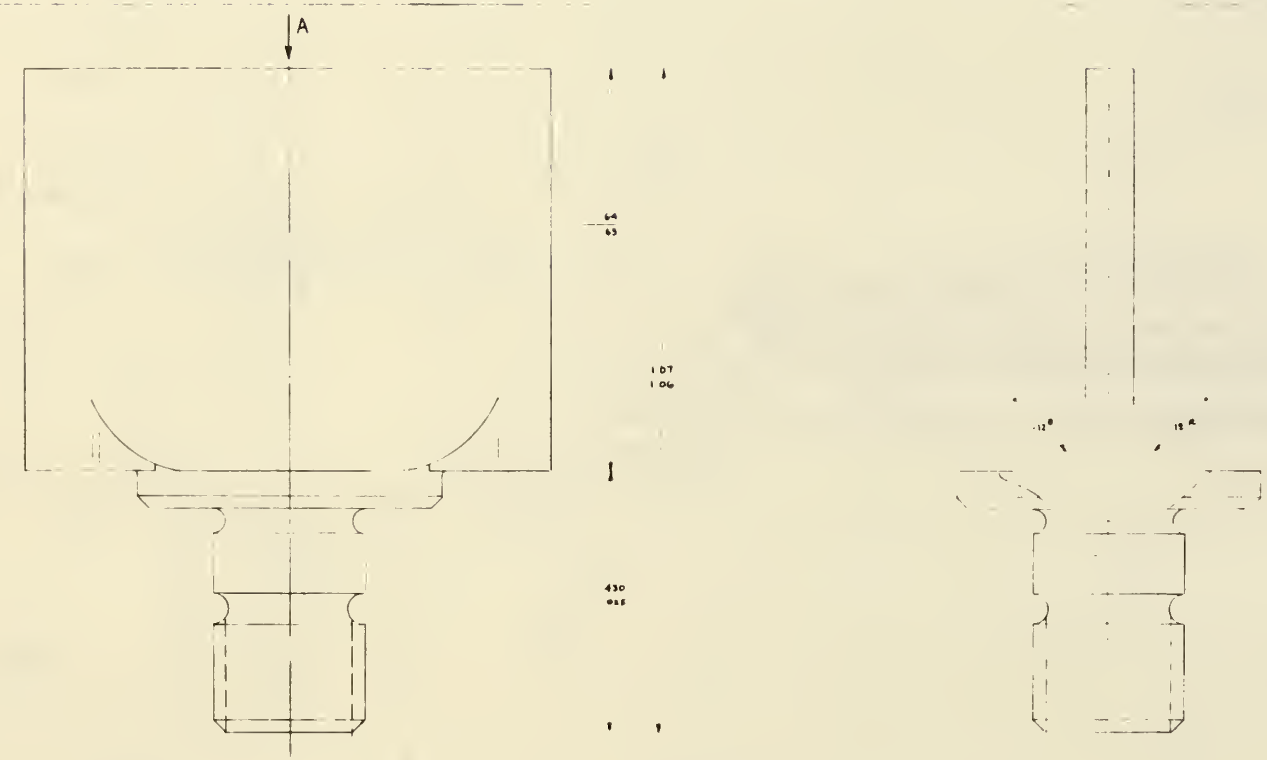

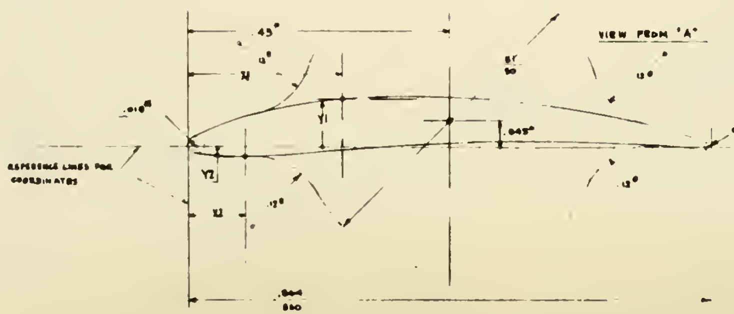

PROFILE COORDINATES

CONVEX SIDE	X1	0	.000	004	008	016	029	060	081	124	168	212	256	300	344	388	432	476	.520	568	607	650	694	.737	.780	.801	840	866
	Y1	0	009	010	014	020	031	039	047	057	068	075	080	.083	084	084	083	.081	077	.072	066	058	050	040	.029	024	-017	0
CONCAVE SIDE	X2	0	004	008	013	020	047	069	.092	135	.178	220	255	.300	347	390	.433	.476	517	.560	603	.646	686	.726	.770	.797	817	.844
	Y2	0	-007	-008	-009	-011	-010	-014	-015	-013	-011	-008	-006	-.003	+.001	004	.006	007	009	009	.010	010	007	005	.003	001	0	0

NOTES

1. COORDINATE Y2 AS SHOWN IN FIGURE IS NEGATIVE
2. DISTANCES .045" AND .43" ARE NOT CRITICAL BUT SHOULD BE EQUAL FOR ALL BLADES
3. FOR MISSING DIMENSIONS SEE DWG 2210-1
4. FOR .012" FILLETS BETWEEN BASE AND PROFILE SEE NOTE 5 OF DWG 2210-1
5. VIEW FROM "A" IS A VIEW FROM THE BLADE TIP TO THE BASE WITH 81/80 DIA

3 | 42 | DIFFUSOR BLADES TYPE B1

NAVAL POSTGRADUATE SCHOOL
DEPT OF AERONAUTICS, TURBO PROPULSION LABORATORY

.008
.002

SHEET 3 OF 4
SCALE 10:1

DIFFUSOR BLADES TYPE B1 | 2210-3

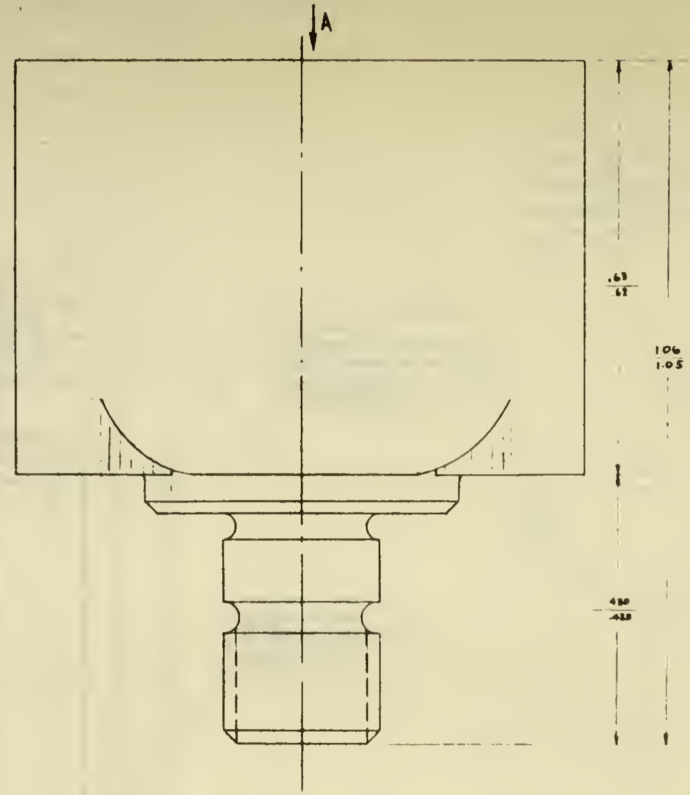

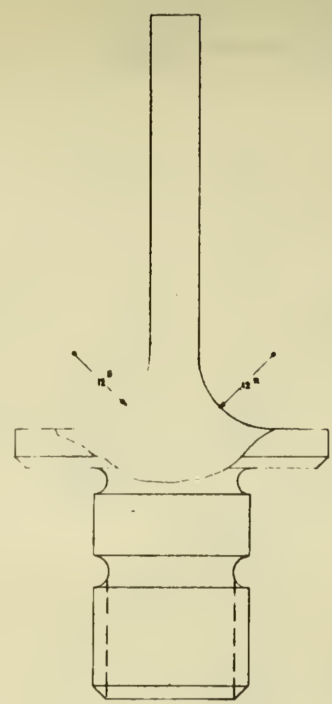

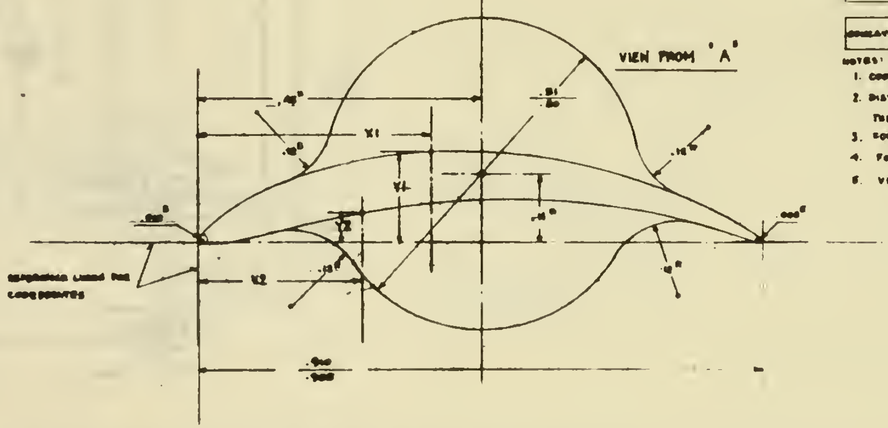

PROFILE COORDINATES

CONVEX SIDE	X1	0	.001	.005	[illegible]	.016	.036	.057	.079	.134	.171	.216	.260	[illegible]	.360	[illegible]	[illegible]	[illegible]	[illegible]	.576	[illegible]	[illegible]	[illegible]	.770	[illegible]	.844	[illegible]	.910
	Y1	0	[illegible]	.012	.016	.026	.042	.057	.070	[illegible]	.110	[illegible]	.124	.141	.146	.148	[illegible]	[illegible]	.137	.131	.120	.107	[illegible]	.075	.063	.042	[illegible]	0
CONCAVE SIDE	X2	0	[illegible]	.011	.016	.030	.055	.079	[illegible]	.148	.175	.237	.281	[illegible]	[illegible]	.411	[illegible]	[illegible]	[illegible]	.587	[illegible]	.676	[illegible]	.768	.814	.857	.861	[illegible]
	Y2	0	[illegible]	-.005	-.005	-.004	-.001	.006	.011	.022	.033	.043	.051	.060	.064	.066	.070	.071	.071	[illegible]	.064	.058	.050	.040	[illegible]	.021	.015	0

NOTES:

1. COORDINATE Y2 IN FIGURE IS A POSITIVE VALUE
2. DISTANCES .11" AND .45" ARE NOT CRITICAL BUT SHOULD BE THE SAME FOR ALL BLADES
3. FOR MISSING DIMENSIONS SEE DWG. 2210-1
4. FOR FILLETS WITH .12R BETWEEN PROFILE AND BASE SEE NOTE 8 OF DWG. 2210-1
5. VIEW FROM "A" IS A VIEW FROM THE BLADE TIP TO ITS BASE WITH .01/.00 DIA

4	42	DIFFUSER BLADES TYPE B2	2024-T4

NAVAL POSTGRADUATE SCHOOL
DEPT. OF AERONAUTICS, TURBO-PROPULSION LABORATORY

SHEET 4 OF 4

DIFFUSER BLADES TYPE B2

2210-4

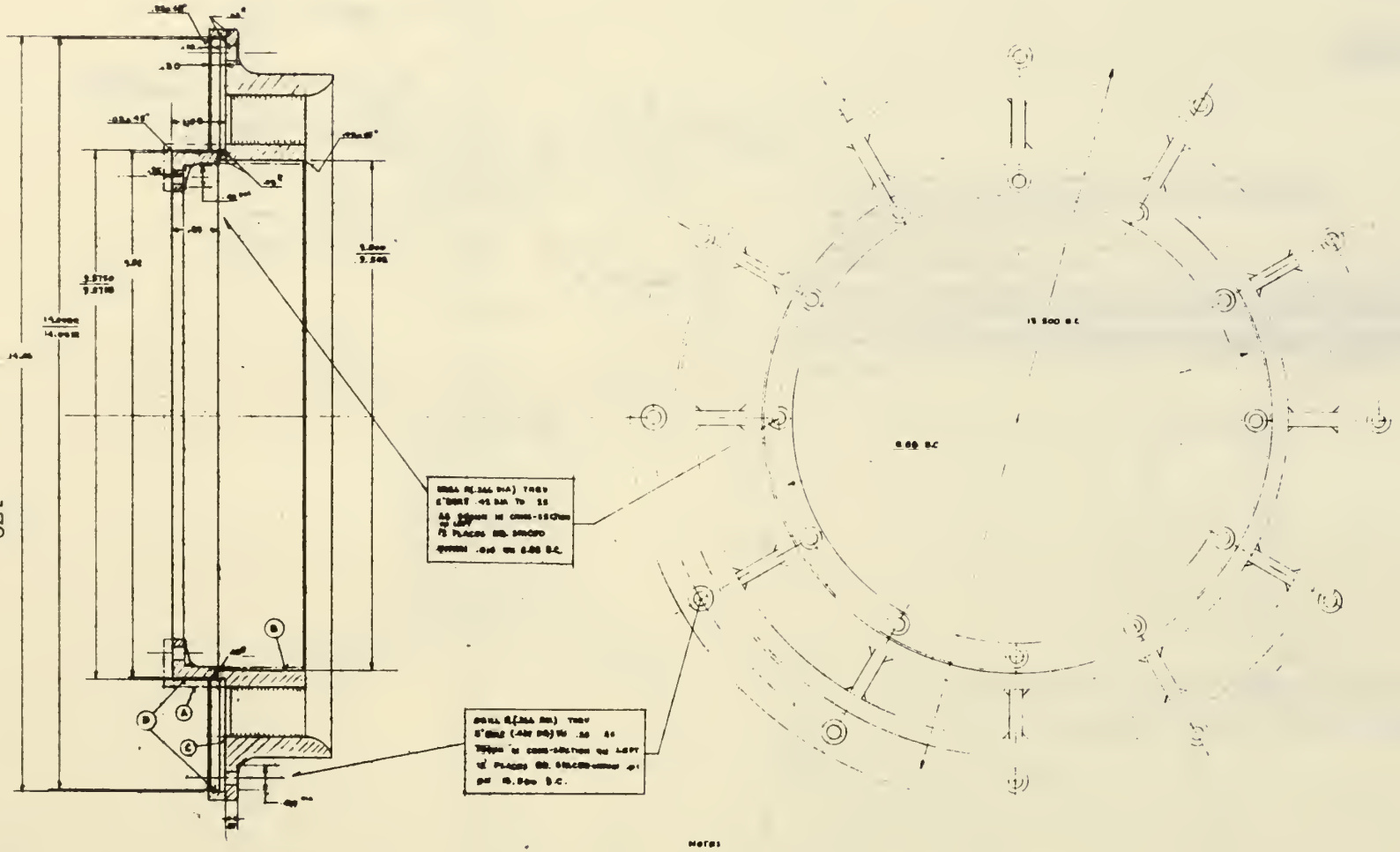

NOTES

1. MACHINED FROM PART 2211-1 AFTER NORMALIZING
2. USE SURFACE (A) OF PART 2211-1 FOR CENTERING ON LATHE
3. SURFACES (B) MUST BE CONCENTRIC WITHIN .001 T.I.R.
4. SURFACE (C) MUST BE SQUARE WITH SURFACES (B)

1	1	SPIDER SUPPORT	
		NAVAL POSTGRADUATE SCHOOL	
		SPIDER SUPPORT	2211

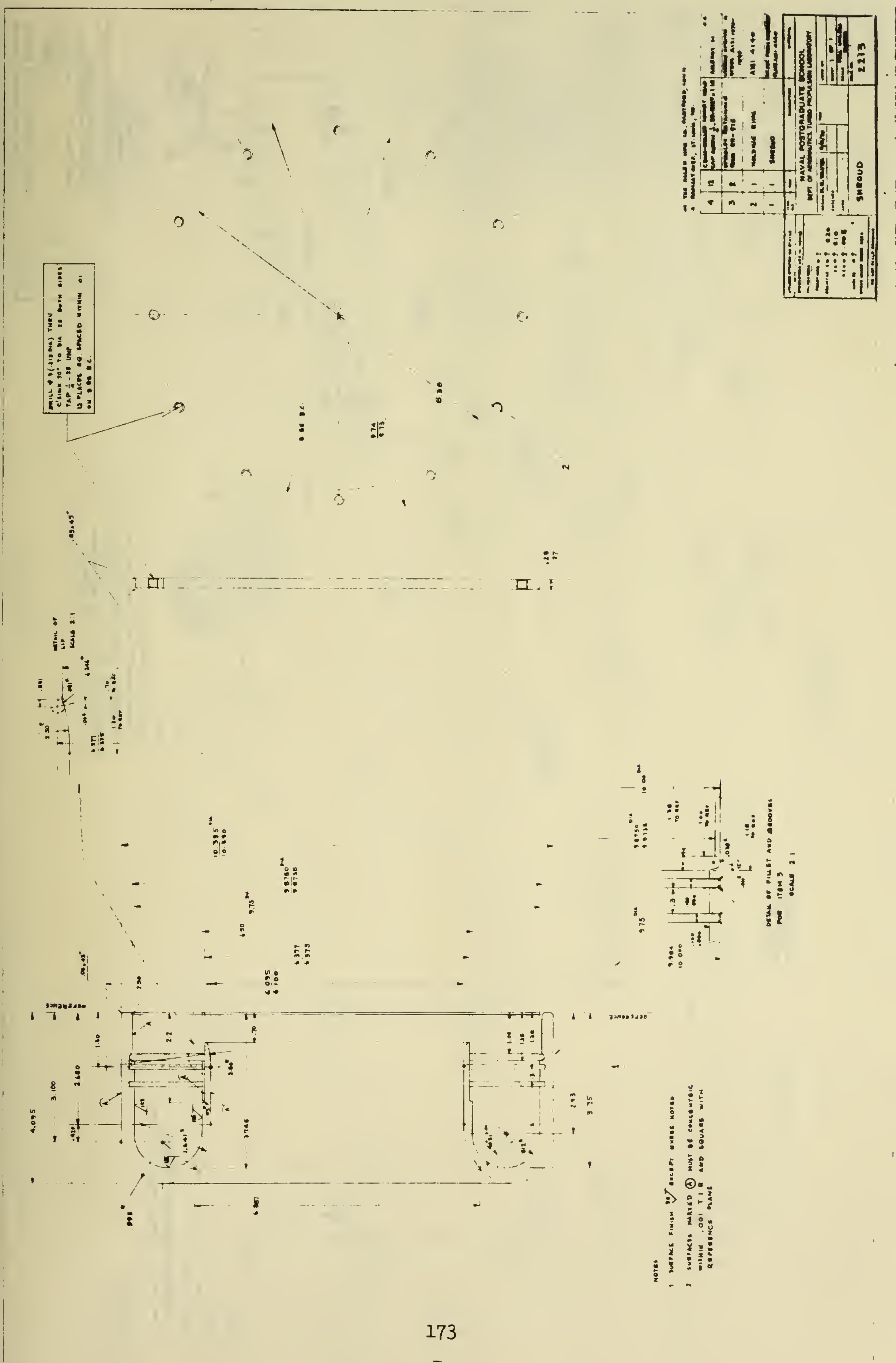
NAVAL POSTGRADUATE SCHOOL
SHROUD
2213
AISI 4140

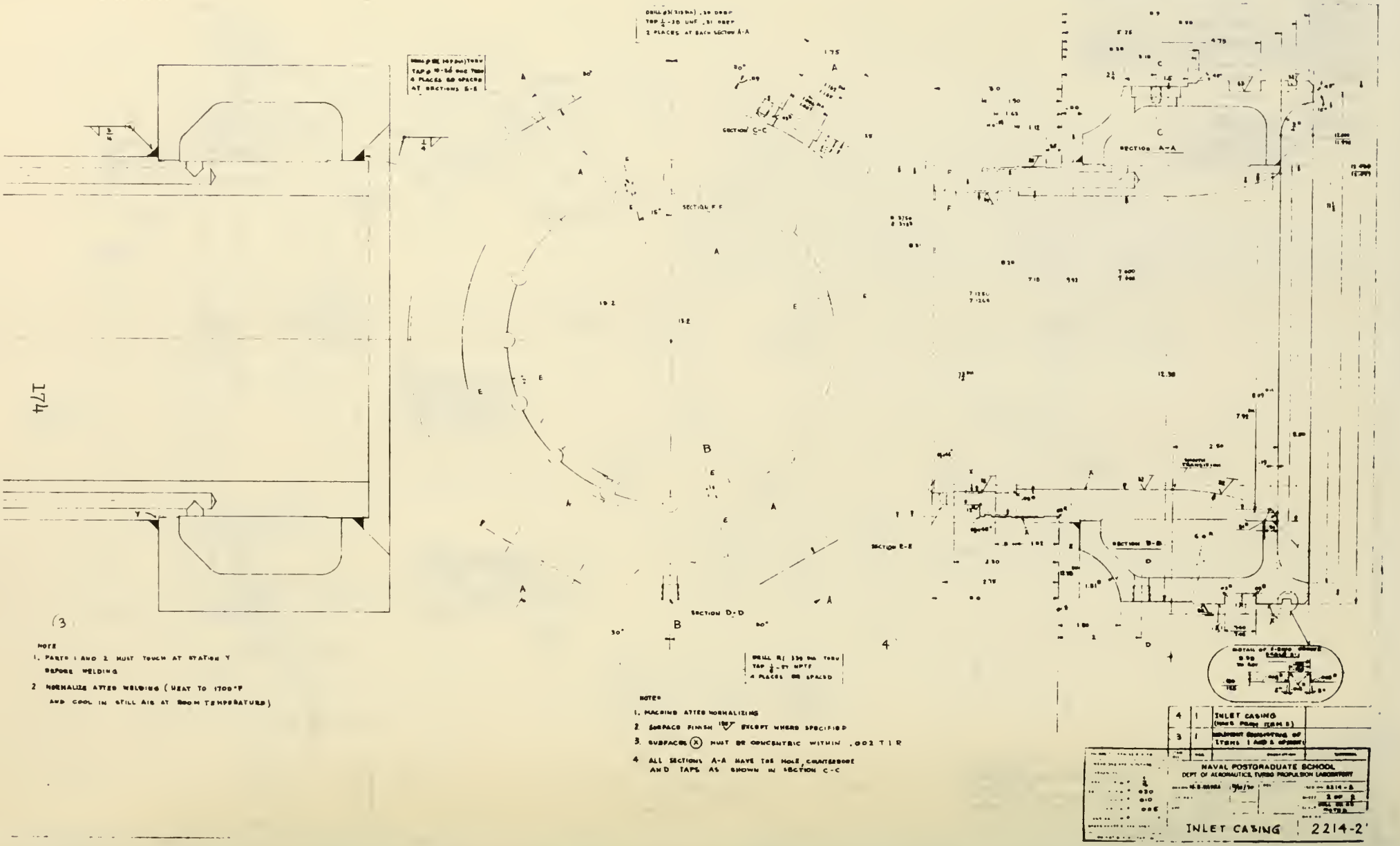

NOTE

1. PARTS 1 AND 2 MUST TOUCH AT STATION Y BEFORE WELDING
2. NORMALIZE AFTER WELDING (HEAT TO 1700°F AND COOL IN STILL AIR AT ROOM TEMPERATURE)

NOTES

1. MACHINE AFTER NORMALIZING
2. SURFACE FINISH 100 EXCEPT WHERE SPECIFIED
3. SURFACES (X) MUST BE CONCENTRIC WITHIN .002 T I R
4. ALL SECTIONS A-A HAVE THE HOLE, COUNTERBORE AND TAPS AS SHOWN IN SECTION C-C

4	1	INLET CASING
3	1	

NAVAL POSTGRADUATE SCHOOL
DEPT OF AERONAUTICS, TURBO PROPULSION LABORATORY

INLET CASING 2214-2

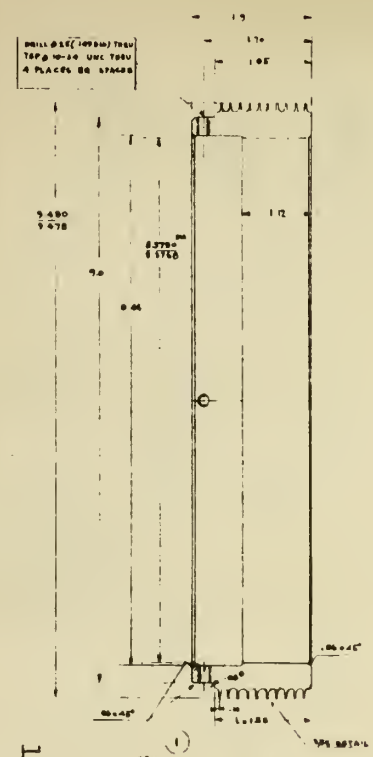

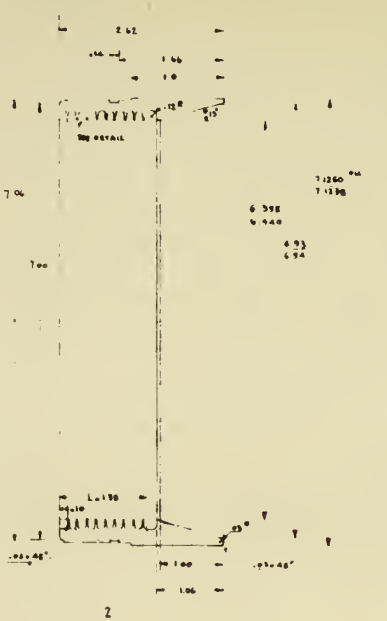

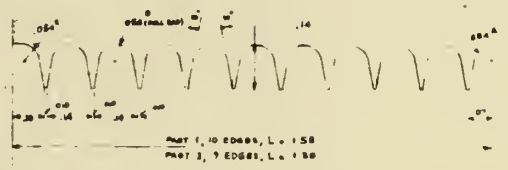

DETAIL OF LABYRINTHS
SCALE 5 : 1

15	4		A1
14	5		SA
13	4		ST
12	5		ST
11	8		Aluminum
10	16		Aluminum
9	8		
8	4		ST. ST. 304
7	8		ST. ST. 304
6	8		ST. ST. 304
5	8		ST. ST. 304
4	2		ST. STL 430
3	1		A1 2024 - T4
2	1		A1 2024 - T4
1	1		A1 2024 - T4

NAVAL POSTGRADUATE SCHOOL
DEPT OF AERONAUTICAL TURBO PROPULSION LABORATORY

LABYRINTHS AND DETAILS

2215

175

DRILL .531 DIA THRU
16 HOLES EQ SPACED
WITHIN .010 ON
22.00 B.C.

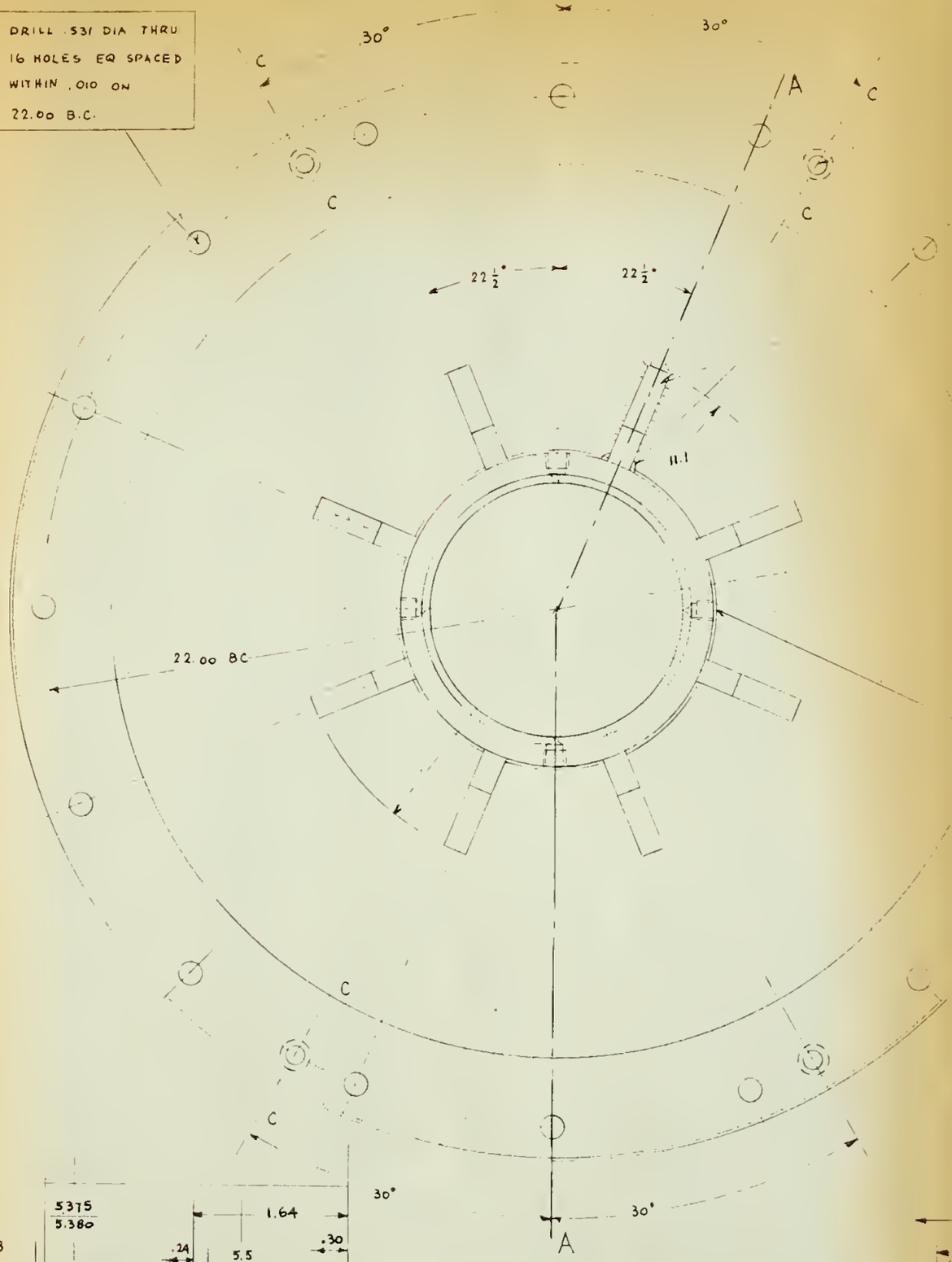

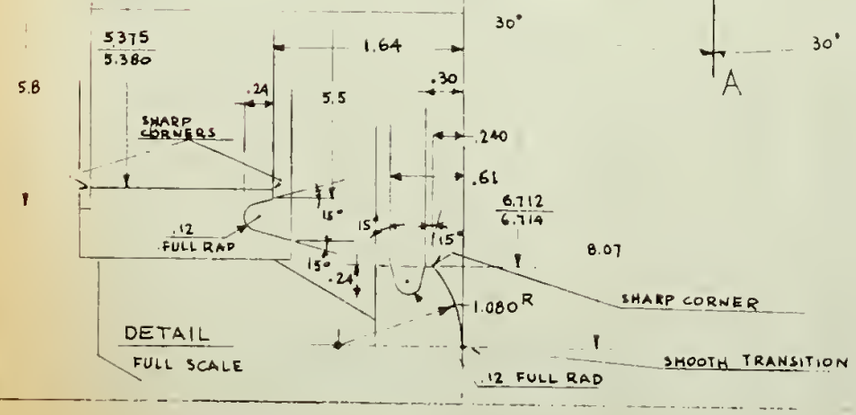

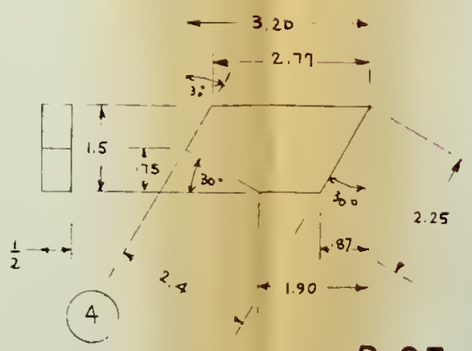

SECTION C-C

DRILL X(.397 DIA) THRU
C'BORE .68 DIA, .44 DEEP
4 PLACES ON 22.00 B.C
AT SECTIONS C-C

8 FINS EQ. SPACED
WELD BOTH SIDES
2 PLACES AT
EACH FIN

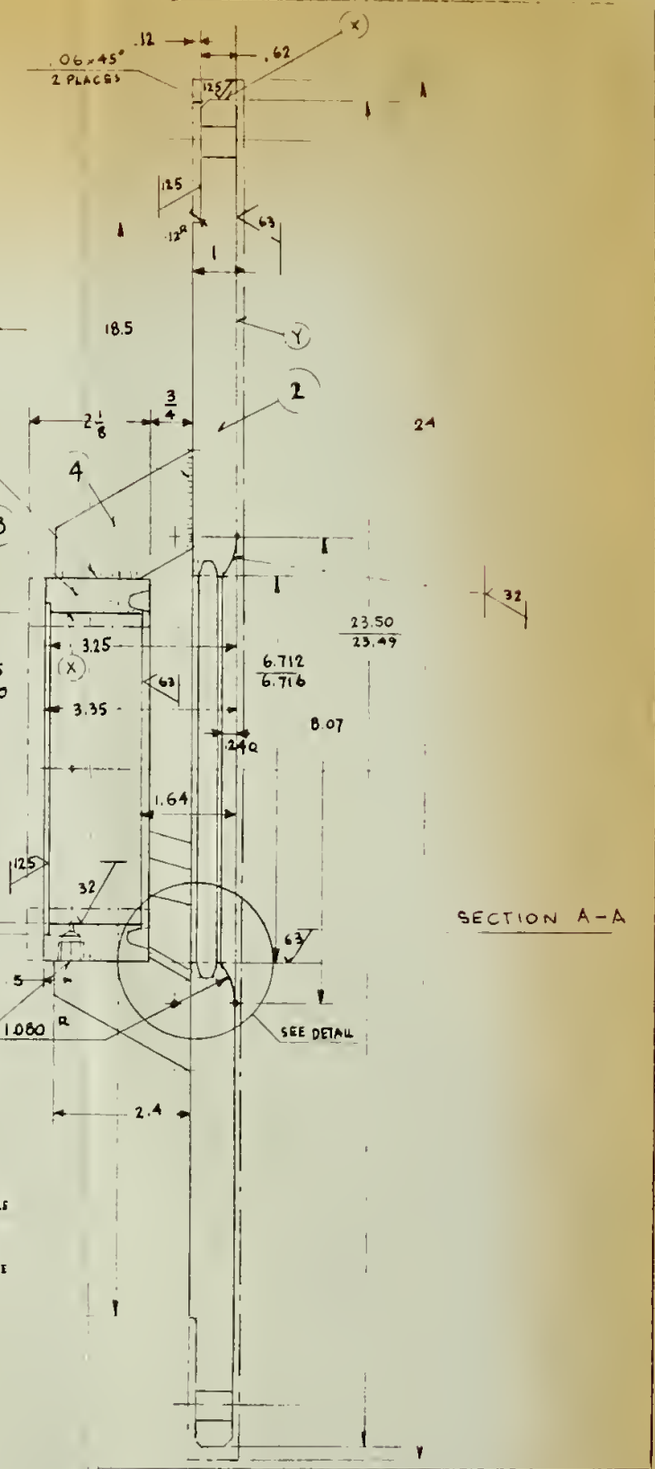

SECTION A-A

(1) NOTES

1. WELDED TYPE CONSTRUCTION WITH THRU WELDS AS INDICATED.
2. BEFORE MACHINING SURFACES WITH √ NORMALIZE WELDMENT (HEAT TO 1700°F AND COOL IN STILL AIR AT ROOM TEMPERATURE
3. SURFACES MARKED (X) MUST BE CONCENTRIC WITHIN .010 T.I.R. AND SQUARE WITH SURFACE (Y)
4. BORE WITH 5.375 / 5.380 MUST HAVE MINIMUM POSSIBLE TAPER

DRILL R(.339 DIA), .44 DEEP
DRILL .062 DIA THRU
TAP ⅛-27 NPTF
4 PLACES EQ. SPACED

ITEM NO.	REQ'D	DESCRIPTION	MATERIAL
4	8	FINS ½ x ½ THICK x 3.20 LG	H.R. STEEL FLAT M 1020
3	1	SEAMLESS STEEL PIPE, 6" NOM. DOUBLE EXTRA STRONG, 6.625 OD x .864 WALL x 2 7/8 LG.	ASTM - A 53
2	1	PLATE 24 OD x 1" THICK	ASTM - A 36
1	1	NOZZLE (MACHINE FROM WELDMENT OF ITEMS 2, 3 AND 4)	

UNLESS OTHERWISE STATED
DIMENSIONS ARE IN INCHES
TOLERANCES
FRACTIONS ± 1/32
DECIMALS XX ± .03
X ± .01
XXX ± .005
ANGLES ± °
BREAK SHARP EDGES .005R
DO NOT SCALE DRAWING

NAVAL POSTGRADUATE SCHOOL
DEPT. OF AERONAUTICS, TURBO PROPULSION LABORATORY

DRAWN M.H. VAVRA	11/15/70	REV	USED ON
CHECKED			SHEET 1 OF 1
APPD			SCALE HALF OR AS NOTED

NOZZLE FRAME

DWG NO. 2216

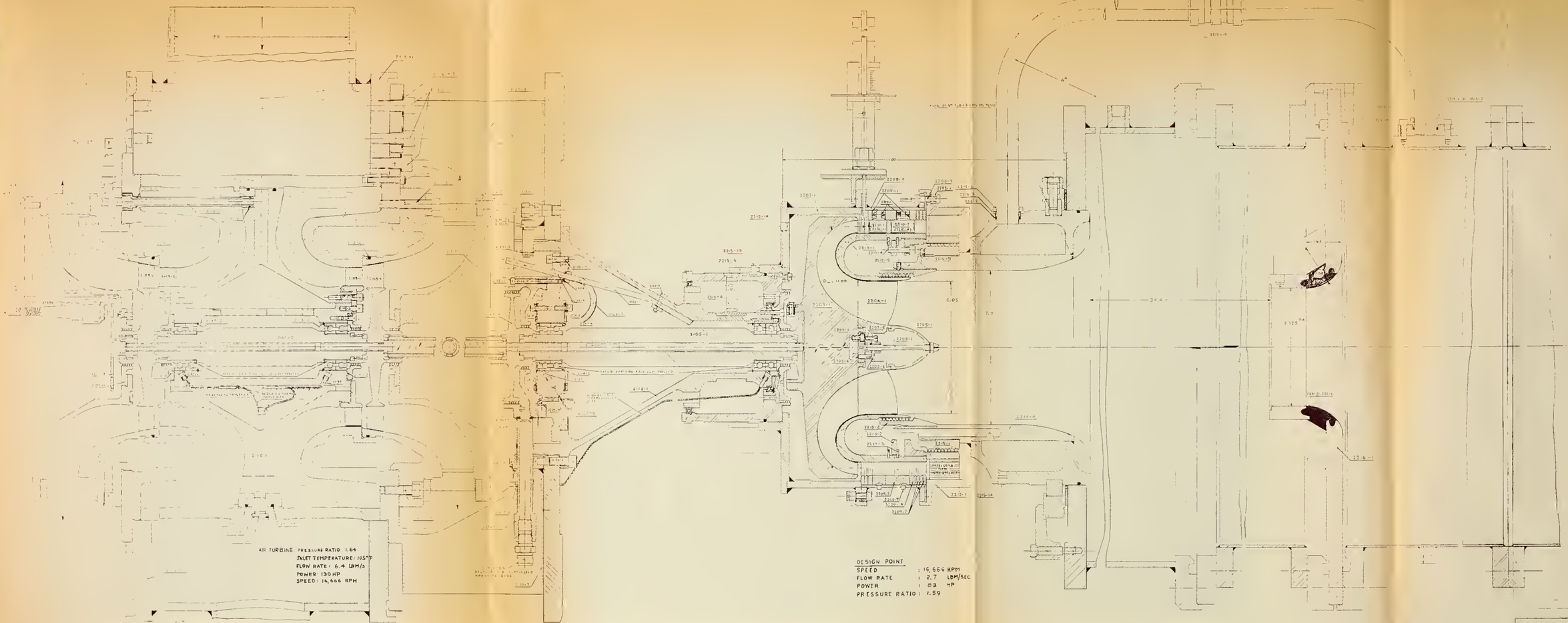

INVESTIGATION OF HYBRID COMPRESSOR CONCEPT
SPONSORED BY
NAVAL AIR SYSTEMS COMMAND, CODE 330
AIR TASK NO A 3307300/186B/3F414 32301
PROJECT ENGINEER H H GUTTMANN AIR-330C

NAVAL POSTGRADUATE SCHOOL DEPT OF AERONAUTICS, TURBO-PROPULSION LABORATORY	
DRAWN M H YAVRA, JULY 7, 1973	SCALE : FULL
TEST COMPRESSOR ASSEMBLY	DWG NO 2222

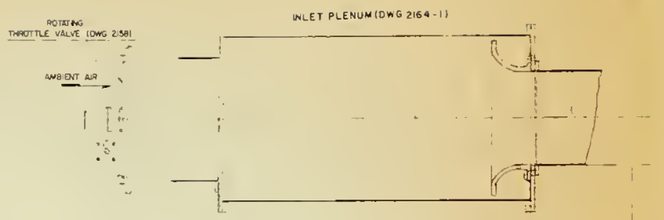

INVESTIGATION OF HYBRID COMPRESSOR CONCEPT
SPONSORED BY
NAVAL AIR SYSTEMS COMMAND
AIR TASK-A3303300/186B/3F41432301
PROJECT ENGINEER K H GUTTMANN, AIR-330C

NAVAL POSTGRADUATE SCHOOL TURBO-PROPULSION LAB, DEPT OF AERONAUTICS	
DRAWN: M H VAVRA, JULY 9, 1973	SCALE: 1/10
INSTALLATION OF HYBRID COMPRESSOR TEST RIG IN CELL 2 OF TURBO-PROPULSION LAB	DWG 2223

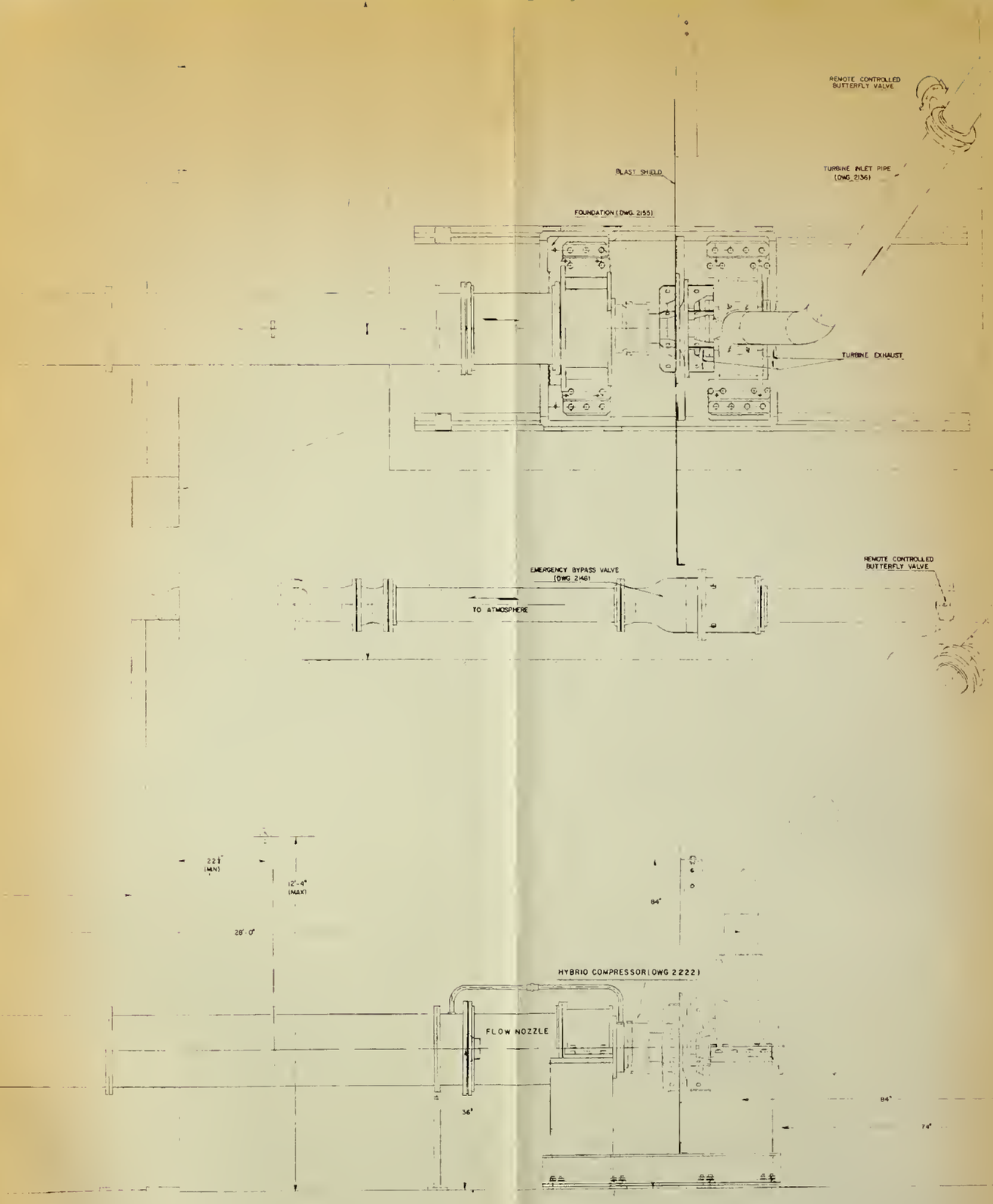

DWG 2223

APPENDIX C

LOSSES IN RADIAL COMPRESSOR WHEELS

The flows in rotors of radial machines are greatly influenced by Coriolis and centripetal accelerations and are difficult to analyze even if viscous effects are ignored. The prediction of the losses in radial impellers constitutes an even more difficult task because of the complex three-dimensional nature of the real flow through such wheels which makes it impossible to apply conventional boundary layer theories or to use loss data for stationary channels or diffusors. At off-design operating conditions the prediction of the flow losses with theoretical means is nearly impossible because of local flow separations that occur in the wheels.

A more detailed discussion on losses in impellers of centrifugal compressors is given in paragraph 5 of Appendix A which also emphasizes the need for more and better experimental data. At present only a limited amount of such data is available in the open literature, for instance in Ref. 2 and Ref. 10. Although not directly applicable to the special rotor of the Hybrid compressor the test data of these references are evaluated in the following to obtain indications how the rotor losses are influenced by the different design parameters.

Reference 10 will be discussed first because it gives the losses in a particular rotor with specified dimensions which is shown in Fig. 12. Hence its pertinent geometrical characteristics are:

$$R_{1o}/R_2 = 0.541$$

$$R_{1i}/R_2 = 0.287$$

$$b_2/R_2 = 0.078$$

The blade angle at R_{1o} is given as 57°.

Figure 13 shows the so-called polytropic impeller efficiency η_{RP}, which is defined in Ref. 11, as a function of β_{1o}, U_2/a_0 and the Mach number M_{W1} of the relative velocity W_{1o} at the inducer tip radius R_{1o}. Figure 13 is an exact reproduction of Fig. 4 of Ref. 10, but with the symbols of this report. The dashed parts of the curves for η_{RP} = constant are extrapolations by the writer. It is noticeable from Fig. 13 that the best rotor performance is obtained for positive incidence angles of about 9° if blockage because of the blade thickness is ignored. Reference 10 states that the inducer blades have a parabolic mean camber line and that their thickness is about 3% of the arc length of the camber line. Figure 14 gives the relations to determine the arc length m of a parabolic blade with axial length L and inlet blade angle β_B. From Fig. 12 there is L = 19.5 mm, and for $\beta_B = 57°$, m = 21.51 mm. Hence the blade thickness t is equal to (0.03) (21.51) = 0.64 mm. In accordance with Eqs. 7 and 8, the flow angle β_{1o}' of Fig. 3b is

$$\tan \beta_{1o}' = \tan \beta_{1o} \left(\frac{s}{s - t/\cos \beta_B} \right) \qquad C(1)$$

For 20 rotor blades, and with the dimensions of Fig. 12,

$$s = \pi(97.4)/20 = 15.30 \text{ mm}$$

and for $t = 0.64$ mm, $\beta_B = 57°$,

$$\tan \beta_{1o}' = \tan \beta_{1o} \, (0.923)$$

In Fig. 13 the angles β_{1o}' of this relation are shown on a special horizontal scale that is labeled β_{1o}'. Hence if the blockage due to the thickness of the blades is taken into account, the optimum incidence angle i' defined by Fig. 3b is still about +7°, which is at variance with

the findings of Ref. 2 (see Fig. 24) where it is shown that incidence angles of about zero at the inducer inlet give the best rotor performance. The same conclusion is made in Ref. 12 on the basis of past experience.

The parametric curves M_{W1} = constant of Fig. 13 were transposed from Fig. 4 of Ref. 10 also. In the following it will be shown that these curves give data that are redundant since M_{W1} is known if U_2/a_0, β_{1o}, and R_{1o}/R_2 are known. Reference 10 defines M_{W1} as the Mach number of the relative velocity W_{1o} at R_{1o}. Independent of whether the absolute velocity V_1 at the inducer inlet is constant or changing along the radius R_1,

$$M_{W1} = \frac{W_{1o}}{a_1} = \frac{\omega R_{1o}}{\sin \beta_{1o}} = \frac{U_2}{R_2} R_{1o} \frac{1}{\sin \beta_{1o}} \qquad C(2)$$

The quantity a_1 is the velocity of sound of the flow at R_{1o} where the static temperature is T_{1o}. Now, with

$$M_{V1} = \frac{V_{1o}}{a_1} = \frac{W_{1o} \cos \beta_{1o}}{a_1} = M_{W1} \cos \beta_{1o}$$

and

$$\frac{a_0}{a_1} = \sqrt{\frac{T_0}{T_{1o}}} = \left[1 + \frac{\gamma - 1}{2} M_{V1}^2\right]^{\frac{1}{2}}$$

there is

$$M_{W1} = \frac{U_2}{a_0} \frac{R_{1o}}{R_2} \frac{1}{\sin \beta_{1o}} \left[1 + \frac{\gamma - 1}{2} M_{W1}^2 \cos^2 \beta_{1o}\right]^{\frac{1}{2}}$$

and

$$M_{W1} = \frac{(U_2/a_0)\,(R_{1o}/R_2)}{\left[\sin^2 \beta_{1o} - \frac{\gamma - 1}{2} \cos^2 \beta_{1o}\,(U_2/a_0)^2\,(R_{1o}/R_2)^2\right]^{\frac{1}{2}}} \qquad C(3)$$

This relation could have been derived directly from Eq. A II(4) but it has been developed here to show that it holds for arbitrary distributions of V_1 vs. R_1 and not only for uniform inlet velocities ahead of the rotor. Equation C(3) can be modified to obtain the angle β_{1o} as a function of U_2/a_0 and M_{W1}, or

$$\sin \beta_{1o} = (U_2/a_0)\,(R_{1o}/R_2) \sqrt{\frac{1/M_{W1}^2 + \frac{\gamma - 1}{2}}{1 + \frac{\gamma - 1}{2}\,(U_2/a_0)^2\,(R_{1o}/R_2)^2}} \qquad C(4)$$

At point A of Fig. 13 the curve $M_{W1} = 0.6$ intersects the line $U_2/a_0 = 0.9$ at an angle β_{1o} of 66.5°, giving $i = 66.5 - 57 = 9.5^\circ$. However for $R_{1o}/R_2 = 0.541$ of the rotor of Fig. 12, $U_2/a_0 = 0.9$, $M_{W1} = 0.6$, and $\gamma = 1.4$, Eq. C(4) gives a flow angle

$$\beta_{1o} = 55.2^\circ$$

so that the incidence angle without blockage is -1.8° instead of $+9.5^\circ$. Figure 15 has been obtained by calculating the angles $\beta_{1o} = \beta_{1o}^*$ from Eq. C(4) with the values of U_2/a_0 along the curves M_{W1} = constant of Fig. 13 that pertain to particular efficiencies η_{RP}. Through the points thus obtained, which are marked by circles in Fig. 15, a new set of curves η_{RP} = constant has been drawn. In Eq. C(4) the value of R_{1o}/R_2 has been taken as 0.541 in accordance with the rotor dimensions of Fig. 12.

Figure 15 shows that the incidence angles are greatly reduced and that their values for optimum efficiencies become smaller with increasing ratios U_2/a_0 .

If Fig. 15 is correct; that is, if the relationship between M_{W1} , U_2/a_0, and η_{RP} in Fig. 13 is valid, but if the flow angles β_{1o} given in this figure are in error, the resulting incidence angles are more in line with experience. Then the argumentation in Ref. 10 based on its Fig. 5, which is presented as Fig. 16 in this report, namely, that positive incidence angles are necessary to obtain favorable velocity distributions along the inducer blades, would be without substance. The curves of Fig. 16 were obtained theoretically by neglecting blade thickness, compressibility and friction. It is very doubtful, however, whether velocity distributions similar to those shown in Fig. 16 occur along the actual inducer blades, not only because effects of blade thickness and leading edge shape were ignored, but primarily because the inducer was treated as a stationary cascade whose flow is not influenced by the impeller downstream of it. Hence no account is taken of Coriolis and centripetal accelerations and the fact that the inducer and impeller blades adjoin at the inducer discharge and form continuous blade surfaces from rotor inlet to rotor discharge. Hence at the station where the inducer and impeller blades join, the velocities on either side of a blade will differ and not be equal as Fig. 16 shows.

It will be tried to support the relationship presented in Fig. 15 by additional data of Ref. 10, namely, those given by its Fig. 3 which are presented here in Fig. 17. This figure shows the polytropic efficiency of the rotor of Fig. 12 at $U_2/a_0 = 0.83$ for three different diffusors.

It is evident from Fig. 18 that the rotor performance is almost independent of the diffusor configurations, although the latter influences the range of operation of the compressor.

The rotor efficiencies of Fig. 17 are given as functions of the flow coefficient φ_1 , defined by

$$\varphi_1 = \frac{Q_1}{U_2 R_2^2} \qquad C(5)$$

where Q_1 is the volume flow rate at the inducer inlet. Because of the curved walls of the inlet duct ahead of the inducer of Fig. 12 the absolute velocity V_1 will vary from the inner radius R_{1i} to the outer radius R_{1o} of the inlet eye. Let $\bar{V}_1$ be the average velocity at the inducer inlet such that

$$Q_1 = A_1 k_{B1} \bar{V}_1 \qquad C(6)$$

where

$$A_1 = \pi R_{1o}^2 \left[1 - \left(\frac{R_{1i}}{R_{1o}} \right)^2 \right]$$

k_{B1} is the blockage factor at station (1). Then, from Eqs. C(5) and C(6)

$$\frac{\bar{V}_1}{a_0} = \frac{\varphi_1}{k_{B1}} \left(\frac{U_2}{a_0} \right) \left(\frac{R_2}{R_{1o}} \right)^2 \frac{1}{\pi \left[1 - (R_{1i}/R_{1o})^2 \right]} \qquad C(7)$$

The weight flow rate $\dot{w}$ through the compressor is

$$\dot{w} = Q_1 \frac{\bar{p}_1}{R_G \bar{T}_1} = \varphi_1 U_2 R_2^2 \frac{(\bar{p}_1/P_0) P_0}{R_G (\bar{T}_1/T_0) T_0} \qquad C(8)$$

$\overline{p}_1$, $\overline{T}_1$ are the flow properties at the radius $\overline{R}_1$ where the velocity $\overline{V}_1$ occurs. Then, for an isentropic process from P_0, T_0 to $\overline{p}_1$, $\overline{T}_1$,

$$\frac{\overline{p}_1/P_0}{\overline{T}_1/T_0} = (\overline{T}_1/T_0)^{1/(\gamma-1)} \qquad C(9)$$

and, since

$$\overline{V}_1^{\,2} = 2 g c_p (T_0 - \overline{T}_1) = \frac{2}{\gamma - 1} a_0^{\,2} \left[1 - \frac{\overline{T}_1}{T_0}\right]$$

or

$$\frac{\overline{T}_1}{T_0} = 1 - \frac{\gamma - 1}{2}\left(\frac{\overline{V}_1}{a_0}\right)^2 \qquad C(10)$$

the dimensionless mass flow rate $(\dot{m})^*$ of Eq. 66 becomes

$$(\dot{m})^* = \frac{(\dot{w}/g)\sqrt{g R_G T_0}}{\pi R_2^{\,2} P_0} = \frac{\varphi_1}{\pi}\left(\frac{U_2}{a_0}\right)\sqrt{\gamma}\left[1 - \frac{\gamma - 1}{2}\left(\frac{\overline{V}_1}{a_0}\right)^2\right]^{1/(\gamma-1)} \qquad C(11)$$

Since by Eq. C(7) the ratio $(\overline{V}_1/a_0)$ is a function of φ_1 and (U_2/a_0) for known impeller dimensions, the dimensionless mass flow rate $(\dot{m})^*$ can be determined for assumed blockage factors k_{B1}.

The change of V_1 along R_1 can be determined approximately by assuming that the curvatures k_m of the generatrices of the axisymmetric stream surfaces at the inducer inlet vary linearly from k_{mi} at R_{1i} to k_{mo} at R_{1o}, where k_{mi} and k_{mo} are the curvatures of the meridional contours at these radii. In accordance with Eq. 11 (122) of Ref. 5

$$V_1 = V_{1i}\, e^{-\int_0^n k_m \, dn} \qquad C(12)$$

where $n = R_1 - R_{1i}$, and V_{1i} is the velocity at R_{1i}. As shown in Art. 3.3 of Ref. 5 the curvatures k_m in Eq. C(12) for the channel of Fig. 12 must be introduced as negative values. The assumed linear variation of k_m is given by

$$k_m = k_{mi} + \frac{k_{mo} - k_{mi}}{R_{1o} - R_{1i}} (R_1 - R_{1i}) \qquad C(13)$$

and the integral of Eq. C(12) becomes

$$-\int_0^n k_m \, dn = R_2 \, k_{mi} \left(\frac{R_1}{R_2} - \frac{R_{1i}}{R_2} \right) + \frac{R_2 \, k_{mo} - R_2 \, k_{mi}}{2\left(\frac{R_{1o}}{R_2} - \frac{R_{1i}}{R_2} \right)} \left(\frac{R_1}{R_2} - \frac{R_{1i}}{R_2} \right)^2 \qquad C(14)$$

On examining Fig. 12 it can be noticed that the rotor drawing presented in Ref. 10 is not to scale. From the measured distances of the figure the radius ratios R_{1o}/R_2 and R_{1i}/R_2 are about 0.59 and 0.275, instead of 0.541 and 0.287 in accordance with the dimensions of Fig. 12. Because of this situation it is not possible to determine the radii of curvature of the meridian contours at R_{1i} and R_{1o} from Fig. 12 with graphical means. Although the approach explained in the following is speculative it is believed that it gives a sufficiently good approximation for k_{mi} and k_{mo}. It is based on the assumption that the meridian contours of the rotor are curves with the equation $r/a = \theta^{-b}$ in polar coordinates. As shown in Fig. 18 and explained in Program No. 110 of Appendix D, such curves have zero curvature at a point P_0 given by r_0/a and θ_0 for any value of b between zero and unity. For angles θ larger than θ_0 the curvatures increase smoothly to reach a maximum value of k_m at point P_m where the tangent to the curve is perpendicular to that at P_0.

The writer has investigated a large number of curves and believes that those with $r/a = \theta^{-b}$ have the smallest curvature k_m at P_m for a given ratio y_0/x_0 of the coordinates of Fig. 18. Three-dimensional flow analyses indicate that smoothly changing curvatures k of the meridian contours of a channel and small values of k produce small changes of the velocities across the width of the channel and along the flow paths. In addition to satisfying these conditions it is seen from Fig. 20 also that contours with $r/a = \theta^{-b}$ establish flow channels that look very much like those of high-performance radial impellers. The inner or hub contour is supposed to be located between station P_0 and P_m of Fig. 20. For this curve

$$y_0/x_0 = \frac{180 - 51.7}{2(44.5)} = 1.4416$$

From Fig. 12 it is apparent that the tip contour does not have zero curvature at the outer rotor diameter of 180 mm, but that it is curved to the diameter where the axial width of the diffusor is 7 mm. It can be seen from Ref. 10 that this diameter is 215 mm. Hence, in accordance with Fig. 20 the tip contour is supposed to extend from P_m' to P_0' having

$$y_0'/x_0' = \frac{215 - 97.4}{2(37.5)} = 1.5680$$

The points P_0 and P_0' correspond to station P_0 of Fig. 18 so that the curvatures of the meridian at these locations are zero.

Since no direct solution of the problem of establishing the exponent b in $r/a = \theta^{-b}$ for given ratios y_0/x_0 is possible, the Calculator Program No. 110 of Appendix D has been established to obtain this relationship with an iterative process. Figure 19 shows b as function of y_0/x_0

and gives the maximum curvature k_m at station P_m of Fig. 18 by the dimensionless quantity $x_0\, k_m$. From Fig. 19 for the hub contour

$$k_m = k_{mi} = \frac{(1.174)}{44.5} = (2.638)(10^{-2})\ \text{mm}^{-1}$$

so that the radius of curvature R_{ci} is

$$R_{ci} = \frac{1}{k_{mi}} = 37.90\ \text{mm}$$

For the tip contour

$$k_m' = k_{mo} = \frac{1.232}{37.5} = (3.285)\ (10^{-2})\ \text{mm}^{-1}$$

or

$$R_{co} = \frac{1}{k_{mo}} = 30.44\ \text{mm}$$

The exponents b were found to be 0.2552 for the inner and 0.3525 for the outer contour. They were used to establish the coordinates of the meridian contours of Fig. 20.

The calculated curvatures k_{mi} and k_{mo} introduced into Eq. C(14) give

$$-\int_0^n k_m\, dn = -\ 0.6815 + 2.3747\ \frac{R_1}{R_2} + 1.1456\ \left(\frac{R_1}{R_2} - 0.287\right)^2 \qquad \text{C(15)}$$

From Eqs. C(12) and C(15) for $R_1/R_2 = R_{1o}/R_2 = 0.541$

$$\frac{V_{1o}}{V_{1i}} = e^{0.67712} = 1.9682$$

or

$$\frac{V_1}{a_0} = \frac{V_{1o}}{a_0}\,(0.5081)\; e^{-\int_0^n k_m\, dn} = \frac{V_{1o}}{a_0}\, X \qquad C(16)$$

Thus, for chosen values of V_{1o}/a_0 the ratios V_1/a_0 at the different radii R_1 are known, and it is possible to determine the corresponding weight flow rates by

$$\dot{w} = k_{B1} \int_{R_{1i}}^{R_{1o}} 2\pi\, R_1\, V_1\, \frac{p_1}{R_G\, T_1}\, dR_1$$

or

$$\dot{w} = 2\pi\, R_2^{\,2}\, k_{B1}\, \frac{P_0}{T_0}\, \frac{a_0}{R_G} \int_{R_{1i}/R_2}^{R_{1o}/R_2} \frac{R_1}{R_2}\, \frac{V_1}{a_0}\, \frac{p_1/P_0}{T_1/T_0}\, d\left(\frac{R_1}{R_2}\right)$$

Similar to Eqs. C(9) and C(10)

$$\frac{p_1/P_0}{T_1/T_0} = \left[1 - \frac{\gamma - 1}{2}\left(\frac{V_1}{a_0}\right)^2\right]^{1/(\gamma-1)}$$

Then, since $R_{1i}/R_2 = 0.287$ and $R_{1o}/R_2 = 0.541$, the dimensionless mass flow rate $(\dot{m})^*$ of Eq. C(11) is obtained also from

$$(\dot{m})^* = 2\, k_{B1} \sqrt{\gamma}\, \left(\frac{V_{1o}}{a_0}\right) \int_{0.287}^{0.541} \left(\frac{R_1}{R_2}\right) X \left[1 - \frac{\gamma - 1}{2}\left(\frac{V_{1o}}{a_0}\, X\right)^2\right]^{1/(\gamma-1)} d\left(\frac{R_1}{R_2}\right) \qquad C(17)$$

where X is defined by Eq. 16.

With Eqs. C(11) and C(17) the flow coefficient φ_1 can be related to V_{1o}/a_0 by determining $\overline{V}_1/a_0$ from Eq. C(7) for particular values of φ_1 and calculating $(\dot{m})^*$ by Eq. C(11). Then, that ratio V_{1o}/a_0 has to be established which,

introduced in Eq. C(16) and used in Eq. C(17), gives the same value of $(m)^*$. Since the same blockage factor k_{B1} is used in both calculating procedures, its influence on the relationship between φ_1 and V_{1o}/a_0 is small, and a constant value $k_{B1} = 0.97$ will be assumed. For the ratios V_{1o}/a_0 thus determined, the flow angle β_{1o} at R_{1o} is given by

$$\tan \beta_{1o} = \frac{\omega R_{1o}}{V_{1o}} = \frac{(U_2/a_0)\,(R_{1o}/R_2)}{(V_{1o}/a_0)} = \frac{0.44903}{(V_{1o}/a_0)} \qquad C(18)$$

The rotor efficiencies η_{PR} of Fig. 17 which hold for $U_2/a_0 = 0.83$ can therefore be related to the flow angle β_{1o} at the tip of the inducer. With the calculated data it is possible also to establish the Mach number M_{W1} at the inducer tip radius by means of Eq. C(3). For $\gamma = 1.4$

$$M_{W1} = \frac{0.44903}{\left[\sin^2 \beta_{1o} - (0.2)\,(0.44903)^2 \cos^2 \beta_{1o}\right]^{\frac{1}{2}}} \qquad C(19)$$

These calculations have been performed on a Monroe 1655 Calculator. In particular, the evaluation of Eq. C(17) for the velocity ratios of Eq. C(16) has been carried out with Program No. 108 of Appendix D. Figure 21 shows the dimensionless mass flow rate $(\dot{m})^*$ as functions of φ_1 and of V_{1o}/a_0. The relationship $(m)^* = f_1(\varphi_1)$ has been obtained from Eqs. C(11) and C(10), and $(m)^* = f_3(V_{1o}/a_0)$ is the result of the calculations with Program No. 108. Whereas $f_1(\varphi_1)$ depends solely on the rotor dimensions which are given by Fig. 12, the accuracy of the function $f_3(V_{1o}/a_0)$ depends on how well the assumed stream surface curvatures correspond to reality.

Figure 21 also shows the rotor efficiency η_{RP} as function of φ_1. This curve has been obtained from the test data of Fig. 17, and represents the best estimate of a continuous curve that can be drawn through all the test points between $\varphi_1 \cong 0.11$ and $\varphi_1 \cong 0.275$. With this composite diagram the flow functions φ_1 can be determined for chosen ratios V_{1o}/a_o, since corresponding values must have the same dimensionless mass flow rate $(\dot{m})^*$. Hence, as shown in Fig. 21, it is also possible to obtain η_{RP} as a function of V_{1o}/a_o. Moreover, since by Eq. C(18) the relationship between the flow angle β_{1o} and V_{1o}/a_o is known for the velocity distribution of Eq. C(16), the rotor efficiency η_{RP} is obtained as function of the angle β_{1o} at the speed ratio $U_2/a_o = 0.83$ for which the data of Fig. 17 hold. Moreover, Eq. C(19) establishes the Mach number M_{W1} for different flow angles β_{1o}. The data thus obtained are marked by circles in Fig. 22. It can be seen that the maximum rotor efficiency occurs at a flow angle of about 55^o; that is, at an incidence angle i of about -2^o. The data points marked by crosses in Fig. 22 are from Fig. 15 for $U_2/a_o = 0.83$. Both curves of η_{RP} have the same maximum at about the same flow angle, but the efficiencies from Fig. 15 decrease more rapidly with flow angle on either side of the maximum than the data from Fig. 21. Figure 15 was obtained from the data of Ref. 10, shown in Fig. 13, by determining the flow angle $(\beta_{1o}{}^*)$ with Eq. C(4) on assuming that U_2/a_o and M_{W1} of Fig. 13 are correct and that the rotor dimensions are those given by Fig. 12. Inspite of the much smaller range of rotor efficiency with inlet flow angle which the data from Fig. 15 exhibit, it is remarkable how well the Mach numbers M_{W1} of the two approaches of Fig. 22 coincide.

For purposes of discussion the curves of η_{PR} and M_{W1} obtained from Fig. 21 are compared in Fig. 23 with the data of Fig. 13 at $U_2/a_0 = 0.83$ which are marked by crosses, and which represent the original values given by Ref. 10. It must be noted, however, that in Fig. 23 the curves from Fig. 13 are plotted against a scale marked β_{1o}** which is shifted by about 12° with respect to the horizontal scale β_{1o} that holds for the data from Fig. 21. This shift has been chosen such that the two curves for η_{RP} coincide as closely as possible.

The conclusions that can be drawn from the preceeding analyses are:

- (1) The curves of Fig. 13 are not consistent because, for the rotor dimensions of Fig. 12, the flow angles β_{1o} must be different than those of Fig. 13 if the velocity ratios U_2/a_0 and the Mach numbers M_{W1} of this figure are assumed to be correct, and doubt exists whether optimum efficiencies are reached at incidence angle i of about +9°.
- (2) If the curves of Fig. 13 are plotted against the flow angle β_{1o}*, obtained from Eq. C(4) to establish the correct relationship between U_2/a_0 and M_{W1}, the resulting curves of Fig. 15 give optimum incidence angle i of about -2°.
- (3) If other original values of Ref. 10 for $U_2/a_0 = 0.83$, presented in Fig. 17, are analyzed with the best possible procedure, the optimum incidence angle i is also about -2° but, as shown in Fig. 22, the range in which the flow angle can vary for a specified off-design efficiency is about twice that of the curves of Fig. 15 described in point (2) above. However, the inlet Mach numbers M_{W1} of the two approaches lie on the same curve.

- (4) If the relations computed from Fig. 17 are compared with the original results of Fig. 13, it is seen from Fig. 23 that the two curves $\eta_{RP} = f(\beta_{1o})$ at $U_2/a_0 = 0.83$ can be made to coincide only if the flow angles of Fig. 13 are reduced by about 12^o. In this case, however, different inlet Mach numbers M_{W1} occur.
- (5) The discrepancies in the data from Ref. 10 make it inadvisable to use Fig. 13 with reduced flow angles, or Fig. 15, where the range of flow angle for given off-design efficiency is very much smaller than that derived from Fig. 17.
- (6) It is not believed that the design criteria of Ref. 10 have general applicability. The inconsistencies in the data could be due to non-uniform inlet velocity distributions because of the shape of the inlet duct and its supporting fins. It is possible also that the flow angle measurements are in error or that the dimensions of the rotor are different from those given by Fig. 12.

Test data of radial compressor wheels are presented also in Ref. 2. The curves of Fig. 23b of Ref. 2 are redrawn in Fig. 24 of this report in a somewhat modified form, and with U_2/a_0 instead of with $U_2/\sqrt{T_0}$ as parameter. There is, in metric units for air,

$$\frac{U_2}{a_0} = \frac{U_2}{\sqrt{\gamma R_G g T_0}} = \frac{U_2}{\sqrt{T_0}} \frac{4.9874}{100}$$

for:

$\gamma = 1.4$

$R_G = \mathcal{R}/M = 847.83/28.964 = 29.272$ $(m/^oK)$

$g = 9.81$ (m/s^2)

The incidence angle i' of Fig. 24 equals

$$i' = \beta_{1o}' - \beta_{Bo}$$

where β_{1o}' is the flow angle at R_{1o} obtained from Eq. C(1) by taking account of the blockage due to the inducer blade thickness, and β_{Bo} is the inducer blade angle at R_{1o}. Reference 2 does not give the dimensions and the inducer blade angles of the rotor for which Fig. 24 has been established. Hence Mach number M_{W1} and peripheral speed ratio U_2/a_0 cannot be related to each other by, say, Eq. C(3). Point D of Fig. 25, which gives the curves of Fig. 24 also corresponds to the design point of the Hybrid impeller with $M_{W1} = 0.4842$; $i' \cong + 0.5^{\circ}$, and $U_2/a_0 = 0.7156$. It can be noticed that for these values of M_{W1} and i' the parameter U_2/a_0 of Figs. 24 and 25 is very nearly equal to 0.7156. It was decided, therefore, to ignore the curves U_2/a_0 = constant in Fig. 24 for the off-design performance calculations of the Hybrid compressor and to assume that $r_e = \eta_R/\eta_{RMAX}$ is only depending on M_{W1} and i' , not only because of the limited information given in Ref. 2 but also because these two quantities seem to be the most important variables that affect the rotor efficiency. The curve labeled "Max. Flow Rate" in Fig. 24 appears to represent the limit at which stable operation is possible, probably because of the flow separations that occur on the pressure, or concave, sides of the inducer blades at these negative incidence angles. The surge limit of Fig. 24 is that which occurs if a non-bladed diffusor is arranged after the impeller. Hence, for bladed diffusors, compressor surge may be initiated by separations in the diffusor at incidence angles i' smaller than those of Fig. 24.

APPENDIX D

CALCULATING PROGRAMS

FOR

MONROE MODEL 1655/56

ELECTRIC PROGRAMMABLE DISPLAY CALCULATOR

WITH

CARD READER CR-1

AND

MONROE MODEL 1880-22

SCIENTIFIC PROGRAMMABLE PRINTING CALCULATOR

PROGRAM No. 102

MONROE CALCULATOR 1655 WITH CARD READER CR-1

Description

Program 102 calculates the dimensionless flow rate of a radial compressor from the conditions at the impeller discharge. From Eq. II (11) of Ref. (a)*,

$$\Phi_2 = \frac{\dot{w}\sqrt{(R_G/g)T_0}}{P_0\ A_2\ k_{B2}} = \mu\sqrt{\gamma}\ \cot\ \alpha_2 \left(\frac{U_2}{a_0}\right) \frac{p_2/P_0}{T_2/T_0}$$

where:

$\dot{w}$ = weight flow rate (lbm/s)

R_G = gas constant (ft-lb/(lbm,$^\circ$R))

g = 32.174 (ft/s^2)

T_0 = total temperature ahead of rotor ($^\circ$R)

P_0 = total pressure ahead of rotor (psia)

$A_2 = 2\pi\ R_2\ b_2$ = rotor discharge area (in.^{2})

k_{B2} = restriction factor (-)

$A_1 = \pi\ (R_{lo}^{\ 2} - R_{li}^{\ 2})$ = rotor inlet area (in.^{2})

k_{B1} = restriction factor (-)

μ = slip factor (-)

$\gamma = c_p/c_v$ (-)

α_2 = absolute flow angle at rotor discharge ($^\circ$)

U_2 = peripheral rotor speed (ft/s)

$a_0 = \sqrt{g\ \gamma\ R_G\ T_0}$

---

*(a) Vavra, M. H., "Basic Elements for Advanced Design of Radial Flow Compressors," in AGARD-LS-39-70, "Advanced Compressors," Techn. Editing & Reprod. Ltd; London 1970.

p_2 = static pressure out rotor discharge (psia)

T_2 = static temperature at rotor discharge ($^{\circ}R$)

From Eqs. I(20) and I(8) of Ref. (a)

$$\frac{p_2}{P_0} = (T_2'/T_0)^{\gamma(\gamma-1)}$$

$$\frac{T_2'}{T} = 1 + (\gamma-1)\,\mu\left(\frac{U_2}{a_0}\right)^2\left[\frac{1}{\Psi^2}\left(1 - \frac{\mu}{2\sin^2\alpha_2}\right) - \frac{1}{2\mu}\left(\frac{1}{\Psi^2} - 1\right)\right]$$

From Eq. I(7) of Ref. (a)

$$\frac{T_2}{T_0} = 1 + (\gamma-1)\,\mu\left(\frac{U_2}{a_0}\right)^2\left(1 - \frac{\mu}{2\sin^2\alpha_2}\right)$$

The velocity coefficient

$$\Psi = \frac{W_2}{W_{2\,is}}$$

establishes the rotor loss in accordance with Ref. (a).

The following quantities will be used during the calculations:

$$A = 1 - \frac{\mu}{2\sin^2\alpha_2}$$

$$B = \frac{1}{2\mu}\left(\frac{1}{\Psi^2} - 1\right)$$

$$C = (\gamma-1)\,\mu\left(\frac{U_2}{a_0}\right)^2$$

$$D = \mu\sqrt{\gamma}\,\cot\alpha_2\left(\frac{U_2}{a_0}\right)$$

Then

$$T_2'/T_0 = F = 1 + C\left(\frac{1}{\Psi^2}A - B\right)$$

$$p_2/P_0 = F^{\gamma/(\gamma-1)}$$

$$T_2/T_0 = 1 + C\ A$$

$$\varphi_2 = D \frac{(p_2/P_0)}{(T_2/T_0)}$$

$$X = \Phi_2\ A_2\ k_{B2} = \frac{\dot{w}\sqrt{(R_G/g)\ T_0}}{P_0}$$

$$\Phi_1 = \frac{X}{A_1\ k_{B1}} = \frac{\dot{w}\sqrt{(R_G/g)\ T_0}}{P_0\ A_1\ k_{B1}}$$

The flow function Φ_1 will be used in program No. 103 to establish the ratios p_1/P_0 and T_1/T_0. The area $A_1 = \pi\ (R_{lo}^{\ 2} - R_{li}^{\ 2})$ must be introduced in square inches.

Enclosures: Operating Instructions (1 page)
Program Listing (4 pages)

OPERATING INSTRUCTIONS PROGRAM No. 102

MONROE CALCULATOR 1655/6 WITH CARD READER CR-1

Set-Up: (RESET); (TO(0)); Depress (LOAD); Read Cards 1-3

Release (LOAD); (TO(0)); Depress (P); (RESUME)

P-COUNT		
0 0 1	ENTER: γ	(RESUME)
0 1 2	" : U_2/a_0	(")
0 1 4	" : α_2	(")
0 2 3	" : μ	(")
0 3 4	" : ψ	(")
1 3 4	" : A_2	(")
1 3 6	" : k_{B2}	(")
1 4 1	" : A_1	(")
1 4 3	" : k_{B1}	(")
1 4 6	RESULTS:	

↑ (1) → T_2/T_0

↑ (0) → p_2/p_0

↑ (4) → $\dfrac{\dot{w}\sqrt{(R_G/g)T_0}}{P_0}$

↑ (3) → $\Phi_2 = \dfrac{\dot{w}\sqrt{(R_G/g)T_0}}{P_0\ A_2\ k_{B2}}$

↑ (5) → $\Phi_1 = \dfrac{\dot{w}\sqrt{(R_G/g)T_0}}{P_0\ A_1\ k_{B1}}$

(RESUME)

TURBO-PROPULSION LABORATORY, DEPT. OF AERONAUTICS, NPS,

PROGRAM No. 102 MONROE 1655 CALCULATOR PAGE 1 OF 4.

FLOW RATE THROUGH RADIAL COMPRESSOR FOR GIVEN

CONDITIONS AT DISCHARGE ..... DATE: AUG 72 BY: M.H.V.R.

BR PT	ADDRESS P	ADDRESS COUNT	COMMAND	CODE	E	A	M	0	1	2	3	4	5	6	7	8	9	X	Y	Z	NOTES
0	0	0	HALT	401	γ																ENTER: γ
		1	STR(2)	441	γ					γ											
		2	−	062																	
		3	1	001																	
		4	÷	072	$\gamma-1$																
		5	RCL(2)	461	γ																
		6	=	020	$\frac{\gamma-1}{\gamma}$																
	0	7	INV	054	$\gamma/(\gamma-1)$																
	1	0	STR(0)	457				$\frac{\gamma}{\gamma-1}$													
	1	1	HALT	401																	ENTER: U_2/a_0
		2	STR(6)	445										U_2/a_0							
	1	3	HALT	401	α_2																ENTER: α_2
		4	SIN/COS	040	$\sin\alpha_2$																
		5	×	070																	
		6	=	020	$\sin^2\alpha_2$																
	1	7	STR(5)	444									$\sin^2\alpha_2$								
1	2	0	INV	054	$\sin^2\alpha_2$																
		1	×	070																	
	2	2	HALT	401	μ																ENTER: μ
		3	STR(4)	443	μ							μ									
		4	÷	072	$\frac{\mu}{\sin^2\alpha_2}$																
		5	2	002																	
		6	−	062	$\frac{\mu}{2\sin^2\alpha_2}$																
	2	7	1	001																	
	3	0	=	020	$-A$																
		1	CHSGN	013	A																
		2	STR(3)	442							A										
	3	3	HALT	401	ψ																ENTER: ψ
		4	INV	054	$1/\psi$																
		5	X	070																	
		6	−	062	$1/\psi^2$																
	3	7	STR(7)	446											$1/\psi^2$						
					E	A	M	0	1	2	3	4	5	6	7	8	9	X	Y	Z	

200

TURBO-PROPULSION LABORATORY, DEPT. OF AERONAUTICS, NPS ,
PROGRAM No. ...102... MONROE 1655 CALCULATOR

DATE: AUG. 72 BY: M.H.V.

BR PT	ADDRESS P COUNT	COMMAND	CODE	E	A	M	0	1	2	3	4	5	6	7	8	9	X	Y	Z	NOTES
							REGISTERS													
2	040	1	001				$\frac{\gamma}{\gamma-1}$		γ	A	μ	$\sin^2\alpha_2$	U_2/a_0	$1/\psi^2$						
	1	÷	072	$1/\psi^2-1$																
	2	2	002																	
	3	÷	072	$\frac{1}{2}(1/\psi^2-1)$																
	4	RCL(4)	463	μ																
	5	=	020	B											B					
	6	STR(8)	447	Y																
	47	RCL(2)	461	γ																
	50	−	062																	
	1	1	001																	
	2	×	070	$\gamma-1$																
	3	RCL(4)	463	μ																
	4	×	070	$\mu(\gamma-1)$																
	5	RCL(6)	465	U_2/a_0																
	6	×	070																	
	57	RCL(6)	465	U_2/a_0																
3	60	=	020	C																
	1	STR(1)	440					C												
	2	RCL(7)	466	$1/\psi^2$																
	3	×	070																	
	4	RCL(3)	462	A																
	5	−	062																	
	6	RCL(8)	467	B																
	67	×	070																	
	70	RCL(1)	460	C																
	1	+	060																	
	2	1	001																	
	3	a^x	074	T_2'/T_0																
	4	RCL(0)	477																	
	5	=	020	P_2/P_0																
	6	STR(0)	457				P_2/P_0													
	7	RCL(1)	460	C																

TURBO-PROPULSION LABORATORY, DEPT. OF AERONAUTICS, NPS ,
PROGRAM No. ...102... MONROE 1655 CALCULATOR PAGE...3 OF 4 .
DATE: AUG. 72 BY: M.H.V

BR PT	ADDRESS P	COUNT		COMMAND	CODE			REGISTERS E	A	M	0	1	2	3	4	5	6	7	8	9	X	Y	Z	NOTES
4	1	0	0	×	0	7	0				P_2/P_0	C	γ	A	μ	$\sin^2\alpha_2$	U_2/a_0							
			1	RCL(3)	4	6	2	A																
			2	+	0	6	0	CA																
			3	1	0	0	1																	
			4	=	0	2	0	T_2/T_0																
			5	STR(1)	4	4	0					T_2/T_0												
			6	1	0	0	1																	
	1	0	7	−	0	6	2																	
	1	1	0	RCL(5)	4	6	4	$\sin^2\alpha_2$																
			1	÷	0	7	2	$\cos^2\alpha_2$																
			2	RCL(5)	4	6	4	$\sin^2\alpha_2$																
			3	×	0	7	0	$\cot^2\alpha_2$																
			4	RCL(2)	4	6	1	γ																
			5	=	0	2	0	$\gamma\cot^2\alpha_2$																
			6	$\sqrt{\ }$	0	5	6	$\sqrt{\gamma\cot^2\alpha_2}$																
	1	1	7	×	0	7	0																	
5	1	2	0	RCL(6)	4	6	5	U_2/a_0																
			1	×	0	7	0																	
			2	RCL(4)	4	6	3	μ																
			3	×	0	7	0																	
			4	I	0	0	1																	
			5	×	0	7	0	D																
			6	RCL(0)	4	7	7	P_2/P_0																
	1	2	7	÷	0	7	2																	
	1	3	0	RCL(1)	4	6	0	T_2/T_0																
			1	×	0	7	0	Φ_2																
			2	STR(3)	4	4	2							Φ_2										
	1	3	3	HALT	4	0	1	A_2																ENTER: A_2
			4	×	0	7	0																	
	1	3	5	HALT	4	0	1	K_{B2}																ENTER: K_{B2}
			6	÷	0	7	2	X																
	1	3	7	STR(4)	4	4	3								X									
								E	A	M	0	1	2	3	4	5	6	7	8	9	X	Y	Z	

202

MUV

BR PT	ADDRESS P COUNT			COMMAND	CODE			E	A	M	0	1	2	3	4	5	6	7	8	9	X	Y	Z	NOTES
6	1	4	0	HALT	4	0	1	A_1			p_2/p_0	T_2/T_0	γ	Φ_2	X	$\sin^2\alpha_2$	U_2/a_0							ENTER: A_1
			1	÷	0	7	2																	
	1	4	2	HALT	4	0	1	k_{B1}																ENTER: k_{B1}
			3	=	0	2	0	Φ_1																
			4	STR(5)	4	4	4									Φ_1								
	1	4	5	HALT	4	0	1				p_2/p_0	T_2/T_0	γ	Φ_2	X	Φ_1								RESULTS:
			6	TO(0)	7	4	0																	
			7																					
			0																					
			1																					
			2																					
			3																					
			4																					
			5																					
			6																					
			7																					
			0																					
			1																					
			2																					
			3																					
			4																					
			5																					
			6																					
			7																					
			0																					
			1																					
			2																					
			3																					
			4																					
			5																					
			6																					
			7																					
								E	A	M	0	1	2	3	4	5	6	7	8	9	X	Y	Z	

PROGRAM No. 103

MONROE CALCULATOR 1655/6 WITH CARD READER CR-1

Description

Program 103 deals with the flow of a perfect gas with $\gamma = c_p/c_v$ = constant that passes through a given area A. Because of boundary layers the effective flow area is supposed to be k_B A. The total pressure P_t and the total temperature T_t of the flow are known. To be determined is the average static pressure p that exists at the flow area k_B A. The equation of continuity can be expressed by a dimensionless flow function Φ where

$$\Phi = \sqrt{\frac{2\gamma}{\gamma-1}\left[\left(\frac{p}{P_t}\right)^{2/\gamma} - \left(\frac{p}{P_t}\right)^{(\gamma+1)/\gamma}\right]}$$

where

$$\Phi = \frac{\dot{w}\sqrt{(R_G/g)T_t}}{k_B A P_t} = \frac{\dot{m}\sqrt{g R_G T_t}}{k_B A P_t}$$

There are:

$\dot{w}$ = weight flow rate (lbm/s)

$\dot{m}$ = mass flow rate (slug/s)

R_G = gas constant (ft-lb/(lbm,$^\circ$R))

g = 32.174 (ft/s^2)

k_B A = effective cross-sectional area of channel where static pressure p occurs

P_t, p (psia)

T_t ($^\circ$R)

A (in.^{2})

Figure D 103 shows a plot of Φ vs. $r = p/P_t$. At the critical pressure ratio r_c the function $\Phi = \Phi_c$ has a maximum, hence no solutions occur if

Φ is larger than Φ_c. There are:

$$r_c = \left(\frac{2}{\gamma + 1}\right)^{\gamma/(\gamma-1)} = \left[\left(\frac{2}{\gamma + 1}\right)^{1/(\gamma-1)}\right]^{\gamma}$$

and

$$\Phi_c = \sqrt{\frac{2\gamma}{\gamma + 1}} \left(\frac{2}{\gamma + 1}\right)^{1/(\gamma-1)}$$

If Φ is smaller than Φ_c two solutions of $r = p/P_t$ are obtained, say, r_I if the velocity at the area A is subsonic, and r_{II} if the flow is supersonic. These pressure ratios must be obtained with an iterative process, by assuming a value of r, say r_i, and verifying whether the corresponding value Φ_i equals the specified flow function Φ.

The following quantities are used in the calculations

$$E1 = 2/\gamma$$

$$E2 = (\gamma+1)/\gamma$$

$$A = 2\gamma/(\gamma-1)$$

$$B = \left(\frac{2}{\gamma + 1}\right)^{1/(\gamma-1)}$$

$$C = \sqrt{\frac{2\gamma}{\gamma + 1}} = \sqrt{\frac{2}{E2}}$$

With,

$$r = p/P_t$$

there are:

$$\Phi = \sqrt{A(r^{E1} - r^{E2})}$$

$$r_c = (p/P_t)_c = B^{\gamma}$$

$$\Phi_c = C\ B$$

Enclosures: Fig. D(103)

Operating Instruction (1 page)

Program Listing (3 pages)

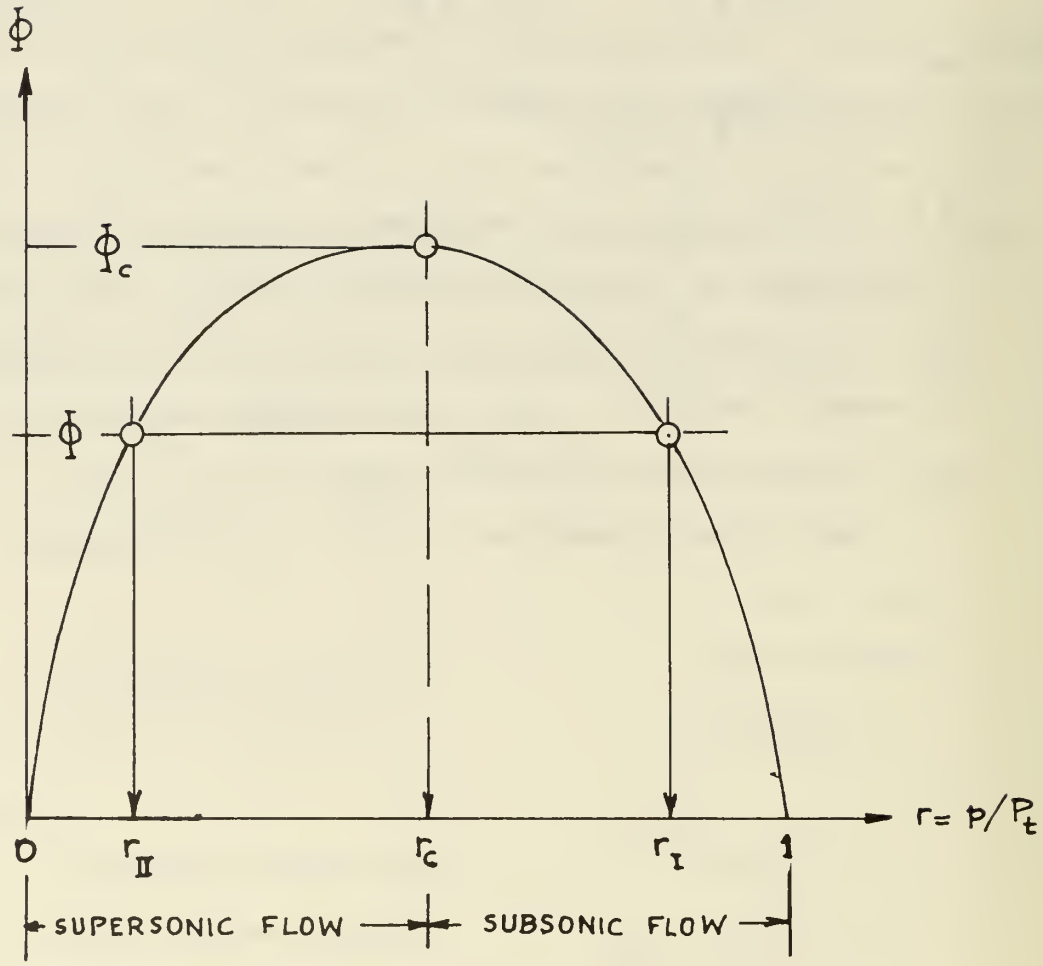

FIG. D(103) ISENTROPIC FLOW FUNCTION Φ

OPERATING INSTRUCTIONS PROGRAM No. 103

MONROE CALCULATOR 1655/6 WITH CARD READER CR-1

Set-Up: (RESET); (TO(0)); Depress (LOAD); Read Cards 1-3

Release (LOAD); (TO(0)); Depress (P); (RESUME)

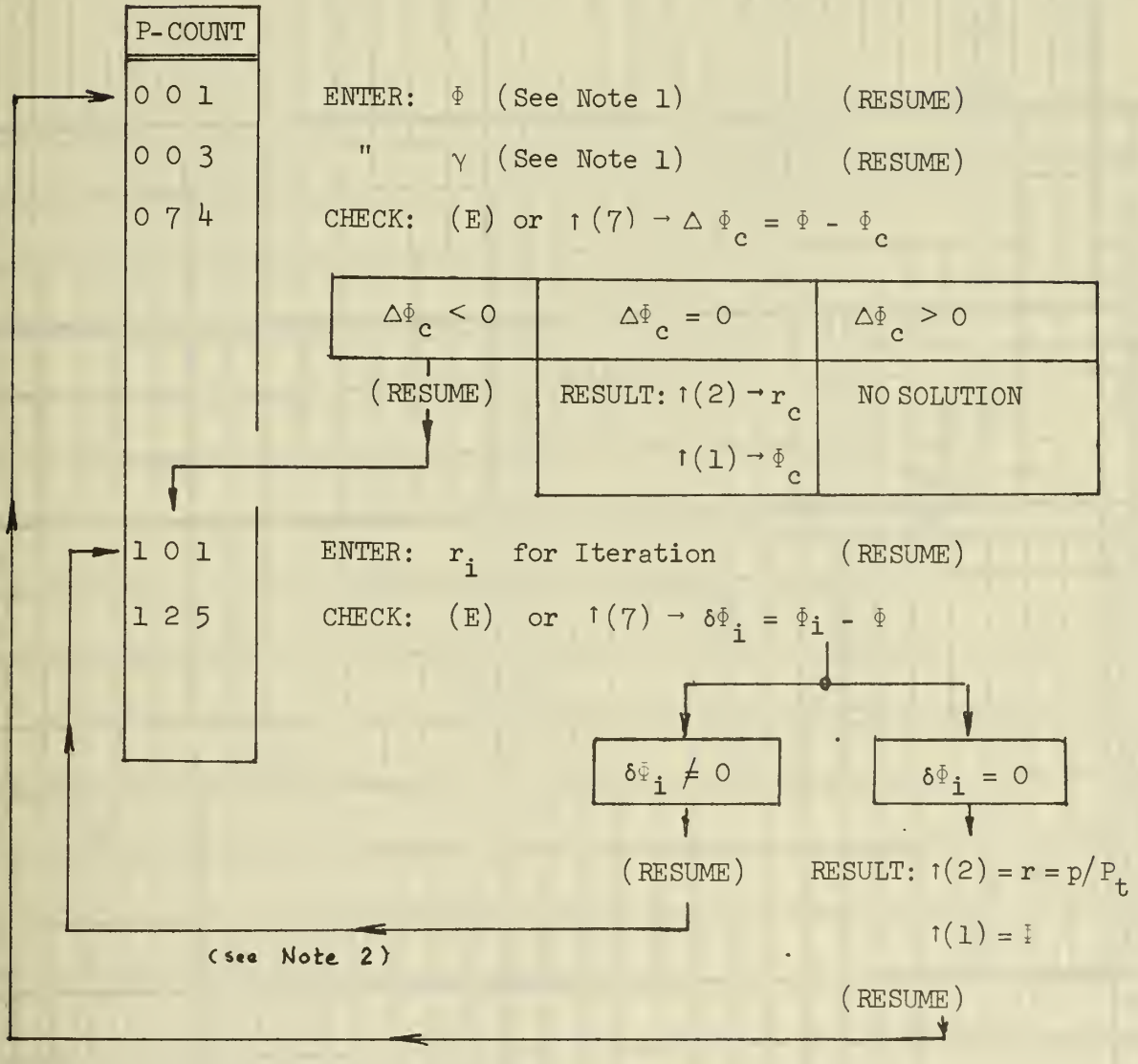

Note 1: If Program 103 is used immediately after Program 102:

Enter at P-Count 1: ↑(5) for Φ

Enter at P-Count 3: ↑(1) for γ

Note 2: Change of r_i (Reg. 2) to r_{i+1} for next iteration:

	SUBSONIC FLOW	SUPERSONIC FLOW
$\delta\Phi_i > 0$	$r_{i+1} > r_i$	$r_{i+1} < r_i$
$\delta\Phi_i < 0$	$r_{i+1} < r_i$	$r_{i+1} > r_i$

TURBO-PROPULSION LABORATORY, DEPT. OF AERONAUTICS, NPS ,
PROGRAM No. 103..... MONROE 1655 CALCULATOR
DETERMINATION OF PRESSURE RATIO FOR GIVEN ISENTROPIC ..... PAGE 1 OF 3.
FLOW FUNCTION FOR DIFFERENT GAMMA ..... DATE: AUG.72 BY: M.H.VA

BR PT	ADDRESS P COUNT	COMMAND	CODE	E	A	M	REGISTERS 0	1	2	3	4	5	6	7	8	9	X	Y	Z	NOTES
0	000	HALT	401	Φ				Φ												ENTER: Φ [A(5) of No. 102]
	001	STR(1)	440																	
	002	HALT	401	γ																ENTER: γ [A(2) of No. 102]
	003	STR(6)	445	γ									γ							
	004	+	060																	
	005	1	001																	
	006	÷	072	$\gamma+1$																
	007	2	002																	
	010	=	020	$\frac{\gamma+1}{2}$																
	011	INV	054	$\frac{2}{\gamma+1}$																
	012	STR(5)	444									$\frac{2}{\gamma+1}$								
	013	X	070																	
	014	RCL(6)	465	γ																
	015	=	020	$\frac{2\gamma}{\gamma+1}$																
	016	$\sqrt{}$	056	C																
	017	STR(4)	443								C									
	020	RCL(6)	465	γ																
	021	—	062																	
	022	1	001																	
	023	=	020	$\gamma-1$																
	024	INV	054	$\frac{1}{\gamma-1}$																
	025	STR(3)	442							$\frac{1}{\gamma-1}$										
	026	RCL(5)	464	$\frac{2}{\gamma+1}$																
	027	a^x	074																	
	030	RCL(3)	462	$\frac{1}{\gamma-1}$																
	031	X	070	B																
	032	STR(2)	441						B											
	033	RCL(4)	463	C																
	034	=	020	Φ_c																
	035	STR(0)	457				Φ_c													
	036	RCL(2)	461	B																
	037	a^x	074																	

TURBO-PROPULSION LABORATORY, DEPT. OF AERONAUTICS, NPS ,
PROGRAM No. ..103.... MONROE 1655 CALCULATOR

PAGE..2.OF..3.
DATE: .AUG.72. BY: ..M.H.V..

BR PT	ADDRESS P COUNT			COMMAND	CODE			E	A	M	0	1	2	3	4	5	6	7	8	9	X	Y	Z	NOTES
2	0	4	0	RCL(6)	4	6	5	γ			Φ_c	Φ	B	$\frac{1}{\gamma-1}$	C	$\frac{2}{\gamma+1}$	γ							
			1	=	0	2	0	r_c																
			2	STR(2)	4	4	1						r_c											
			3	RCL(3)	4	6	2	$\frac{1}{\gamma-1}$																
			4	×	0	7	0																	
			5	RCL(6)	4	6	5	γ																
			6	×	0	7	0																	
		4	7	2	0	0	2																	
		5	0	=	0	2	0	A																
			1	STR(5)	4	4	4									A								
			2	2	0	0	2																	
			3	÷	0	7	2																	
			4	RCL(6)	4	6	5	γ																
			5	=	0	2	0	E1																
			6	STR(4)	4	4	3								E1									
		5	7	RCL(6)	4	6	5	γ																
3		6	0	+	0	6	0																	
			1	1	0	0	1																	
			2	÷	0	7	2	$\gamma+1$																
			3	RCL(6)	4	6	5	γ																
			4	=	0	2	0	E2																
			5	STR(3)	4	4	2							E2										
			6	RCL(1)	4	6	0	Φ																
		6	7	−	0	6	2																	
		7	0	RCL(0)	4	7	7	Φ_c																
			1	=	0	2	0	$\Phi-\Phi_c$																
			2	STR(7)	4	4	6											$\Phi-\Phi_c$						
		7	3	HALT	4	0	1	$\Phi-\Phi_c$			Φ_c		r_c											CHECK: $\Phi-\Phi_c = ?$
			4	0			0																	
			5	0			0																	
			6	0			0																	
			7	0			0																	
								E	A	M	0	1	2	3	4	5	6	7	8	9	X	Y	Z	

TURBO-PROPULSION LABORATORY, DEPT. OF AERONAUTICS, NPS,
PROGRAM No. 103 .... MONROE 1655 CALCULATOR
PAGE 3 OF 3
DATE: AUG. 72 BY: M.H.V.

BR PT	ADDRESS P	COUNT	COMMAND	CODE	REGISTERS E	A	M	0	1	2	3	4	5	6	7	8	9	X	Y	Z	NOTES
4	1	0 0	HALT	4 0 1	r_i			Φ_c	Φ	r_c	E2	E1	A	γ							ENTER: r_i for iteration
		1	STR(2)	4 4 1	r_i					r_i											
		2	a^x	0 7 4																	
		3	RCL(3)	4 6 2	E2																
		4	=	0 2 0	r_i^{E2}																
		5	STR(0)	4 5 7				r_i^{E2}													
		6	RCL(2)	4 6 1	r_i																
1	0	7	a^x	0 7 4																	
1	1	0	RCL(4)	4 6 3	E1																
		1	−	0 6 2	r_i^{E1}																
		2	RCL(0)	4 7 7	r_i^{E2}																
		3	X	0 7 0																	
		4	RCL(5)	4 6 4	A																
		5	=	0 2 0																	
		6	$\sqrt{\ }$	0 5 6	Φ_i																
1	1	7	STR(0)	4 5 7				Φ_i													
5	1	2 0	−	0 6 2																	
		1	RCL(1)	4 6 0	Φ																
		2	=	0 2 0	Φ_i-Φ																
		3	STR(7)	4 4 6											Φ_i-	Φ					
1	2	4	HALT	4 0 1	Φ_i-Φ			Φ_i	Φ	r_i	E2	E1	A	γ	Φ_i-	Φ					CHECK: $\Phi_i = \Phi$?
		5	SFSNS	5 2 3																	Depr.(SENSE) if $\Phi_i = \Phi$
		6	SKF1	5 4 0																	
1	2	7	JUMP 00	6 0 0																	
1	3	0	TO(0)	7 4 0																	
		1																			
		2																			
		3																			
		4																			
		5																			
		6																			
		7																			
					E	A	M	0	1	2	3	4	5	6	7	8	9	X	Y	Z	

210

PROGRAM No. 104

MONROE CALCULATOR 1655/1656 WITH CARD READER CR-1

Description

This program can be used to determine the flow properties at the inlet of a radial compressor rotor provided the absolute velocity V_1 at this station is axial and uniform. The following quantities must be known:

$$\Phi_1 = \frac{\dot{w}\sqrt{(R_G/g)\ T_0}}{P_0\ A_1\ k_{B1}} = \frac{\dot{m}\sqrt{R_G\ g\ T_0}}{P_0\ A_1\ k_{B1}} = \text{dimensionless flow function}$$

p_1/P_0 = ratio of static and total pressure at inlet

U_2/a_0 = speed ratio

R_{1o}/R_2 = ratio of outer radius at inlet and outer rotor radius

$\gamma = c_p/c_v$ = specific heat ratio

The program determines:

T_1/T_0 = ratio of static and total temperatures at inlet

V_1/a_0 = ratio of absolute velocity at inlet and velocity of sound at T_0

W_{1o}/a_0 = ratio of relative velocity at R_{1o} and velocity of sound at T_0

β_{1o} = relative flow angle at R_{1o}

$M_{W1} = W_{1o}/a_1$ = Mach number of W_{1o}

Symbols:

$\dot{w}$ = weight flow rate (lbm/s)

$\dot{m}$ = mass flow rate (slug/s)

R_G = gas constant (ft-lb/(lbm,^oR)

g = 32.174 (ft/s^2)

T_0 = total inlet temperature (^oR)

P_0 = total inlet pressure (psia)

$A_1 = \pi\ (R_{1o}^2 - R_{1i}^2)$ = area of inlet eye of rotor ($in.^2$)

k_{Bl} = restriction factor (-)

p_1 = static pressure at inlet (psia)

T_1 = static temperature at inlet (^oR)

U_2 = peripheral rotor speed at outer radius R_2 (ft/s)

$$a_0 = \sqrt{g\ \gamma\ R_G\ T_0} \qquad \text{(ft/s)}$$

R_{1i} = inner radius at inlet eye (in.)

R_{1o} = outer radius at inlet eye (in.)

R_2 = outer radius of impeller (in.)

Although English units are used in the above list, the program can be used for any consistent system of units.

Derivations:

$$T_1/T_0 = (p_1/P_0)^{(\gamma-1)/\gamma}$$

$$\dot{w} = A_1\ k_{Bl}\ V_1\ \frac{p_1}{R_G\ T_1} = A_1\ k_{Bl}\ \frac{V_1}{a_0}\ \frac{(p_1/P_0)}{(T_1/T_0)}\ \frac{\sqrt{g\ \gamma\ R_G\ T_0}}{R_G}\ \frac{P_0}{T_0}$$

or

$$\Phi_1 = \sqrt{\gamma}\ \frac{V_1}{a_0}\ \frac{(p_1/P_0)}{(T_1/T_0)}$$

and

$$\frac{V_1}{a_0} = \frac{\Phi_1}{\sqrt{\gamma}}\ \frac{T_1/T_0}{(p_1/P_0)}$$

The peripheral speed U_{1o} at R_{1o} is

$$U_{1o} = (R_{1o}/R_2)\ U_2$$

For axial entry

$$W_{1o}^2 = V_1^2 + U_{1o}^2$$

$$\tan\beta_{1o} = U_{1o}/V_1$$

Thus

$$\frac{W_{1o}}{a_0} = \sqrt{\left(\frac{V_1}{a_0}\right)^2 + \left(\frac{U_2}{a_0}\right)^2 \left(\frac{R_{1o}}{R_2}\right)^2}$$

$$\tan\beta_{1o} = \frac{(R_{1o}/R_2)(U_2/a_0)}{(V_1/a_0)}$$

and

$$M_{W1} = \frac{W_{1o}}{a_1} = \frac{W_{1o}}{a_0}\ \frac{a_0}{a_1} = \frac{W_{1o}/a_0}{\sqrt{T_1/T_0}}$$

The flow angle β_{1o}', by taking account of the blade thickness, is

$$\tan\beta_{1o}' = \left(1 - \frac{t_u}{s}\right) \tan\beta_{1o} = k \tan\beta_{1o}$$

where

$$t_u = \frac{t}{\cos\beta_B}$$

$$s = \frac{2\pi R_{1o}}{Z_R}$$

where:

t = actual blade thickness at R_{1o}

β_B = blade inlet angle at R_{1o}

Z_R = number of rotor blade

Also

$$\cot\beta_{1o}' = \frac{(V_1/a_0)/k}{(R_{1o}/R_2)(U_2/a_0)}$$

with

$$k = 1 - \frac{t}{\cos\beta_B} \frac{Z_R}{2\pi R_{1o}}$$

If β_B is the blade angle at R_{1o}, the incidence angle i' is

$$i' = \beta_{1o}' - \beta_B$$

Enclosures: Operating Instructions (1 page)
Program Listing (3 pages)

OPERATING INSTRUCTIONS PROGRAM No. 104

MONROE CALCULATOR 1655/6 WITH CARD READER CR-1

Set-Up: (RESET); (TO(0)); Depress (LOAD); Read Cards 1-2

Release (LOAD); (TO(0)); Depress (P); (RESUME)

P-COUNT		
0 0 1	ENTER: Φ_1 (see note)	(RESUME)
0 0 3	" p_1/p_0 (see note)	(")
0 0 5	" γ	(")
0 3 6	" U_2/a_0	(")
0 4 0	" R_{10}/R_2	(")
0 6 7	" k	(")
0 7 6	" β_B	(")
1 0 1	RESULTS: ↑ (4) → (T_1/T_0)	
	↑ (3) → (V_1/a_0)	
	↑ (2) → (W_{1o}/a_0)	
	↑ (1) → β_{1o} (°)	
	↑ (0) → β'_{1o} (°)	
	↑ (5) → M_{W1}	
	↑ (7) → i'(°)	
	(RESUME)	

Note: If Program 104 is used immediately after Program 103, enter:

at P-Count 001: ↑ (1) to obtain Φ,

at P-Count 003: ↑ (2) to obtain p_1/P_0

TURBO-PROPULSION LABORATORY, DEPT. OF AERONAUTICS, NPS, PAGE 1 OF 3.

PROGRAM No. 104 ..... MONROE 1655 CALCULATOR ..... DATE: AUG. 72 BY: M.H. VAVRA

INLET CONDITIONS OF RADIAL COMPRESSOR WITH AXIAL INLET FLOW

BR PT	ADDRESS P	ADDRESS COUNT		COMMAND	CODE			REGISTERS E	A	M	0	1	2	3	4	5	6	7	8	9	X	Y	Z	NOTES
0	0	0	0	HALT	4	0	1																	ENTER: Φ_1 [↑(1) of PROG. 103]
			1	STR(6)	4	4	5										Φ_1							
	0	0	2	HALT	4	0	1																	ENTER: P_1/P_0 [↑(2) of PROG. 103]
			3	STR(5)	4	4	4									P_1/P_0								
	0	0	4	HALT	4	0	1	γ																ENTER: γ [↑(6) of PROG. 103]
			5	STR(3)	4	4	2	γ						γ										
			6	−	0	6	2																	
		0	7	1	0	0	1																	
		1	0	÷	0	7	2	$\gamma-1$																
			1	RCL(3)	4	6	2	γ																
			2	=	0	2	0	$\frac{\gamma-1}{\gamma}$																
			3	STR(4)	4	4	3								$\frac{\gamma-1}{\gamma}$									
			4	RCL(3)	4	6	2																	
			5	$\sqrt{\ }$	0	5	6	$\sqrt{\gamma}$																
			6	STR(3)	4	4	2							$\sqrt{\gamma}$										
		1	7	RCL(5)	4	6	4	P_1/P_0																
−		2	0	a^x	0	7	4																	
			1	RCL(4)	4	6	3	$\frac{\gamma-1}{\gamma}$																
			2	X	0	7	0	T_1/T_0																
			3	STR(4)	4	4	3	T_1/T_0							T_1/T_0									
			4	RCL(6)	4	6	5	Φ_1																
			5	÷	0	7	2																	
			6	RCL(3)	4	6	2	$\sqrt{\gamma}$																
		2	7	÷	0	7	2																	
		3	0	RCL(5)	4	6	4	P_1/P_0																
			1	X	0	7	0	V_1/a_0																
			2	STR(3)	4	4	2							V_1/a_0										
			3	=	0	2	0	$(V_1/a_0)^2$																
			4	STR(7)	4	4	6											$(V_1/a_0)^2$						
	0	3	5	HALT	4	0	1	U_2/a_0																ENTER: U_2/a_0
			6	X	0	7	0																	
	0	3	7	HALT	4	0	1	R_{10}/R_2																ENTER: R_{10}/R_2
								E	A	M	0	1	2	3	4	5	6	7	8	9	X	Y	Z	

215

M U V. 2/72/1

N 104

TURBO-PROPULSION LABORATORY, DEPT. OF AERONAUTICS, NPS, PAGE 2 OF 3
PROGRAM No. 104 ... MONROE 1655 CALCULATOR DATE: AUG. 72 BY: M.H.V.

BR PT	ADDRESS P	COUNT	COMMAND	CODE	E	A	M	0	1	2	3	4	5	6	7	8	9	X	Y	Z	NOTES
					REGISTERS																
2	0	4 0	×	070	C						V_1/a_0	T_1/T_0	P_1/P_0	Φ_1	$(V_1/a_0)^2$					·	$C = (U_2/a_0)(R_{10}/R_2)$
		1	STR(0)	457				C													
		2	+	060	C^2																
		3	RCL(7)	466	$(V_1/a_0)^2$																
		4	=	020	$W_1/a_0)^2$																
		5	√	056	W_1/a_0																
		6	STR(2)	441						W_1/a_0											
	4	7	RCL(3)	462	V_1/a_0																
	5	0	X	076																	
		1	RCL(0)	477																	
		2	=	020	$\beta_{10}{}^R$																
		3	R→°	046	$\beta_{10}{}^\circ$				β_{10}												
		4	STR(1)	440					β_{10}												
		5	RCL(4)	463	T_1/T_0																
		6	√	056	$\sqrt{T_1/T_0}$																
	5	7	÷	072																	
3	6	0	RCL(2)	462	W_1/a_0																
		1	=	020	$1/M_{W1}$																
		2	INV	054	M_{W1}																
		3	STR(5)	444									M_{W1}								
		4	RCL(3)	462	V_1/a_0																
		5	÷	072																	
	6	6	HALT	401	k																ENTER: k
	6	7	X	076	kV_1/a_0																
	7	0	RCL(0)	477	C																
		1	=	020	$\beta_{10}{}'^R$																
		2	R→°	046	$\beta_{10}{}'$																
		3	STR(0)	457	$\beta_{10}{}'$			β_{10}'													
		4	−	062																	
	7	5	HALT	401	β_B																ENTER: β_B
		6	=	020	i'																
	7	7	STR(7)	446											i'						
					E	A	M	0	1	2	3	4	5	6	7	8	9	X	Y	Z	

216

BR PT	ADDRESS P COUNT	COMMAND	CODE	REGISTERS	NOTES
4	1 0 0	HALT	4 0 1	0: β_{10}'; 1: β_{10}; 2: W_1/a_0; 3: V_1/a_0; 4: T_1/T_0; 5: M_{W1}; 6: Φ_1; 7: i_1	RESULTS
	1	TO(0)	7 4 0		

PROGRAM NO. 105

MONROE CALCULATOR 1655/6 WITH CARD READER CR-1

Description

In Ref. (a)* the so-called adiabatic rotor efficiency η_R of a radial compressor wheel is related to the wheel efficiency η_W and to the velocity ratio

$$\Psi = \frac{W_2}{W_{2is}}$$

which is a convenient measure to express the rotor losses for performance calculations.

From Eq. a(21); that is, Eq. (21) of Ref. (a),

$$\Psi = \frac{W_2/W_{1o}}{\left[1 - \eta_W + \eta_W(W_2/W_{1o})^2\right]^{\frac{1}{2}}}$$

From Eq. a(27)

$$\eta_W = \frac{\eta_R - C}{1 - C}$$

where, from Eq. a(25),

$$C = \frac{1 - (R_{1o}/R_2)^2}{(R_{1o}/R_2)^2 \cot^2\beta_{1o} + 2\mu\left(1 - \mu/[2 \sin^2 \alpha_2]\right)}$$

From Eq. II(5) of Ref. (a)

$$\frac{W_2}{W_{1o}} = \frac{\left[1 - 2\mu\left(1 - \mu/[2 \sin^2\alpha_2]\right)\right]^{\frac{1}{2}} \sin\beta_{1o}}{R_{1o}/R_2}$$

---

*See page 1 of Program 102

The following quantities are supposed to be known:

R_{1o}/R_2 = ratio of outer radius at impeller inlet and impeller exit radius

α_2 = absolute flow angle at impeller exit

μ = impeller slip factor

β_{1o} = relative flow angle at outer radius at impeller inlet

η_R = adiabatic rotor efficiency [see Eq. a(12)]

To be determined are:

η_W = wheel efficiency [see Eq. a(15)]

W_2/W_{1o} = ratio of relative velocity at impeller exit and relative velocity at outer radius at impeller inlet

$\Psi = W_2/W_{2is}$ = ratio of actual and isentropic relative velocities at impeller exit

The following quantities are used for the calculations

$$A = 2\mu \left(1 - \frac{\mu}{2 \sin^2 \alpha_2} \right)$$

$$B = \sqrt{1 - A}$$

Then

$$C = \frac{1 - (R_{1o}/R_2)^2}{(R_{1o}/R_2)^2 \cot^2 \beta_{1o} + A} = \frac{D}{E}$$

$$W_2/W_{1o} = \frac{B \sin \beta_{1o}}{R_{1o}/R_2}$$

$$F = \left[1 - \eta_W + \eta_W (W_2/W_{1o})^2 \right]^{\frac{1}{2}}$$

$$\Psi = \frac{W_2/W_{1o}}{F}$$

Enclosures: Operating Procedure (1 page)
Program Listing (3 pages)

OPERATING INSTRUCTIONS PROGRAM No. 105

MONROE CALCULATOR 1655/6 WITH CARD READER CR-1

Set-Up: (RESET); (TO(0)); Depress (LOAD); Read Cards 1-3

Release (LOAD); (TO(0)); Depress (P); (RESUME)

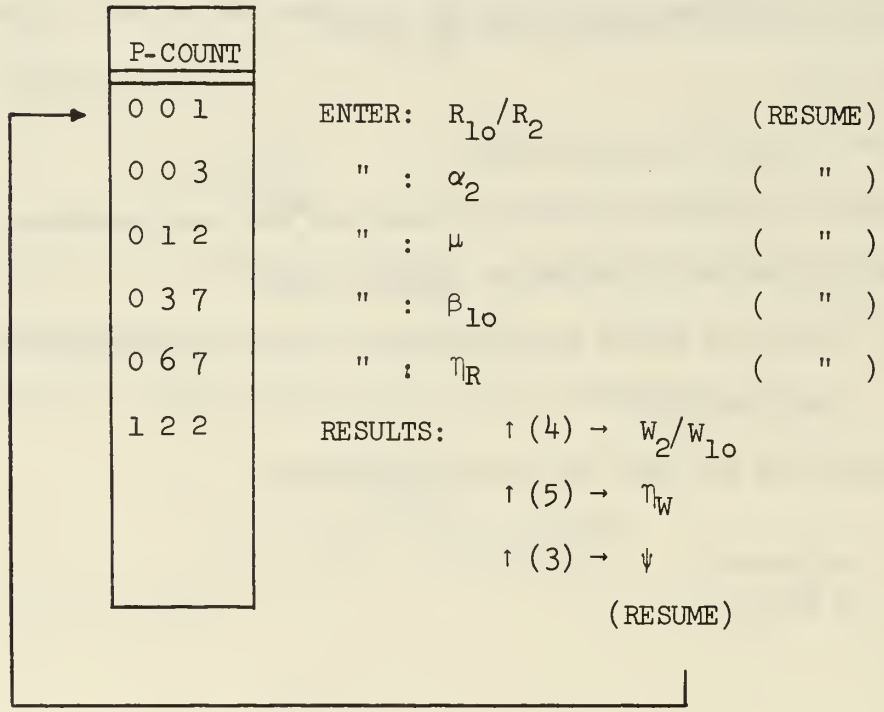

TURBO-PROPULSION LABORATORY, DEPT. OF AERONAUTICS, NPS ,
PROGRAM No. 105 ..... MONROE 1655 CALCULATOR
RELATION BETWEEN ROTOR EFFICIENCIES AND VELOCITY RATIO.....
OF RADIAL COMPRESSOR IMPELLER .....

DATE: AUG. 72 . BY: M.H. YAVRA

BR PT	ADDRESS P COUNT	COMMAND	CODE	REGISTERS E	A	M	0	1	2	3	4	5	6	7	8	9	X	Y	Z	NOTES
0	000	HALT	401	R_{10}/R_2																ENTER: R_{10}/R_2
	001	STR(6)	445										R_{10}/R_2							
	002	HALT	401	α_2																ENTER: α_2
	003	SIN/COS	040	$\sin\alpha_2$																
	004	x	070																	
	005	x	070	$\sin^2\alpha_2$																
	006	2	002																	
	007	=	020	$2\sin^2\alpha_2$																
	010	STR(1)	440					$2\sin^2\alpha_2$												
	011	HALT	401																	ENTER: μ
	012	STR(2)	441	μ					μ											
	013	÷	072																	
	014	RCL(1)	460	$2\sin^2\alpha_2$																
	015	−	062	$\frac{\mu}{2\sin^2\alpha_2}$																
	016	1	001																	
	017	x	070																	
1	020	2	002																	
	021	x	070																	
	022	RCL(2)	461	μ																
	023	+	060	$-A$																
	024	1	001																	
	025	−	062	$1-A$																
	026	STR(1)	440					$1-A$												
	027	1	001																	
	030	=	020	$-A$																
	031	CHSGN	013	$+A$																
	032	STR(2)	441							A										
	033	RCL(1)	460	$1-A$																
	034	√	056	B																
	035	STR(1)	440					B												
	036	HALT	401	β_{10}																ENTER: β_{10}
	037	SIN/COS	040	$\sin\beta_{10}$					B	A			R_{10}/R_2							

TURBO-PROPULSION LABORATORY, DEPT. OF AERONAUTICS, NPS, PAGE 2 OF 3.
PROGRAM No. 105 MONROE 1655 CALCULATOR DATE: AUG. 72 BY: M.H.Y.

BR PT	ADDRESS P	COUNT	COMMAND	CODE	REGISTERS E	A	M	0	1	2	3	4	5	6	7	8	9	X	Y	Z	NOTES
2	0	4 0	STR(3)	442	$\sin\beta_{10}$				B	A	$\sin\beta_{10}$			R_{10}/R_2							
		1	2.FUNC	036	$\cos\beta_{10}$																
		2	÷	072																	
		3	RCL(3)	462	$\sin\beta_{10}$																
		4	×	070	$\cot\beta_{10}$																
		5	RCL(6)	465	R_{10}/R_2																
		6	×	070	$\frac{R_{10}}{R_2}\cot\beta_{10}$																
	4	7	+	060	$(R_{10}/R_2)\cot\beta_{10}]^2$																
	5	0	RCL(2)	461	A																
		1	=	020	E																
		2	STR(4)	443								E									
		3	RCL(6)	465	R_{10}/R_2																
		4	×	070																	
		5	−	062	$(R_{10}/R_2)^2$																
		6	1	001																	
	5	7	÷	072	−D																
3	6	0	RCL(4)	463	E																
		1	+	060	−C																
		2	STR(4)	443								−C									
		3	1	001																	
		4	=	020	1−C																
		5	STR(5)	444									1−C								
0	6	6	HALT	401	η_R																ENTER: η_R
	6	7	+	060																	
	7	0	RCL(4)	463	−C																
		1	÷	072	η_R−C																
		2	RCL(5)	464	1−C																
		3	=	020	η_W																
		4	STR(5)	444									η_W								
		5	RCL(1)	460	B																
		6	×	070																	
	7	7	RCL(3)	462	$\sin\beta_{10}$																
					E	A	M	0	1	2	3	4	5	6	7	8	9	X	Y	Z	

TURBO-PROPULSION LABORATORY, DEPT. OF AERONAUTICS, NPS ,
PROGRAM No. ...105... MONROE 1655 CALCULATOR

DATE: AUG.72 BY: M.H.V.

BR PT	ADDRESS P COUNT	COMMAND	CODE	E	A	M	0	1	2	3	4	5	6	7	8	9	X	Y	Z	NOTES
4	1 0 0	÷	0 7 2					B	A	$\sin\beta_{10}$	$-C$	η_w	R_{10}/R_2							
	1	RCL(6)	4 6 5	R_{10}/R_2																
	2	×	0 7 0	W_2/W_{10}																
	3	STR(4)	4 4 3								W_2/W_{10}									
	4	×	0 7 0	$(W_2/W_{10})^2$																
	5	RCL(5)	4 6 4	η_w																
	6	−	0 6 2																	
	1 0 7	RCL(5)	4 6 4	η_w																
	1 1 0	+	0 6 0																	
	1	1	0 0 1																	
	2	=	0 2 0	F^2																
	3	√	0 5 6	F																
	4	÷	0 7 2																	
	5	RCL(4)	4 6 3	W_2/W_{10}																
	6	=	0 2 0	$1/\psi$																
	1 1 7	· INV	0 5 4	ψ																
5	1 2 0	STR(3)	4 4 2							ψ										
	1 2 1	HALT	4 0 1	ψ						ψ	$\frac{W_2}{W_{10}}$	η_w								RESULTS:
	2	TO(0)	7 4 0																	
	3																			
	4																			
	5																			
	6																			
	7																			
	0																			
	1																			
	2																			
	3																			
	4																			
	5																			
	6																			
	7																			

PROGRAM NO. 106

MONROE CALCULATOR 1655/6 WITH CARD READER CR-1

Description

This program is used to determine the flow properties at the discharge of a radial compressor wheel with the following equations of Ref. (a)*.

Eq. I (6): $$\frac{T_{t2}}{T_0} = 1 + (\gamma-1)\,\mu\left(\frac{U_2}{a_0}\right)^2$$

Eq. I (7): $$\frac{T_2}{T_0} = 1 + (\gamma-1)\,\mu\left(\frac{U_2}{a_0}\right)^2\left[1 - \frac{\mu}{2\sin^2\alpha_2}\right]$$

Eq. I (8): $$\frac{T_2'}{T_0} = 1 + (\gamma-1)\,\mu\left(\frac{U_2}{a_0}\right)^2\left[\frac{1}{\psi^2}\left(1 - \frac{\mu}{2\sin^2\alpha_2}\right) - \frac{1}{2\mu}\left(\frac{1}{\psi^2} - 1\right)\right]$$

Eq. I(20): $$\frac{p_2}{p_0} = \left(\frac{T_2'}{T_0}\right)^{\gamma/(\gamma-1)}$$

Eq. I(19): $$\frac{p_{t2}}{p_0} = \left(\frac{p_2}{p_0}\right)\left(\frac{T_{t2}/T_0}{T_2/T_0}\right)^{\gamma/(\gamma-1)}$$

Eq. II(6): $$M_{v2} = \frac{\mu\ U_2/a_0}{\sin\alpha_2\sqrt{T_2/T_0}}$$

Input data are:

$$\frac{U_2}{a_0} = \frac{\text{peripheral speed of impeller at discharge}}{\text{velocity of sound at total inlet temperature } T_0}$$

α_2 = absolute flow angle at impeller exit

μ = rotor slip factor

* See page 1 of Program 102

$$\gamma = c_p/c_v$$

$$\psi = W_2/W_{2is} \quad = \text{velocity ratio}$$

The calculated values are :

T_0 = total temperature at impeller inlet

P_0 = total pressure at impeller inlet

T_2 = static temperature at impeller exit

p_2 = static pressure at impeller exit

T_{t2} = total temperature at impeller exit

P_{t2} = total pressure at impeller exit

M_{V2} = Mach number of absolute velocity V_2 at impeller exit = $V_2/\sqrt{g\gamma R_G T_2}$

The following quantities are established during the calculations

$$A = (\gamma-1)\ \mu \left(\frac{U_2}{a_0}\right)^2$$

$$B = 1 - \frac{\mu}{2 \sin^2 \alpha_2}$$

$$C = \frac{1}{2\mu}\left(\frac{1}{\psi^2} - 1\right)$$

$$D = \frac{\mu^2\left(U_2/a_0\right)^2}{\sin^2 \alpha_2}$$

$$E = \gamma/(\gamma-1)$$

Then:

$$\frac{T_{t2}}{T_0} = 1 + A$$

$$\frac{T_2}{T_0} = 1 + AB$$

$$\frac{T_2'}{T_0} = 1 + \left[A \frac{1}{\Psi^2} B - C\right]$$

$$M_{V2} = \sqrt{\frac{D}{T_2/T_0}}$$

Enclosures: Operating Instructions (1 page)

Program Listing (3 pages)

OPERATING INSTRUCTIONS PROGRAM No. 106

MONROE CALCULATOR 1655/6 WITH CARD READER CR-1

Set-Up: (RESET); (TO(0)); Depress (LOAD); Read Cards 1-3

Release (LOAD); (TO(0)); Depress (P); (RESUME)

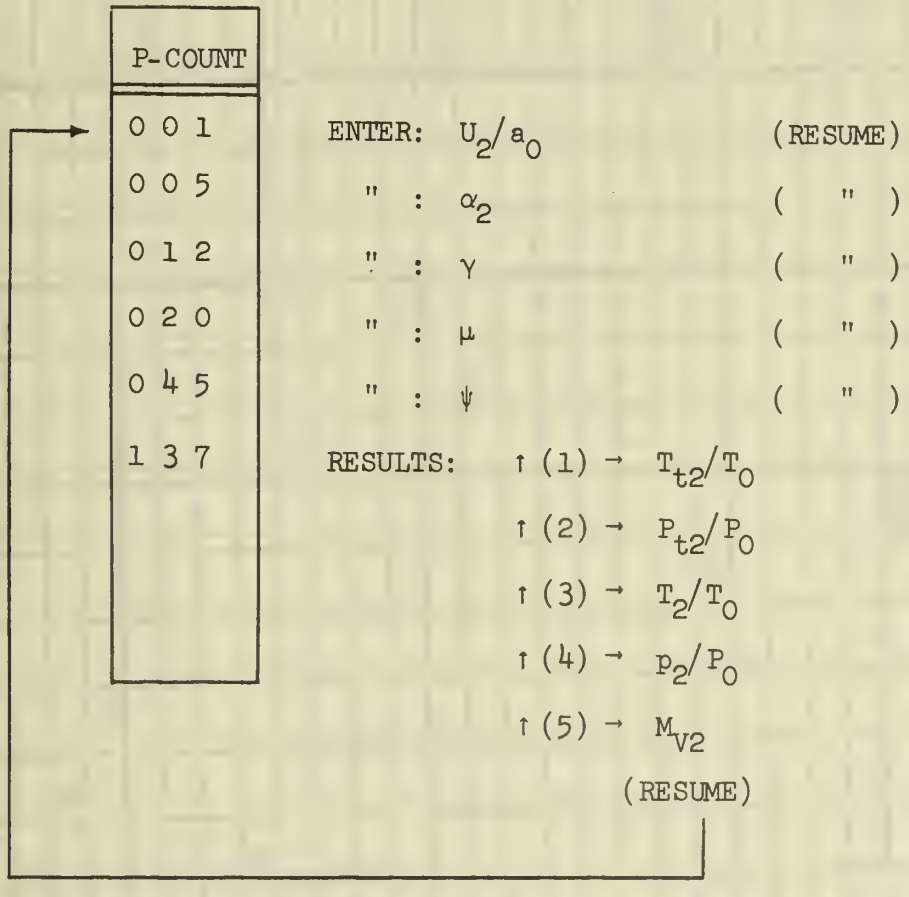

Note: N-switch must be in "Down" position.

TURBO-PROPULSION LABORATORY, DEPT. OF AERONAUTICS, NPS,
PROGRAM No. 106 ..... MONROE 1655 CALCULATOR
CONDITIONS AT DISCHARGE OF IMPELLER OF RADIAL COMPRESSOR.....
PAGE 1 OF 3.
DATE: AUG. 72
BY: M.H. VA

BR PT	ADDRESS P	ADDRESS COUNT		COMMAND	CODE			REGISTERS E	A	M	0	1	2	3	4	5	6	7	8	9	X	Y	Z	NOTES
0	0	0	0	HALT	4	0	1	U_2/a_0																ENTER: U_2/a_0
			1	X	0	7	0																	
			2	=	0	2	0	$(U_2/a_0)^2$																
	0		3	STR(6)	4	4	5										$(U_2/a_0)^2$							
	0	0	4	HALT	4	0	1	α_2																ENTER: α_2
			5	SIN/COS	0	4	0	$\sin\alpha_2$																
			6	X	0	7	0																	
			7	=	0	2	0	$\sin^2\alpha_2$																
	0	1	0	STR(5)	4	4	4									$\sin^2\alpha_2$								
	0	1	1	HALT	4	0	1	γ																ENTER: γ
			2	STR(7)	4	4	6	γ										γ						
			3	−	0	6	2																	
			4	1	0	0	1																	
			5	X	0	7	0	$\gamma-1$																
			6	STR(8)	4	4	7												$\gamma-1$					
	0	1	7	HALT	4	0	1	μ																ENTER: μ
1	0	2	0	STR(9)	4	5	0													μ				
			1	X	0	7	0	$(\gamma-1)/\mu$																
			2	RCL(6)	4	6	5	$(U_2/a_0)^2$																
			3	=	0	2	0	A																
			4	STR(1)	4	4	0					A												
			5	RCL(7)	4	6	6	γ																
			6	÷	0	7	2																	
			7	RCL(8)	4	6	7	$\gamma-1$																
	0	3	0	=	0	2	0	E																
			1	STR(2)	4	4	1						E											
			2	RCL(9)	4	7	0	μ																
			3	÷	0	7	2																	
			4	2	0	0	2																	
			5	÷	0	7	2	$\mu/2$																
			6	RCL(5)	4	6	4	$\sin^2\alpha_2$																
	0	3	7	−	0	6	2																	
								E	A	M	0	1	2	3	4	5	6	7	8	9	X	Y	Z	

TURBO-PROPULSION LABORATORY, DEPT. OF AERONAUTICS, NPS,
PROGRAM No. 106 ... MONROE 1655 CALCULATOR
PAGE 2 OF 3.
DATE: AUG. 72 ... BY: M.H.V.

BR PT	ADDRESS P	ADDRESS COUNT	COMMAND	CODE	E	A	M	0	1	2	3	4	5	6	7	8	9	X	Y	Z	NOTES
2	0	4 0	f	001					A	E			$\sin^2\alpha_2$	$(U_2/a_0)^2$	χ	$\gamma-1$	μ				
		1	=	020	-B																
		2	CHSGN	013	B																
		3	STR(3)	442							B										
	0	4 4	HALT	401	ψ																ENTER: ψ
		5	INV	054	$1/\psi$																
		6	×	070																	
		7	−	062	$1/\psi^2$																
	0	5 0	STR(7)	446											$1/\psi^2$						
		1	1	001																	
		2	÷	072	$1/\chi^2-1$																
		3	2	002																	
		4	÷	072																	
		5	RCL(9)	470	μ																
229		6	=	020	C																
		7	STR(4)	443								C									
3	0	6 0	RCL(9)	470	μ																
		1	×	070																	
		2	×	070	μ^2																
		3	RCL(6)	465	$(U_2/a_0)^2$																
		4	÷	072																	
		5	RCL(5)	464	$\sin^2\alpha_2$																
		6	=	020	D																
		7	STR(5)	444									D								
	0	7 0	RCL(7)	466	$1/\chi^2$																
		1	×	070																	
		2	RCL(3)	462	B																
		3	−	062																	
		4	RCL(4)	463	C																
		5	×	070																	
		6	RCL(1)	460	A																
	0	7 7	+	060																	
					E	A	M	0	1	2	3	4	5	6	7	8	9	X	Y	Z	

TURBO-PROPULSION LABORATORY, DEPT. OF AERONAUTICS, NPS ,
PROGRAM No. 106 MONROE 1655 CALCULATOR

DATE: AUG. 72 BY: M.H.V.

BR PT	P	ADDRESS COUNT	COMMAND	CODE	E	A	M	0	1	2	3	4	5	6	7	8	9	X	Y	Z	NOTES
					REGISTERS																
4		00	1	001					A												
		01	a^x	074	T_2'/T_0																
		02	RCL(2)	461	E																
		03	=	020	P_2/P_0																
		04	STR(4)	443								P_2/P_0									
		05	RCL(1)	460	A																
		06	X	070																	
		07	RCL(3)	462	B																
1	10	08	+	060																	
		11	−	001																	
		12	=	020	T_2/T_0																
		13	STR(3)	442	T_2/T_0						T_2/T_0										
		14	INV	054	T_0/T_2																
		15	X	070																	
		16	RCL(5)	464	D																
		17	=	020																	
1	20	5	$\sqrt{\ }$	056	M_{12}																
		21	STR(5)	444									M_{12}								
		22	−	001	1																
		23	+	060																	
		24	RCL(1)	460	A																
		25	÷	072	T_{t2}/T																
		26	STR(1)	440					T_{t2}/T_0												
		27	RCL(3)	462	T_2/T_0																
1	30	0	a^x	074	T_{t2}/T_2																
		31	RCL(2)	461	E																
		32	X	070																	
		33	RCL(4)	463	P_2/P_0																
		34	=	020	P_{t2}/P_0																
		35	STR(2)	441						P_{t2}/P_0											
1	36		HALT	401					$\frac{T_{t2}}{T_0}$	$\frac{P_{t2}}{P_0}$	$\frac{T_2}{T_0}$	$\frac{P_2}{P_0}$	M_{12}								RESULTS
		37	TO(0)	740																	

PROGRAM NO. 108

MONROE CALCULATOR 1655 WITH CARD READER CR-1

Description

This program calculates Eq. C(17) of Appendix C.

$$(\dot{m})^* = 2k_{B1}\sqrt{\gamma}\int_{0.287}^{0.541}\left(\frac{R_1}{R_2}\right) X \left(\frac{V_{1o}}{a_0}\right)\left[1 - \frac{\gamma-1}{2}\left(X\frac{V_{1o}}{a_0}\right)^2\right]^{1/(\gamma-1)} d\left(\frac{R_1}{R_2}\right)$$

where $X = \dfrac{V_1/a_0}{V_{1o}/a_0}$

For five equal increments of R_1/R_2 between 0.287 and 0.541 the ratio X can be calculated from Eqs. C(15) and C(16). The following table gives the data that have to be entered in the program in the order required, starting from i = 0. The quantity z_i is used in the process of integration.

i	0	1	2	3	4	5
X_i	0.5081	0.5749	0.6544	0.7493	0.8631	1.0
$(R_1/R_2)_i$	0.287	0.3378	0.3886	0.4394	0.4902	0.541
z_i	2	1	1	1	1	2

With $\Delta(R_1/R_2) = (0.541 - 0.287)/5 = 0.0508$ and

$$N_i = \left(\frac{R_1}{R_2}\right)_i X_i \left[\frac{V_{1o}}{a_0}\right]\left[1 - \frac{\gamma-1}{2}\left(X_i\frac{V_{1o}}{a_0}\right)^2\right]^{1/(\gamma-1)}$$

there is with the trapezoidal method of integration

$$\int_{0.287}^{0.541} = \left(N_0/2 + N_1 + N_2 + N_3 + N_4 + N_5/2\right)\Delta\left(\frac{R_1}{R_2}\right)$$

or

$$S = \int_{0.287}^{0.541} = 0.0508 \sum_{i=0}^{5} N_i/z_i$$

Hence

$$(m)^* = 2k_{Bl} \sqrt{\gamma}\, S$$

Further, from Eq. C(18)

$$\cot \beta_{1o} = \frac{V_{1o}/a_0}{(U_2/a_0)\,(R_{1o}/R_2)} = \frac{V_{1o}/a_0}{0.44903}$$

From Eq. C(19)

$$M_{W1} = \frac{0.44903}{\left[\sin^2\beta_{1o} - \frac{\gamma-1}{2}\,(0.44903)^2 \cos^2\beta_{1o}\right]^{\frac{1}{2}}}$$

The program can be used for different values of γ, k_{Bl}, U_2/a_0 and R_{1o}/R_2. It can be adapted also to integrations with more than five equal increments between R_{1i}/R_2 and R_{1o}/R_2. In this case the increment $\Delta(R_1/R_2)$ must be entered in addresses 75 to 103 (octal).

Enclosures: Operating Instruction (1 page)

Program Listing (4 pages)

OPERATING INSTRUCTIONS PROGRAM No. 108

MONROE CALCULATOR 1655/6 WITH CARD READER CR-1

Set-Up: (RESET); (TO(0)); Depress (LOAD); Read Cards 1-4;

Release (LOAD); (TO(0)); Depress (P); (RESUME)

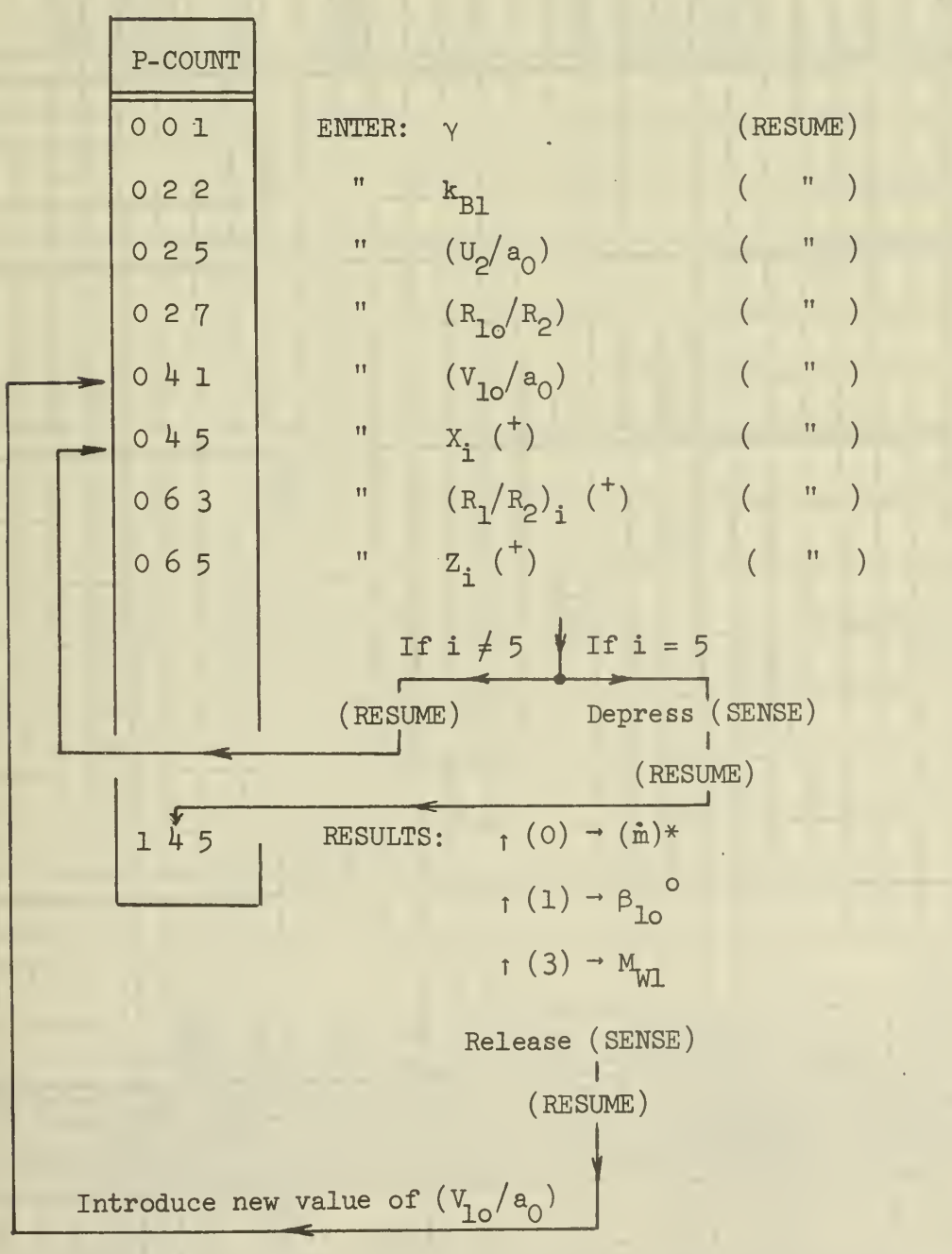

(+) Enter val with equal indices i of Table on p. 1 of Program Descripti sequentially for i = 0, 1, 2, 3, 4, 5.

TURBO-PROPULSION LABORATORY, DEPT. OF AERONAUTICS, NPS, PAGE 1 OF 4.

PROGRAM No. 108..... MONROE 1655 CALCULATOR DATE: 8/4/72

MASS FLOW RATE AT INDUCER INLET AS FUNCTION OF $V_{1\sigma}/a_0$ ..... BY: M.H. Vavra

EQ.: C(17) OF HYBRID COMPRESSOR DESIGN REPORT.....

BR PT	ADDRESS P	ADDRESS COUNT		COMMAND	CODE			REGISTERS E	A	M	0	1	2	3	4	5	6	7	8	9	X	Y	Z	NOTES
0	0	0	0	HALT	4	0	1	γ																ENTER: γ
			1	STR (1)	4	4	0	γ				γ												
			2	-	0	6	2																	
			3	1	0	0	1																	
			4	÷	0	7	2	$\gamma-1$																
			5	STR(2)	4	4	1						$\gamma-1$											
			6	2	0	0	2																	
		0	7	=	0	2	0	$\frac{\gamma-1}{2}$																
		1	0	STR(5)	4	4	4									$\frac{\gamma-1}{2}$								
			1	RCL(2)	4	6	1	$\gamma-1$																
			2	INV	0	5	4	$\frac{1}{\gamma-1}$																
			3	STR (4)	4	4	3								$\frac{1}{\gamma-1}$									
			4	RCL(1)	4	6	0	γ																
			5	$\sqrt{\ }$	0	5	6	$\sqrt{\gamma}$																
			6	x	0	7	0																	
		1	7	2	0	0	2																	
-		2	0	x	0	7	0	$2\sqrt{\gamma}$																
		2	1	HALT	4	0	1	k																ENTER: $k_{B1} = k$
			2	=	0	2	0	$2k\sqrt{\gamma}$																
			3	STR (6)	4	4	5										$2k\sqrt{\gamma}$							
		2	4	HALT	4	0	1	U_2/a_0																ENTER: U_2/a_0
			5	x	0	7	0																	
		2	6	HALT	4	0	1	R_{10}/R_2																ENTER: R_{10}/R_2
		2	7	=	0	2	0	b																$b = (U_2/a_0)(R_{10}/R_2)$
		3	0	STR(2)	4	4	1						b											
			1	0			0																	
			2	0			0																	
			3	0			0																	
			4	0			0																	
			5	0			0																	
			6	0			0																	
		3	7	STR (0)	4	5	7				0	γ	b.		$\frac{1}{\gamma-1}$	$\frac{\gamma-1}{2}$	$2k\sqrt{\gamma}$							Clears (0)
								E	A	M	0	1	2	3	4	5	6	7	8	9	X	Y	Z	

234

M U N 9/62

TURBO-PROPULSION LABORATORY, DEPT. OF AERONAUTICS, NPS, PROGRAM No. 108 MONROE 1655 CALCULATOR — PAGE 2 OF 4 — DATE: 8/4/72 — BY: M.H.V.

BR PT	ADDRESS P	COUNT	COMMAND	CODE	E	A	M	0	1	2	3	4	5	6	7	8	9	X	Y	Z	NOTES
2	0	4 0	HALT	4 0 1	v			0	γ	b		$\frac{1}{\gamma-1}$	$\frac{\gamma-1}{2}$	$2k\sqrt{\gamma}$							ENTER: $(V_{1_0}/a_0) = v$
		1	STR(1)	4 4 0					v												
	4	2	RCL(1)	4 6 0	v																
		3	X	0 7 0																	
	4	4	HALT	4 0 1	X_i																ENTER: (X_i); $i=0\to 5, 1$
		5	X	0 7 0	$v X_i$																
		6	STR(3)	4 4 2							$v X_i$										
	4	7	X	0 7 0	$(v X_i)^2$																
	5	0	RCL(5)	4 6 4	$\frac{\gamma-1}{2}$																
		1	=	0 2 0	c_i																$c_i = \frac{\gamma-1}{2}(v X_i)^2$
		2	CHSGN	0 1 3	$-c_i$																
		3	+	0 6 0																	
		4	1	0 0 1																	
		5	a^x	0 7 4	$1-c_i$																
		6	RCL(4)	4 6 3	$\frac{1}{\gamma-1}$																
235	5	7	X	0 7 0	q_i																$q_i = (1-c_i)^{1/(\gamma-1)}$
3	6	0	RCL(3)	4 6 2	$v X_i$																
		1	X	0 7 0																	
	6	2	HALT	4 0 1	$(R_1/R_2)_i$																ENTER: $(R_1/R_2)_i$; $i=0\to 5, 1$
		3	÷	0 7 2	N_i																
	6	4	HALT	4 0 1	z_i																ENTER: z_i; $i=0\to 5, 1$
		5	+	0 6 0	N_i/z_i																If $i=5$, depress [SENSE]
		6	RCL(0)	4 7 7	◐																◐ $\sum_{1}^{i-1}(N_i/z_i)$
	6	7	=	0 2 0	◎																◎ $\sum_{1}^{i}(N_i/z_i)$
	7	0	STR(0)	4 5 7	◎																
		1	SFSNS	5 2 3																	
		2	SKF1	5 4 0																	
		3	JUMP 42	6 4 2																	
		4	X	0 7 0	$\sum_{1}^{5}(N_i/z_i)$																
	7	5	•	0 1 2																	
	7	6	0	0 0 0																	$\Delta R/R_2 = .050800$
	7	7	5	0 0 5					v	b	$v X_i$	$\frac{1}{\gamma-1}$	$\frac{\gamma-1}{2}$	$2k\sqrt{\gamma}$							
					E	A	M	0	1	2	3	4	5	6	7	8	9	X	Y	Z	

M.H.V. 2/24/72.

TURBO-PROPULSION LABORATORY, DEPT. OF AERONAUTICS, NPS, PAGE 3 OF 4
PROGRAM No. ..108.... MONROE 1655 CALCULATOR DATE: 8/4/72 BY: M.H.V

BR PT	ADDRESS P	ADDRESS COUNT	COMMAND	CODE	E	A	M	0	1	2	3	4	5	6	7	8	9	X	Y	Z	NOTES
4	1	0 0	0	0					v	b	vX_i	$\frac{1}{\gamma-1}$	$\frac{\gamma-1}{2}$	$2k\sqrt{\gamma}$							
		1	8	0 1 0																	$\Delta R/R_2 = .050800$
		2	0	0																	
	1	0 3	0	0	5																
		4	×	0 7 0	$\Sigma(N_i/\beta_i)\frac{\Delta R}{R_2}$																
		5	RCL(6)	4 6 5	$2k\sqrt{\gamma}$																
		6	=	0 2 0	$(\dot{m})^*$																
	1	0 7	STR(0)	4 5 7				$(\dot{m})^*$													
	1	1 0	RCL(1)	4 6 0	v																
		1	÷	0 7 2																	
		2	RCL(2)	4 6 1	b																
		3	𝒳	0 7 6	$\cot\beta_{10}$																
		4	1	0 0 1																	
		5	=	0 2 0	$\beta_{10}{}^R$																
236		6	R→°	0 4 6	$\beta_{10}{}^\circ$																
	1	1 7	STR(1)	4 4 0	$\beta_{10}{}^\circ$				$\beta_{10}{}^\circ$												
5	1	2 0	SIN/COS	0 4 0	$\sin\beta_{10}$																
		1	×	0 7 0																	
		2	=	0 2 0	$\sin^2\beta_{10}$																
		3	STR(3)	4 4 2							$\sin^2\beta_{10}$										
		4	2. FUNC	0 3 6	$\cos\beta_{10}$																
		5	×	0 7 0																	
		6	RCL(2)	4 6 1	b																
	1	2 7	×	0 7 0	$b\cos\beta_{10}$																
	1	3 0	×	0 7 0	$b^2\cos^2\beta_{10}$																
		1	RCL(5)	4 6 4	$\frac{\gamma-1}{2}$																
		2	−	0 6 2	d																$d = \frac{\gamma-1}{2} b^2\cos^2\beta_{10}$
		3	RCL(3)	4 6 2	$\sin^2\beta_{10}$																
		4	=	0 2 0	f																$f = d - \sin^2\beta_{10}$
		5	CHSGN	0 1 3	$-f$																$-f = \sin^2\beta_{10} - \frac{\gamma-1}{2} b^2\cos^2\beta_{10}$
		6	√	0 5 6	$\sqrt{-f}$																
	1	3 7	INV	0 5 4	$1/\sqrt{-f}$			$(\dot{m})^*$	β_{10}°	b	$\sin^2\beta_{10}$	$\frac{1}{\gamma-1}$	$\frac{\gamma-1}{2}$	$2k\sqrt{\gamma}$							
					E	A	M	0	1	2	3	4	5	6	7	8	9	X	Y	Z	

TURBO-PROPULSION LABORATORY, DEPT. OF AERONAUTICS, NPS ,
PROGRAM No. 108 ..... MONROE 1655 CALCULATOR

DATE: 8/4/72 BY: M.H.V.

BR	ADDRESS	COMMAND	CODE	E	A	M	0	1	2	3	4	5	6	7	8	9	X	Y	Z	NOTES
6	1 4 0	x	0 7 0																	
	1	RCL(2)	4 6 1	b			$(\dot{m})^*$	β_{10}	b	$\sin^2\beta_{10}$	$\frac{1}{\gamma-1}$	$\frac{\gamma-1}{2}$	$2k\sqrt{\theta}$							
	2	=	0 2 0	M_{W1}																
	3	STR(3)	4 4 2							M_{W1}										RESULTS
1	4 4	HALT	4 0 1				$(\dot{m})^*$	β_{10}		M_{W1}										
	5	0	0																	Clears (0)
	6	STR(0)	4 5 7																	
1	4 7	TO(2)	7 4 2																	To repeat with new value γ_{10}/a_0
	0																			
	1																			
	2																			
	3																			
	4																			
	5																			
	6																			
	7																			
	0																			
	1																			
	2																			
	3																			
	4																			
	5																			
	6																			
	7																			

REGISTERS

M.H.V. 2/25/72

PROGRAM No. 109

MONROE CALCULATOR 1655 WITH CARD READER CR-1

Description

This program calculates the flow conditions after an axial row of blades for known entrance conditions. Figure D(109)1 shows such as cascade located between station (e) and station (d). It is assumed that the conditions at the mean radii R_{me} and R_{md}, at entrance and discharge, respectively, are representative of the average flow properties ahead of and after the cascade. The effective flow area at station (e) is taken as

$$A_e \, k_{Be} = 2\pi \, R_{me} \, h_e \, k_{Be}$$

where k_{Be} is a blockage factor that takes account of the boundary layers at the inner and outer wall contours. Similarly, at discharge station (d)

$$A_d \, k_{Bd} = 2\pi \, R_{md} \, h_d \, k_{Bd}$$

Figure D(109)2 shows a diffusor cascade of a subsonic axial compressor where the flow angle is reduced from α_e to α_d. Figure D(109)4 shows a stator of a turbine blading where the subsonic velocity V_e ahead of the row is accelerated to a supersonic velocity V_d because of the converging-diverging area change of the flow channel. Figures D(109)3 and 5 represent the flow processes in the bladings of Fig. D(109)2 and 4, respectively in entropy diagrams, by assuming that the processes are adiabatic and that the fluids have constant specific heat ratios γ. In general, from the equation of continuity

$$A_e \, k_{Be} \, \rho_e \, V_e \cos \alpha_e = A_d \, k_{Bd} \, \rho_d \, V_d \cos \alpha_d$$

With ρ_e and ρ_d from

$$\rho = p/g\ R_G\ T$$

and the Mach numbers M_e and M_d from

$$M = V/\sqrt{g\ \gamma\ R_G\ T}$$

there is

$$M_d = \frac{A_e\ k_{Be}}{A_d\ k_{Bd}} \quad \frac{\cos\ \alpha_e}{\cos\ \alpha_d} \quad \frac{p_e}{\sqrt{T_e}} \quad M_e \quad \frac{\sqrt{T_d}}{p_d}$$

To obtain dimensionless relations the static pressure p and the static temperatures T will be taken as multiples of the constants P_0 and T_0, respectively. Then

$$M_d = K\ \frac{\sqrt{T_d/T_0}}{(p_d/P_0)} \qquad \text{D109(1)}$$

where

$$K = \frac{A_e\ k_{Be}\ \cos\ \alpha_e}{A_d\ k_{Bd}\ \cos\ \alpha_d}\ M_e\ \frac{p_e/P_0}{\sqrt{T_e/T_0}} \qquad \text{D109(2)}$$

The dimensionless quantity K is known from the cascade geometry and the inlet conditions. It is assumed that the ratios P_{te}/P_0, T_{te}/T_0 and the Mach number M_e are known, where P_{te} and T_{te} are the total pressure and the total temperature at station (e). Then, from

$$T_{te} = T_e \left[1 + \frac{\gamma-1}{2}\ M_e^2\right]$$

and

$$P_{te} = p_e \left[1 + \frac{\gamma-1}{2}\ M_e^2\right]^{\gamma/(\gamma-1)}$$

there are

$$\frac{T_e}{T_0} = \frac{T_{t2}/T_0}{1 + \frac{\gamma-1}{2} M_e^2} \qquad \text{D109(3)}$$

and

$$\frac{p_e}{P_0} = \frac{P_{te}/P_0}{\left[1 + \frac{\gamma-1}{2} M_e^2\right]^{\gamma/(\gamma-1)}} \qquad \text{D109(4)}$$

These quantities establish the value of K of Eq. 2, if the flow areas, the blockage factors, and the flow angles at stations (e) and (d) are known.

Since $T_{td} = T_{te}$ for an adiabatic process, there is similar to Eq. 3

$$\frac{T_d}{T_0} = \frac{T_{te}/T_0}{1 + \frac{\gamma-1}{2} M_d^2} \qquad \text{D109(5)}$$

The losses in the row of the blade are expressed by the total pressure loss coefficient Y_t defined by

$$Y_t = \frac{P_{te} - P_{td}}{P_{te} - p_e} \qquad \text{D109(6)}$$

Hence

$$\frac{P_{td}}{P_0} = \frac{P_{te}}{P_0} - Y_t \left(\frac{P_{te}}{P_0} - \frac{p_e}{P_0}\right) \qquad \text{D109(7)}$$

and, similar to Eq. 4,

$$\frac{p_d}{P_0} = \frac{P_{td}/P_0}{\left[1 + \frac{\gamma-1}{2} M_d^2\right]^{\gamma/(\gamma-1)}} \qquad \text{D109(8)}$$

Because of the above exponential expression it is not possible to obtain a closed solution for M_d by substituting Eqs. 5 and 8 into Eq. 1. It is necessary to choose a particular value $M_d = M_d^*$, which is used to determine

T_d/T_0 and p_d/P_0 by Eqs. 5 and 8. These values are introduced into Eq. 1., and M_d^* must be iterated until the result of Eq. 1 equals M_d^*. For given flow conditions at station (e) there always occur two solutions, one for which M_d is subsonic, the other for which M_d is supersonic.

All input data are dimensionless with the exception of the cross-sectional areas A_e and A_d. The dimensions of these areas are arbitrary but the units for A_e and A_d must be equal. As seen from the operating instructions, the calculated ratios p_e/P_0 and T_e/T_0 must be read before the iteration for M_d. If the condition $M_d = M_d^*$ has been satisfied, the final results are obtained by depressing the (SENSE) switch.

The velocity V_d after the cascade is

$$V_d = M_d \, a_0 \sqrt{\frac{T_d}{T_0}}$$

where a_0 is the velocity of sound corresponding to T_0. The velocity V_d is obtained with the keyboard operation

↑(8) √ x ↑(0) x (Value of a_0) =

at P-Count 173.

Enclosures: Figure D(109)

Operating Instruction (1 page)

Program Listing (4 pages)

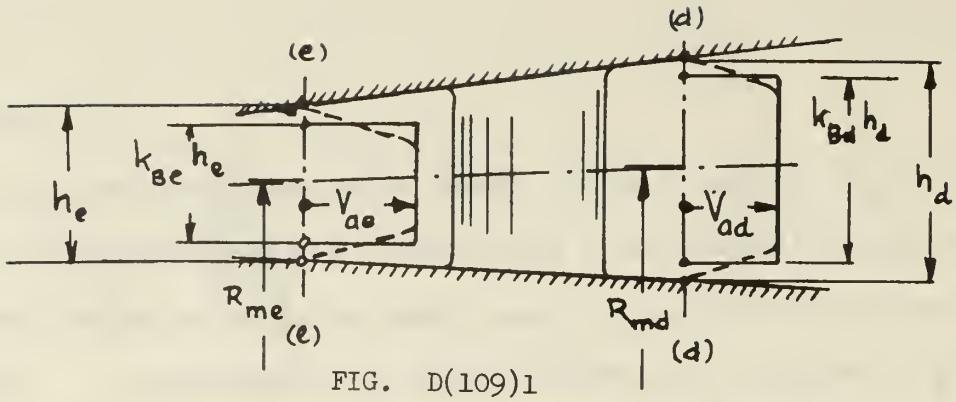

FIG. D(109)1

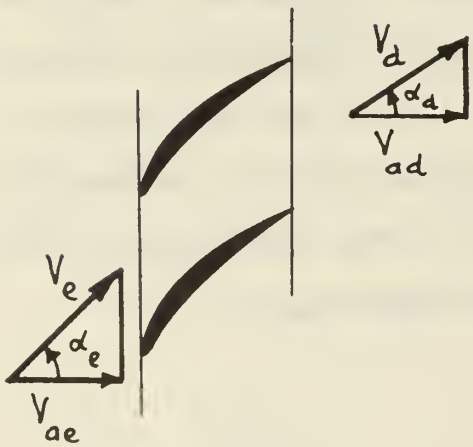

FIG. D(109)2

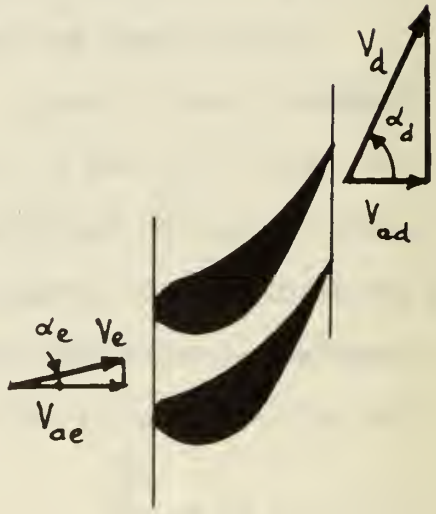

FIG. D(109)4

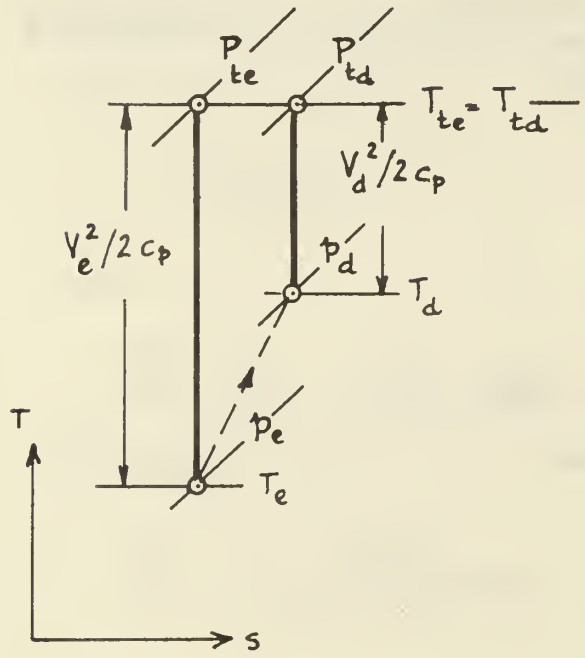

FIG. D(109)3

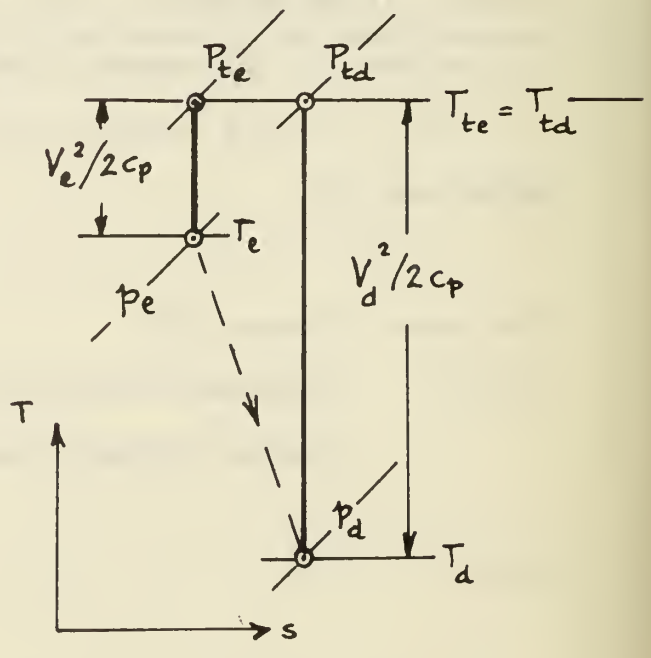

FIG. D(109)5

FIG. D(109) FLOW THROUGH CASCADE

OPERATING INSTRUCTIONS PROGRAM No. 109

MONROE CALCULATOR 1655 WITH CARD READER CR-1

Set-Up: (RESET); (TO(0)); Depress (LOAD); Read Cards 1-4

Release (LOAD); (TO(0)); Depress (P); (RESUME)

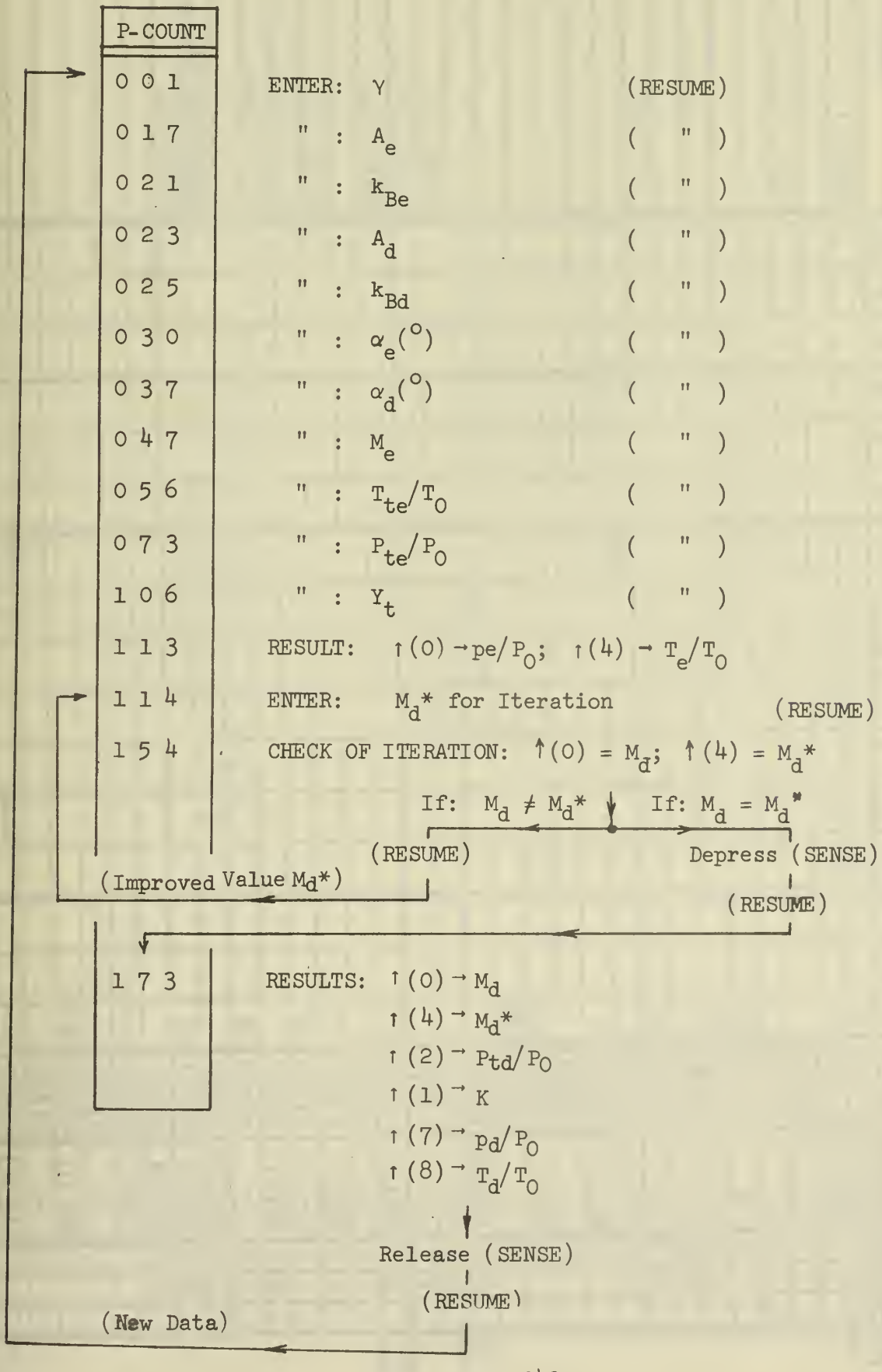

TURBO-PROPULSION LABORATORY, DEPT. OF AERONAUTICS, NPS, PAGE 1 OF 4

PROGRAM No. 109 MONROE 1655 CALCULATOR DATE: 8/6/72. BY: M.H. Vay

FLOW CONDITIONS AFTER CASCADE FOR GIVEN INLET CONDITIONS, ... FLOW DEFLECTION AND TOTAL PRESSURE LOSS COEFFICIENT ...

BR PT	ADDRESS P	ADDRESS COUNT	COMMAND	CODE			REGISTERS E	A	M	0	1	2	3	4	5	6	7	8	9	X	Y	Z	NOTES
0	0	0	HALT	4	0	1	γ																ENTER: γ
		1	STR(1)	4	4	0					γ												
		2	−	0	6	2																	
		3	1	0	0	1																	
		4	÷	0	7	2	$\gamma-1$																
		5	STR(2)	4	4	1	$\gamma-1$					$\gamma-1$											
		6	2	0	0	2																	
	0	7	=	0	2	0	$\frac{\gamma-1}{2}$																
	1	0	STR(6)	4	4	5										$\frac{\gamma-1}{2}$							
		1	RCL(1)	4	6	0	γ																
		2	÷	0	7	2																	
		3	RCL(2)	4	6	1	$\gamma-1$																
		4	=	0	2	0	$\frac{\gamma}{\gamma-1}$																
	1	5	STR(5)	4	4	4									$\frac{\gamma}{\gamma-1}$								
	1	6	HALT	4	0	1																	ENTER: A_e
	1	7	×	0	7	0																	
−	2	0	HALT	4	0	1																	ENTER: k_{be}
		1	÷	0	7	2																	
	2	2	HALT	4	0	1																	ENTER: A_d
		3	÷	0	7	2																	
	2	4	HALT	4	0	1																	ENTER: k_{Bd}
		5	=	0	2	0	B																
		6	STR(1)	4	4	0					B												$B=(A_e k_{be})/(A_d k_{Bd})$
	2	7	HALT	4	0	1	α_e																ENTER: $\alpha_e°$
	3	0	SIN/COS	0	4	0																	
		1	2.FUNCT	0	3	6	$\cos\alpha_e$																
		2	×	0	7	0																	
		3	RCL(1)	4	6	0	B																
		4	=	0	2	0																	
		5	STR(1)	4	4	0					$B\cos\alpha_e$												
	3	6	HALT	4	0	1	α_d																ENTER: $\alpha_d°$
	3	7	SIN/COS	0	4	0																	
							E	A	M	0	1	2	3	4	5	6	7	8	9	X	Y	Z	

244

MUV 2/70

TURBO-PROPULSION LABORATORY, DEPT. OF AERONAUTICS, NPS ,
PROGRAM No. ..109..... MONROE 1655 CALCULATOR

DATE: 8/6/72 BY: M.H.V.

BR PT	ADDRESS P COUNT	COMMAND	CODE	E	A	M	0	1	2	3	4	5	6	7	8	9	X	Y	Z	NOTES
2	4 0	2.FUNCT	0 3 6	$\cos\alpha_d$								$\frac{\gamma}{\gamma-1}$	$\frac{\gamma-1}{2}$							
	1	÷	0 7 2																	
	2	RCL(1)	4 6 0	$B\cos\alpha_e$																
	3	=	0 2 0	$(B\cos\alpha_e/\cos\alpha_d)^{-1}$																
	4	INV	0 5 4	$B\cos\alpha_e/\cos\alpha_d$																
	5	X	0 7 0																	
	4 6	HALT	4 0 1	M_e																ENTER: M_e
	4 7	STR(2)	4 4 1						M_e											
	5 0	=	0 2 0	C																
	1	STR(1)	4 4 0					C												$C=\frac{A_e k_{Be}}{A_d k_{Bd}}\frac{\cos\alpha_e}{\cos\alpha_d} M_e$
	2	RCL(2)	4 6 1	M_e																
	3	TO(6)	7 4 6	Z_{1e}																
	4	X	0 7 0																	
	5 5	HALT	4 0 1	T_{te}/T_0																ENTER: T_{te}/T_O
	6	STR(3)	4 4 2							T_{te}/T_0										
	5 7	=	0 2 0	T_e/T_0																
3	6 0	STR(4)	4 4 3								T_e/T_0									
	1	√	0 5 6	$\sqrt{T_e/T_0}$																
	2	INV	0 5 4	$1/\sqrt{T_e/T_0}$																
	3	X	0 7 0																	
	4	RCL(1)	4 6 0	C																
	5	=	0 2 0	C'																$C' = C/\sqrt{T_e/T_0}$
	6	STR(1)	4 4 0					C'												
	6 7	RCL(2)	4 6 1	M_e																
	7 0	TO(7)	7 4 7	Z_{2e}																
	1	X	0 7 0																	
	7 2	HALT	4 0 1	P_{te}/P_0																ENTER: P_{te}/P_0
	3	STR(2)	4 4 1						P_{te}/P_0											
	4	X	0 7 0	P_e/P_0																
	5	STR(0)	4 5 7				P_e/P_0													
	6	RCL(1)	4 6 0	C'																
	7 7	=	0 2 0	K																

BR PT	ADDRESS P COUNT	COMMAND	CODE	E	A	M	0	1	2	3	4	5	6	7	8	9	X	Y	Z	NOTES
4	100	STR(1)	440	K			p_e/P_0	K	P_{te}/P_0	T_{te}/T_0	T_e/T_0	$\frac{\gamma}{\gamma-1}$	$\frac{\gamma-1}{2}$							
	1	RCL(0)	477	p_e/P_0																
	2	−	062																	
	3	RCL(2)	461	P_{te}/P_0																
	4	X	070	$\frac{P_e-P_{te}}{P_0}$																
	105	HALT	401	Y_t																ENTER: Y_t
	6	+	060	$Y_t\frac{P_e-P_{te}}{P_0}$																
	107	RCL(2)	461	P_{te}/P_0																
	110	=	020	P_{td}/P_0																
	1	STR(2)	441						P_{td}/P_0											
	112	HALT	401				p_e/P_0				T_e/T_0									RESULTS: ↑(0) → p_e/P_0; ↑(4) → T_e/T_0
	113	HALT	401	M_d^*																ENTER: M_d^* for Iteration
	114	STR(4)	443	M_d^*							M_d^*									
	5	To(7)	747	Z_{2d}^*																
	6	x	070																	
	117	RCL(2)	461	P_{td}/P_0																
5	120	=	020	p_d/P_0																
	1	STR(7)	446											p_d/P_0						
	2	INV	054	P_0/p_d																
	3	x	070																	
	4	RCL(1)	460	K																
	5	=	020	KP_0/p_d																
	6	STR(0)	457				$K\frac{P_0}{p_d}$													
	127	RCL(4)	463	M_d^*																
	130	To(6)	746	Z_{1d}^*																
	1	x	070																	
	2	RCL(3)	462	T_{te}/T_0																
	3	=	020	T_d/T_0																
	4	STR(8)	447	T_d/T_0											T_d/T_0					
	5	√	056	$\sqrt{T_d/T_0}$																
	6	X	070																	
	137	JUMP 50	650																	
				E	A	M	0	1	2	3	4	5	6	7	8	9	X	Y	Z	

TURBO-PROPULSION LABORATORY, DEPT. OF AERONAUTICS, NPS,
PROGRAM No. 109 MONROE 1655 CALCULATOR
PAGE 4 OF 4
DATE: 8/6/72 BY: M.H.V.

BR PT	ADDRESS P	ADDRESS COUNT	COMMAND	CODE	E	A	M	0	1	2	3	4	5	6	7	8	9	X	Y	Z	NOTES
6	1	4 0	X	070	M								$\frac{\gamma}{\gamma-1}$	$\frac{\gamma-1}{2}$							
		1	X	070	M^2																
		2	RCL(6)	465	$\frac{\gamma-1}{2}$																
		3	+	060	$\frac{\gamma-1}{2}M^2$																SUBROUTINE: $Z_1 = f_1(M,\gamma)$
		4	1	001																	
		5	=	020	Z_1^{-1}																
		6	INV	054	Z_1																$Z_1 = 1/(1+\frac{\gamma-1}{2}M^2)$
1	4	7	RCLP	557	Z_1																
1	5	0	RCL(0)	477	$K\frac{P_0}{P_d}$			$K\frac{P_0}{P_d}$	K	P_{td}/P_0	T_{td}/T_0	M_d^*	$\frac{\gamma}{\gamma-1}$	$\frac{\gamma-1}{2}$	P_d/P_0	T_d/T_0					
		1	=	020	M_d																
		2	STR(0)	457				M_d													
1	5	3	HALT	401																	CHECK: $M_d = M_d^*$?. If $M_d = M_d^*$ depress [SENSE]
		4	SFSNS	523																	
		5	SKFI	540																	
		6	JUMP 13	613																	
247	1	5 7	JUMP 72	672																	
7	1	6 0	X	070	M																
		1	X	070	M^2																
		2	RCL(6)	465	$\frac{\gamma-1}{2}$																SUBROUTINE $Z_2 = f_2(M,\gamma)$
		3	+	060	$\frac{\gamma-1}{2}M^2$																
		4	1	001																	
		5	a^x	074	$1+\frac{\gamma-1}{2}$	M^2															
		6	RCL(5)	464	$\frac{\gamma}{\gamma-1}$																
1	6	7	=	020	Z_2^{-1}																
1	7	0	INV	054	Z_2																$Z_2 = 1/[(1+\frac{\gamma-1}{2}M^2)^{\gamma/(\gamma-1)}]$
		1	RCLP	557																	
1	7	2	HALT	401				M_d	K	P_{td}/P_0	T_{td}/T_0	M_d^*	$\frac{\gamma}{\gamma-1}$	$\frac{\gamma-1}{2}$	P_d/P_0	T_d/T_0					RESULTS
		3	TO(0)	740																	
		4																			
		5																			
		6																			
		7																			
					E	A	M	0	1	2	3	4	5	6	7	8	9	X	Y	Z	

PROGRAM NO. 110

MONROE CALCULATOR 1655 WITH CARD READER C-R1

Description

The curve of Fig. D(110)has the characteristics that its curvature k at the point P_o is zero and that k increases gradually with increasing angle θ. To be found is that curve which has the angle $\delta_m = \pi/2$ between the tangents of the curve at P_o and P_m such that particular distances x_o/a and y_o/a are obtained. For

$$r/a = \theta^{-b} \qquad 110(1)$$

there is *

$$\tan \Psi = - \frac{\theta}{b} \qquad 110(2)$$

For $0 < b < 1$ there is $\pi/2 < \Psi < \pi$ and since

$$\vartheta = \Psi - \pi/2$$

one obtains

$$\cot \vartheta = - \tan (\Psi - \pi/2) = \theta/b \qquad 110(3)$$

and

$$\sin \vartheta = \sqrt{\frac{1}{1 + (\theta/b)^2}} \qquad 110(4)$$

where $0 < \vartheta < \pi/2$

The curvature k at $P(r/a, \theta)$ is

$$k = \frac{1 - b(1-b)/\theta^2}{a\theta^{-b}\left[1+(b/\theta)^2\right]^{3/2}} \qquad 110(5)$$

---

*Vavra, M. H., "Aerothermodynamics and Flow in Turbomachines," pp. 293/298, John Wiley & Sons, New York, 1960.

At P_o $(r_o/a, \theta_o)$ the curvature k_o is zero, hence, by Eq. 5

$$\theta_o = \sqrt{b(1-b)} \qquad 110(6)$$

From Eq. 1

$$\frac{r_o}{a} = \theta_o^{-b} = [b(1-b)]^{-\frac{b}{2}} \qquad 110(7)$$

and from Eq. 4

$$\vartheta_o = \sin^{-1} \sqrt{\frac{1}{1 + (\theta_o/b)^2}} \qquad 110(8)$$

From Fig. D(110) for $P(r/a, \theta)$

$$\delta = (\theta + \vartheta) - (\theta_o + \vartheta_o) = E - E_o$$

and for $P_m\left(\frac{r_m}{a}, \theta_m\right)$, where $\delta_m = \pi/2$,

$$\delta_m = \frac{\pi}{2} = (\theta_m + \vartheta_m) - (\theta_o + \vartheta_o) = E_m - E_o \qquad 110(9)$$

where, according to Eq. 4

$$\vartheta_m = \sin^{-1} \sqrt{\frac{1}{1 + (\theta_m/b)^2}} \qquad 110(10)$$

From Fig. D(110) the coordinates x_o/a and y_o/a are

$$\frac{x_o}{a} = \frac{r_o}{a} \cos \vartheta_o - \frac{r_m}{a} \sin \vartheta_m \qquad 110(11)$$

$$\frac{y_o}{a} = \frac{r_o}{a} \sin \vartheta_o + \frac{r_m}{a} \cos \vartheta_m \qquad 110(12)$$

From Eq. 3

$$\frac{b}{\theta} = \tan \vartheta$$

Hence

$$1 + (b/\theta)^2 = 1 + \tan^2 \vartheta = \frac{1}{\cos^2 \vartheta}$$

Introduced into Eq. 5, with Eqs. 1 and 6,

$$a\,k = \frac{1 - (\theta_o/\theta)^2}{r/a} \cos^3 \vartheta \qquad 110(13)$$

Hence at P_m the curvature k_m is obtained from

$$a\,k_m = \frac{1 - (\theta_o/\theta_m)^2}{r_m/a} \cos^3 \vartheta_m \qquad 110(14)$$

It is not possible to calculate the parameters of a curve with $\delta_m = \pi/2$ that has a given ratio y_o/x_o with a closed solution. It is necessary to choose a value of b which establishes θ_o, r_o/a and ϑ_o. Then the angle θ_m must be varied until $\delta_m = 90^o$ by Eq. 9. With θ_m, the quantities r_m/a and ϑ_m are obtained from Eqs. 1 and 10. Then the coordinates x_o/a and y_o/a of Eqs. 11 and 12 establish the ratio y_o/x_o. If this ratio differs from that of the desired curve the quantity b must be varied until agreement is reached

From Eqs. 11 and 14 it is possible also to express the curvature k_m as a multiple of $1/x_o$ or

$$k_m\, x_o = (a\,k_m)\ (x_o/a) \qquad 110(15)$$

Enclosures: Figure D(110)

Operating Instruction (1 page)

Program Listing (4 pages)

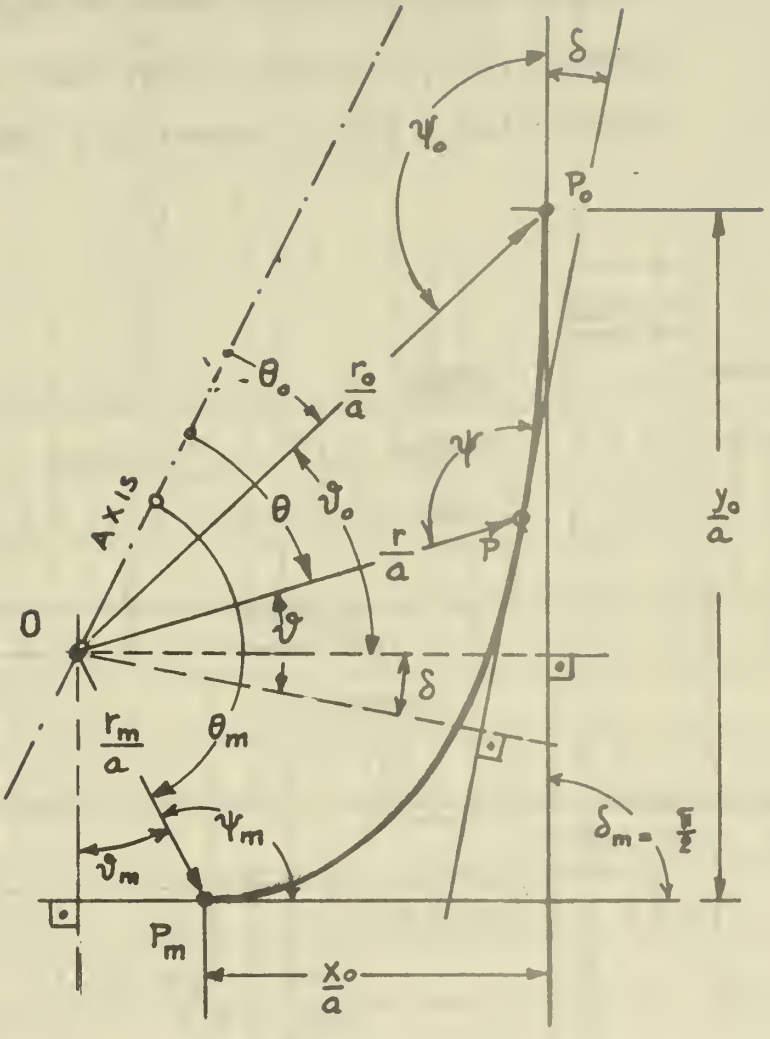

FIG. D(110) CURVE $r/a = \theta^{-b}$

OPERATING INSTRUCTIONS PROGRAM No. 110

MONROE CALCULATOR 1655/6 WITH CARD READER CR-1

Set-Up: (RESET); (TO(0)); Depress (LOAD); Read Cards 1-4

Release (LOAD); TO(0)); Depress (P); (RESUME)

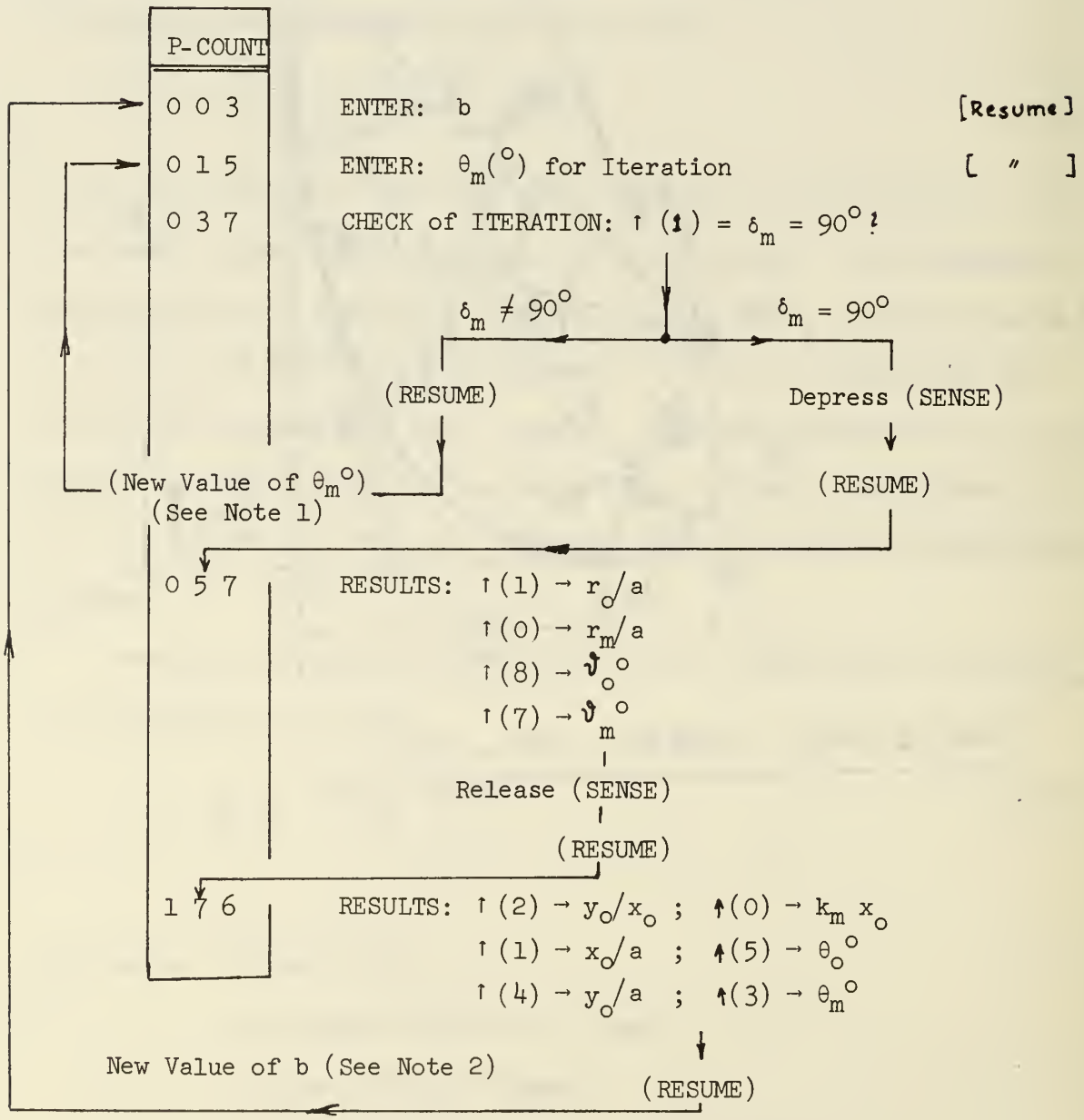

Note 1: $\delta_m < 90^\circ$ → Increase θ_m ; $\delta_m > 90^\circ$ → Decrease θ_m

Note 2: To increase y_o/x_o → Increase b

To decrease y_o/x_o → Decrease b

TURBO-PROPULSION LABORATORY, DEPT. OF AERONAUTICS, NPS, PAGE 1 OF 4.
PROGRAM No. 110 MONROE 1655 CALCULATOR DATE: 8/7/72. BY: M.H. Vavra
CALCULATION OF CURVE r/a = Θ-b WITH ZERO CURVATURE .....
AT ONE POINT AND δmax = 90° .....

BR PT	ADDRESS P	COUNT		COMMAND	CODE			REGISTERS E	A	M	0	1	2	3	4	5	6	7	8	9	X	Y	Z	NOTES
0	0	0	0	1	0	0	1	1																
			1	−	0	6	2																	
		0	2	HALT	4	0	1	b																ENTER: b
			3	STR (6)	4	4	5										b							
			4	×	0	7	0	1−b																
			5	RCL(6)	4	6	5	b																
			6	=	0	2	0	b(1-b)																
		0	7	√	0	5	6	θ_o^R																
		1	0	STR(5)	4	4	4	θ_o^R								θ_o^R								
			1	TO (7)	7	4	7	$\sin\vartheta_o$																
			2	SIN⁻¹/COS⁻¹	0	4	2	ϑ_o^R																
			3	STR (4)	4	4	3								ϑ_o^R									
		1	4	HALT	4	0	1	$\theta_m°$																ENTER: $\theta_m°$ ($0 \le \theta_m \le 180°$)
			5	SIN/COS	0	4	0																	
			6	2FUNCT	0	3	6	$\cos\theta_m$																
		1	7	SIN⁻¹/COS⁻¹	0	4	2																	
1		2	0	2FUNCT	0	3	6	θ_m^R																
			1	STR (3)	4	4	2	θ_m^R						θ_m^R										
			2	TO (7)	7	4	7	$\sin\vartheta_m$																
			3	SIN⁻¹/COS⁻¹	0	4	2	ϑ_m^R																
			4	STR (2)	4	4	1	ϑ_m^R					ϑ_m^R											
			5	+	0	6	0																	
			6	RCL(3)	4	6	2	θ_m^R																
		2	7	−	0	6	2																	
		3	0	RCL(5)	4	6	4	θ_o^R																
			1	−	0	6	2																	
			2	RCL(4)	4	6	3	ϑ_o^R																
			3	=	0	2	0	δ_m^R																
			4	R → °	0	4	6	$\delta_m°$																$\delta_m = \vartheta_m + \theta_m - (\theta_o + \vartheta_o)$
			5	STR(1)	4	4	0					$\delta_m°$												
		3	6	HALT	4	0	1																	CHECK: $\delta_m = 90°$? If true: [SENSE]
		3	7	SFSNS	5	2	3																	
								E	A	M	0	1	2	3	4	5	6	7	8	9	X	Y	Z	

TURBO-PROPULSION LABORATORY, DEPT. OF AERONAUTICS, NPS ,
PROGRAM No. 110 MONROE 1655 CALCULATOR

DATE: 8/7/72 BY: M.H.Y.

BR PT	ADDRESS P COUNT	COMMAND	CODE	REGISTERS E	A	M	0	1	2	3	4	5	6	7	8	9	X	Y	Z	NOTES
2	040	SKF 1	540					δ_m°	ϑ_m^R	θ_m^R	ϑ_o^R	θ_o^R	b							
	1	JUMP 14	614																	
	2	RCL(5)	464	θ_o^R																
	3	TO(6)	746	r_o/a				r_o/a												
	4	STR(1)	440																	
	5	RCL(3)	462	θ_m^R																
	6	TO(6)	746	r_m/a																
	7	STR(0)	457				r_m/a													
	50	RCL(2)	461	ϑ_m^R																
	1	R→°	046	ϑ_m°																
	2	STR(7)	446											ϑ_m°						
	3	RCL(4)	463	ϑ_o^R																
	4	R→°	046	ϑ_o°																
	5	STR(8)	447												ϑ_o°					
	56	HALT	401				r_m/a	r_o/a						θ_m°	ϑ_o°					RESULTS: $\frac{r_m}{a}, \frac{r_o}{a}$; ϑ_m°; ϑ_o°
	57	RCL(8)	467	ϑ_o^e																
3	60	SIN/COS	040	$\sin\vartheta_o$																
	1	x	070																	
	2	RCL(1)	460	$\frac{r_o}{a}$																
	3	=	020	$\frac{r_o}{a}\sin\vartheta_o$																
	4	STR(4)	443								$\frac{r_o}{a}\sin\vartheta_o$									
	5	2.FUNC	036	$\cos\vartheta_o$																
	6	x	070																	
	67	RCL(1)	460	r_o/a																
	70	=	020	$\frac{r_o}{a}\cos\vartheta_o$					$\frac{r_o}{a}\cos\vartheta_o$											
	1	STR(1)	440																	
	2	RCL(2)	461	ϑ_m^R																
	3	R→°	046	ϑ_m°																
	4	SIN/COS	040	$\sin\vartheta_m$																
	5	x	070																	
	6	RCL(0)	477	r_m/a																
	7	—	062	$\frac{r_m}{a}\sin\vartheta_m$																

TURBO-PROPULSION LABORATORY, DEPT. OF AERONAUTICS, NPS, PAGE 3 OF 4
PROGRAM No. 110 .... MONROE 1655 CALCULATOR DATE: 8/7/72 BY: M.H.V.

BR PT	ADDRESS P	COUNT	COMMAND	CODE	E	A	M	0	1	2	3	4	5	6	7	8	9	X	Y	Z	NOTES
4	1	0	RCL(1)	460	$\frac{r_o}{a}\cos\vartheta_o$			r_m/a	$\frac{r_o}{a}\cos\vartheta_o$	ϑ_m^R	θ_m^R	$\frac{r_o}{a}\sin\vartheta_o$	θ_o^R	b							
		1	=	020	$-\frac{x_o}{a}$																
		2	CHSGN	013	x_o/a																
		3	STR(1)	440					x_o/a												
		4	2.FUNCT	036	$\cos\vartheta_m$																
		5	×	070																	
		6	RCL(0)	477	r_m/a																
1	0	7	+	060	$\frac{r_m}{a}\cos\vartheta_m$																
1	1	0	RCL(4)	463	$\frac{r_o}{a}\sin\vartheta_o$																
		1	=	020	y_o/a																
		2	STR(4)	443								y_o/a									
		3	RCL(5)	464	θ_o^R																
		4	÷	072																	
		5	RCL(3)	462	θ_m^R																
		6	×	070	θ_o/θ_m																
1	1	7	÷	062	$(\theta_o/\theta_m)^2$																
5	1	2	0	+	001																	
		1	÷	072	$\frac{(\theta_o}{(\theta_m)^2}-1$																
		2	RCL(0)	477	r_m/a																
		3	=	020	$-Y$																
		4	CHSGN	013	Y																$Y=(1-(\theta_o/\theta_m)^2)/(r_m/a)$
		5	STR(0)	457				Y													
		6	RCL(2)	461	ϑ_m^R																
1	2	7	R → °	046	ϑ_m°																
1	3	0	SIN/COS	040																	
		1	2.FUNCT	036	$\cos\vartheta_m$																
		2	a^x	074																	
		3	3	003																	
		4	×	070	$\cos\vartheta_m^3$																
		5	RCL(0)	477	Y																
		6	×	070	$a\,k_m$																
1	3	7	JUMP 45	645																	
					E	A	M	0	1	2	3	4	5	6	7	8	9	X	Y	Z	

255

TURBO-PROPULSION LABORATORY, DEPT. OF AERONAUTICS, NPS ,
PROGRAM No. ...110.... MONROE 1655 CALCULATOR

DATE: ..8/7/72. BY: M.H.V.

BR PT	ADDRESS P COUNT	COMMAND	CODE	E	A	M	REGISTERS 0	1	2	3	4	5	6	7	8	9	X	Y	Z	NOTES
6	140	a^x	074	θ									b							
	1	RCL(6)	465	b																SUBROUTINE:
	2	=	020	θ^b																$r/a = \theta^{-b}$
	3	INV	054	θ^{-b}																
	4	RCLP	557	r/a																
145	5	RCL(1)	460	x_o/a			Y	x_o/a	ϑ_m^R	θ_m^R	y_o/a	θ_o^R	b							
	6	=	020	$x_o k_m$																
147	7	STR(0)	457				$x_o k_m$													
150	0	RCL(4)	463	y_o/a																
	1	÷	072																	
	2	RCL(1)	460	x_o/a																
	3	=	020	y_o/x_o					y_o/x_o											
	4	STR(2)	441																	
	5	RCL(5)	464	θ_o^R																
	6	R→°	046	θ_o°																
157	7	JUMP 71	671																	
160	0	÷	072	θ									b							
	1	RCL(6)	465	b																SUBROUTINE:
	2	×	070	θ/b																$\sin\vartheta = \frac{1}{\sqrt{1+(\theta/b)^2}}$
	3	+	060	$(\theta/b)^2$																
	4	1	001																	
	5	=	020	$1+(\theta/b)^2$																
	6	$\sqrt{}$	056																	
167	7	INV	054	$\sin\vartheta$																
170	0	RCL P	557																	
171	1	STR(5)	444	θ_o°			$x_o k_m$	x_o/a	y_o/x_o	θ_m^R	y_o/a	θ_o°	b							
	2	RCL(3)	462	θ_m^R																
	3	R→°	046	θ_m°						θ_m°										
	4	STR(3)	442																	
175	5	HALT	401				$x_o k_m$	x_o/a	y_o/x_o	θ_m°	y_o/a	θ_o°	b							RESULTS: $\frac{y_o}{x_o}$; $\frac{y_o}{\alpha}$; $\frac{x_o}{\alpha}$; $x_o k_m$; θ_o°, θ_m°
	6	TO(0)	740																	
	7																			
7																				

PROGRAM NO. 517

MONROE CALCULATOR 1880-22

Description

Program 517 calculates the conditions after the diffusor, the honeycomb flow straightener, and the discharge duct of the Hybrid compressor. Details of these calculations are given in Section III.3 of "Hybrid Compressor Design Report." The compressor is supposed to operate as an exhauster such that the static pressure (p_6) at the compressor discharge is 14.7 psia. The total temperature at the impeller inlet (T_0) is taken to be 520°R. Basic data to be used in the program are the conditions after the rotor obtained by the method described in Section III.2 of "Hybrid Compressor Design Report."

Both diffusor rows are considered as a unit and it is assumed that the flow angle α_4 after the second diffusor blade row is constant, equal to 21°. The program contains program 109, described in Appendix D, which by an iterative procedure establishes the Mach number $M_{V4} = M_4$ of the flow after the diffusor with losses that are a multiple of its design pressure loss coefficient.

After calculating the diffusor performance program 517 determines the overall compressor performance in accordance with Section III.4. Examples of print-outs are given in Tables XI and XII of the aforementioned report.

Enclosures: Operating Instructions (1 page)

List of Print-Out of Results (1 page)

Program Listing (12 pages)

Main Data Storage (1 page)

Set-Up: Read 2 Magnetic Cards starting at Branch Point 0 0

P-COUNT		
0 0 4 3	ENTER: $(k_{B2}/k_{B4}) \cos \alpha_4 = 1.161\ 218$	(RESUME)
0 0 4 7	" : $(Y_t)_{i=i_o} = 0.2089$	(")
0 0 5 1	" : $V_S/V_4 = 1.039$	(")
0 0 5 5	" : $V_5/V_4 = 0.8764$	(")
0 0 5 9	" : $V_6/V_4 = 0.722$	(")
0 0 7 9	" : α_4 (°) = 21°	(")
0 0 8 5	" : α_2 (°)	(")
0 0 9 4	" : T_{t2}/T_0	(")
0 0 9 8	" : P_{t2}/T_0	(")
0 1 0 2	" : T_2/T_0	(")
0 1 0 6	" : p_2/P_0	(")
0 1 1 0	" : M_{V2}	(")
0 1 4 1	" : $Y_t/(Y_t)_{i=i_o}$	(")
0 1 6 7	" : M_4* FOR ITERATION	(")
0 2 3 5	PRINT-OUT: IDENTIFIER -4. $\Delta M = M_4 - M_4$* M_4*	

IF $\Delta M \neq 0$ (RESUME)

IF $\Delta M \cong 0$ ENTER: 0 (RESUME)

0 4 3 9	ENTER: $\dot{w}\sqrt{(R_G/g)T_0}/P_0$	(RESUME)
0 4 6 7	" : U_2/a_0	(")

PRINT-OUT OF RESULTS
(see list attached)

SEE NOTE

NOTE: After "Print-out of Results" the program automatically returns to P-Count 0085 for new data.

PROGRAM 517

MONROE CALCULATOR 1880-22

LIST OF PRINT-OUT OF RESULTS:

. . . . . .

U_2/a_0

α_2 (°)

P_{t4}/P_0

p_4/P_0

T_4/T_0

$M_{V4} = M_4$

V_4/a_0

P_{t4}'/P_0

p_4'/P_0

P_{t4}''/P_0

p_4'/P_0

P_{t5}/P_0

P_{t6}/P_0

p_6/P_0

P_0 (psia)

$\dot{w}$ (lbm/s)

HP (HP)

N (rpm)

η_T (–)

. . . . . .

MONROE 1080

PROGRAM # VA517 OFF-DESIGN PERFORMANCE HYBRID PAGE 1 OF 12 DATE: 6/73 BY: MHV

STEP	SYMBOL	COMMAND	COMMENTS	ENTER	STORE	PRINT
00 0		2				
1		9				
2		.				
3		3				
4		6				
5		4				
6		0				
7		7				
8		7	$E = \sqrt{(R_a/g)}\, T_0$			
9		↓( )( )				
01 0		2				
1		0	*		E → 20	
2		1				
3		7				
4		6				
5		.				
6		5				
7		4	$F = R_a (\gamma/(\gamma-1)\, T_0/550$			
8		↓( )( )				
9		2				
02 0		1	*		F → 21	
1		2				
2		3				
3		2				
4		9				
5		0				
6		.				
7		2				
8		1				
9		↓( )( )	$G = a_0\ 720/(\pi D_2)$			
03 0		2				
1		2			G → 22	
2		/				
3		/				
4		/				
5		/	NO OP.			
6		/				
7		/				
8		/				
9		/				
04 0		SET D.P.				
1		4				
2		HALT	ENTER: $C = \frac{k_{B2}}{k_{B4}} / \cos\alpha_4 = 1.16218$	C		
3		↓( )( )				
4		0				
5		0			C → 00	
6		HALT	ENTER: $(Y_t)_{i=i_0} = 0.2089 = Y_{t0}$	Y_{t0}		
7		↓( )( )				
8		0				
9		1			Y_{t0} → 01	

MHV 2/7/73

PROGRAM # VA 517 — MONROE 1080 — PAGE 2 OF 12 DATE: 6/73 BY: MHV

STEP	SYMBOL	COMMAND	COMMENTS	ENTER	STORE	PRINT
050		HALT	ENTER: $V_5/V_4 = 1.039$	V_5/V_4		
1		↓( )( )				
2		0				
3		2			$V_5/V_4 \rightarrow 02$	
4		HALT	ENTER: $V_5/V_4 = 0.8764$	V_5/V_4		
5		↓( )( )			$V_5/V_4 \rightarrow 03$	
6		0				
7		3				
8		HALT	ENTER: $V_6/V_4 = 0.722$	V_6/V_4		
9		↓( )( )				
060		0				
1		4			$V_6/V_4 \rightarrow 04$	
2		•				
3		4	$\gamma-1$			
4		÷				
5		1				
6		•				
7		4	γ			
8		=	$(\gamma-1)/\gamma$			
9		↓( )( )				
070		0				
1		5			$\frac{\gamma-1}{\gamma} \rightarrow 05$	
2		3				
3		•				
4		5	$\gamma/(\gamma-1)$			
5		↓( )( )				
6		0			$\frac{\gamma}{\gamma-1} \rightarrow 06$	
7		6				
8		HALT	ENTER: $\alpha_4 = 21$	α_4		
9		↓( )( )				
080		0				
1		7			$\alpha_4 \rightarrow 07$	
2	+	IND/SYMB	↕ SYMBOL. ADDRESS +			
3		+	↓			
4		HALT	ENTER: α_2	α_2		
5		↓( )( )				
6		2				
7		9			$\alpha_2 \rightarrow 29$	
8		SIN/COS				
9		2NDFUNC	$\cos \alpha_2$			
090		↓( )( )				
1		1				
2		0			$\cos\alpha_2 \rightarrow 10$	
3		HALT	ENTER: T_{t2}/T_0	T_{t2}/T_0		
4		↓( )( )				
5		1				
6		1			$T_{t2}/T_0 \rightarrow 11$	
7		HALT	ENTER: P_{t2}/P_0	P_{t2}/P_0		
8		↓( )( )				
9		1				

MHV 2/7/73

PROGRAM # VA 517 — MONROE 1080 — PAGE 3 OF 12 DATE: 6/73 BY: MHV

STEP	SYMBOL	COMMAND	COMMENTS	ENTER	STORE	PRINT
100		2			$P_{t2}/P_0 \rightarrow 12$	
101		HALT	ENTER: T_2/T_0	T_2/T_0		
102		↓( )( )				
103		1				
104		3			$T_2/T_0 \rightarrow 13$	
105		HALT	ENTER: P_2/P_0	P_2/P_0		
106		↓( )( )				
107		1				
108		4			$P_2/P_0 \rightarrow 14$	
109		HALT	ENTER: $M_{V2} = M_2$	M_{V2}		
110		↓( )( )				
111		1				
112		5			$M_2 \rightarrow 15$	
113		↑( )( )				
114		1				
115		3	T_2/T_0			
116		$\sqrt{}$	$\sqrt{T_2/T_0}$			
117		1/x	$1/\sqrt{T_2/T_0}$			
118		X				
119		↑( )( )				
120		1				
121		5	M_2			
122		X				
123		↑( )( )				
124		1				
125		4	P_2/P_0			
126		X				
127		↑( )( )				
128		1				
129		0	$\cos \alpha_2$			
130		X				
131		↑( )( )				
132		0				
133		0	C			
134		=	K			
135		↓( )( )				
136		0				
137		8			K → 08	
138		/	↑ NO OP			
139		/				
140		HALT	ENTER: Y_t / Y_{to}	Y_t/Y_{to}		
141		X				
142		↑( )( )				
143		0				
144		1	Y_{to}			
145		CHSGN	$-Y_{to}$			
146		X				
147		(				
148		↑( )( )				
149		1				

MHV 2/7/73

PROGRAM # VA 517 MONROE 1880 PAGE 4 OF 12 DATE: 6/73 BY: MHV

STEP	SYMBOL	COMMAND	COMMENTS	ENTER	STORE	PRINT
150		2	P_{t2}/P_0			
151		−				
152		↑( )( )				
153		1				
154		4	P_2/P_0			
155		)				
156		+				
157		↑( )( )				
158		1				
159		2	P_{t2}/P_0			
160		=	P_{t4}/P_0			
161		↓( )( )				
162		3				
163		0			$P_{t4}/P_0 \rightarrow 40$	
164	X	IND/SYMB	SYMBOL. ADDRESS X			
165		X				
166		HALT	ENTER: M_4^* FOR ITERATION OF M_4	M_4^*		
167		↓( )( )				
168		1				
169		6			$M_4^* \rightarrow 16$	
170		X				
171		X	M_4^{*2}			
172		•				
173		2	$(\gamma-1)/2$			
174		+				
175		1				
176		a^x	$1+\frac{\gamma-1}{2}M_4^{*2} = A1$			
177		↓( )( )				
178		1				
179		7			$A1 \rightarrow 17$	
180		↑( )( )				
181		0				
182		6	$\gamma/(\gamma-1) = 3.5$			
183		=	$\left(1+\frac{\gamma-1}{2}M_4^{*2}\right)^{3.5} =$			
184		1/x				
185		X				
186		↑( )( )				
187		1				
188		0	P_{t4}/P_0			
189		=	P_4/P_0			
190		↓( )( )				
191		1				
192		1			$P_4/P_0 \rightarrow 31$	
193		↑( )( )				
194		1				
195		1	T_{t2}/T_0			
196		÷				
197		↑( )( )				
198		1				
199		7	A1			

MHV 2/7/73

PROGRAM # VA 517 MONROE 1080 PAGE 5 OF 12 DATE: 6/73 BY: MHV

STEP	SYMBOL	COMMAND	COMMENTS	ENTER	STORE	PRINT
200		=	T_4/T_0			
201		↓( )( )				
202		3				
203		2			$T_4/T_0 \rightarrow 32$	
204		√	$\sqrt{T_4/T_0}$			
205		÷				
206		↑( )( )				
207		3				
208		1	p_4/p_0			
209		×				
210		↑( )( )				
211		0				
212		8	K			
213		=	M_4			
214		↓( )( )				
215		3				
216		3			$M_4 \rightarrow 33$	
217		−				
218		↑( )( )				
219		1				
220		6	M_4^*			
221		=	$\Delta M = M_4 - M_4^*$			
222		↓( )				
223		0			$\Delta M \rightarrow 0$	
224		4	↑ PRINT IDENTIFIER −4.			
225		CHSGN				
226	EC	177	↓			−4.
227		↑( )				
228		0	ΔM			
229		PRINT A				ΔM
230		↑( )( )				
231		1				
232		6	M_4^*			
233		PRINT A				M_4^*
234		HALT	IF $\Delta M \cong 0$; ENTER: 0			
235		JUMP	↑			
236		=	GO TO S.A ÷ IF $\Delta M = 0$			
237		IND/SYMB				
238		÷	↓			
239		JUMP	↑ GO TO S.A. × IF $\Delta M \neq 0$ FOR			
240		IND/SYMB	BETTER APPROXIMATION OF M_4			
241		×	↓			
242	÷	IND/SYMB	↑ SYMBOL. ADDRESS ÷			
243		÷	↓			
244		↑( )( )				
245		3				
246		2	T_4/T_0			
247		√	$\sqrt{T_4/T_0}$			
248		×				
249		↑( )( )				

MHV 2/7/73

PROGRAM # VA 517 MONROE 1880 PAGE 6 OF 12 DATE: 6/73 BY: MHV

STEP	SYMBOL	COMMAND	COMMENTS	ENTER	STORE	PRINT
250		3				
1		3	M_4			
2		×	V_4/a_0			
3		↓( )( )				
4		3				
5		4			$V_4/a_0 \rightarrow 34$	
6		(				
7		↑( )( )				
8		0				
9		7	α_4			
260		SIN/COS				
1		)	SIN α_4			
2		×	$(V_4/a_0) \sin\alpha_4$			
3		×	$[(V_4/a_0)\sin\alpha_4]^2$			
4		•				
5		2	$(\gamma-1)/2$			
6		+				
7		↑( )( )				
8		3				
9		2	T_4/T_0			
270		=	T_4^*/T_0			
1		1/x	T_0/T_4^*			
2		X				
3		↑( )( )				
4		1				
5		1	T_{t2}/T_0			
6		a^x	$(T_{t2}/T_0)(T_0/T_4^*)$			
7		↑( )( )				
8		0				
9		6	$\gamma/(\gamma-1) = 3.5$			
280		×				
1		↑( )( )				
2		3				
3		1	P_4/P_0			
4		=	P_{t4}'/P_0			
5		↓( )( )				
6		3				
7		5			$\frac{P_{t4}'}{P_0} \rightarrow 35$	
8		↑( )( )				
9		3				
290		4	V_4/a_0			
1		×				
2		↑( )( )				
3		0				
4		2	$V_S/V_4 = 1.039$			
5		×	V_S/a_0			
6		×	$(V_S/a_0)^2$			
7		•				
8		2	$(\gamma-1)/2 = .2$			
9		CHSGN	$-.2$			

MHV 2/7/73

PROGRAM # VA 517 MONROE 1080 PAGE 7 OF __ DATE: 6/73 BY: MHV

STEP	SYMBOL	COMMAND	COMMENTS	ENTER	STORE	PRINT
300		+				
301		↑( )( )				
302		1				
303		1	T_{t2}/T_0			
304		÷	T_4'/T_0			
305		↑( )( )				
306		1				
307		1	T_{t2}/T_0			
308		a^x				
309		↑( )( )				
310		0				
311		6	$\gamma/(\gamma-1) = 3.5$			
312		×				
313		↑( )( )				
314		3				
315		5	P_{t4}'/P_0			
316		×	P_4'/P_0			
317		↓( )( )				
318		3				
319		6			$\frac{P_4'}{P_0} \rightarrow 36$	
320		/	NO OP			
321		•				
322		3				
323		+	$.3(P_4'/P_0)$			
324		(				
325		•				
326		7				
327		×				
328		↑( )( )				
329		3				
330		5	P_{t4}'/P_0			
331		)	$.7(P_{t4}'/P_0)$			
332		÷	P_{t4}''/P_0			
333		↓( )( )				
334		3				
335		7			$\frac{P_{t4}''}{P_0} \rightarrow 37$	
336		↑( )( )				
337		3				
338		5	P_{t4}'/P_0			
339		×				
340		↑( )( )				
341		3				
342		6	P_4'/P_0			
343		=	P_4''/P_0			
344		↓( )( )				
345		3				
346		8			$\frac{P_4''}{P_0} \rightarrow 38$	
347		↑( )( )				
348		3				
349		4	V_4/a_0			

MHV 2/7/73

PROGRAM # VA 517 MONROE 1880 PAGE 8 OF 12 DATE: 6/73 BY: MHV

STEP	SYMBOL	COMMAND	COMMENTS	ENTER	STORE	PRINT
350		X				
1		↑( )( )				
2		0				
3		3	$V_5/V_4 = 0.8764$			
4		X	V_5/a_0			
5		X	$(V_5/a_0)^2$			
6		•				
7		2	$(\gamma-1)/2$			
8		CHSGN	$-.2$			
9		+				
360		↑( )( )				
1		1				
2		1	T_{t2}/T_0			
3		=	T_5/T_0			
4		1/X	T_0/T_5			
5		X				
6		↑( )( )				
7		1				
8		1	T_{t2}/T_0			
9		a^x	T_{t2}/T_5			
370		↑( )( )				
1		0				
2		6	$\gamma/(\gamma-1) = 3.5$			
3		X				
4		↑( )( )				
5		3				
6		8	p_4''/P_0			
7		X	P_{t5}/P_0			
8		↓( )( )				
9		3				
380		9			$\frac{P_{t5}}{P_0} \rightarrow 39$	
1		•				
2		6	0.6			
3		+	$0.6\ (P_{t5}/P_0)$			
4		(				
5		↑( )( )				
6		3				
7		8	p_4''/P_0			
8		X				
9		•				
390		4				
1		)				
2		=	P_{t6}/P_0			
3		↓( )( )				
4		4				
5		0			$\frac{P_{t6}}{P_0} \rightarrow 40$	
6		↑( )( )				
7		3				
8		4	V_4/a_0			
9		X				

MHV 2/7/73

PROGRAM # VA 517 MONROE 1880 PAGE 9 OF 12 DATE: 6/73 BY: MHV

STEP	SYMBOL	COMMAND	COMMENTS	ENTER	STORE	PRINT
400		↑( )( )				
401		0				
402		4	$V_6/V_4 = .722$			
403		x	V_6/a_0			
404		x	$(V_6/a_0)^2$			
405		·				
406		2	$(\gamma-1)/2 = .2$			
407		CHSGN	$-.2$			
408		+				
409		↑( )( )				
410		1				
411		1	T_{t2}/T_0			
412		÷	T_6/T_0			
413		↑( )( )				
414		1				
415		1	T_{t2}/T_0			
416		a^x	T_6/T_{t2}			
417		↑( )( )				
418		0				
419		6	$\gamma/(\gamma-1) = 3.5$			
420		x				
421		↑( )( )				
422		4				
423		0	P_{t6}/P_0			
424		=	P_6/P_0			
425		↓( )( )				
426		4				
427		1			$\frac{P_6}{P_0} \rightarrow 41$	
428		1/x	P_0/P_6			
429		x				
430		1				
431		4	$P_{ATM} = 14.7$ psia			
432		·				
433		7				
434		=	P_0 (psia)			
435		↓( )( )				
436		4				
437		2			$P_0 \rightarrow 42$	
438		HALT	ENTER : $X = \dot{w}\sqrt{(R_G/g)\,T_0/P_0}$	X		
439		X				
440		↑( )( )				
441		4				
442		2	P_0			
443		÷				
444		↑( )( )				
445		2				
446		0	E			
447		x	$\dot{w}$ (lbm/s)			
448		↓( )( )				
449		4				

MHV 2/7/73

PROGRAM # VA 517 MONROE 1080 PAGE 10 OF 12 DATE: 6/73 BY: MHV

STEP	SYMBOL	COMMAND	COMMENTS	ENTER	STORE	PRINT
45 0		3			$\dot{w} \rightarrow 43$	
1		(				
2		↑( )( )				
3		1				
4		1	T_{t2}/T_0			
5		−				
6		1				
7		)	$(T_{t2}/T_0) - 1$			
8		×				
9		↑( )( )				
46 0		2				
1		1	F			
2		=	HP			
3		↓( )( )				
4		4				
5		4			HP → 44	
6		HALT	ENTER: U_2/a_0	U_2/a_0		
7		↓( )( )				
8		2				
9		8			$U_2 \rightarrow 28$	
47 0		×			a_0	
1		↑( )( )				
2		2				
3		2	G			
4		=	N (rpm			
5		↓( )( )				
6		4				
7		5			N → 45	
8		↑( )( )				
9		3				
48 0		0	P_{t4}/P_0			
1		a^x				
2		↑( )( )				
3		0				
4		5	$(\gamma-1)/\gamma = .4/1.4$			
5		−	$(P_{t4}/P_0)^{\gamma-1/\gamma}$			
6		1				
7		÷	$(P_{t4}/P_{t0})^{\frac{\gamma-1}{\gamma}} - 1$			
8		(				
9		↑( )( )				
49 0		1				
1		1	T_{t2}/T_0			
2		−				
3		1				
4		)	$(T_{t2}/T_0) - 1$			
5		=	η_T			
6		↓( )( )				
7		4				
8		6			$\eta_T \rightarrow 46$	
9	EC	176	PRINT LINE OF DOTS			....

MHV 2/7/73

PROGRAM # VA 517 MONROE 1880 PAGE 11 OF 12 DATE: 6/73 BY: MHV

STEP	SYMBOL	COMMAND	COMMENTS	ENTER	STORE	PRINT
500		2				
501		8	SET-UP POINTER 28 (FIRST REG.			
502		↓( )	TO BE PRINTED & STR. 49			
503		•				
504		↓( )( )				
505		4				
506		9				
507	PRINT A	IND/SYMB	SYMBOL. ADDRESS "PRINT A"			
508		PRINT A				
509		↑( )( )	RCL ACC. TO POINTER			
510		IND/SYMB				
511		PRINT A				DATA
512		SET D.P	SET DEC. POINT TO 4			
513		4				
514		1				
515		↑( )( )	ADD 1 TO POINTER, STR 49			
516		+	AND SET UP NEW POINTER			
517		4				
518		9				
519		↓( )( )				
520		4				
521		9				
522		↓( )				
523		•				
524		−				
525		4				
526		5				
527		=	NEW POINTER − 45			
528		BRANCH	IF NEW POINTER = 45, I.E. IF N			
529		=	IS TO BE PRINTED SET DP TO ZERO			
530		IND/SYMB	WITH S.R. Φ			
531		Φ				
532		↑( )( )				
533		4				
534		9	NEW POINTER			
535		−				
536		4				
537		7				
538		=	NEW POINTER −47			
539		JUMP				
540		=	GO TO S.A. √ IF NEW POINTER			
541		IND/SYMB	= 47, OR DO NOT PRINT			
542		√				
543		JUMP	GO TO S.A "PRINT A" IF NEW			
544		IND/SYMB	POINTER ≤ 46			
545		PRINT A				
546	√	IND/SYMB	SYMBOL. ADDRESS √			
547		√				
548	EC	176	PRINT LINE OF DOTS			....
549		JUMP				

MHV 2/7/73

PROGRAM # VA S17 MONROE 1080 PAGE 12 OF 12 DATE: 6/73 BY: MHV

STEP	SYMBOL	COMMAND	COMMENTS	ENTER	STORE	PRINT
550		IND/SYMB	JUMP TO S.A. ADD. + TO			
551		+	PROCESS NEW DATO			
552	Φ	IND/SYMB	SUBROUTINE Φ SETS D.POINT TO 0			
553		Φ	FOR PRINTING OF N			
554		SET D.P				
555		0				
556		RESUME				
557						
558						
559						
560						
561						
562						
563						
564						
565						
566						
567						
568						
569						
570						
571						
572						
573						
574						
575						
576						
577						
578						
579						
580						
581						
582						
583						
584						
585						
586						
587						
588						
589						
590						
591						
592						
593						
594						
595						
596						
597						
598						
599						

MHV 2/7/73

PROGRAM: VA 517 OFF-DESIGN HYBRID COMPRESSOR — PAGE: 51 OF 1 DATE 6/73 BY: MHV

MAIN STORAGE BOOKKEEPING

REGISTER	CONTENTS 1	CONTENTS 2	CONTENTS 3
00	$C = (k_{B2}/k_{B4})/\cos 21° = 1.16$	1 218	
01	$Y_{to} = .2089$		
02	$V_S/V_4 = 1.039$		
03	$V_5/V_4 = .8764$		
04	$V_6/V_4 = .722$		
05	$(\gamma-1)/\gamma = .4/1.4$		
06	$\gamma/(\gamma-1) = 1.4/.4 = 3.5$		
07	$\alpha_4 = 21°$		
08	K		
09			
10	$\cos \alpha_2$		
11	T_{t2}/T_0		
12	P_{t2}/P_0		
13	T_2/T_0		
14	p_2/P_0		
15	$M_{V2} = M_2$		
16	M_4^*		
17	$A1 = 1+[(\gamma-1)/2]\,M_4^{*2}$		
18			
19			
20	$E = 29.364\,077$		
21	$F = 176.54$		
22	$G = 23290.21$		
23			
24			
25			
26			
27			
28	U_2/a_0	PRINT-OUT OF INPUT	
29	α_2		
30	P_{t4}/P_0		
31	p_4/P_0		
32	T_4/T_0		
33	M_4	LINE UP	
34	V_4/a_0	OF CALCULATED DATA	
35	P_{t4}'/P_0	FOR PRINTING.	
36	p_4'/P_0		
37	P_{t4}''/P_0		
38	p_4''/P_0		
39	P_{t5}/P_0		
40	P_{t6}/P_0		
41	p_6/P_0		
42	P_0 (psia)		
43	$\dot{w}$ (lbm/s)		
44	HP		
45	N (rpm)		
46	η_T		
47			
48			
49	POINTER		

M.H.V. 2/1/73

DISTRIBUTION LIST

		No. of Copies
1.	Defense Documentation Center Cameron Station Alexandria, Virginia 22314	12
2.	Library Code 0212 Naval Postgraduate School Monterey, California 93940	2
3.	Superintendent Naval Postgraduate School Monterey, California 93940	1
4.	Provost Code 02 Naval Postgraduate School Monterey, California 93940	1
5.	Dean of Research Code 023 Naval Postgraduate School Monterey, California 93940	1
6.	Chairman Department of Aeronautics Code 57 Naval Postgraduate School Monterey, California 93940	1
7.	Turbo-Propulsion Laboratory Department of Aeronautics Naval Postgraduate School Monterey, California 93940	5
8.	Commanding Officer Naval Air Systems Command Navy Department Washington, D. C. 20360	1
9.	Asst. Commander for Research & Technology Naval Air Systems Command Navy Department Washington, D. C. 20360	1

10. Dr. Frank Tanczos — 1
Code 03
Naval Air Systems Command
Navy Department
Washington, D. C. 20360

11. Mr. I. Silver — 1
Code 03B
Naval Air Systems Command
Navy Department
Washington, D. C. 20360

12. Dr. Edward S. Lamar — 1
Chief Scientist, AIR-03C
Naval Air Systems Command
Navy Department
Washington, D. C. 20360

13. Dr. H. J. Mueller — 1
Research Administrator
Code 310A
Naval Air Systems Command
Navy Department
Washington, D. C. 20360

14. Mr. E. A. Lichtman — 1
Naval Air Systems Command
Code 330
Navy Department
Washington, D. C. 20360

15. Mr. Karl H. Guttmann — 2
Code 330C
Naval Air Systems Command
Navy Department
Washington, D. C. 20360

16. Rear Admiral C. O. Holmquist, USN — 1
Chief of Naval Research
Office of Naval Research
Arlington, Virginia 22218

17. Commanding Officer — 6
Naval Air Propulsion Test Center
Attn: Mr. E. Stawski
Trenton, New Jersey 08628

18. Mr. Eric Lister — 1
R & T Division
Naval Air Propulsion Test Center
Trenton, New Jersey 08628

19. Mr. Elmer G. Johnson — 1
Director, Fluid Dynamics Facilities
Research Laboratories (ARL)
Wright-Patterson AFB, Ohio 45433

20. Mr. R. A. Langworthy — 1
Army Aviation Materiel Laboratories
Department of the Army
Fort Eustis, Virginia 23604

21. National Aeronautics and Space Administration — 1
Lewis Research Center (Library)
2100 Brookpark Road
Cleveland, Ohio 44135

22. Prof Dr. Ing. Karl Bammert — 1
Institut fuer Stroemungsmaschinen
Technische Hochschule Hannover
3 Hannover, Germany

23. Prof M. Berchtold — 1
Institut fuer Thermodynamik
Eidg. Technische Hochschule
Sonneggstr. 3
8006 Zurich
Switzerland

24. Dr. V. Beglinger — 1
Manager of Development
Brown Bovery-Sulzer Turbomachinery Ltd
Ch-8023 Zurich
Switzerland

25. Library — 1
AiResearch Mfg. Corporation
Division of Garrett Corporation
402 South 36th Street
Phoenix, Arizona 85034

26. CAG Library — 1
The Boeing Company
Seattle, Washington 98124

27. Prof Jacques Chauvin — 1
von Karman Institute
Chaussee de Waterloo 72
1640 Rhode-Saint-Genese
Belgium

28. Mr. Jean Fabri — 1
ONERA
29, Ave. de al Division Leclerc
92 Chatillon
Franch

29. Dr. Robert Goulard — 1
Director, Project SQUID
Jet Propulsion Center
Purdue University
Lafayette, Indiana 47907

30. Dr. Robert E. Henderson — 1
Director of Research
Detroit Diesel Allison Division
General Motors
P. O. Box 894
Indianapolis, Indiana 46206

31. Dr. B. Lakshminarayana — 1
Professor of Aerospace Engineering
The Pennsylvania State University
233 Hammond Building
University Park, Pennsylvania 16802

32. Library — 1
General Electric Company
Aircraft Engine Technology Division
DTO Mail Drop H43
Cincinnati, Ohio 45215

33. Library — 1
Pratt and Whitney Aircraft
Post Office Box 2691
West Palm Beach, Florida 33402

34. Library — 1
Pratt and Whitney Aircraft
East Hartford, Connecticut 06108

35. Prof Dr. Ing. H. Marcinowski — 1
Institut fuer Stroemungsmaschinen
Universitaet (T. H.) Karlsruhe
Karlsruhe, Germany

36. Prof Gordon C. Oates — 1
Department of Aeronautics and Astronautics
University of Washington
Seattle, Washington 98105

37. Dr. Bruce A. Reese — 1
Director, Jet Propulsion Center
School of Mechanical Engineering
Purdue University
Lafayette, Indiana 47907

38. Dr. W. Schlachter — 1
Brown, Boveri-Sulzer Turbomachinery Ltd
Dept. TDE
Escher Wyss Platz
CH-8023 Zurich
Switzerland

39. Prof Dr. Ing. H. Schlichting — 1
Institut fuer Stroemungsmechanik
Technische Hochschule Braunschweig
Bienroder Weg 3
93 Braunschweig, Germany

40. Dr. George K. Serovy — 1
Professor of Mechanical Engineering
208 Mechanical Engineering Building
Iowa State University
Ames, Iowa 50010

41. Dr. J. Surugue — 1
Director, Energie et Propulsion
ONERA
29 Ave. de la Division Leclerc
92 Chatillon
France

42. Dr. W. Tabakoff — 1
Professor, Department of Aerospace Engineering
University of Cincinnati
Cincinnati, Ohio 45221

43. Prof Dr. W. Traupel — 1
Institut fur Thermische Turbomaschinen
Eidg, Technische Hochschule
Sonneggstr. 3
8006 Zurich
Switzerland

44. Dr. Arthur J. Wennerstrom — 1
Chairman, ASME Turbomachinery Committee
ARL/LF
Wright-Patterson AFB
Dayton, Ohio 45433

REPORT DOCUMENTATION PAGE

READ INSTRUCTIONS BEFORE COMPLETING FORM

1. REPORT NUMBER: NPS-57Va73071A	2. GOVT ACCESSION NO.
3. RECIPIENT'S CATALOG NUMBER	
4. TITLE (and Subtitle): Design Report of Hybrid Compressor and Associated Test Rig	5. TYPE OF REPORT & PERIOD COVERED: Final Report to July 1973
	6. PERFORMING ORG. REPORT NUMBER
7. AUTHOR(s): Michael H. Vavra	8. CONTRACT OR GRANT NUMBER(s): Airtask No. A3303300/186B/3F41432301
9. PERFORMING ORGANIZATION NAME AND ADDRESS: Department of Aeronautics, Naval Postgraduate School, Monterey, Calif 93940	10. PROGRAM ELEMENT, PROJECT, TASK AREA & WORK UNIT NUMBERS: N.A.
11. CONTROLLING OFFICE NAME AND ADDRESS: Naval Air Systems Command, AIR 330C, Washington, D. C. 20360	12. REPORT DATE: July 1973
	13. NUMBER OF PAGES: 279
14. MONITORING AGENCY NAME & ADDRESS (if different from Controlling Office)	15. SECURITY CLASS. (of this report): Unclassified
	15a. DECLASSIFICATION/DOWNGRADING SCHEDULE

16. DISTRIBUTION STATEMENT (of this Report)

Approved for public release and sale; distribution unlimited.

17. DISTRIBUTION STATEMENT (of the abstract entered in Block 20, if different from Report)

18. SUPPLEMENTARY NOTES

19. KEY WORDS (Continue on reverse side if necessary and identify by block number)

Hybrid compressor concept.
Aerodynamic Design
Design- and Off-Design Performance
Losses in Radial Compressor Wheels
Performance of Drive Air Turbine

20. ABSTRACT (Continue on reverse side if necessary and identify by block number)

This report presents the aerodynamic calculations and describes the mechanical features of a test rig that has been designed at the Turbopropulsion Laboratory, Department of Aeronautics, for research work on a special type of centrifugal compressor. This so-called Hybrid compressor consists of a centrifugal rotor with 180° flow deflection in the meridional plane followed by an axial flow diffusor. The report establishes a method to predict the off-design performance of the subject compressor, which can be applied also to conventional centrifugal compressors. Extensive use is made of modern programmable calculators, and

Item 19 continued:

Description of Test Rig
Torque Measurement
Programs for Programmable Calculators

Item 20 continued:

programs are presented to show the effectiveness of these tools in engineering endeavors.